INTRACELLULAR TRAFFICKING OF THE INVASION-PROMOTING CELL SURFACE PROTEINASE MT1-MMP



Valentina Gifford
Christ Church
University of Oxford

Supervised by:
Dr. Yoshifumi Itoh
Prof. Michael Dustin
Submitted: Trinity Term 2020

This thesis is submitted to the Nuffield Department of Orthopaedics Rheumatology and Musculoskeletal Science, University of Oxford, in partial fulfilment of the requirements for the degree of Doctor of Philosophy

Declaration

I hereby declare that this thesis is my own original work and that all sources have been acknowledged and cited in the bibliography section. This work has not been submitted before as fulfilment of another degree or qualification to this or any other University.

Valentina Gifford

Date 28/07/2020

Abstract

Membrane type-1 matrix metalloproteinase (MT1-MMP) is a type I transmembrane proteinase that has been shown to promote the progression of different diseases, including rheumatoid arthritis (RA) and cancer, by enhancing cellular invasion. MT1-MMP promotes cellular invasion by degrading pericellular extracellular matrix (ECM) at the leading edge of migrating cells. MT1-MMP has been shown to localise to various motility-associated structures, including lamellipodia, filopodia, invadopodia, and podosomes. However, the molecular mechanisms of MT1-MMP localisation to these structures are not well-understood. Dr. Itoh's research group and others have found that MT1-MMP cell surface exposure is achieved by intracellular trafficking of MT1-MMP-containing vesicles along microtubules and that kinesin superfamily motor proteins (KIFs) play a role. We have employed a siRNA library to screen for the responsible KIFs and found that the knockdown (KD) of four KIFs (KIF13A, KIF3A, KIF9, KIF1C) notably affected MT1-MMP-mediated cellular functions at the cell-matrix interface of human fibrosarcoma cells (HT1080). Interestingly, the KD of these KIFs did not affect the overall level of MT1-MMP at the cell surface, but it significantly influenced MT1-MMP localisation at the substrate-attached side of the plasma membrane. Live cell imaging experiments confirmed that KIF13A, KIF3A and KIF9 associates with MT1-MMP-positive vesicles. These experiments also showed that when cells are cultured atop a substratum, KIF13A and KIF3A collaborate to transport MT1-MMP within the central cytoplasmic areas. However, only KIF13A seemed to reach the cell periphery to deliver the proteinase to the tips of motility-associated structures. Bioinformatic analysis revealed that the expression profile of KIF13A and KIF9 is altered in several cancer types and that

these two motor proteins might have cancer-specific roles, partially related to their involvement in MT1-MMP intracellular trafficking. Taken together these findings shed light on KIF-dependent MT1-MMP cell surface exposure and suggest KIF-driven MT1-MMP intracellular trafficking mechanisms as potential targets to control the un-wanted cell invasion that sustains the progression of diseases like RA and cancer.

Acknowledgements

I would like to thank my supervisor Dr. Yoshifumi Itoh for his constant support and encouragement throughout this DPhil. I would also like to thank my co-supervisor Prof. Michael Dustin for his support and feedback. Huge thanks go to Dr. Angus Wann for the continuous scientific and moral support he provided me and for his invaluable help in proof-reading this thesis. I am grateful to Prof. Afsie Sabokbar for always being there to encourage me and for her irreplaceable advices.

Huge thanks go to Noriko Ito and to Dr. Stefan Balint for helping me develop my laboratory skills and perform experiments.

I wish to thank all the members of the osteoarthritis centre for being amazing colleagues and for making me smile. Particular thanks go to Dr. Hayat Muhammad, who has been always extremely supportive.

Above all, I would like to thank my family and my fiancé Federico, for their love, support and never-ending faith in me.

Table of contents

CHAPTER 1: 26

1.1 CELL MIGRATION 27

1.2 MATRIX METALLOPROTEINASES (MMPS) 28

1.3 MEMBRANE TYPE-I MATRIX METALLOPROTEINASE (MT1-MMP) 32

1.3.1 Substrates of MT1-MMP 32

1.3.2 Regulation of MT1-MMP 36

1.4 INTRACELLULAR TRAFFICKING BY KINESIN SUPERFAMILY MOTOR PROTEINS (KIFS) 44

1.4.1 Kinesin superfamily motor proteins (KIFs) 45

1.4.2 MT1-MMP intracellular trafficking by KIFs 59

1.4.3 Selection of KIFs to study intracellular trafficking of MT1-MMP-containing vesicles 60

1.4.4 KIF13A 63

1.4.5 KIF3A 65

1.4.6 KIF9 66

1.4.7 KIF1C 66

1.5 AIMS OF THE THESIS 67

CHAPTER 2: 71

2.1 CELL CULTURE 73

2.1.1 Cells and cell culture reagents 73

2.1.2 Cell culture conditions 74

2.1.3 Cryopreservation of cells 74

2.1.4 Transient transfection 74

2.1.5 Gene silencing 75

2.1.6 Establishment of stable HT-1080 cells expressing NanoLuc® luciferase 75

2.1.7 Transduction of stable HT-1080 cells expressing NanoLuc® luciferase 76

2.2 MOLECULAR BIOLOGY 77
2.2.1 Reagents and materials 77
2.2.2 General solutions 78
2.2.3 RT-PCR and cDNA synthesis 79
2.2.4 PCR reaction 79
2.2.5 DNA electrophoresis 80
2.2.6 Quantification of DNA bands 81
2.2.7 DNA fragment purification 81
2.2.8 Restriction digestion 81
2.2.9 Ligation of DNA fragments 82
2.2.10 Fusion of DNA fragments 82
2.2.11 Bacterial electroporation 82
2.2.12 DNA plasmid purification 83
2.2.13 Molecular cloning of constructs 84
2.2.14 Cloning of Tet-off TRIPZ inducible lentiviral shRNA constructs 87
2.2.15 Packaging lentiviral shRNA constructs 88
2.3 SDS PAGE GEL ELECTROPHORESIS 88
2.3.1 Reagents and materials 88
2.3.2 General solutions 89
2.3.3 SDS-PAGE procedure 90
2.4 WESTERN BLOTTING 91
2.4.1 Reagents and materials 91
2.4.2 Antibodies 92
2.4.3 General solutions 92
2.4.4 Procedure 92
2.4.5 Quantification of protein bands 93
2.5 ZYMOGRAPHY 93
2.5.1 Reagents and materials 93
2.5.2 Gel composition 94
2.5.3 General solutions 94

2.5.4 Procedure 95
2.5.5 Quantification of gelatinolytic bands 95
2.6 IMMUNOCYTOCHEMISTRY 96
2.6.1 Reagents 96
2.6.2 General solutions 96
2.6.3 Antibodies 97
2.6.4 Procedure 97
2.7 FLUORESCENT-GELATIN FILM DEGRADATION ASSAY 98
2.7.1 Reagents and materials 98
2.7.2 Preparation of fluorescently labelled gelatin 99
2.7.3 Coating of glass cover slips 99
2.7.4 Culture of cells on gelatin-coated cover slips 100
2.7.5 Image analysis 100
2.8 COLLAGEN FILM DEGRADATION ASSAY 101
2.8.1 Reagents and materials 101
2.8.2 Collagen-coating of 12-well dish 101
2.8.3 Culture of cells on collagen-coated dishes and collagen staining 102
2.8.4 Image analysis 102
2.9 CELL SURFACE BIOTINYLATION 103
2.9.1 Reagents and materials 103
2.9.2 General solutions 103
2.9.3 Procedure 103
2.10 TRANSWELL COLLAGEN INVASION ASSAY 104
2.10.1 Reagents and materials 104
2.10.2 Procedure 104
2.10.3 Transwell invasion quantification 105
2.11 MICROCARRIER BEADS INVASION ASSAY 105
2.11.1 Reagents and materials 105
2.11.2 Procedure 106

2.11.3 Quantification of cellular invasion through the collagen matrix 107

2.12 WOUND-HEALING ASSAY 108

2.12.1 Reagents and materials 108

2.12.2 Procedure 108

2.12.3 Quantification of wound closure 108

2.13 LIVE CELL IMAGING 109

2.13.1 Reagents and materials 109

2.13.2 General Solutions 109

2.13.3 Procedure 109

2.13.4 Tracking of MT1-RFP-positive vesicles trafficked by GFP-tagged KIFs 110

2.14 IMAGE ACQUISITION 110

2.15 IMAGE PROCESSING AND ANALYSIS 111

2.16 ANALYSIS OF GENOMIC ALTERATIONS OF *KINESIN* GENES IN CANCER 113

CHAPTER 3: 117

3.1 INTRODUCTION 119

3.2 RESULTS 120

3.2.1 MT1-MMP-dependent F-gelatin film degradation by HT-1080 cells is inhibited by KD of KIF13A, KIF3A, KIF1C and enhanced by KD of KIF9 120

3.2.2 MT1-MMP-dependent F-gelatin film degradation by HT-1080 cells is not affected by overexpression of GFP-tagged KIF13A, KIF3A, KIF9 and KIF1C 125

3.2.3 MT1-MMP-dependent collagen film degradation by HT-1080 cells is inhibited by KD of KIF13A, KIF3A, KIF1C and enhanced by KD of KIF9 127

3.2.4 MT1-MMP-dependent proMMP-2 activation by HT-1080 cells is inhibited by KD of KIF13A, KIF3A, KIF1C and enhanced by KD of KIF9 129

3.2.5 The KD of KIF13A, KIF3A, KIF9 and KIF1C does not affect MT1-MMP cell surface expression 132

3.2.6 The KD of KIF13A, KIF3A and KIF9 alters MT1-MMP localisation to the cell matrix interface 134

3.2.7 The KD of KIF13A, KIF3A and KIF9 affects MT1-MMP-mediated cell invasion through a microporous membrane 136

3.2.8 The KD of KIF13A, KIF3A, KIF9 and KIF1C diminishes MT1-MMP-dependent cell migration in 3D collagen 138

3.2.9 MT1-MMP-dependent collagen film degradation by RASFs is inhibited by KD of KIF13A, KIF3A, KIF1C and enhanced by KD of KIF9 141

3.2.10 MT1-MMP-dependent gelatin film degradation by MDA-MB-231 cells is not affected by KD of KIF13A, KIF3A, KIF9 and KIF1C 143

3.2.11 MT-Loop region is dispensable for efficient MT1-MMP-dependent gelatin film degradation by MDA-MB-231 cells 145

3.3 DISCUSSION 147

CHAPTER 4: 159

4.1 INTRODUCTION 161

4.2 RESULTS 162

4.2.1 KIF13A, KIF3A, KIF9 and KIF1C KD influences MT1-MMP intracellular distribution in HT-1080 cells 162

4.2.2 MT1-MMP localisation to the MTOC, cis-Golgi and trans-Golgi 165

4.2.3 MT1-MMP co-localisation with Rab5 and Rab7 168

4.2.4 Co-localisation of GFP-tagged KIFs and MT1-RFP in HT-1080 cells cultured on a gelatin matrix 170

4.2.5 Co-localisation of GFP-tagged KIFs and MT1-RFP in HT-1080 cells cultured in a 3D collagen matrix 175

4.2.6 GFP-tagged KIF13A, KIF3A and KIF9-v1 transport MT1-RFP-positive vesicles.179

4.2.7 GFP-tagged KIF13A and KIF3A collaboratively transport MT1-RFP-containing vesicles 187

4.2.8 KD of KIF3A or KIF13A diminishes KIF9-induced increase of MT1-MMP-dependent gelatinolytic activity of HT-1080 cells 194

4.3 DISCUSSION 199

CHAPTER 5: 209

5.1 INTRODUCTION 211

5.2 RESULTS 213

5.2.1 MT1-MMP-dependent F-gelatin film degradation by NanoLuc® luciferase-expressing HT-1080 cells is inhibited by the KD of KIF13A, KIF3A and KIF1C and enhanced by the KD of KIF9 213

5.2.2 Characterisation of NanoLuc® luciferase-expressing HT-1080 stably expressing TRIPZ inducible lentiviral shRNAs targeting KIF13A or KIF9 214

5.2.3 Genomic alterations of Kif13a and Kif9 genes across The Cancer Genome Atlas (TCGA) studies 217

5.3 DISCUSSION 221

CHAPTER 6: 233

6.1 GENERAL DISCUSSION 233

6.2 FUTURE PROSPECTS 240

6.3 CONCLUSIONS 241

CHAPTER 7: 245

List of Figures

FIGURE 1.1: THREE STEP THEORY OF CELL INVASION 28

FIGURE 1.2: MMPS MULTI-DOMAIN STRUCTURE [14] 29

FIGURE 1.3: A MODEL OF THE CELL SURFACE ACTIVATION OF PROMMP-2 BY MT1-MMP [14] 35

FIGURE 1.4: KINESIN DOMAIN ORGANISATION 48

FIGURE 1.5: ORGANISATION OF MICROTUBULES 49

FIGURE 1.6: DOMAIN STRUCTURE-BASED CLASSIFICATION OF KINESINS 50

FIGURE 1.7: 'HAND-OVER HAND' MODEL FOR KINESIN MOTILITY 58

FIGURE 1.8: MT1-MMP CELL SURFACE EXPOSURE IS ACHIEVED BY TARGETED VESICLE TRANSPORT. 61

FIGURE 1.9: SELECTION OF KIFS TO STUDY MT1-MMP INTRACELLULAR TRAFFICKING IN HT1080 CELLS 63

FIGURE 2.1: CLONING AND EXPRESSION OF GFP-TAGGED KIFS AND HALO-TAGGED KIFS 86

FIGURE 2.2: QUANTIFICATION OF GELATINOLYTIC BANDS 96

FIGURE 2.3: SET UP OF TRANSWELL INVASION ASSAY 105

FIGURE 2.4: SET UP OF MICROCARRIER BEADS INVASION ASSAY 107

FIGURE 3.1: THE KD OF KIF13A, KIF3A, KIF9 AND KIF1C ALTERS MT1-MMP-MEDIATED GELATIN FILM DEGRADATION IN HT-1080 CELLS 119

FIGURE 3.2: GELATIN FILM DEGRADATION IS DEPENDENT ON ENDOGENOUS MT1-MMP IN HT-1080 CELLS 121

FIGURE 3.3: THE KD OF KIF13A, KIF3A, KIF9 AND KIF1C ALTERS MT1-MMP-MEDIATED GELATIN FILM DEGRADATION IN HT-1080 CELLS 122

FIGURE 3.4: THE KD OF KIF5B DOES NOT ALTER MT1-MMP-MEDIATED GELATIN FILM DEGRADATION IN HT-1080 CELLS 122

FIGURE 3.5: EFFICIENCY OF KIF KD IN HT-1080 CELLS 124

FIGURE 3.6: THE KD OF KIF13A, KIF3A, KIF9 AND KIF1C DOES NOT ALTER MT1-MMP EXPRESSION AT THE MRNA LEVEL 125

FIGURE 3.7: OVEREXPRESSION OF GFP-TAGGED KIFS DOES NOT INFLUENCE MT1-MMP-DEPENDENT GELATIN FILM DEGRADATION BY HT-1080 CELLS 126

FIGURE 3.8: GELATIN FILM DEGRADATION IS MEDIATED BY ENDOGENOUS MT1-MMP IN HT-1080 CELLS 127
FIGURE 3.9: THE KD OF KIF13A, KIF3A, KIF9 AND KIF1C ALTERS MT1-MMP-MEDIATED COLLAGEN FILM DEGRADATION IN HT-1080 CELLS 128
FIGURE 3.10: PRO-MMP-2 ACTIVATION IS ONLY DEPENDENT ON ENDOGENOUS MT1-MMP IN HT-1080 CELLS 129
FIGURE 3.11: THE KD OF KIF13A, KIF3A, KIF9 AND KIF1C ALTERS MT1-MMP-MEDIATED PROMMP-2 ACTIVATION AND MT1-MMP PROCESSING 131
FIGURE 3.12: THE KD OF KIF13A, KIF3A, KIF9 AND KIF1C DOES NOT AFFECT THE OVERALL AMOUNT OF MT1-MMP ON THE CELL SURFACE 133
FIGURE 3.13: THE KD OF KIF13A, KIF3A, KIF9 AND KIF1C MODIFIES MT1-MMP LOCALISATION AT THE SUBSTRATE-ATTACHMENT SIDE 135
FIGURE 3.14: TRANSWELL INVASION IS ONLY DEPENDENT ON ENDOGENOUS MT1-MMP IN HT-1080 CELLS 137
FIGURE 3.15: THE KD OF KIF13A, KIF3A, KIF9 AND KIF1C ALTERS MT1-MMP-DEPENDENT TRANSWELL INVASION 138
FIGURE 3.16: CELL MIGRATION THROUGH 3D COLLAGEN IS ONLY DEPENDENT ON ENDOGENOUS MT1-MMP 139
FIGURE 3.17: THE KD OF KIF13A, KIF3A, KIF9 AND KIF1C DIMINISHES MT1-MMP-DEPENDENT CELL MIGRATION IN 3D COLLAGEN 140
FIGURE 3.18: THE KD OF KIF13A, KIF3A, KIF9 AND KIF1C DOES NOT AFFECT WOUND CLOSURE . 141
FIGURE 3.19: THE KD OF KIF13A, KIF3A, KIF9 AND KIF1C ALTERS MT1-MMP-MEDIATED COLLAGEN FILM DEGRADATION BY RASFS 142
FIGURE 3.20: EFFICIENCY OF KIF KD IN MDA-MB-231 CELLS 144
FIGURE 3.21: THE KD OF KIF13A, KIF3A, KIF9, KIF1C AND KIF5B DOES NOT AFFECT MT1-MMP-MEDIATED GELATIN FILM DEGRADATION BY MDA-MB-231 145
FIGURE 3.22: MT1-LOOP REGION IS NOT REQUIRED FOR EFFICIENT MT1-MMP MEDIATED GELATIN FILM DEGRADATION BY MDA-MB-231 146
FIGURE 3.23: MULTIPLE KIFS REGULATE MT1-MMP INTRACELLULAR TRAFFICKING 155

FIGURE 4.1: MT1-MMP DISTRIBUTION IN THE CYTOPLASM AND ITS ACCUMULATION AT THE RUFFLING MEMBRANE STRUCTURES AND PERINUCLEAR AREA 164
FIGURE 4.2: MT1-MMP LOCALISATION TO THE MTOC, CIS- AND TRANS-GOLGI 167
FIGURE 4.3: MT1-MMP CO-LOCALISATION WITH RAB5 AND RAB7 169
FIGURE 4.4: GFP-TAGGED KIFS AND MT1-RFP CO-LOCALISATION IN HT-1080 CULTURED ON GELATIN-COATED COVER GLASS 174
FIGURE 4.5: GFP-TAGGED KIFS AND MT1-RFP CO-LOCALISATION IN HT-1080 CULTURED IN A 3D COLLAGEN MATRIX 178
FIGURE 4.6: KIF13A TRANSPORTS MT1-MMP-CONTAINING VESICLES AT THE RUFFLING MEMBRANE STRUCTURES AND THE SUBSTRATE-ATTACHMENT SIDE 181
FIGURE 4.7: KIF3A TRANSPORT MT1-MMP-CONTAINING VESICLES AROUND THE PERINUCLEAR AREA 183
FIGURE 4.8: KIF9-V1-GFP AND MT1-RFP POSITIVE VESICLES LOCALISES AT THE PERINUCLEAR AREA 184
FIGURE 4.9: KIF9-V2-GFP AND KIF1C DO NOT DIRECTLY CONTRIBUTE TO MT1-MMP INTRACELLULAR TRAFFICKING MECHANISMS 186
FIGURE 4.10: EFFECT OF CONCOMITANT KD OF KIF13A AND KIF3A ON MT1-MMP-MEDIATED GELATIN FILM DEGRADATION 188
FIGURE 4.11: KIF13A AND KIF3A COLLABORATIVELY TRANSPORT MT1-MMP-CONTAINING VESICLE 193
FIGURE 4.12: EFFECT OF KIF3A AND KIF9 CO-KD ON MT1-MMP-MEDIATED GELATIN FILM DEGRADATION 196
FIGURE 4.13: KIF3A AND KIF9-V1 TRANSPORT MT1-MMP-CONTAINING VESICLES AROUND THE NUCLEAR AREA 197
FIGURE 4.14: EFFECT OF KIF13A AND KIF9 CO-KD ON MT1-MMP-MEDIATED GELATIN FILM DEGRADATION 198
FIGURE 4.15: KIF13A AND KIF3A COLLABORATE TO TRAFFIC MT1-MMP TO THE CELL SURFACE ... 205
FIGURE 5.1: SCHEMATIC REPRESENTATION OF AN EXPERIMENTAL PULMONARY METASTATIC MODEL 212
FIGURE 5.2: THE KD OF KIF13A AND KIF9 ALTERS MT1-MMP-MEDIATED GELATIN FILM DEGRADATION BY LUCIFERASE-LABELLED HT1080 CELLS 213

FIGURE 5.3: CHARACTERISATION OF NANOLUC® LUCIFERASE-LABELLED HT1080 STABLY EXPRESSING TET-ON TRIPZ INDUCIBLE LENTIVIRAL SHRNAS TARGETING KIF13A OR KIF9 216
FIGURE 5.4: ANALYSIS OF *KIF13A* AND *KIF9* GENE MUTATIONS IN TCGA PANCANCER ATLAS STUDIES 218
FIGURE 5.5: ANALYSIS OF *KIF13A* AND *KIF9* GENE AMPLIFICATIONS AND DEEP DELETIONS IN TCGA PANCANCER ATLAS STUDIES 220
FIGURE 5.6: SCHEMATIC REPRESENTATION OF A POSSIBLE EXPERIMENTAL SETUP 223
FIGURE 5.7: KIF13A IS AN UNFAVOURABLE PROGNOSTIC MARKER FOR LIVER CANCER..... 226
FIGURE 5.8: KIF9 IS A FAVOURABLE PROGNOSTIC MARKER FOR RENAL AND COLORECTAL CANCERS 227

List of Tables

TABLE 1.1: NOMENCLATURE OF KINESIN SUPERFAMILY MOTOR PROTEINS (KIFS)..... 51

TABLE 2.1: LIST OF PRIMERS USED FOR RT-PCR..... 79

TABLE 2.2: DREAM TAQ GREEN DNA POLYMERASE STANDARD REACTION SETUP..... 80

TABLE 2.3: PHUSION HOT START II HIGH-FIDELITY DNA POLYMERASE STANDARD REACTION SETUP . 80

TABLE 2.4: QUICK-FUSION CLONING KIT STANDARD REACTION SETUP..... 82

TABLE 2.5: SDS-PAGE RESOLVING GEL COMPOSITION 90

TABLE 2.6: SDS-PAGE STACKING GEL COMPOSITION 90

TABLE 2.7: SDS-PAGE RESOLVING GEL COMPOSITION FOR ZYMOGRAPHY 94

TABLE 4.1: AVERAGE VELOCITIES AND DIAMETERS OF MT1-RFP-POSITIVE VESICLES TRANSPORTED BY KIF13A-GFP, KIF3A-GFP AND KIF9-V1-GFP..... 185

TABLE 4.2: AVERAGE VELOCITIES OF MT1-RFP-POSITIVE VESICLES TRANSPORTED BY KIF13A-GFP AND KIF3A-HALOTAG..... 190

List of Abbreviations

2D: Two dimensional

3D: Three dimensional

5-HT_{1A}: Serotonin type 1A

A431: Squamous carcinoma cells

ACC: Adrenocortical carcinoma

ADP: Adenosine diphosphate

AP-1: Adaptor protein 1

AP-2: Adaptor protein 2

APS: Ammonium persulfate

ARF6: ADP-ribosylation factor 6

ATP: Adenosine triphosphate

BSA: Bovine serum albumin

C-terminus: COOH-terminus

CIP: Calf intestinal alkaline phosphatase

COS-7: African green monkey SV40-transformed kidney epithelial cells

DAPI: 4,6-diamidino-2-phenylindole

DIC: Differential interference contrast

DLBC: Diffuse large B-cell lymphoma

DMEM: Dulbecco's Modified Eagle's Medium

DMSO: Dimethyl sulfoxide

ECM: Extracellular matrix

EDTA: Ethilenediaminetetraaetic acid

ERM: Ezrin/radixin/moesin

FAs: Focal adhesions

FBS: Fetal bovine serum

FHA: Forkhead-associated domain

FI: Fluorescence intensity

GAPs: GTPase-activating proteins

GBM: Glioblastoma multiforme

GEFs: Guanine nucleotide exchange factors

GPI: Glycosylphosphatidylinositol

HEK 293: Human embryonic kidney 293 cells

HIF-2α: Hypoxia-inducible factor 2α

HT-1080: Human fibrosarcoma cells

HeLa: Human Henrietta Lacks cell line

HER2: Human epidermal growth factor receptor

IRM: Interference reflection microscopy

Ig: Immunoglobulin

KAP: Kinesin associate protein

KD: Knockdown

KHCs: Kinesin heavy chains

KIF: Kinesin superfamily motor protein

KLC: Kinesin light chain

LB: Luria-Bertani

LGG: Brain lower grade glioma

LPR: Low-density lipoprotein receptor

LPS: Lipopolysaccharide

MAPs: Microtubule associate proteins

MDA-MB-231: Human breast cancer cell line

MMPs: Matrix metalloproteinases

MMTV: Mouse mammary tumor virus

MT-MMPs: Membrane-type matrix metalloproteinases

MTOC: Microtubule organising centre

N-WASP: Neural Wiskott-Aldrich Syndrome protein

N-terminus: NH2-terminus

NA: Numerical aperture

NEDD9: Neural precursor cell expressed developmentally down-regulated 9

NT: Non-targeting

PA: Phosphatidic acid

PCC: Pearson's correlation coefficient

PCPG: Pheochromocytoma and paraganglioma

PCs: Pro-protein convertases

PLD2: Phospholipase D2

PET: Polyethylene terephthalate

PKC: Protein kinase C

PVDF: Polyvinylidene difluoride

Pro: Pro-domain

RA: Rheumatoid arthritis

RASFs: Rheumatoid arthritis synovial fibroblasts

RECK: Reversion-inducing cysteine-rich protein with kazal motifs

ROI: Region of interest

RT-PCR: Reverse transcription polymerase chain reaction

RT: Room temperature

SD: Standard deviation

SDS: Sodium dodecyl sulphate

TAE: Tris-acetate-EDTA

TBS: Tris-buffered saline

TCGA: The Cancer Genome Atlas

TE: Tris-EDTA buffer

THY1+: thymus cell antigen 1 positive

TIMP: Tissue inhibitor of metalloproteinase

TIRF: Total internal reflection fluorescence

TKS4: Tyr kinase substrate with four SH3 domains

TKS5: Tyr kinase substrate with five SH3 domains

TNBC: Triple negative breast cancer

TRE: Tetracycline reporter element

Tet: Tetracycline

VAMP7: Vesicle-associated protein 7

WASH: Wiskott-Aldrich Syndrome protein with Scar homolog

WASP: Wiskott-Aldrich Syndrome protein

WAVE: WASP family verprolin homologous protein

ccRCC: Kidney renal clear cell carcinoma

rtTA3: Reverse tetracycline transactivator

shRNA: Short hairpin RNA

siRNA: Small interfering RNA

tTA: Tetracycline transactivator

CHAPTER 1:

INTRODUCTION

1.1 Cell migration

Cell migration is a fundamental biological process that plays a crucial role in various physiological phenomena like embryonic development, immune response and wound healing (1). Cell migration is physiologically highly regulated and when it becomes uncontrolled it can lead to the development of diseases like rheumatoid arthritis (RA) and cancer (2). Thus, understanding the mechanisms of cell migration is of great importance for both the life science and medical science fields.

Abercrombie and colleagues (3-5) were the first to describe two-dimensional (2D) cell migration, studying fibroblasts moving on a flat substratum. 2D migration studies are useful to analyse the fundamental aspects of cell migration. However, they do not reproduce physiological cell movement *in vivo*, where cells are completely embedded in the extracellular matrix (ECM), that acts as a physical barrier and is characterised by a variable composition, density and stiffness (6). Lance Liotta and co-workers (7) proposed the 'three-step model of invasion', that describes cell migration through the ECM. The model states that cell migration is achieved through the cyclical repetition of the following three steps (Figure 1.1): cell attachment to the ECM through cell adhesion molecules such as integrins; local ECM degradation by proteinases; cell migration through the degraded ECM space (7). Cells can successfully carry out these three steps when integrin-mediated cell adhesion, cytoskeletal re-arrangements and proteinase activity are coordinated in a spatiotemporal manner (6). Proteinase-dependent cell migration is also known as mesenchymal-type migration (6). However, when cells move within a three-dimensional (3D) matrix, they can also adopt the amoeboid-type migration, which does not require proteolytic activities:

cells squeeze through pre-existing pores within the matrix, adjusting their shape and employing actomyosin-based forces (8). It is now clear that cells can switch from the mesenchymal- to the amoeboid-type migration when ECM pore size is large enough for them to squeeze their nuclei through (9). Nevertheless, if pore size is not big enough, cells need to create a path to migrate through the ECM, employing proteinases like matrix metalloproteinases (MMPs) (10) (11).

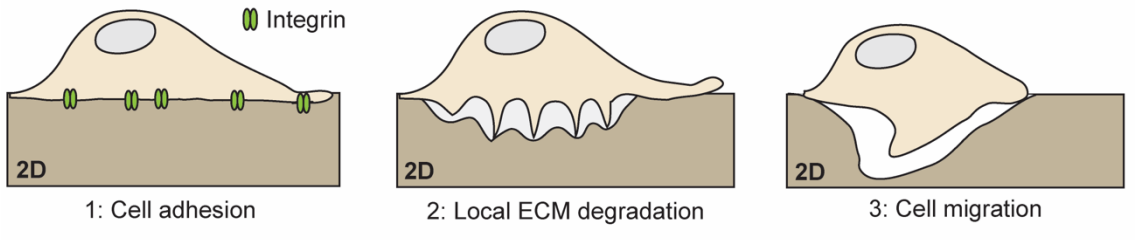


Figure 1.1: Three step theory of cell invasion

1: The cell recognises the ECM and attaches to that through adhesion molecules like integrins. 2: Proteinases are recruited, and local ECM degradation is achieved. 3: The cell body migrates through the degraded area.

1.2 Matrix Metalloproteinases (MMPs)

MMPs are zinc-dependent proteinases that belong to the large superfamily of metzincin (12). MMPs can collectively degrade all the components of the ECM (13). In humans, there are 23 different MMPs, categorised depending on their domain structure or their substrate specificity (12). MMPs can also be grouped into soluble MMPs, which are secreted in the extracellular milieu, and into membrane-type MMPs (MT-MMPs), which are anchored to the cell surface (14)

(Figure 1.2). The majority of soluble MMPs are characterised by a multi-domain structure made up of a signal peptide (SP), a pro-domain (Pro), a catalytic domain (Cat), a hinge region (L1) and a hemopexin domain (Hpx) (Figure 1.2) (14).

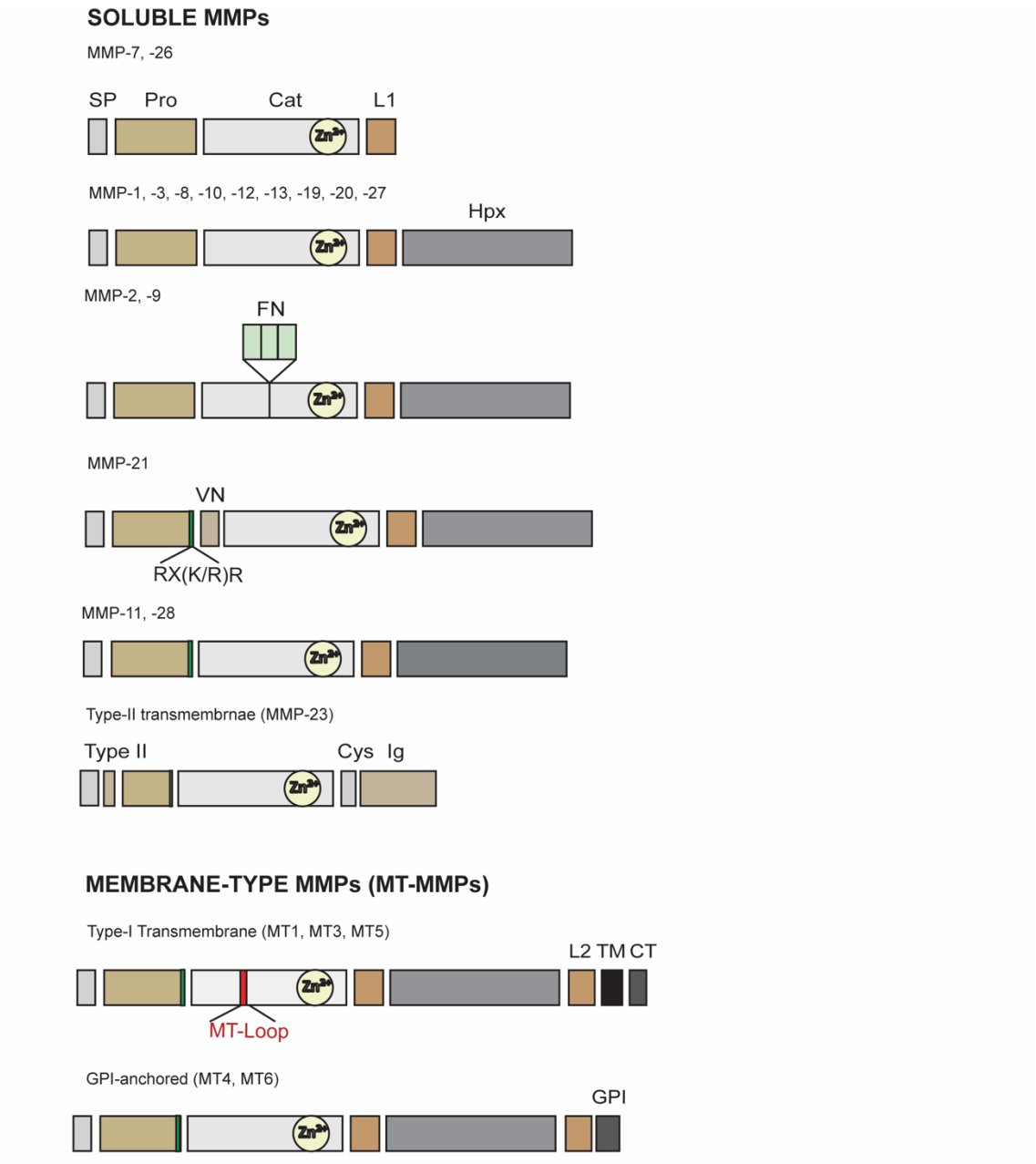


Figure 1.2: MMPs multi-domain structure [14]

SP: signal peptide; Pro: pro-domain; Cat: catalytic domain; L1: linker peptide 1; Hpx: hemopexin domain; FN: fibronectin type II repeats; VN: vitronectin type domain; type II: membrane type II

domain; Cys: cysteine-rich domain; Ig: immunoglobulin; L2: linker peptide 2; TM: transmembrane domain; CT: cytoplasmic tail; GPI: GPI-anchor signal sequence.

The signal peptide is used to direct the proteinases to the cell surface for secretion (15). The pro-domain is 80 amino acids long and contains a conserved cysteine residue, which maintains the enzyme latent (12). The cysteine interacts with the catalytic Zn^{2+} through its SH group (12). Upon proteolytic activation, the Zn^{2+} becomes available for the interaction with a water molecule and the catalytic activity can take place (12). The catalytic domain is approximatively 170 amino acids long and consists of four α-helices, five stranded β-sheets and connecting loops. The catalytic site contains the consensus sequence HEXGHXXGXXH, characterised by a conserved glutamate residue and three histidine residues that coordinate with the catalytic Zn^{2+} (16). Downstream of the consensus sequence there is a methionine residue, also named 'Met-turn', which plays a crucial role in maintaining the structural integrity of the catalytic site (16). This 'Met turn' is conserved and it is the reason behind the name 'Metzincin'. Binding of a substrate to the catalytic domain, causes the displacement of the water molecule interacting with the catalytic Zn^{2+}. The carbonyl group of the substrate peptide bond is subjected to a nucleophilic attack by the displaced water molecule. This step is facilitated by the conserved glutamate residue, which acts as a general base, drawing a proton from the water molecule (17). The invagination S_1' is localised to the right of the catalytic Zn^{2+} and it accommodates the substrate side chain that becomes the new NH_2 (N)-terminus after the peptide bond cleavage (17). The S_1' is the most variable portion of the catalytic domain among the MMPs and therefore it determines substrate specificity and selectivity (18). The hinge

region (L1) connects the catalytic and the hemopexin domains and is characterised by a proline-rich sequence of variable length, which provides structural constraint (19). The hemopexin domain is about 210 amino acids long. It features four stranded antiparallel β-sheets stabilised by a Ca^{2+} cation in the middle (12). This domain can act as interface for protein interaction and for some MMPs, as binding site for their respective endogenous inhibitors, the tissue inhibitors of metalloproteinases (TIMPs). For instance, the proMMP-2 hemopexin domain interacts with the COOH (C)-terminal domain of TIMP-2, facilitating the formation of proMMP-2-TIMP-2 complex on the cell surface (20). The hemopexin domain is also important for MMP-1, MMP-2, MMP-8, MMP-13 and MMP-14 collagenolytic activity (21).

MT-MMPs are characterised by the typical domain structure of MMPs, but in addition, they are anchored to the cell surface through either a transmembrane domain (TM), followed by a cytoplasmic tail (CT) (MT1-, MT-2, MT-3, and MT5-MMPs), or a glycosylphosphatidylinositol (GPI)-anchor (MT4-, MT6-MMPs) at their C-terminus (Figure 1.2) (14). The pro-peptide of all MT-MMPs contains the basic amino acid motif (RX(K/R)R) at its C-terminus, which can be recognised by pro-protein convertases (PCs), such as furin (14). MT-MMPs are activated by PCs within the trans Golgi and are expressed as active forms on the cell surface. Besides MT-MMPs, RX(K/R)R amino acid motif is also present in other MMPs such as MMP-11, MMP-21 and MMP-28, which can also be activated by PCs (22). TM-type MT-MMPs possess a unique eight-amino acid loop insertion in their catalytic domain named the MT-Loop (Figure 1.2) (22).

MT1-MMP is the most studied and well characterised proteinase among MT-MMPs. This proteinase has been shown to be the sole MMP to promote cell

migration through collagen-rich matrices (23) and it has been associated with a variety of physiological processes like wound healing, immune response, skeletal development and angiogenesis (22). On the other hand, MT1-MMP has also been implicated with multiple pathological conditions like RA (24), atherosclerosis (25), inflammation (26), cancer growth, invasion and metastasis (27).

1.3 Membrane type-I matrix metalloproteinase (MT1-MMP)

MT1-MMP was characterised for the first time in invasive cancer cells as cell surface activator of proMMP-2 (28). It is now known that this proteinase is also expressed in many other cell types such as adipocytes, chondrocytes, endothelial cells, epithelial cells, fibroblasts, mesenchymal stem cells, myeloid cells, neuronal cells, osteoclasts, osteoblasts, B cells and T cells (14). As described above, MT1-MMP consists of the typical domain structure of MMPs and it is tethered to the cell surface through a transmembrane domain (Figure 1.2).

1.3.1 Substrates of MT1-MMP

ECM components

MT1-MMP degrades a wide array of ECM components, including fibrillar collagen types I, II, III, fibronectin, fibrin/fibrinogen, laminin-1, -2, -4, -5, vitronectin, aggrecan, and perlecan (22). Collagens are the most abundant proteins of the ECM and they are the major structural elements of most tissues (29). Collagens can be classified into three major groups: fibrillar collagens, fibril-

associated collagen, and sheet-forming collagens. Fibrillar collagens account for more than 90% of all collagen types (29). Collagen type I is the most abundant of fibrillar collagens (30). It is highly expressed in connective tissues and represent an important component of the interstitial matrix (30). Collagen type II is a fundamental component of cartilage and is also found in vitreous humor; collagen type III has a primary role in maintaining the structural integrity of cardiovascular and visceral tissues (30). Fibrillar collagen monomer is a complex of three long and parallel left-handed polyproline II helices, twisted together and forming a right-handed triple helical structure (31). Collagen monomers aggregate to form fibrils, which associate to generate thicker fibres in tissues. At neutral pH, fibrillar collagens can only be hydrolysed by MMP-1, MMP-2, MMP-8, MMP-13 and MT1-MMP, which are known as collagenases (32). MT1-MMP collagenolytic activity plays a primary role *in vivo*. MT1-MMP-deficient mice die within the first 16 weeks after birth, due to developmental abnormalities (33, 34). Null mice present dwarfism, osteopenia, osteoclast-mediated arthritis, fibrosis of soft tissue and develop a progressive cranial dysmorphism (33, 34). Overall, skeletal development and connective tissue remodelling during post-natal development are impaired. More recently, it has been reported that MT1-MMP plays a primary role in tendons' development by releasing collagen fibres from the fibripositors and inducing the formation of new fibres (35). Therefore, MT1-MMP-dependent collagenolysis is essential for stromal remodelling after birth.

Soluble MMPs

MT1-MMP activates proMMP-2 on the cell surface (28). Active MMP-2 degrades collagen type IV, a major component of the basement membrane, that cannot be directly degraded by MT1-MMP (28). The basement membrane is a

thin and dense matrix sheet, produced and organised by epithelial cells. The basement membrane has a primary role in supporting tissue architecture, separating the epithelium from the surrounding stroma (36). When primary epithelial cancer cells invade and metastasise to distal organs, they have to migrate through their own basement membrane. Basement membrane transmigration is mediated by MT1-MMP, that is expressed on the cell surface of cancer cells. The proteinase activates proMMP-2 produced by stromal cells, allowing basement membrane degradation and transmigration by cancer cells (28). MT1-MMP-dependent proMMP-2 activation has been shown to support the growth of gastric cancer cells and support their transmigration through their own basement membrane (37). MT1-MMP-dependent proMMP-2 activation model is well-accepted and it has also been reviewed recently (Figure 1.3) (14). Briefly, MT1-MMP homo-dimerises on the cell surface through its hemopexin and transmembrane domains; one MT1-MMP molecule of the dimer is inhibited by a molecule of tissue inhibitor of metalloproteinase 2 (TIMP-2), which binds to the catalytic domain of the proteinase through its N-terminal inhibitory domain. Exposed TIMP-2 C-terminal domain binds to proMMP-2 hemopexin domain and a $(MT1\text{-}MMP)_2$-TIMP-2-proMMP-2 complex is generated (14). The MT1-MMP molecule, free from TIMP-2, cleaves proMMP-2 pro-domain, generating an intermediate form that undergoes an auto-catalytic activation to produce active MMP-2 (22). MT1-MMP also activates proMMP-13 on the cell surface (38). The detailed mechanism of this activation process has not been clarified yet but, it has been reported that TIMP-2 is dispensable and MMP-13 C-terminal domain is essential (39). It is not clear how MT1-MMP-dependent proMMP-13 contribute to cellular invasiveness.

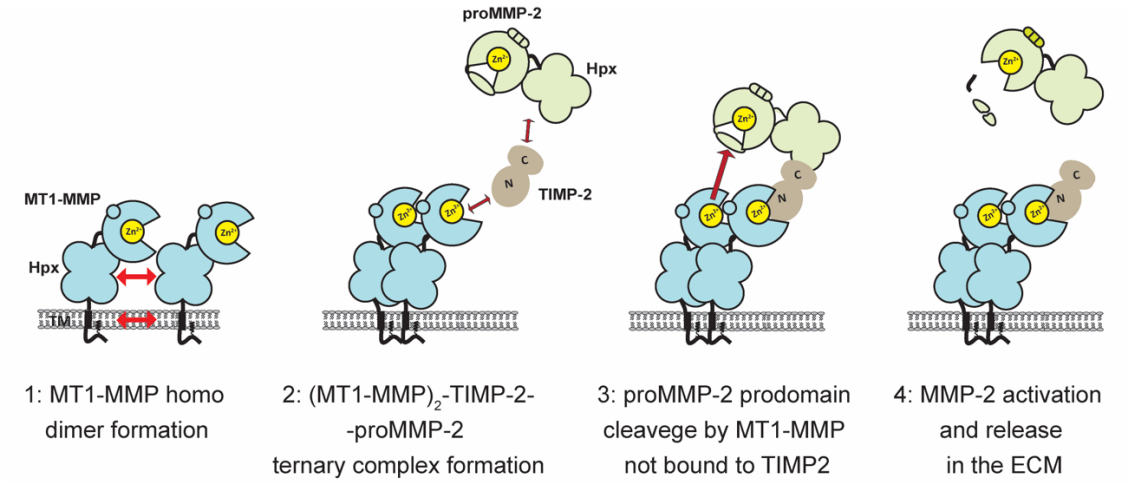


Figure 1.3: A model of the cell surface activation of proMMP-2 by MT1-MMP [14]

1: MT1-MMP forms a homo-dimeric complex though its hemopexin and transmembrane domains on the cell surface. 2: A molecule of TIMP-2 inhibits one of the MT1-MMP molecules in the complex, interacting through its N-terminal inhibitory domain with the catalytic domain of MT1-MMP. TIMP-2 interacts though its C-terminal domain with proMMP-2 hemopexin domain and a $(MT1\text{-}MMP)_2$-TIMP-2-proMMP-2 ternary complex is formed. 3: MT1-MMP, not bound to TIMP-2, cleaves proMMP-2 in the middle of the pro-domain and triggers the auto-catalytic activation of the intermediate MMP-2. 4: MMP-2 is released as active form in the ECM.

Cell surface molecules

MT1-MMP cleaves several cell adhesion molecules including the hyaluronan receptor CD44 (40), the transmembrane heparan sulphate proteoglycan Syndecan 1 (41), pro-αv integrin (42, 43) and ICAM-1 (44). Among these adhesion molecules, CD44 has been shown to interact with MT1-MMP, mediating indirect MT1-MMP association with cytoskeletal actin and its localisation to the lamellipodial membrane structure (45). MT1-MMP-dependent CD44 shedding has been found to support cell migration on a hyaluronan-based matrix (40). Shedding of Syndecan 1, pro-αv integrin and ICAM-1 have likewise

been reported to support cellular motility (41, 44, 46). MT1-MMP cleaves also other cell surface proteins like low-density lipoprotein receptor (LPR-1) (47) and ADAM-9, that are consequently inactivated (48). LPR-1 cleavage by MT1-MMP control different pathways depending on the cell type: in cancer cells, it regulates the fate of MMP-2 and other proteinases (47); in human chondrocytes, it negatively controls LPR-1-dependent endocytosis of MMP-13 and aggrecanases (49); in vascular smooth muscle cells, it regulates de-differentiation processes (50). Taken together these data suggest that MT1-MMP highly influences signalling within the cellular microenvironment by cleaving cell surface molecules.

1.3.2 Regulation of MT1-MMP

Given its wide variety of biological functions, MT1-MMP activity is tightly regulated at different levels (51).

Gene regulation

Very little is known about how MT1-MMP gene expression is controlled in specific tissues. MT1-MMP gene has nine exons and 10 introns and exon-intron boundaries are similar to those observed in other MMPs (52). MT1-MMP promoter lacks the conserved TATA box in position -25 and the adaptor protein 1 (AP-1) binding site in position -80 that are both present in other conventional promoters like MMP-1, -3, -9, -13 (52). MT1-MMP promoter contains numerous binding sites within 2 kb upstream the translation start site; these sites include EGR1, Nkx-2, CARG Box, E-Box, Lyf1, c-Myc and AP-4 and have been shown to influence the promoter activity (52, 53). NF-kB binding site is located 2.16 kb upstream the translational start site and regulate MT1-MMP gene expression in some cell types (54). For instance, histone acetyltransferase Tip 60 decreases

MT1-MMP transcription in glioblastoma cells upon inhibition of NF-kB signalling pathway (54). Sp1 binding site has also been reported to control the activity of MT1-MMP promoter (52). It is located 125 bp upstream the translational start site and it regulates MT1-MMP gene expression in prostate cancer cell lines (55), melanoma cells (56) and in von Hippel-Lindau renal carcinoma cells by co-operating with hypoxia-inducible factor 2α (HIF-2α) (57, 58). Snail is a zinc finger transcription factor that supports MT1-MMP up-regulation in fibroblasts (59, 60). There are multiple stimuli that have been reported to induce MT1-MMP production. When fibroblasts, endothelial and epithelial cells are cultured in 3D collagen matrices, they up-regulate MT1-MMP expression (53, 61, 62). In non-transformed human fibroblasts, DDR2 acts as receptor to mediate collagen-induced MT1-MMP expression (63). Type 1 insulin like growth factor regulates MT1-MMP transcription in highly invasive Lewis lung carcinoma cells, thus increasing their invasive potential (64). Fibroblast growth factor 1 has also been reported to induce the transcription of MT1-MMP in prostate carcinoma cell line (65). The proto-oncogenic transcription factor FBI-1 has been found to interact with MT1-MMP promoter 600 bp upstream the translational start site, enhancing the expression of the proteinase in human ovarian cancer cells (66). Oncoproteins have also been shown to influence MT1-MMP expression. Oncoproteins from high-risk human papillomaviruses increase *Mt1-mmp* gene transcription, enhancing invasion by cervical cancer cells (67). MT1-MMP is up-regulated by phorbol ester in human fibrosarcoma (HT-1080) cells (68) and by concanavalin A in fibroblasts (38), human breast cancer (MDA-MB-231) cells (69) and HT-1080 cells (70). Hence, MT1-MMP gene regulation is controlled by multiple stimuli that indirectly influence the wide variety of biological functions

mediated by this proteinase. A better understanding of the mechanisms that regulate MT1-MMP transcription would help controlling the enhanced MT1-MMP-dependent cellular invasion that is observed in multiple cancer types.

Activation of MT1-MMP zymogen (proMT1-MMP)

MT1-MMP is synthesised in the rough endoplasmic reticulum as pre-pro-enzyme and the signal peptide is removed by a signal peptidase. The pro-enzyme is further processed in the trans Golgi by PCs, which remove the pro-domain (28). These enzymes can either recognise a RRKR motif at the C-terminus of the pro-domain and directly cleave it (28), or they can carry out an alternative processing recognising the KAMRRPR motif within the pro-domain (71). Furin has been shown to recognise only the RRKR motif to activate proMT1-MMP (71). Thus, MT1-MMP is expressed on the cell surface in its active form.

Inhibition by endogenous inhibitors

TIMP-2, -3 and -4 but not TIMP-1 can inhibit MT1-MMP on the cell surface (14). As previously discussed, TIMP-2 plays an important role in MT1-MMP-mediated proMMP-2 activation (28). Although TIMP-2 has been described to inhibit MT1-MMP by many scientists (12, 72), TIMP-2 null mice do not exhibit alteration of ECM architecture or an excess of MT1-MMP activity (73). Therefore, TIMP-2 may mainly sustain proMMP-2 activation rather than inhibiting MT1-MMP activity *in vivo*. On the contrary, TIMP-3 null mice exhibit enhanced ECM degradation (74) and TIMP-3 null cells show increased proMMP-2 activation (75). Hence, TIMP-3 plays a prominent role in inhibiting MT1-MMP and safeguarding the ECM turnover. Reversion-inducing cysteine-rich protein with kazal motifs (RECK), testican 3 and its variant N-tes have also been reported to inhibit MT1-MMP (76) (77).

MT1-MMP processing to lower molecular weight species

MT1-MMP proteinase activity on the cell surface can also be downregulated by proteolytic processing (78, 79). Active MT1-MMP (60 kDa) can be processed by MMP-2 or MT1-MMP itself to 44 - 45 kDa species that lack the catalytic domain (78-80). Although this processing downregulates MT1-MMP proteinase activity, it is the result of the functional activation of the proteinase (78-80) and processed MT1-MMP can be replenished by newly synthesised enzyme on the cell surface.

Endocytosis and recycling

Endocytosis is an important regulatory mechanism to control the cell surface level of MT1-MMP and it has been shown to occur through at least two different means: the clathrin- and caveolae-dependent pathways (51, 81). Clathrin-mediated endocytosis requires the interaction between the LLY^{573} motif, in the cytoplasmic tail of MT1-MMP, with the adaptor protein 2 (AP-2) of the clathrin adaptor complex (81, 82). Clathrin-mediated endocytosis also requires the palmitoylation at Cys^{574} downstream LLY^{573} (83). It has been shown that altering clathrin-mediated MT1-MMP internalisation, decreases the ability of the proteinase to promote cell migration (82, 83). Hence, endocytosis is not only a means to decrease MT1-MMP cell surface expression but also a way to constantly replace it with newly secreted proteinase molecules (14). Recently, it has been found that clathrin light chain B knockdown (KD) decreases MT1-MMP cell surface expression in endometrial cancer cells, diminishing their invasion through collagen matrices (84).

Endocytosis has also been shown to be driven by other mechanisms. In human Henrietta Lacks (HeLa) and HT-1080 cells, protein kinase C (PKC) has

been shown to phosphorylate Thr^{567} and this phosphorylation has been found to be required for MT1-MMP endocytosis (85). Recently, it has also been demonstrated that in breast carcinoma cells, MT1-MMP interacts with ERM (ezrin/radixin/moesin) proteins through its cytoplasmic tail and this interaction is important for the subcellular localisation and internalisation of the proteinase (86). In triple negative breast cancer cells (MDA-MB-231), MT1-MMP internalisation has been found to be promoted by Endophilin A2 (87). Therefore, MT1-MMP endocytosis is controlled by different mechanisms and some of them are cell-type specific.

After MT1-MMP has been internalised, it is recycled back to the cell surface (82). MT1-MMP recycling has been shown to be indispensable for promoting cell migration and invasion (88).

Polarised localisation on the cell surface

MT1-MMP is a membrane-tethered enzyme and its polarised localisation across the cell surface can determine the directionality of migration (22). When cells migrate, they attach to the ECM through adhesion molecules and MT1-MMP is localised to these adhesion sites to achieve local ECM proteolysis (89). Cytoskeletal rearrangements direct the formation of membrane protrusions to generate a leading edge (89). MT1-MMP has been found to localise to these motility-associated structures, including filopodia, lamellipodia, podosomes and invadopodia (14, 90-93).

Filopodium is a thin (0.1 - 0.3 μm) actin-rich finger-like protrusive structure, that is thought to be employed by cells to sense the surrounding ECM (94). Filopodia formation is directed by cdc42, a small GTPase of the Rho family that activates WASP (Wiskott-Aldrich Syndrome protein) and N-WASP (neural-

WASP) inducing actin filament nucleation (94). Fisher et al. (95) have shown that cdc42 and MT1-MMP generate a molecular complex at filopodia, directing the formation of single cell invasion tunnels by HT-1080 cells cultured in a 3D matrix. Co-localisation of MT1-MMP and cdc42 at filopodia has been found to mediate the formation of membrane protrusion and drive invasion of oral squamous carcinoma cells (96). Moreover, it has been observed that expression of constitutively active cdc42 in HT-1080 cells induces MT1-MMP dimerisation almost exclusively at filopodia (92).

Lamellipodium is a thin, (0.1 - 0.2 μm) actin-rich, sheet-like membrane protrusion developed by cells migrating on a flat substratum (97). Several research groups have reported that WASP family verprolin homologous protein 2 (WAVE-2) is crucial for lamellipodia formation (98-101). In particular, Suetsugu et al. (101), have shown that WAVE-2 directs the generation of peripheral ruffles and its depletion reduces the extension of the leading edge as well as the persistency of directionality during cell migration. MT1-MMP localises to lamellipodia through the interaction of its hemopexin domain with CD44 (45). CD44 cytoplasmic domain binds to the actin cytoskeleton through the ERM proteins, indirectly associating MT1-MMP to the actin filaments (45, 102).

Podosomes and invadopodia, which can collectively named ‘invadosomes’, are membrane protrusions that establish close contact with the ECM (103, 104). They both possess an actin-rich core surrounded by scaffolding and adhesion molecules and are enriched with ECM-degrading enzymes and Tyr-phosphorylated proteins (105). MT1-MMP, cortactin, N-WASP, TKS4 (adaptor proteins Tyr kinase substrate with four SH3 domains) and TKS5 (adaptor proteins Tyr kinase substrate with five SH3 domains), have been all

found to localise to either podosomes and invadopodia and to contribute to their structure and functions (106). Although podosomes and invadopodia are characterised by a similar architecture, some molecular differences have been identified: podosomes are usually smaller than invadopodia, which can have diameters and lengths of up to 8 μm and 5 μm respectively (107); podosomes are highly dynamic structures, whose half-life is limited to few minutes, whereas invadopodia can be stable for hours (106); a cell can form more than 100 podosomes but usually no more than 10 invadopodia (107). Podosomes are found in smooth muscle cells and monocytes, whereas invadopodia in cancer cells (105). In macrophages, MT1-MMP localisation to podosomes contributes to their ECM degrading capacity (108-110). It has been reported that MT1-MMP also acts as a memory device for the localised reformation of podosomes after their dissolution (91). MT1-MMP localisation to invadopodia is a highly controlled process, driven by several endo/exocytic circuities, which have been extensively reviewed but have not been completely understood yet (93, 111).

MT1-MMP has also been shown to localise to focal adhesions (FAs), integrin-rich cell adhesion complexes that mediate cell-ECM interactions (112, 113). MT1-MMP localisation to FAs has been shown to depend on the MT-Loop sequence in the catalytic domain and if impaired, to reduce cellular invasion (112). Although the precise mechanism of MT1-MMP localisation to FAs is still unclear, it is reasonable to speculate that FAs may act as precursors of the leading edge, during cell migration and invasion.

Endo/exocytic circuities

Endo/exocytic circuities guarantee that MT1-MMP is constantly trafficked towards the dynamic leading edge of migrating cells. These circuities are under

the control of Rab GTPases. Rab GTPases are small GTPases that are activated by guanine nucleotide exchange factors (GEFs), who convert them into their GTP-bound forms, and de-activated by GTPase-activating proteins (GAPs), who catalyse the formation of their corresponding GDP-bound forms (114). When Rabs are active, they can recruit effector molecules and control a wide variety of intracellular vesicle trafficking mechanisms (114). In primary human macrophages, it has been found that Rab5a, Rab8a, Rab14 and Rab22 are involved in MT1-MMP intracellular trafficking (110). Rab5a plays a role in MT1-MMP endocytosis; Rab8a controls MT1-MMP exocytic transport from the trans Golgi to the plasma membrane; Rab14 and Rab22a regulate MT1-MMP recycling to the cell surface (110). In MDA-MB-231 cells and human mammary epithelial MCF10A cells, Rab5a mediates Rab4- and RABENOSYN-5-dependent endo/exocytic circuities of MT1-MMP and α3 integrin, promoting ECM degradation (115). Rab2a was also found to influence MT1-MMP-dependent ECM degradation and invasion in breast cancer cells, directing MT1-MMP trafficking from the late endosome to the cell surface, through the interaction with the late endosomal complex VPS39 (116). On the other hand, in HT-1080 cells, MT1-MMP trafficking from late endosomes to the plasma membrane is mediated by Rab7 and vesicle-associated protein 7 (VAMP7), which co-localises with MT1-MMP at proteolytic sites (85, 117). In carcinoma and sarcoma cell lines, Rab5 has been demonstrated to be indispensable for flotillin-dependent MT1-MMP endocytosis, which proceeds the recycling of the proteinase towards invadosomes (118).

Rab GTPases are not the only molecules that have been found involved in MT1-MMP endo/exocytic circuities. Chloride intracellular channel 3 regulates

MT1-MMP recycling from late endosomes, directly affecting breast cancer cell invasion and metastasis (119). The Wiskott-Aldrich Syndrome protein with Scar homolog (WASH) has also been found to regulate MT1-MMP trafficking from late endosomes to invadopodia in breast cancer cells (120). In MDA-MB-231 cells, coronin 1C promotes MT1-MMP trafficking from endosomal structures to invadopodia, increasing their invasiveness (121). Neural precursor cell expressed developmentally down-regulated 9 (NEDD9) and adenosine diphosphate (ADP)-ribosylation factor 6 (ARF6) have been also reported to control MT1-MMP trafficking to late endosomes in breast cancer cells (122).

Endo/exocytic circuities are not the only processes that grant a constant supply of MT1-MMP to the dynamic leading edge of migrating cells. MT1-MMP intracellular trafficking by kinesin superfamily motor proteins (KIFs) have also been found to regulate MT1-MMP polarised localisation on the cell surface (108). Unfortunately, the mechanisms that control the interplay between KIFs and the endo/exocytic pathways described above, are still largely unknown.

1.4 Intracellular trafficking by Kinesin superfamily motor proteins (KIFs)

Intracellular vesicle trafficking is one of the major means to regulate polarised localisation of MT1-MMP on the cell surface (108, 123). Intracellular vesicle transport is powered by molecular motors that carry cargoes along the cytoskeletal tracks, converting chemical energy into mechanical work (124). There are three types of cytoplasmic motors: myosins, which move along actin filaments, kinesins and dyneins, which travel along microtubule filaments (124).

Kinesins have been shown to play a crucial role in trafficking MT1-MMP-containing vesicles to the cell surface (14, 22, 108, 125).

1.4.1 Kinesin superfamily motor proteins (KIFs)

KIFs are molecular motors that unidirectionally transport cargoes, such as organelles, mRNAs and protein complexes, along the microtubule filaments by hydrolysing adenosine triphosphate (ATP) molecules (126). The first kinesin was identified in 1985 by Vale and colleagues (127, 128), who were studying squid fast axonal transport employing video-enhanced differential interference contrast (DIC) microscopy, developed few years earlier by Robert Allen and Scott Brady (129). Vale and colleagues (127) isolated the first molecular motor from squid nervous system using adenylyl-imidodiphosphate, a non-hydrolysable analogue of ATP, and column chromatography. The isolated protein was named Kinesin, from the Greek Kinein that means to move. Meanwhile, Brady and colleagues (130) independently isolated from the chicken brain a microtubule ATPase with the same properties and molecular weight of Kinesin. Over the last 25 years, biochemical, genetic and bioinformatic approaches have led to the identification of 45 genes that encode KIFs in mouse and human genomes (131). Each of these *kinesin* genes can encode for more than one molecular motor through alternative mRNA splicing (131).

Kinesin domain organisation

All kinesins contain a motor domain, also known as the head, a coiled-coil stalk, which mediates protein dimerisation and can regulate motor activity and a tail (Figure 1.4) (132). The motor domain structure was described for the first time

in 1996 by Kull and colleagues (133), who complexed it with an ADP molecule and subjected it to X-ray crystallography (133). Kinesin motor domain (~350 amino acids) was found to be much smaller than that of dynein (~1000 amino acids) and myosin (~850 amino acids) and to exhibit evident structural similarities with the core of the catalytic domain of myosin (133). Its structure primarily consists of a core of eight parallel β-sheets, flanked on both sides by three α-helices; the nucleotide binding pocket and the microtubule binding interface are at the opposite sides of the eight β sheets (133) and they are highly conserved across all KIFs (133, 134). The nucleotide binding pocket (ATP binding site) contains a conserved motif (GxxxxGKT/S) that generates a phosphate-binding loop (P-loop), located between β-strand 3 and α-helix 2 (135). This motif binds with the β-phosphate of the ATP molecule. The motor domain binding site consists of two other highly conserved motifs: switch-1 (NxxSSR), comprising β-strand 5, loop 8 and loop 11, and switch-2 motif (DxxGxE), made up of α-helix 4, loop 12 and α-helix 5 (135). These two motifs undergo conformational changes depending on the presence or absence of the ATP's γ-phosphate and the microtubule binding cycles (135). The motor domain structure also comprises a family-specific neck linker, located before or after the core, and a cover strand, positioned opposite to the neck linker (136). The neck linker is a 12 - 18 amino acid sequence that acts as an important structural and force generation element. Rice and co-workers (137) were the first to show that the neck linker can adopt two distinct conformations: it can be flexible when the motor domain is ADP-bound or nucleotide-free or, it can be docked along the core in the ATP-bound state (138). This model has been further extended more recently and it has been shown that the neck linker coordinates processive stepping of motor domains

along the microtubule filaments (139, 140). The neck linker also generates mechanical force but the exact mechanisms have not been elucidated completely. Recently, it has been reported that if the ATP-dependent neck linker docking to the motor domain core is unpaired, the force output is significantly decreased, whereas motor processivity and speed are increased (141). The cover strand has also been shown to be a crucial element for force generation and forward movement (142).

The stalk or coiled-coil region is characterised by an α-helical structure; it follows the neck linker and grants functional and/or regulatory characteristics to the various kinesin families (132). Some KIFs are characterised by a flexible region with a non α-helical structure, connecting the neck linker with the stalk and named hinge 1, that contributes to inhibiting the binding of the motor domain to the microtubule filaments (143). The stalk is also characterised by another non α-helical structure called hinge 2, that helps the stalk to kink and swivel (144). Additionally, the coiled-coil region mediates protein dimerisation and coordinates processive movement along the microtubule filaments (132).

The globular tail domain mediates the cargo-binding affinity of kinesins and it can directly or indirectly interact with the cargoes (145). Conventional kinesin forms a tetramer made up of two kinesin heavy chains (KHCs), comprising the motor domain, the neck linker and the stalk and two kinesin light chains (KLCs) (Figure 1.4) (146) (147). KLCs bind to the heavy chain tail and mediate the interaction with cargoes thorough several binding partners like c-Jun N-terminal kinase-interacting proteins (148). Kinesins can also directly bind to their cargoes through adaptor molecules. AP-1 complex, Fodrin and Rab6 are

only few of the numerous adaptors that link KIFs to their specific cargoes (149-151).

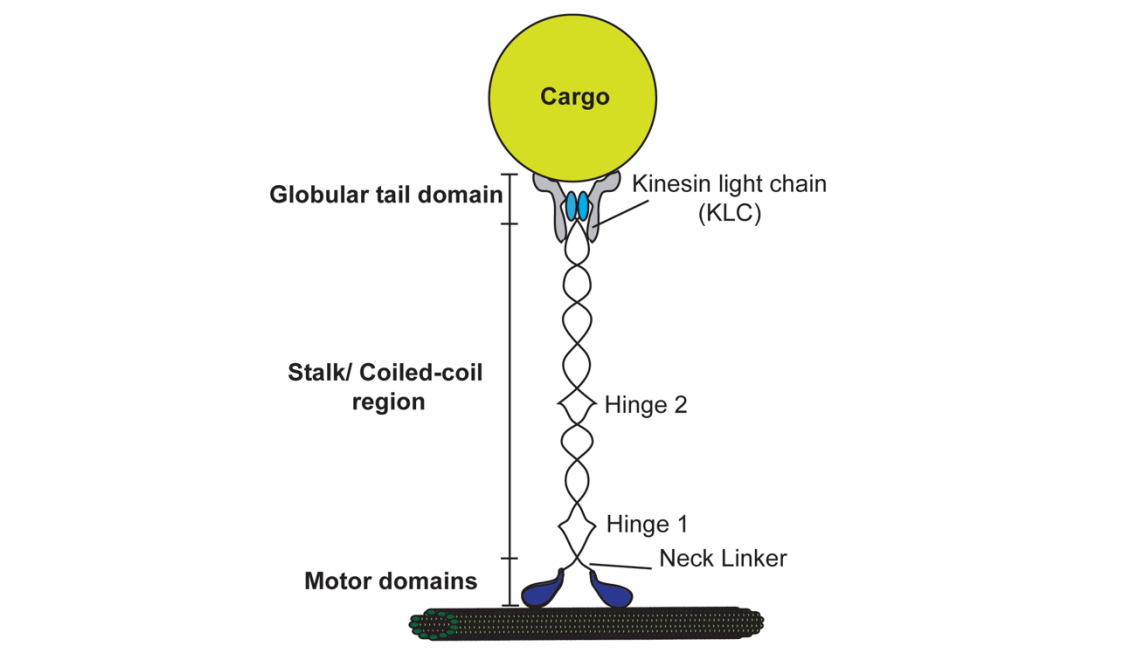


Figure 1.4: Kinesin domain organisation

A typical kinesin consists of a motor domain, connected through a neck linker with a stalk or coiled coil region and a globular tail domain. The stalk is characterised by two non-α-helical structures named hinge 1 and hinge 2. Conventional kinesin interacts with the cargo through kinesin light chains (KLCs), represented in grey.

Depending on the position of the motor domain, kinesins can be classified into three major types: N-type in which the motor domain is found at the N-terminus; M-type, in which the motor domain is located in the middle of the protein sequence; C-type, in which the motor domain is localised at the C-terminus (152). Microtubule filaments are polarised polymers because they are made up of α/β tubulin heterodimers that further polymerise and are intrinsically polarised (153). Alpha tubulins are exposed at one end, known as ‘minus’ end, while β tubulins at

the other, identified as ‘plus’ end (153). In most of the cells, the minus ends are stably anchored to the microtubule organising centre (MTOC) and have a slow dynamic, whereas plus ends constantly undergo polymerisation and de-polymerisation processes, growing and shrinking rapidly (Figure 1.5) (154).

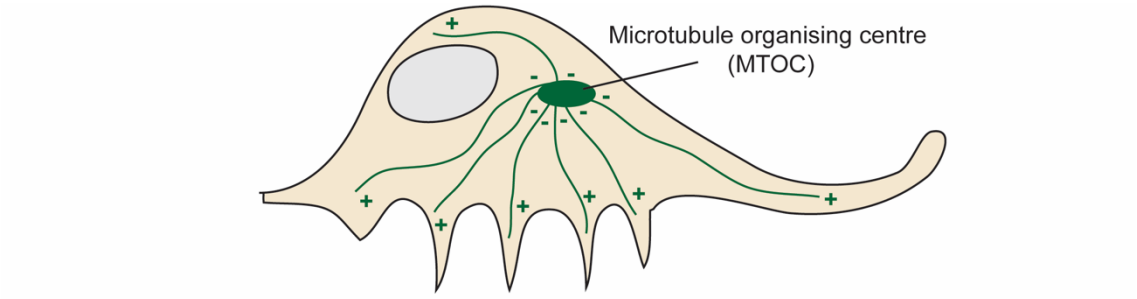


Figure 1.5: Organisation of microtubules

Microtubule filaments are polarised polymers made up of α/β tubulin heterodimers. Minus ends are stably anchored to the MTOC, whereas plus ends develop towards the cell periphery and are characterised by a rapid dynamic.

Domain structure-based classification of kinesins is entirely matching the functional classification in plus-end directed motors, minus-end directed motors and non-motors (Figure 1.6) (135). N-type kinesins move towards the plus ends, C-type towards the minus ends, whereas M-type do not possess any motor activity (Figure 1.6) (135).

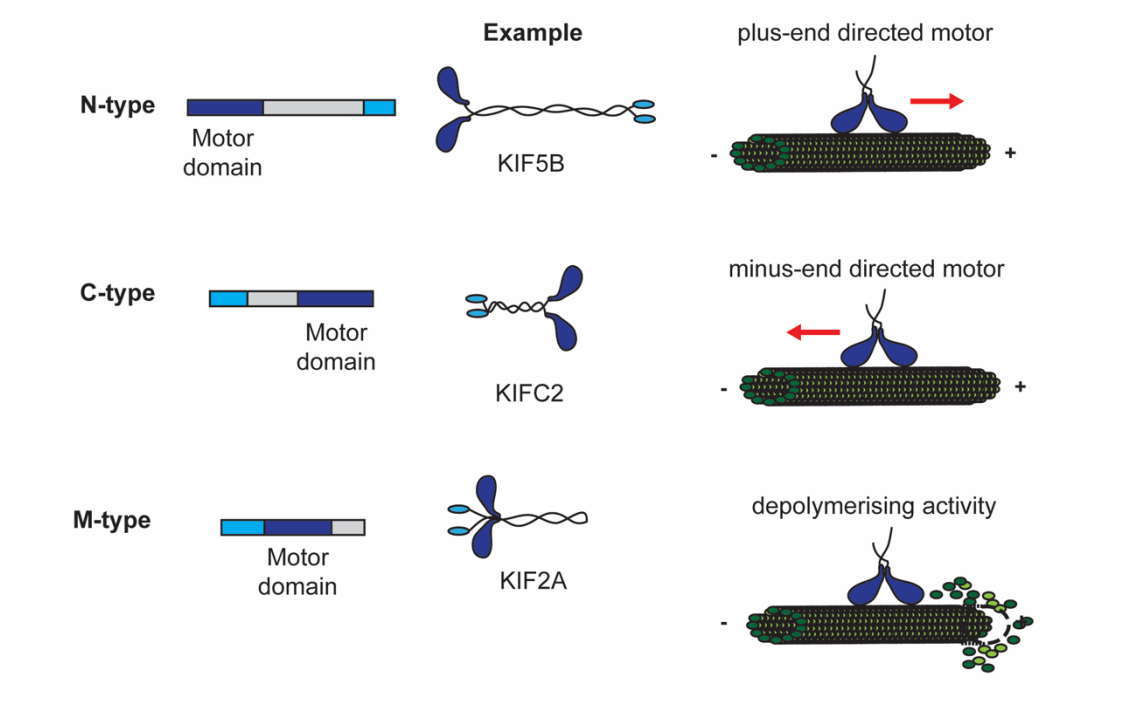


Figure 1.6: Domain structure-based classification of kinesins

Kinesins are classified in N-type, C-type and M-type depending on the position of their motor domain. KIF5B is an example of N-type kinesin; it has its motor domain at the N-terminus and it travels towards the plus-end of microtubule filaments. KIFC2 is an example of C-type kinesin; it has its motor domain at the C-terminus and mediates minus-end directed motility. KIF2A is an example of M-type kinesin. The motor domain is present in the middle of the protein sequence and it mediates depolymerisation of the microtubule filaments.

Kinesin families

Until 2004 KIFs were named by different criteria and researchers were experiencing growing confusion and difficulties in communication. Therefore, Lawrence and colleagues (155) developed the first standardised kinesin nomenclature, that is still in use today.

Table 1.1: Nomenclature of kinesin superfamily motor proteins (KIFs)

Type	Family		Gene name
N	Kinesin-1		KIF5A, KIF5B, KIF5C
N	Kinesin-2		KIF3A, KIF3B, KIF3C, KIF17
N	Kinesin-3		KIF1A, KIF1B (-v1, -v2), KIF1C, KIF13A, KIF13B, KIF14, KIF28, KIF16A, KIF16B
N	Kinesin-4		KIF4A, KIF4B, KIF21A, KIF21B, KIF7, KIF27
N	Kinesin-5		KIF11
N	Kinesin-6		KIF20A, KIF20B, KIF23 (-v1, -v2)
N	Kinesin-7		KIF10
N	Kinesin-8		KIF18A, KIF18B, KIF19A, KIF19B
N	Kinesin-9		KIF6, KIF9 (-v1, -v2, -v3)
N	Kinesin-10		KIF22
N	Kinesin-11		KIF26A, KIF26B
N	Kinesin-12		KIF12, KIF15
M	Kinesin-13		KIF2A, KIF2B, KIF2C, KIF24
C	Kinesin-14	A	KIFC1
		B	KIFC2, KIFC3, KIF25 (v-1, v-2)

KIFs were divided in 14 families (Table 1.1) in accordance to phylogenetic analysis (131, 156). These 14 families bear the name Kinesin followed by an Arabic number and large subfamilies are referred to with the name of their family, appended with a letter (155). Among these families, Kinesin-13 is the sole to contain M-type KIFs and Kinesin-14 the only one to comprise C-type KIFs (126). The other families are only grouping N-type KIFs.

Kinesin-1 family members are characterised by the typical domain organisation described in Figure 1.4 and they have both a cargo-binding domain and a light-chain-binding domain that binds a KLC (157). KIF5B is the only family member ubiquitously expressed, whereas KIF5A and KIF5C are neuron specific (158). Members of this family have been reported to transport organelles and to mediate nuclear movement (159).

Kinesin-2 family comprises KIF3A, KIF3B, KIF3C and KIF17. Members of this family have been shown to be involved in spermatogenesis (160), intraflagellar transport (161) and organelle trafficking (162). KIF3A forms heterodimers with KIF3B or KIF3C, whereas KIF3B does not associate with KIF3C (163). KIF3A/3B heterodimer is formed by association with the kinesin associated protein (KAP) adaptor molecule, that instead does not seem to bind KIF3A/3C heterodimer (163). KIF3A/3B/KAP has been extensively studied over the years for its prominent role in cilia-dependent signal transduction pathways, like Hedgehog-signalling pathway (164, 165). Hence, its role in ciliogenesis has been proposed to be the reason why *Kif3a*, *Kif3b* and *Kap* genes are indispensable for development (163). KIF17 is expressed in multiple cell types including neuronal cells and has been found to be a fast and processive motor (163).

Kinesin-3 family motors have the typical N-type kinesins' domain organisation but are characterised by specific structural features, which set them apart from the other N-type motors (166): the neck linker contains a β-sheet and a helix; the tail interacts with a forkhead-associated (FHA) domain and it contains short coiled-coils used for binding regulators and cargoes (166). These structural features make Kinesin-3 motors highly processive and able to 'walk' long distances along the microtubule filaments (166). These KIFs have been reported to transport organelles and to be important for neuronal cells (159). They can exist as monomers or homodimers and the switch between these two forms is considered a crucial regulatory process (166).

Kinesin-4 family was once referred to as chromokinesin family because some of the members bind to chromosomes. Members of this group have a highly

conserved neck β-sheet and coiled-coil stalk and have been found to transport organelles (167) and to be involved in chromosomal movement (168).

The only member of Kinesin-5 family in human is KIF11 also known as Eg5. As other members of this family in mammals, yeast and plants, KIF11 forms homotetramers acting as mitotic motors and essential for bipolar formation (159). Over the last years, KIF11 has been extensively studied for its role in the progression of several cancer types and recently its overexpression has been linked with poor prognosis of breast cancer (169).

Kinesin-6 family groups three members: KIF23, KIF20A and KIF20B. The family's name derives from Rabkinesin-6, the original name of KIF20A. These KIFs have a highly conserved motor domain, containing the longest loop 6 of all kinesins (170). The function of loop 6 has not been clarified yet, but it has been proposed that this region may act as interface for cytosolic factors and regulators (159). Members of this family are involved in cytokinesis (43, 171) and mitosis (172).

KIF10 also known as CENP-E is the only member of kinesin-7 family in humans and it is the first kinesin that was identified to associate with kinetochore (173). KIF10 is important for chromosome congression and alignment; it interacts with unanchored kinetochores during mitosis and it employs plus-end directed microtubule filaments to move mono-oriented chromosomes to the spindle equator; it also collaborates with dynein and chromokinesins to achieve chromosome congression (174, 175).

Kinesin-8 family motors have a prominent role in controlling microtubule dynamics throughout the cell cycle (176). These KIFs are microtubule destabilizers by either depolymerizing microtubule filaments at the plus ends or

by acting as microtubule capping factors, preventing both shrinkage and growth (177). They have been reported to control astral and mitotic spindle length, to mediate chromosome alignment during metaphase and chromosome segregation during anaphase (176).

Kinesin-9 family name was taken from KIF9. These motors are characterised by a conserved amino acid sequence in the neck linker (159). This family has been studied less than others and functions of its members are still largely unknown. KIF6 rs20455 polymorphism has been linked with a higher risk of coronary heart disease and has been shown to influence the response to statin therapy (178). KIF9 has been found to act as regulator of podosomes in human macrophages (179) and to mediate nuclei positioning during skeletal differentiation (180).

KIF22 (also known as KID) is the only identified kinesin-10 motor in humans. This KIF is characterised by the typical N-type kinesin domain organisation with a C-terminal tail containing a DNA binding site (181). KIF22 has been reported to play a role in bipolar organisation of spindle microtubule filaments, chromosome stability and movement (182).

Kinesin-11 family motors KIF26A and KIF26B are still largely unknown. These two KIFs do not function as microtubule-based motors because they lack the conserved amino acid sequence required for motor activity (183, 184). Nevertheless, they both bind to microtubule filaments. These kinesins have been reported to play crucial roles in signaling pathways: KIF26A functions as a key player of the cell growth signaling pathway for the development of enteric nervous system (183); KIF26A maintains intracellular calcium homeostasis and positively

impacts on nociceptive perception (185); KIF26B plays an important role in the signaling pathway that sustains kidney development (184).

KIF12 and KIF15 make up the Kinesin-12 family. These KIF share a family specific neck β-sheet and have different roles during mitosis (126) (159). KIF15 is believed to be important for spindle elongation and bipolarity, whereas KIF12 for cytokinesis (181).

Kinesin-13 family motors are M-type KIFs and they use the energy of ATP hydrolysis to depolymerize microtubule filaments (186). These motors have a prominent role in regulating microtubule dynamics and they can depolymerize microtubule filaments at both ends (187). They exert important functions during mitosis because they are required for spindle assembly, regulate spindle microtubule dynamics, kinetochore-microtubule attachments and chromosome segregation (129).

Kinesin-14 family motors are C-type KIFs, hence their MD is located at the C-terminus of the amino acid sequence and they have a minus-end directed motility. This family is divided into two subfamilies: Kinesin-14A and Kinesin-14B (159). These motors regulate MTOC and spindle assembly; they can influence microtubule organisation and sliding or crosslinking microtubule filaments (188). During cell division, they participate in chromosome segregation and contribute to spindle organisation (188). These KIFs also take part in a tug-of-war with kinesin-5 motors regulating microtubule nucleation (188).

Kinesin regulation

As previously discussed, KIFs play important roles in intracellular trafficking, cell division, cell motility and ciliary functions. Hence, they are tightly regulated to ensure that they are only active at the right time and place (189).

Mechanisms of regulation can either be intrinsic or extrinsic to the kinesin motors themselves. Majority of KIFs are intrinsically regulated by autoinhibitory mechanisms. Autoinhibition has been extensively studied and described for Kinesin-1 and it has now been also accepted as a regulatory mechanism for motors belonging to kinesin-2 and kinesin-3 families (141). Autoinhibition depends on the generation of intramolecular interactions that block the ATPase and/or the microtubule-binding activity of the motor domain (190, 191). In Kinesin-1 tail domain, the QIAKPIRP amino acid sequence has been shown to bind to switch-1 preventing ADP release from the nucleotide pocket and thus ATPase activity (192, 193). Similar mechanism has been described for kinesin-2 and kinesin-3 motors (194, 195). Autoinhibition can also prevent processive motility of MDs. For instance, KLC domains have been shown to separate the motor domains of Kinesin-1, preventing processive movement (196). Autoinhibition can be relieved by phosphorylation and cargo binding (189).

Kinesin activity can also be regulated by a wide range of extrinsic mechanisms. Motor-based transport is highly controlled at the start, when KIFs interact with their specific cargoes, and it is also influenced by the state of microtubule filaments (189). The association of KIFs with their cargos is mediated by adaptor molecules like Rab GTPases (197). Echard et al. (151) were the first to describe a GTP-dependent interaction between Rab6A and KIF20A and by now many more Rab GTPases have been described to interact with KIFs and influence their interaction with cargoes (197, 198). KIF-mediated transport is also highly regulated by microtubule tracks. Kinesin motor domains can recognise different types of microtubule filaments' modifications: tubulin isoforms can undergo post-translational modifications like polyglutamylation, acetylation and

de-tyrosination; microtubule-associated proteins (MAPs) can interact with microtubule filaments affecting KIF-dependent transport (199).

Mitotic kinesins are regulated by multiple extrinsic mechanisms: KIFs' protein expression oscillates during cell cycle as a result of ubiquitylation, increased synthesis, transcription or degradation (189); KIFs can be sequestered in the cytoplasm or the nucleus until the right time (189); the small GTPase Ran releases kinesin-importin complexes resulting in motor-mitotic spindle interactions. Kinesin-14 family proteins HSET/XCTK2 control spindle length by cross-linking and sliding microtubules. Importin-β and the small guanosine tri-phosphatase Ran mediate chromosome loading of the human chromokinesin. Aurora kinases, Polo-like kinases and cyclin-dependent kinases phosphorylate KIFs granting their activation at the right time during cell cycle (189).

The mechanisms of kinesin motor motility

KIFs exert fundamental functions in eukaryotic cells, unidirectionally transporting mRNAs, protein complexes and organelles along microtubule filaments. Kinesin motors obtain the energy supply for their movement from ATP hydrolysis that is carried out at the motor domain, where chemical energy is converted in mechanical energy (200). Kinesin-1 was the first to be described more than 30 years ago (127) and since then a lot of progress has been made in understanding how the energy from ATP turnover is converted into motion. Kinesin-1 has been shown to take 8 nm steps, alternatively advancing one motor domain at the time (201-203). Each step is a cycle in which the motor domain binds and unbinds the microtubule filament, ATP is hydrolysed and ADP and phosphate are released (200). During each cycle, the motor domain can adopt three main states, whose structures have been determined by X-ray

crystallography and high resolution cryo-EM (204). The motor domain can bind to the microtubule filaments in its nucleotide-free or ATP-bound state, or it can detach from the microtubule filaments and bind to ADP (Step 1, Figure 1.7) (204). Each cycle starts with the motor domain bound to a microtubule filament in its nucleotide-free state (Step 1, Figure); ATP binding produces a reorientation of nucleotide-binding subdomains (switch-1, switch-2, P-loop), which causes the neck linker to dock to the motor domain (204) (Step 2, Figure 1.7). Neck linker docking blocks the motor domain in its ATP-bound state until the ATPase activity takes place, a phosphate is released and the motor domain detaches from the microtubule (Step 4, Figure 1.7); the nucleotide-free state of the motor domain is characterised by a flexible neck linker which be docked or un-docked (204). The neck linker is blocked in its un-docked state once the motor domain binds again to a microtubule filament and the cycle starts over (200). It has been shown that single KIFs can move along microtubule filaments without falling off (205). Nevertheless, most KIFs form dimers through their coiled coil regions and move along microtubule filaments processively. This processivity can be well represented by the 'hand-over-hand' model (Figure 1.7), in which one motor domain is always bound to the microtubule and the dimer motor domains alternately step on the microtubule filaments during movement (204, 206).

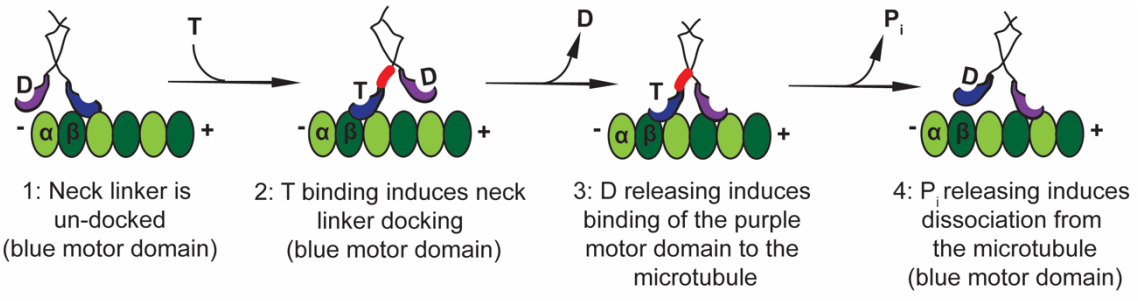


Figure 1.7: 'Hand-over hand' model for kinesin motility

1: The blue motor domain is bound to the microtubule filament and its neck linker is un-docked. 2: The blue motor domain binds to an ATP (T) molecule, which causes neck linker docking (red line). 3: The purple motor domain dissociates from an ADP (D) molecule and binds to the microtubule filaments; its neck linker is un-docked; 4: The T molecule bound to the blue motor domain is hydrolysed and a phosphate (Pi) group is released; the blue motor domain dissociates from the microtubule filament.

As previously discussed, kinesin motors can either travel towards the microtubule plus ends (N-type) or the microtubule minus ends (C-type). Generation of KIF chimeras has highlighted that movement directionality is mainly determined by the neck linker (207). Moreover, it has also been found that the neck linker grants KIFs the ability to navigate around obstacles like MAPs on the microtubule surface (208).

1.4.2 MT1-MMP intracellular trafficking by KIFs

Precise mechanisms of MT1-MMP intracellular trafficking by KIFs are still largely unknown. Remacle and colleagues (209) provided the first experimental evidences that MT1-MMP closely associates with microtubule filaments in fixed specimens and that the microtubular cytoskeleton is required for the intracellular trafficking of the proteinase in both malignant and non-malignant cells. A few years later, Wiesner and co-workers (108) presented novel findings on MT1-MMP intracellular trafficking in primary human macrophages. They showed that MT1-MMP-positive vesicles bidirectionally travel along microtubule filaments; anterograde transport is powered by KIF5B, KIF3A/KIF3B, whereas retrograde movement is mediated by dynein (108). KIF5B has also been found to traffic MT1-MMP to the cell surface in breast cancer cells (210, 211). In gastric cancer cells,

KIF1B has been demonstrated to regulate leptin-mediated MT1-MMP exposure to the cell surface (212). This KIF has also been shown to transport MT1-MMP-positive vesicles in glioma cells.

1.4.3 Selection of KIFs to study intracellular trafficking of MT1-MMP-containing vesicles

Although MT1-MMP intracellular trafficking by KIFs was described for the first time more than 10 years ago, basic mechanisms of this process remain largely unknown. KIFs powering MT1-MMP transport in the various cell types are yet to be determined. Moreover, it is unknown which adaptor molecules are required for this process.

Studies carried out in Dr. Itoh's laboratory have shown that in mouse embryonic fibroblasts expressing MT1-MMP red fluorescent protein (MT1-RFP), the proteinase localised within intracellular vesicles aligned along the microtubule filaments (Figure 1.8). Live cell imaging of these cells also revealed that MT1-MMP-containing vesicles moved bidirectionally along microtubule filaments and dynamically accumulated at the tips of growing membrane protrusions (Figure 1.8). These results were consistent with what had been previously reported by other authors and strongly supported the hypothesis that MT1-MMP cell surface exposure is achieved by targeted vesicle transport, powered by KIFs.

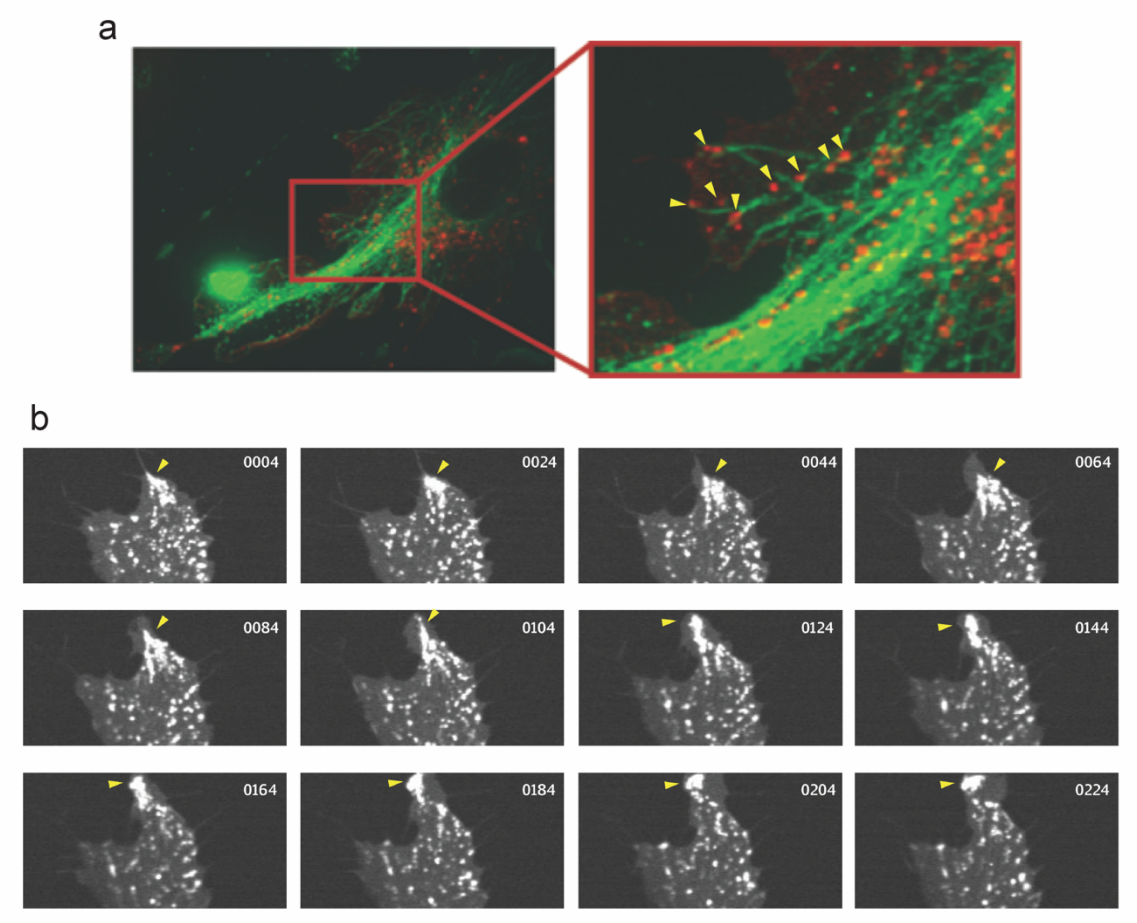
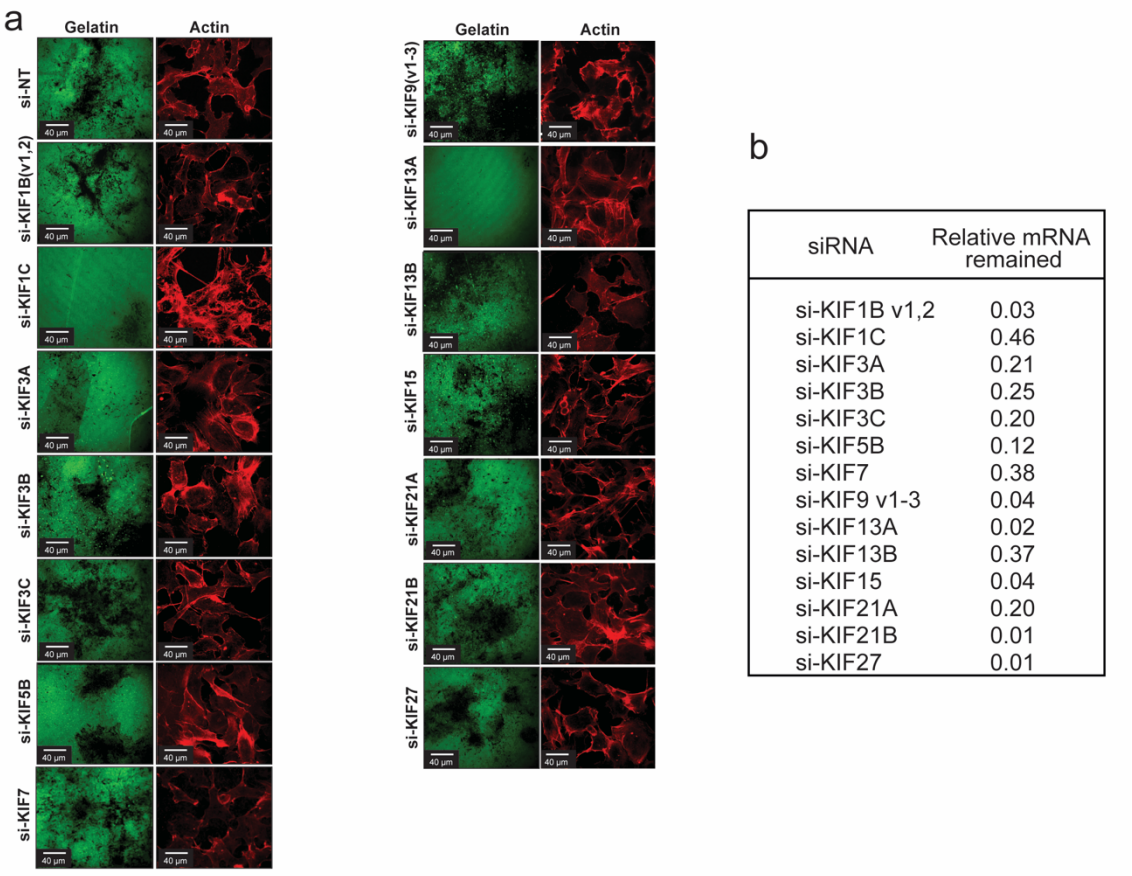


Figure 1.8*: MT1-MMP cell surface exposure is achieved by targeted vesicle transport

a Mouse embryonic fibroblast expressing MT1-RFP (red) were stained for microtubules with an anti-α-tubulin antibody (green). Left panel is a wide view of the image and right panel is an expanded view of the red marked area. The enlarged view shows the area where lamellipodia is expanding. Yellow arrows point MT1-RFP-contianing vesicles, interacting with the microtubule filaments. **b** Mouse embryonic fibroblasts expressing MT1-RFP were subjected to live cell imaging by confocal microscopy. Image time sequence is shown. A new membrane structure is formed between 44 and 64 seconds and MT1-RFP is gradually accumulated to this structure. Yellow arrows point at MT1-RFP accumulation areas.

* Dr. Itoh's group unpublished data

To better understand MT1-MMP intracellular trafficking mechanisms, Dr. Itoh's research group attempted to identify the responsible KIFs. Since potential candidates should mediate plus-end directed motilities, only N-kinesins were taken into consideration. In humans, there are 39 N-type KIFs but excluding those only expressed in neuronal cells or involved in mitotic processes, only 17, including splicing forms, were chosen as potential regulators of MT1-MMP cell surface exposure. To test the role of these KIFs, Dr. Itoh's laboratory employed a gene silencing approach. Human fibrosarcoma HT-1080 cells were transfected with siRNAs targeting these 17 KIFs and subjected to fluorescent-gelatin film degradation assay (Chapter 2, Paragraph 2.7). As shown in Figure 1.9, the KD of four KIFs resulted in notable changes: silencing *Kif13a*, *Kif3a* and *Kif1c* decreased MT1-MMP-mediated gelatinolytic activity of HT-1080 cells, whereas silencing *Kif9* gene enhanced it. Therefore, it was hypothesised that MT1-MMP vesicle trafficking in HT-1080 cells is powered by KIF13A, KIF3A, KIF9 and KIF1C.



siRNA	Relative mRNA remained
si-KIF1B v1,2	0.03
si-KIF1C	0.46
si-KIF3A	0.21
si-KIF3B	0.25
si-KIF3C	0.20
si-KIF5B	0.12
si-KIF7	0.38
si-KIF9 v1-3	0.04
si-KIF13A	0.02
si-KIF13B	0.37
si-KIF15	0.04
si-KIF21A	0.20
si-KIF21B	0.01
si-KIF27	0.01

Figure 1.9[*]: Selection of KIFs to study MT1-MMP intracellular trafficking in HT1080 cells

a HT1080 cells were transfected with siRNAs targeting the indicated KIFs and subjected to gelatin film degradation assay. Scale bars are 40 μm. **b** Efficiency of KD was evaluated measuring the amount of relative mRNA remained employing reverse transcription (RT)-PRC.

1.4.4 KIF13A

KIF13A was identified for the first time in 2000 by Nakagawa and co-workers (149). KIF13A belongs to the subfamily KIF13, within the Kinesin-3 family (213). As for the other Kinesin-3 family members, KIF13A activation and consequent high processivity depend on its dimerization (213). Dimerization is prevented by a proline-dependent shift of the neck coil and coiled coil-1 axis,

[*] Dr. Itoh's group unpublished data

which is released upon cargo binding (213). KIF13A was found to transport mannose-6-phosphate receptor from the Golgi network to the plasma membrane, interacting with the β1 subunit of the AP-1 complex (149). It has been also reported that AP-1 collaborates with KIF13A to create peripheral recycling endosomal subdomains to deliver cargoes to maturing melanosomes in melanocytes (214). The importance of KIF13A for the endosomal network is not limited to melanocytes. Delevoye and colleagues (215) have

a model according to which KIF13A and Rab11 control the development of recycling endosome tubules from sorting endosomes. More recently, it has been reported that Rab10 is essential for recycling tubular endosome formation and that KIF13A is a Rab10-interacting protein (216). KIF13A transports the Z protein of the arenavirus Lassa virus as well as the viral ribonucleoproteins during infection with influenza A (217, 218). KIF13A has also been found to traffic serotonin type 1A (5-HT_{1A}) receptor controlling anxiety (219). Interestingly, KIF13A-dependent transport of 5-HT_{1A} receptor to the cell surface has been associated with stress adaptation in mouse hippocampal neuronal cells (220). KIF13A-dependent trafficking has also been associated with blebby amoeboid migration because it regulates cell surface exposure of RhoB, a small GTPase that controls membrane blebbing (221). Overall, KIF13A seems to have a prominent role for the endosomal network as well as being involved in the transport of various cargoes. Members of the Kinesin-3 family have a high processivity and have adapted over time to drive long-distance intracellular and axonal transport (213). Therefore, KIF13A makes a good candidate for MT1-MMP intracellular trafficking.

1.4.5 KIF3A

KIF3A was initially identified by Kondo and co-workers (222) in 1994 as a motor protein for the anterograde fast axonal transport. Since then, KIF3A has been extensively studied and it is now one of the best characterised kinesins. As previously mentioned, KIF3A associates with KIF3B through KAP and generates KIF3A/KIF3B/KAP heterotrimeric complex that has been reported to mediate the axonal transport of membrane organelle in neuronal cells (162). KIF3A also associates with KIF3C and forms an heterodimer highly expressed in the central nervous system (223). Overall, KIF3A complexes have been found to mediate transport between the endoplasmic reticulum and the Golgi and to regulate trafficking of protein complexes within cilia and flagella (224). This transport within cilia is indispensable during embryogenesis for the development of left-right asymmetry (224). KIF3A-dependent trafficking is essential for the development of spermatozoa and male fertility (225). KIF3A has also been reported to regulate trafficking and release of HIV virion containing compartments in primary human macrophages (226). Recently, KIF3A has been indicated to play a role in epithelium apoptosis and bronchial inflammation in asthma (227). In general, KIF3A is ubiquitously expressed and plays a role in a wide variety of physiological processes. As previously discussed, KIF3A/3B has been reported to mediate MT1-MMP-containing vesicle anterograde transport in primary human macrophages (108). Hence, it is likely that KIF3A might regulate MT1-MMP cell surface exposure in other cell types, including fibroblasts.

1.4.6 KIF9

KIF9 was described for the first time as cytoskeletal binding partner of the Ras-related GTPase Gem, that mediates sprouting of endothelial cells and reorganisation of their actin cytoskeleton (228). Unfortunately, this KIF is still very poorly characterised. It is known that it is an important regulator of macrophage podosomes and influences the matrix-degrading capabilities of these motility-associated structures (179). Recently, it has been shown that KIF9 is highly expressed in mouse testis and is essential for sperm motility and male mouse fertility (229). Given that KIF9 functions are still largely unknown, its potential role in MT1-MMP intracellular trafficking mechanisms would bring a great contribution for its characterisation.

1.4.7 KIF1C

KIF1C is expressed ubiquitously and mediates anterograde trafficking from the Golgi network to the endoplasmic reticulum as well as anterograde transport of various cargoes (230, 231). Among those, there are α5β1 integrin vesicles (231) and dense core vesicles, trafficked through the interaction of KIF1C with Rab6 GTPases and bicaudal D-related protein 1 (232). KIF1C has been shown to regulate podosome dynamics (233, 234) and contributes to Golgi organisation through Rab6a (235). Overall, only few KIF1C cargoes have been identified and given that this KIF is ubiquitously expressed it is likely that its involvement in more trafficking pathways has yet to be described.

1.5 Aims of the thesis

MT1-MMP contributes to the development of various pathological processes including RA and cancer by enhancing cell migration and invasion (14). Localisation of MT1-MMP to the leading edge of migrating cells is a critical step for the proteinase to promote cellular invasion (72). However, the precise mechanism of MT1-MMP cell surface exposure has not been clarified yet. Dr. Itoh's research group and others have found that MT1-MMP localisation to the cell surface is achieved by intracellular trafficking of MT1-MMP-containing vesicles along the microtubule filaments and that KIFs play a role. Dr. Itoh's research group has also found that four KIFs (KIF13A, KIF3A, KIF9, KIF1C) are potentially involved in MT1-MMP intracellular trafficking in HT-1080 cells. Therefore, the aim of this thesis is to investigate the role of these KIFs in MT1-MMP cell surface exposure and MT1-MMP-dependent cell migration and invasion.

Aims of this thesis are to:

Chapter 3:

- Characterise KIFs involved in cell surface localisation of MT1-MMP

Chapter 4:

- Investigate the dynamic regulation of KIF13A, KIF3A, KIF9 and KIF1C in orchestrating MT1-MMP cell surface exposure

Chapter 5:

- Study the role of KIF13A and KIF9 in the metastatic potential of HT-1080 cells
- Analyse the expression profile of *Kif13a* and *Kif9* genes in various cancer types employing data from the cancer genome atlas (TCGA)

Accomplishing these aims will provide new insights into the mechanisms of cellular invasion within tissue matrices and contribute to the understanding of the pathogenesis of the diseases in which MT1-MMP-dependent cellular invasion plays a role.

CHAPTER 2:

MATERIALS AND METHODS

2.1 Cell culture

2.1.1 Cells and cell culture reagents

Cells were obtained from the following sources: African green monkey SV40-transformed kidney epithelial cells (COS-7) and human fibrosarcoma cells (HT-1080) were from ECACC; human embryonic kidney 293 cells (HEK 293) were a kind gift of Dr. Balint (Kennedy Institute of Rheumatology, Oxford); human Henrietta Lacks cell line (HeLa) was from ATTC Cultures; human breast cancer cell line (MDA-MB-231) was a kind gift of Prof. Couchman (University of Copenhagen); human rheumatoid arthritis synovial fibroblasts (RASFs) from three different donors were supplied by of Dr. Itoh.

Materials were obtained from the following sources: Dulbecco's Modified Eagle's Medium (DMEM), penicillin, streptomycin, versene/trypsin from Lonza Biosciences; fetal bovine serum (FBS) from GIBCO; Tetracycline (Tet) system-approved FBS from Takara Bio; 10x RPMI-1640 media, sterile dimethyl sulfoxide (DMSO), puromycin, doxycycline, polybrene and Scienceware® cloning discs from Sigma-Aldrich, Opti-MEM reduced-serum medium and Hygromycin B from Invitrogen; TransIT®-2020 Reagent from Mirus Bio; pNL3.2 CMV vector and Nano-Glo® luciferase assay system from Promega; INTERFERin® from Polyplus transfection; ON-TARGETplus SMARTpool siRNA to KIF5B, KIF3A, KIF13A, KIF1C and non-targeting (NT) siRNA from Dharmacon.; GM6001 (Ilomastat) and Marimastat from Elastin Producs; Corning® CoolCell™ Freezer Container from Merck Biosciences; TIMP-1 and DX2400 were supplied by Dr. Itoh.

2.1.2 Cell culture conditions

Cell lines were cultured in DMEM supplemented with 100 U/mL penicillin, 100 µg/mL streptomycin and 10% (v/v) FBS at 37°C, in a humidified incubator with 5% CO_2. Cells were passaged every 3 - 4 days using trypsin-EDTA. RASFs were cultured in DMEM supplemented with 100 U/mL penicillin, 100 µg/mL streptomycin and 20% (v/v) FBS. They were passaged every 4 days and cultured for up to 8 weeks.

2.1.3 Cryopreservation of cells

A confluent 10 cm^2 cell culture dish was harvested using trypsin-EDTA and centrifuged at 1500 rpm for 3 minutes. Cell pellet was resuspended in 3 mL of DMEM containing 50% (v/v) FBS and 10% (v/v) DMSO. 1 mL aliquots were transferred to cryovials and stored at –80°C in a Corning® CoolCell™ Freezer Container 12 - 18 hours. Cryovials were transferred to liquid nitrogen storage.

2.1.4 Transient transfection

Cells were transfected with expression plasmids using Trans-IT-2020 Reagent according to the manufacturer's instructions. Briefly, cells were seeded at 5 x 10^4/ well in a 12-well plate, 24 hours prior to transfection. 0.5 – 1µg of DNA were diluted in Opti-MEM reduced-serum medium and incubated for 5 minutes. 1.5 – 3µL of Trans-IT were added and the mixture was mixed gently before being incubated 15 – 30 minutes at room temperature (RT). The transfection mixture was added drop-wise to cells that were incubated 36 – 48 hours.

2.1.5 Gene silencing

Gene silencing was performed using INTERFERin (Polyplus-transfection). 0.6 µL of the target specific siRNA were diluted in 200 µL of Opti-MEM reduced-serum medium to a concentration of 10 nM, in a sterile Eppendorf tube. After, 4 µL of INTERFERin were added and mixed gently and the transfection mixture was incubated at RT 15 - 30 minutes. The transfection mixture was transferred to a single well of a 12-well plate and 5 x 10^4 of cells in 1 ml of DMEM, were added drop-wise and incubated for 72 hours. Gene-silencing effect was confirmed by either Western blot (WB) or reverse transcription polymerase chain reaction (RT-PCR).

2.1.6 Establishment of stable HT-1080 cells expressing NanoLuc® luciferase

The pNL3.2 CMV vector was used to establish a stable NanoLuc® luciferase-expressing cell line. PNL3.2 CMV vector (GenBank Accession Number KF853603) expresses NanoLuc luciferase, a luminescent reporter 100-fold brighter than either *Photinus pyralis* and *Renilla reniformis* luciferases. This vector also encodes a hygromycin resistance gene used for generating the stable cell line. To establish HT-1080 cells stably expressing NanoLuc luciferase, cells were transfected with 1 µg of pNL3.2 CMV vector, using TransIT transfection reagent. Un-transfected HT-1080 cells were used as control. After 48 hours, conditioned medium was replaced with fresh DMEM containing 10% (v/v) FBS and 100 µg/ml of hygromycin B. Hygromycin B concentration was raised gradually to 400 µg/ml when all the control cells had perished. Ten clones were isolated among hygromycin-resistant cells using Scienceware® cloning discs (Ø

3.2 mm) and grown separately. Nano-Glo® luciferase assay system (Promega, Madison, USA) was used for the detection of NanoLuc luciferase in the isolated clones. This assay system provides fumarimazine, a reagent that generates a glow-type signal in the presence of NanoLuc luciferase. Luminescence was measured with FLUOstar Omega microplate reader and the colony expressing the highest luminescence signal in the linear dynamic range was selected.

2.1.7 Transduction of stable HT-1080 cells expressing NanoLuc® luciferase

HT-1080 cells stably expressing NanoLuc® luciferase were plated in a 12-well plate (5×10^4/well) and cultured for 24 hours in DMEM, supplemented with 10% (v/v) of Tet system approved FBS. Un-transfected HT-1080 cells stably expressing NanoLuc luciferase were used as control. Medium was supplemented with 1 µg/ml of doxycycline when transducing with Tet-off TRIPZ inducible shRNA-expressing lentiviral particles. Tet-on and Tet-off TRIPZ inducible shRNA-expressing lentiviral particles were generated as explained below (Paragraph 2.2.14). Medium was replaced with 500 µL of viral supernatant and 1 µg/ml of polybrene and transduced cells were centrifuged for 60 minutes at 2500 rpm at 24°C. Then, transduced cells were incubated overnight at 37°C. Viral supernatant was discarded and replaced with fresh medium, supplemented with 1 µg/ml of puromycin to start antibiotic selection. Cells were incubated with puromycin until all control cells had perished, usually 48 hours after the antibiotic was added. After the selection, medium was replaced with DMEM supplemented with 10% (v/v) of Tet system approved FBS and TRIPZ inducible lentiviral shRNA-transduced cells were left to recover for 48 hours. Medium was

supplemented with doxycycline if cells were transduced with Tet-off TRIPZ inducible shRNA-expressing viral particles. After, shRNA constructs' expression was induced removing or adding doxycycline depending on TRIPZ vector being designed to enable the shRNA expression in the presence or absence of tetracycline. 48 hours later, I checked the expression of the TurboRFP reporter to assess transduction efficiency.

2.2 Molecular Biology

2.2.1 Reagents and materials

Reagents were purchased from the following sources: Luria-Bertani (LB) media, LB agar, electrophoresis grade agarose, dNTP Mix (10 mM each), PureLink™ Quick Gel Extraction Kit and High-Capacity cDNA Reverse transcription kit from Invitrogen; PureYield Plasmid Midiprep System and pHTN HaloTag CMV-neo expression vector from Promega; PCL-CTiG vector from Addgene; EZ Load Molecular Rulers from Bio-Rad; DNA grade ethanol (C_2H_5OH), ampicillin and carbenicillin from Merck Biosciences; NEBuilder HiFi DNA Assembly Mix from Biolabs; GelRed® Nucleic Acid Gel Stain from Biotium; restriction enzymes, CloneJET PCR Cloning Kit, Dream Microtubule Aq Green DNA polymerase, Phusion Hot Start II High-Fidelity DNA polymerase and Rapid DNA ligation kit from Fermentas; DH5α competent *E.coli* and T4 DNA polymerase from NEB; Quick Fusion cloning kit from Biotool; calf intestinal alkaline phosphatase (CIP) from BioLabs; TRIPZ inducible lentiviral shRNAs targeting KIF13A (clone id: V3THS_373145) and KIF9 (clone id: V2THS_87885), TRIPZ inducible lentiviral NT shRNA control and Trans-lentiviral shRNA Packaging kit from Dharmacon; Tet system approved FBS from Takara Bio.

Constructs were confirmed by sequencing, employing the TubeSeq Service from Eurofins Genomics. All reagents were of molecular biology grade. Deionised water (dH_2O) was autoclaved before use in order to destroy DNases.

2.2.2 General solutions

- Tris-EDTA buffer (TE): TE lipopolysaccharide (LPS)-free buffer was used to store DNA and contained: 10 mM Tris-HCl and 1 mM EDTA, pH 8.0
- LB agar and LB broth: LB agar and LB broth were prepared according to the manufacturer's instructions. LB agar was allowed to cool down to about 50°C, before adding a selection antibiotic; the solution was poured into 10 cm^2 bacteriological petri dishes and left to set. Petri dishes were stored at 4°C
- Carbenicillin stock solution was made at 50 mg/mL in dH_2O and used at the 50 µg/mL concentration
- Ampicillin stock solution was made at 50 mg/mL in dH_2O and used at the 50 µg/mL concentration
- Solution I: 50mM glucose, 10 mM EDTA, 25 mM Tris-HCl pH 8.0 (stored at 4°C)
- Solution II: 0.2 N NaOH, 1% sodium dodecyl sulfate (SDS) (prepared just before use)
- Solution III: 3M potassium acetate (CH_3COOK), 2M acetic acid (CH_3CCOH)

2.2.3 RT-PCR and cDNA synthesis

Total cellular RNA was isolated using RNAqueous-Micro Kit according to the manufacturer's instructions. cDNA was synthesised using the High Capacity cDNA Reverse Trascription Kit, according to the manufacturer's instructions. PCR was performed using Dreamicrotubuleaq DNA polymerase, according to the standard protocol and specific primers (Table 2.1) were used to assess mRNA levels of genes of interest.

Table 2.1: List of primers used for RT-PCR

Gene	Forward Primer	Reverse Primer	Expected size (bp)
KIF13A	TTTCCAGTAGGAGGAGTC	AAGTTGTTGCGGTGAAGG	194
KIF3A	TGCAAAGTCAGAGATGGC	AGCTGCCATTCTCCTATG	191
KIF9_v1	TCGCCCCTTTCTCTACC	CGCTTGATGGCATTGATG	223
KIF9_v2	TCGCCCCTTTCTCTACC	CGCTTGATGGCATTGATG	402
KIF9_v3	TCGCCCCTTTCTCTACC	CGCTTGATGGCATTGATG	400
KIF1C	TTCCAGCCCAAAAAGCAC	CGGACCTTCTCTCTCATC	277
KIF5B	GCTACAAGAGTTAAAAAGAGTGCT	TCACACTTGTTTGCCTCCTCCAG	470
GADPH	TTCACCACCATGGAGAAGGC	GGTCCCTCCGATGCCTGC	246
MT1-MMP	GGGACCTACGTACCCACACA	TAGCGCTTCCTTCGAACATT	330

2.3.4 PCR reaction

PCRs were performed using Dreamicrotubuleaq Green DNA polymerase according to the manufacturer's reaction setup (Table 2.2). When the PCR product was used for cloning, Phusion Hot Start II High-Fidelity DNA polymerase was employed, using the reaction setup suggested by the manufacturer's (Table 2.3). Primer A and primer B recommended final concentration was in the range

0.2 – 1 µM so the specific volume (X) was calculated according to the primer concentration.

Table 2.2: Dream Taq Green DNA polymerase standard reaction setup

Component	Volume (µL)
10x Dream Taq Buffer	2
dNTPs mix (2 mM each)	0.4
Forward primer (10 mM)	0.5
Reverse primer (10 mM)	0.5
Template DNA (10 pg–1 µg)	1
Dream Taq DNA polymerase	0.1
Nuclease-free dH_2O	15.5

Table 2.3: Phusion Hot Start II High-Fidelity DNA polymerase standard reaction setup

Component	Volume (µL)
5x Phusion HF Buffer	10
10 mM dNTPs mix	1
Primer A	X
Primer B	X
Template DNA	X
Phusion Hot Start II DNA polymerase	0.5
Nuclease-free dH_2O	Add to 50 µL

2.2.5 DNA electrophoresis

DNA electrophoresis was carried out using either 1% (w/v) or 2% (w/v) agarose gels in 0.5x Tris-acetate-EDTA (TAE) buffer. Before pouring the agarose solution into the casting plates, GelRed (1/10,000) was added. DNA was electrophoresed at 130 V in 0.5x TAE buffer for usually 30 minutes. DNA bands were visualised with Syngene's G:BOX Chemi XX6.

2.2.6 Quantification of DNA bands

DNA bands were quantified by Fiji software (National Institutes of Health, Bethesda, MD, USA). I employed the 'rectangle' tool to frame DNA bands in each lane and the 'gel' command in the 'analyse' menu to generate a histogram representing the intensity of each band. Each peak, corresponding to a DNA band, was enclosed with the 'line' tool and the area underneath was selected and quantified with the 'wand' tool. GADPH bands were used to normalise intensities of the bands of interest within the same experiment. Mean band intensities were plotted using Prism (GraphPad software, Inc.) and statistical significance was calculated using either a parametric unpaired T test or a one-way ordinary ANOVA with Tukey's multiple comparison test.

2.2.7 DNA fragment purification

DNA was electrophoresed on agarose gel containing GelRed (1/10,000) and DNA bands were visualised using a dark reader transilluminator. Fragments of interest were excised with a minimal amount of agarose and purified using PureLink™ Quick Gel Extraction Kit, according to the manufacturer's instructions. DNA was eluted in 20 to 50 µL of dH_2O, depending on the expected DNA concentration.

2.2.8 Restriction digestion

Restriction digestions were carried out in 10 or 20 µL reaction volume, according to the manufacturer's instructions.

2.2.9 Ligation of DNA fragments

Ligation of PCR-generated fragments into pJET1.2 cloning vector was carried out using CloneJET PCR Cloning kit, following the manufacturer's instructions. This vector carries a lethal restriction enzyme gene in the site of ligation that is expressed if ligation fails. Consequently, only bacteria expressing recombinant pJET1.2 can form colonies. Ligation of PCR-generated fragments into pSG6 or pHTN HaloTag CMV-neo expression vectors was carried out using T4 DNA polymerase according to the manufacturer's instructions. Where stated, expression vectors were dephosphorylated using CIP before ligation.

2.2.10 Fusion of DNA fragments

The Quick-Fusion Cloning kit was employed for directional cloning of gel-purified inserts into expression vectors as an alternative to conventional cloning method. The fusion cloning reaction was setup according to the manufacturer's instructions (Table 2.4).

Table 2.4: Quick-Fusion Cloning kit standard reaction setup

Component	Quantity
Linearized vector	20 – 100 ng
Insert	10 – 100 ng
Fusion enzyme	1 µL
5x Fusion buffer	0.5 µL
dH_2O	15.5 µL

2.2.11 Bacterial electroporation

1 µL of ligation or fusion reaction mixture was added to 50 µL of electrocompetent DH5α *E. coli*. Bacteria/DNA mixture was transferred into an ice-

cold 0.2 cm electroporation cuvette and pulsed in a BTX Electro Cell manipulator (Qbiogene) with 2100 V for 5 milliseconds. Bacteria/DNA mixture was diluted with 400 µL of LB media and transferred to an Eppendorf tube. Bacteria were grown at 37°C for 1 hour with agitation. 10 – 100 µL of bacterial culture were spread onto a LB agar plate containing the selection antibiotic and grown overnight at 37°C.

2.2.12 DNA plasmid purification

Eight colonies were usually picked from different areas of a LB agar plate using a P20 pipette tip. Each colony was inoculated into 5 ml of liquid LB media supplemented with 50 µg/ml of ampicillin and grown overnight at 37°C with agitation. Bacteria were harvested by spinning 3 ml of culture at maximum speed for 1 minute. The cell pellet was resuspended completely in 100 µL of ice-cold solution I and then, 200 µL of solution II were added. Samples were left on ice for 5 minutes and then they were added with 150 µL of solution III and mixed well. Samples were incubated again on ice for 5 minutes. After, 10 µL of chloroform were added and samples were centrifuged at full speed for 5 minutes to pellet bacterial DNA and protein debris. The supernatant was transferred to a fresh Eppendorf tube and mixed with 100% ethanol in a 1:2 ratio. Samples were centrifuged at full speed for 10 minutes to pellet plasmid DNA. The pellet was washed once with 1 ml of 70% ethanol, centrifuged at full speed for 2 minutes and dried on a heat block set at 37°C. After, the pellet was dissolved in 50 µL of TE containing 50 µg/ml of RNase and incubated at 37°C for 30 minutes. DNA isolated from the eight selected colonies was digested by restriction enzymes to identify correct clones. Once a clone had been identified, it was inoculated into 5

ml of LB, supplemented with 50 µg/ml of ampicillin and grown overnight at 37 °C with agitation. DNA was isolated and purified using PureYield Plasmid Midiprep System, according to the manufacturer's instructions.

2.2.13 Molecular cloning of constructs

The construct encoding human MT1-RFP was supplied by of Dr. Itoh. RFP was inserted into the cytoplasmic domain of FLAG-tagged MT1 after Cys574 with a spacer of two glycines. The remaining cytoplasmic domain of FLAG-tagged MT1 (Gln575-Val582) was attached to the C-terminus of RFP. Constructs encoding KIF13A (GenBank Accession Number NM_001105568), KIF3A (GenBank Accession Number NM_001300791.2), KIF9-v1 and KIF9-v2 (GenBank Accession Numbers NM_022342.5 and NM_180922.4 respectively) and KIF1C (GenBank Accession Number NM_006612.6) in pSG6 vector were kindly provided by Dr. Itoh. Constructs encoding KIF13A-GFP, and KIF9-v2-GFP in pSG6 vector were supplied by of Dr. Itoh. The GFP-tag was introduced at the N-terminus of full length KIFs using three glycines as linker peptide. KIF3A-GFP, KIF9-v1-GFP and KIF1C-GFP were based on the expression vector pSG6. KIF3A-GFP and KIF1C-GFP were constructed by overlap extension PCR method. The following primers were used for KIF3A-GFP: forward flanking primer containing the EcoRI site (5'-ATACGACTCACTATAGGGCGAATTCGAGCCACCATGGTGAGCAAGGGCGC C-3'), reverse primer (5'-CGGCATTCCACCTCCCTTGTACACTCATCCATGCCGTG-3'), forward chimera primer for AcGFP-KIF3A (5'-TACAAGGGAGGTGGAATGCCGATCGGTAAATCAGA-3'), flanking reverse

primer (5'-CCTCTTCATCATCATCTTCC-3'). The following primers were used for KIF1C-GFP: forward flanking primer containing the SmaI site (5'-AARRCGAGCTCGGTACCCGCCACCATGGTGAGCAAGGGCGCC-3'), reverse primer (5'-GCCATTCCACCTCCCTTGTACAGCTCATCCATGCCGTG-3'), forward chimera primer for AcGFP-KIF1C (5'-TACAAGGGAGGTGGAATGGCTGGTGCCTCGGTCAA-3'), flanking reverse primer (5'-AATAAGATCTGGATCCCCTCACACAGCTGCCCCACTCTC-3'). The PCR products for the two constructs were cloned into pSG6 expression vector using Quick-Fusion Cloning kit. Eight colonies were analysed for each construct for the presence of the correct inserts using restriction enzyme digestion (figure 2.1 a). A single positive clone for each mutant was sent for DNA sequencing and further analysed for protein expression by WB using an anti-KIF3A and an anti-KIF1C antibody (Figure 2.1 b). GFP-tagged KIF9-v1 was generated by restriction enzyme cloning. KIF9-v1 and GFP-tagged KIF9-v2 were digested with SacI and KpnI. The GFP-containing fragment from KIF9-v2-GFP was ligated into KIF9-v1 vector. Eight colonies were analysed for the presence of the correct insert using restriction enzyme digestion and they were compared to KIF9-v1 and KIF9-v2 cut with the same restriction enzymes (Figure 2.1 a). A single positive clone was sent for DNA sequencing and further analysed for protein expression using an anti-KIF9 antibody (Figure 2.1 b).

KIF3A-HaloTag and KIF9-v2-HaloTag were based on the expression vector pHTN HaloTag CMV-neo (Gen Bank Accession Number JF920304) that is configured to append HaloTag to the N-terminus of the fused protein. KIF3A-HaloTag was generated sub-cloning KIF3A into pHTN HaloTag CMV-neo. KIF9-v2-HaloTag was generated sub-cloning KIF9-v2 into pHTN HaloTag CMV-neo.

KIF9-v2 insert was cut off the expression vector pSG6 by BglII and SacI digestion and it was blunt ended. PHTN HaloTag CMV-neo was digested with SacI, blunt ended and CIP treated. Then, KIF9-v2 insert was ligated into the linearized vector. For each construct, eight colonies were analysed for the presence of the correct inserts using restriction enzyme digestion (Figure 2.1 a). For each mutant, a single positive clone was sent for DNA sequencing and further analysed for protein expression by WB using an anti-KIF3A and an anti-KIF9 antibody (Figure 2.1 b).

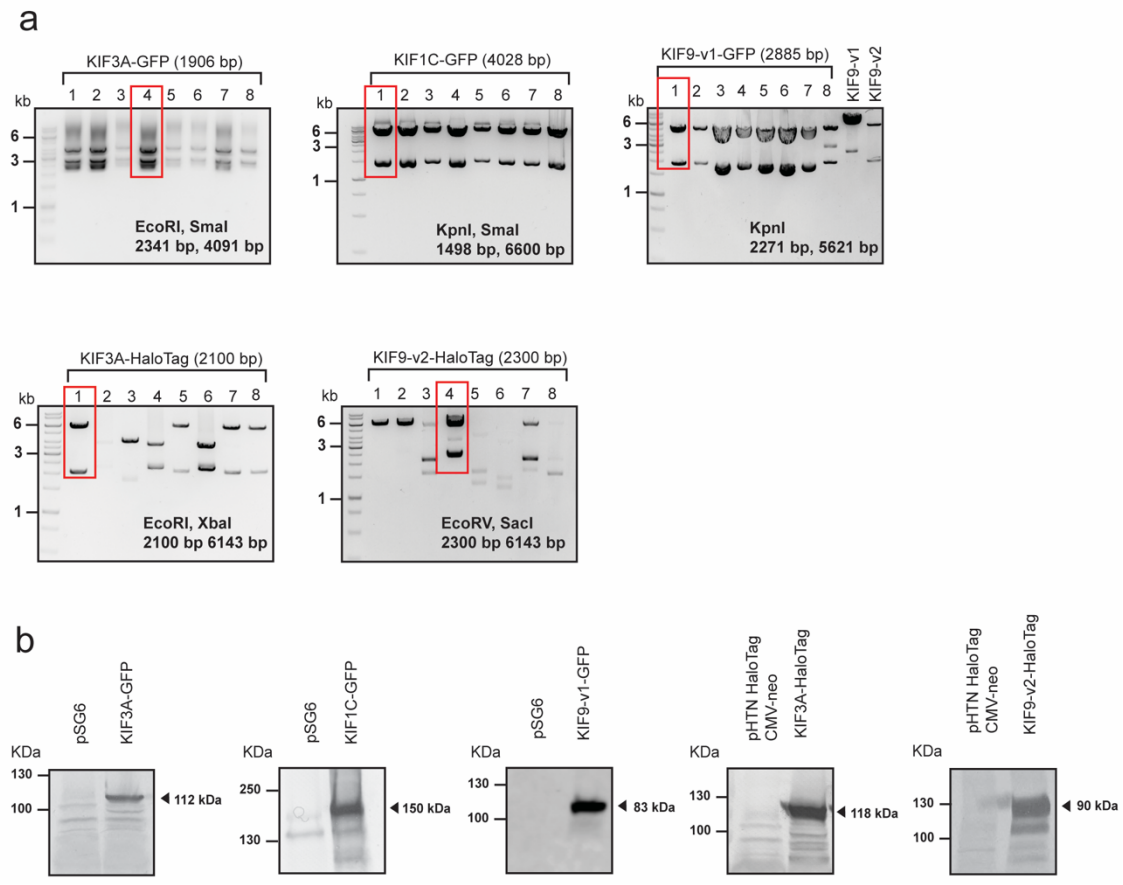


Figure 2.1: Cloning and expression of GFP-tagged KIFs and Halo-tagged KIFs

a Restriction enzyme digestion of DNA extracted from eight different colonies of DH5α competent E. coli transformed with constructs encoding GFP-tagged and Halo-tagged KIFs. Selected clones are highlighted by a red rectangular frame. Restrictions enzymes utilised and bands expected

sizes are shown at the right bottom corner of each DNA gel. **b** Expression of the mutants in HT-1080 cells. HT-1080 cells were transiently transfected with mock vector or plasmid DNA encoding KIF3A-GFP, KIF1C-GFP, KIF9-v1-GFP, KIF3A-HaloTag, KIF9-v2-HaloTag. 48 hours later cells were lysed and subjected to WB analysis using anti-KIF3A, anti-KIF1C and anti-KIF9 antibodies. Calculated molecular sizes of the mutants are at the right of the corresponding protein band.

2.2.14 Cloning of Tet-off TRIPZ inducible lentiviral shRNA constructs

TRIPZ inducible lentiviral shRNAs targeting KIF13A (clone id: V3THS_373145) and KIF9 (clone id: V2THS_87885) and TRIPZ inducible lentiviral non-silencing shRNA control, were converted to a tetracycline-off (Tet-off) configuration. The TRIPZ vector is designed to enable the expression of an shRNA in the presence of doxycycline. This expression is induced by a reverse tetracycline transactivator (rtTA3) that binds and activates expression from tetracycline response element (TRE) promoters. These promoters control the expression of a TurboRFP reporter, that is used to assess the promoter activity and the efficiency of the construct delivery into the cells, and of a puromycin resistance gene, that is employed to select stable cell lines. To convert TRIPZ vector to a Tet-off capable vector, rtTa3 was cleaved by BamHI restriction digestion. PCL-CTiG vector was used as template to amplify the tetracycline transactivator (tTA) by PCR, using the following primers: forward primer (5'-TTGCGGCCGCGGATCCTACCCACCGTACTCGTCAA-3'), reverse primer (5'-AGACGCTAGCGGATCGCCACCATGGCTAGATTAGCTAAAAGT-3'). The amplified tTA insert and the BamHI-digested TRIPZ vectors were gel-purified and the final Tet-off TRIPZ inducible lentiviral constructs were made by fusion. These constructs were used to transiently transfect HT-1080 cells stably expressing

NanoLuc luciferase, to confirm whether TurboRFP/shRNA expression was induced in the absence of doxycycline.

2.2.15 Packaging lentiviral shRNA constructs

To generate Tet-on and Tet-off TRIPZ shRNA-expressing lentiviral particles, we employed Trans-lentiviral shRNA Packaging kit. This packaging mix contains five plasmids that encode structural proteins and enzymes, necessary to produce lentiviral particles. Human embryonic kidney cells (HEK 293), cultured in DMEM supplemented with 10% (v/v) of Tet system approved FBS, were transfected with 0.5 µg of Trans-lentiviral packaging mix and two µg of either TRIPZ Tet-on inducible lentiviral shRNA constructs or the corresponding Tet-off capable vectors that we cloned. After 48 hours, cells transfected with Tet-on or Tet-off TRIPZ inducible lentiviral shRNA constructs were examined microscopically for the presence of TurboRFP and transfection efficiency was assessed. After 24 hours, viral supernatant was collected and it was centrifuged at 1600× g at 4°C for 10 minutes to pellet cell debris. Viral supernatant was aliquoted and transferred to a sterile microfuge tube to be store at -80°C until used.

2.3 SDS page gel electrophoresis

2.3.1 Reagents and materials

Reagents and materials were purchased from the following sources: SDS, glycine, β-mercaptoethanol and amediol from Sigma-Aldrich; 30% (w/v) acrylamide/bis-acrylamide from Severn Biotech.; N,N,N',N'-

Tetramethylethylenediamine (TEMED), hydrochloric acid (HCl), ethylenediaminetetraacetic acid (EDTA), sodium azide (NaN_3), bromophenol blue and butanol (C_4H_9OH) from Merck Biosciences; ammonium persulfate (APS) from Acros Organics; Pre-stained Precision Protein Standards from BioRad; ATTO gel casting kit equipment AE-6401 and gel electrophoreses system AE-6450 from ATTO corporation.

2.3.2 General solutions

- Acrylamide solution: 30% acrylamide, 0.8% (w/v) BIS (N, N'-methylene-bis- acrylamide)
- 4x Lower gel buffer: 110 mM amediol (2-amino-2-methyl-1,3-propanediol), 47 mM HCl, 0.02% NaN_3
- 4x Upper gel buffer: 84 mM amediol, 62 mM HCl, 0.02% NaN_3
- 50% Sucrose solution: 50% (w/v) sucrose, 0.03% (v/v) toluene, 0.02% NaN_3
- APS: 10% Ammonium persulfate in dH_2O
- Butanol solution: 50% (v/v) butanol in dH_2O
- TNC buffer: 50mM Tris-HCl pH 7.5, 150 mM NaCl, 10mM $CaCl_2$, 0.02% NaN_3
- 4x Lower reservoir buffer: 62.5 mM amediol, 50mM HCl
- 4x Upper reservoir buffer: 41mM amediol, 40 mM glycine, 0.4% SDS
- 2x Loading buffer: 0.2 g SDS, 5 ml of 4x upper gel buffer, 0.5 ml of 1% bromophenol blue, 4 ml of glycerol, 1ml of dH_2O

- 2x Reducing loading buffer: 0.2 g SDS, 5 ml of 4x upper gel buffer, 0.5 ml of 1% bromophenol blue, 4 ml of glycerol, 0.4 ml of 0.5 M EDTA pH 8.0, 100 µL of β-mercaptoethanol, 0.6 ml of dH_2O
- 1x Reducing loading buffer: 2x reducing loading buffer diluted in TNCGel composition

Table 2.5: SDS-PAGE resolving gel composition

Reagents	6% Resolving lower gel	7.5 % Resolving lower gel
30 % acrylamide	1200 µL	1500 µL
Lower gel buffer	1500 µL	1500 µL
50% Sucrose	1200 µL	1290 µL
dH_2O	2000 µL	1710 µL
APS	42 µL	42 µL
TEMED	4.5 µL	4.5 µL

Table 2.6: SDS-PAGE stacking gel composition

Reagents	Stacking upper gel
30 % acrylamide	320 µL
Lower gel buffer	642 µL
50% Sucrose	642 µL
dH_2O	963 µL
APS	31.5 µL
TEMED	6.75 µL

2.3.3 SDS-PAGE procedure

ATTO gel casting kit equipment was used to prepare SDS-PAGE gels. Resolving lower gel solution was poured between the two glass plates and 1ml

of butanol solution was used to ensure a flat interface between lower and upper gel. The resolving lower gel solution was left to polymerise for 30 minutes at RT. The butanol solution was discarded and the lower gel interface was washed three times with dH_2O. A 1 mm thick, 15-well comb was inserted on top of the lower resolving gel to form the sample wells. The stacking upper gel solution was applied and incubated at RT for 10 minutes to fully polymerise. The gel casting equipment was placed in the gel electrophoreses system that was previously filled with 1x lower reservoir buffer in the lower compartment. 1x upper reservoir buffer was poured in the upper compartment. The comb was removed from the upper gel and the sample wells were washed twice with 1x upper reservoir buffer. Unless differently specified, cells were lysed in 1x reducing loading buffer and lysates were boiled on a heat block for 20 minutes. Samples were applied to washed wells and 5 µL of pre-stained protein standard were applied to one well. Gels were electrophoresed at 150 V until the dye front has reached the bottom of the resolving gel (~55 - 60 minutes) and then they were used for WB.

2.4 Western blotting

2.4.1 Reagents and materials

Reagents and materials were purchased from the following sources: albumin from bovine serum (BSA, lyophilised powder), Tween 20, Trizma base and skimmed milk powder and ethanol (C_4H_5OH) from Sigma-Aldrich; sodium chloride (NaCl) from Merck Biosciences; polyvinylidene difluoride (PVDF) membranes, Trans-Blot Turbo Transfer System, Trans-Blot Turbo 5x Transfer buffer and transfer stacks from Bio-Rad.

2.4.2 Antibodies

The following primary antibodies were used: rabbit anti-MT1-MMP monoclonal antibody (clone EP1264Y, ab51074, abcam, 1:5000), mouse anti-MT1-MMP monoclonal antibody (clone 222-1D, 1:1000), rabbit anti-KIF1C polyclonal antibody (ab72238, abcam, 1:1000), rabbit anti-KIF3A polyclonal antibody (ab11259, abcam, 1:500), mouse anti-actin monoclonal antibody (clone C4, sc47778, Santa Cruz, 1:1000), mouse anti-α-tubulin (clone B-7, sc5286, Santa Crutz, 1:500).

The following secondary antibodies were used: IRDye 680RD goat anti-mouse IgG (H + L) (926-68070, LI-COR, 1:10000), IRDye 800CW goat ant-rabbit IgG (H + L) (926-32211, LI-COR, 1:10000).

2.4.3 General solutions

- Transfer buffer: 200 ml of 5x Trans-Blot Turbo Transfer buffer, 200 ml of ethanol, 600 ml of dH_2O
- 5% skimmed milk solution: 5 g skimmed milk powder, 10mM Tris-HCl pH 7.5, 150mM NaCl, 0.02% NaN_3
- Washing buffer (TBST): 50mM Tris-HCl pH 7.5, 150mM NaCl, 0.02% (v/v) NaN_3, 0.05% (v/v) Tween 20

2.4.4 Procedure

After samples were separated by SDS-PAGE, proteins on the gel were transferred to a PVDF membrane by using the Trans-Blot Turbo Transfer System, according to the manufacturer's instructions. After the transfer was completed, PVDF membrane was blocked using 5% skimmed milk solution for 50 minutes.

Membrane was washed three times for 5 minutes with 1x washing buffer and then it was incubated overnight at 4°C on a shaker with a primary antibody in 1% (w/v) BSA in Tris-buffered saline (TBS). Membrane was washed again three times for 5 minutes with 1x washing buffer and then it was incubated for 45 minutes at RT with the specific fluorescently-labelled secondary antibody in 1% (w/v) BSA in TBS supplemented with 0.02% (w/v) SDS and 0.2% (w/v) Tween 20. Membrane was washed twice with washing buffer for 15 minutes and scanned by Odyssey CLx imaging system (LI-COR).

2.4.5 Quantification of protein bands

WB membranes were quantified by Fiji software. I used the 'rectangle' tool to frame protein bands in each lane and the 'gel' command in the 'analyse' menu to generate a histogram representing the intensity of each band. Each peak, corresponding to a protein band, was enclosed with the 'line' tool and the area underneath was selected and quantified with the 'wand' tool. Actin or tubulin bands on the same blot were used to normalise intensities of the protein of interest. Mean band intensities were plotted using Prism (GraphPad software, Inc.) and statistical significance was calculated using either a parametric unpaired T test or a one-way ordinary ANOVA with Tukey's multiple comparison test.

2.5 Zymography

2.5.1 Reagents and materials

Reagents and materials were purchased from the following sources: gelatin and Triton-X 100 were from Sigma Aldrich, calcium chloride ($CaCl_2$), zinc

chloride ($ZnCl_2$), methanol (CH_3OH), formic acid (HCOOH), acetic acid (CH_3COOH) and Coomassie Brilliant Blue R-250 were from Merck Biosciences; PureCol collagen from Inamed Biomaterials.

2.5.2 Gel composition

To prepare the 7.5% resolving gel (Table 2.6), acrylamide was co-polymerised with gelatin at a final concentration of 0.8 mg/ml. The stacking upper gel was made following the same recipe reported previously (Table 2.6).

Table 2.7: SDS-PAGE resolving gel composition for zymography

Reagents	7.5% Resolving lower gel
30 % acrylamide	1200 µL
Lower gel buffer	1500 µL
50% Sucrose	1200 µL
2.8 mg/ml Gelatin	2000 µL
APS	42 µL
TEMED	4.5 µL

2.5.3 General solutions

- Gelatin solution: 2.8 mg/ml gelatin in dH_2O
- Washing buffer: 50 mM Tris-HCl pH 7.5, 5mM $CaCl_2$, 5 µM $ZnCl_2$, 0.02% (v/v) NaN_3, 2.5% (v/v) Triton-X 100
- Staining solution: 0.125 % (w/v) Coomassie Brilliant Blue R-250, 62.5 % (v/v) methanol, 25 % (v/v) acetic acid
- De-staining solution: 30 % (v/v) methanol, 1 % (v/v) formic acid

2.5.4 Procedure

HT-1080 cells transfected with siRNAs targeting specific KIFs were cultured in serum-free DMEM with or without PureCol collagen (final concentration 50 µg/ml) for 24 hours. Medium was recovered and mixed with 2x loading buffer in a 1:1 ratio. Then, it was subjected to SDS-PAGE without heat denaturation. Gels were washed four times for 15 minutes with 20 ml of washing buffer and then incubated overnight at 37°C in fresh washing buffer. Gels were then stained with Coomassie Brilliant Blue R-250 for 30 minutes and de-stained until digested areas were clearly detectable against the blue background. Gels were scanned with an image II scanner (GE Healthcare).

2.5.5 Quantification of gelatinolytic bands

Gelatinolytic bands were quantified by Fiji software. Bands corresponding to proMMP-2 (P), intermediate MMP-2 (I) and active MMP-2 (A) in the same lane were enclosed by a rectangular frame using the ‘rectangular’ tool. A histogram was generated as described previously for the quantification of WB gels. This histogram was generally characterised by two distinct peaks corresponding to P and A respectively and one referring to I. Areas underneath peaks were measured using the ‘wand’ tool. The percentage of processed proMMP-2 over the total was calculated as follow:

$$Processed\ proMMP-2\ (\%) = \frac{Area\ Peaks\ (I+A)}{Area\ Peaks(\ P+I+A)} * 100$$

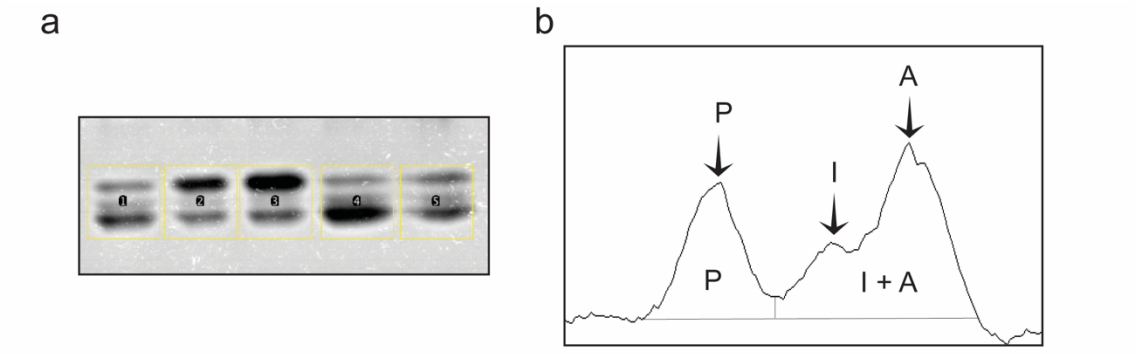


Figure 2.2: Quantification of gelatinolytic bands

a Example of a zymography gel inverted by Fiji. Bands of interest are enclosed by a yellow rectangular frame in each lane and are numbered. **b** Example of histogram related to one lane. Black arrows point peaks corresponding to proMMP-2 (P), intermediate form (I) and active MMP-2 (A).

2.6 Immunocytochemistry

2.6.1 Reagents

Reagents were obtained from the following sources: formaldehyde (HCOH) from Sigma Aldrich; goat serum from Dako; round Ø 18 mm cover glass from VWR collection; ProLong Diamond mounting solution, Alexa 488-conjugated phalloidin (1:500), Alexa 568-conjugated phalloidin (1:500), Dylight 650 phalloidin (1:300), 4,6-diamidino-2-phenylindole (DAPI) (1:500) from Invitrogen.

2.6.2 General solutions

- Blocking solution: 3% (w/v) BSA, 5% (v/v) goat serum, 1 mM $CaCl_2$ in TBS
- 4% formaldehyde solution: 37% formaldehyde solution diluted in phosphate buffered saline (PBS) to adjust to the final concentration
- Washing solution: PBS, 0.02% (v/v) NaN_3

- Permeabilising solution: PBS, 0.1% (v/v) Triton-X 100

2.6.3 Antibodies

The following primary antibodies were used: rabbit anti-MT1-MMP monoclonal antibody (clone EP1264Y, ab51074, abcam, 1:2500), mouse anti-human β1 integrin monoclonal antibody (clone 12G10, ab30394, Millipore, 1:500), mouse anti-FLAG M2 monoclonal antibody (F3165, Merck, 1:500), mouse anti-α-tubulin (clone B-7, sc5286, Santa Crutz, 1:500), rat anti-HA high affinity monoclonal antibody (clone 3F10, Roche, 1:1000), mouse anti-GM130 (cis-Golgi marker) polyclonal antibody (ab169276, 1:100), mouse anti-TGN38 (trans-Golgi marker) monoclonal antibody (clone A-5, sc-166224, Santa Cruz, 1:100), mouse anti-Rab5 monoclonal antibody (clone 1, BD Transduction laboratories, 1:100).

The following secondary antibodies were used: Alexa 488-conjgated goat anti-mouse IgG (A11029, Invitrogen, 1:500), Alexa 488-conjugated goat anti-rabbit IgG (A11034, Invitrogen, 1:500), Alexa 568-conjgated goat anti-mouse IgG (A11031, Invitrogen, 1:500), Alexa 568-conjugated goat anti-rabbit IgG (A11036, Invitrogen, 1:500), DyLight650-conjugated goat anti-rabbit IgG (SA5-10034, Invitrogen, 1:500).

2.6.4 Procedure

Transfected cells were cultured onto coverslips coated with un-labelled or fluorescently-labelled gelatin and incubated from 1 to 15 hours, depending on the experiment. After the incubation, cells were fixed with 4% formaldehyde solution for 15 minutes at RT. Cells were washed three times for 5 minutes with washing solution and, where stated, they were permeabilised with 0.1% (v/v) Triton-X 100

in PBS for 15 minutes at RT. Cells were incubated for 1 hour with blocking solution and then with the appropriate primary antibody, diluted in blocking solution, for 2 hours at RT. After, cells were again washed three times for 5 minutes with washing buffer and they were incubated with the specific secondary antibody, diluted in blocking solution, for 1 hour at RT. Where specified, cells were incubated for 1 hour at RT with phalloidin and DAPI diluted in blocking solution, to respectively visualise actin filaments and nuclei. After washing all the unbound material, cells were mounted in ProLong Diamond mounting solution on glass slides. Transfected cells were also embedded in type I-A collagen. 200 µL of cell suspension (3 x 10^6 cells/ml) were suspended in 500 µL of ice-cold neutralised collagen type I-A (collagen type I-A was neutralised as described in Paragraph 2.11.2). 150 µL of this cell suspension were used to coat one well of a glass-bottomed 8-well chamber and left to to set at 37°C for 1 hour. 1 ml of DMEM, supplemented with 10% FBS, was used to cover the polymerised collagen. Cells were left to elongate in the collagen matrix for 4 to 6 hours and then, they were fixed with 4% formaldehyde solution for 1 hour at RT. Cells were washed three times for 30 minutes with washing solution and stored at 4°C in washing solution before being imaged.

2.7 Fluorescent-Gelatin film degradation assay

2.7.1 Reagents and materials

Reagents and materials were obtained from the following sources: Alexa Fluor-488 NHS ester from Invitrogen; gelatine type A from porcine skin, dimethylformamide (C_2H_6NCHO), sodium bicarbonate ($NaHCO_3$) and 25% (v/v) glutaraldehyde from Sigma Aldrich; ammonium chloride (NH_4Cl) from Fisons;

Slide-A-Lyzer G2 Dialysis Cassettes from Thermo Fisher; Cover glass round Ø 18mm from VWR collection.

2.7.2 Preparation of fluorescently labelled gelatin

Alexa Fluor 488 NHS ester was used to label gelatin using the following protocol. 20 mg of type A gelatin from porcine skin were dissolved in 1 ml of 0.1 M $NaHCO_3$ by gently heating in the microwave. 250 µg of dye were dissolved in 25 µL of dimethylformamide and were added drop-wise to 250 µL of the prepared gelatin solution in a 1.5 ml Eppendorf tube. The mixture was stirred for 1 hour at RT. After, 50 µL of 2M Tris-HCl pH 7.5, 50 µL of 10x PBS and 150 µL of dH_2O were added to the mixture to stop the reaction, giving a concentration of 10 mg/ml gelatin. The solution was dialysed against 1L of PBS for 2 - 4 hours, to remove the unbound dye using a Slide-A-Lyzer G2 Dialysis Cassette. The final volume was measured and the gelatin was diluted 10 times with 50% glycerol in PBS to give a concentration of 1 mg/ml. 1 ml aliquots were stored at -20°C.

2.7.3 Coating of glass cover slips

Labelled gelatin was diluted to a concentration of 50 µg/ml in d-H_2O and the solution was incubated for 20 minutes at 60ºC on a thermo-block. Diluted gelatin was used to coat cover glass (round Ø 18mm) for 20 minutes at RT; cover slips were fixed using 1% (v/v) glutaraldehyde for 5 minutes; the excess of free glutaraldehyde was neutralized using 1M ammonium chloride for 15 minutes. A single cover slip was placed into a well of a 12-well plate and it was washed with 70% (v/v) ethanol to sterilise. It was then washed twice with DMEM and once with DMEM, supplemented with 10% FBS, before being used for the experiments.

The same procedure was applied to coat cover slips with non-labelled gelatin (20 mg/ml).

2.7.4 Culture of cells on gelatin-coated cover slips

Transfected cells were seeded on top of a single cover slip at a concentration between 5 x 10^4 and 1.5 x 10^5 cells/ml, depending on the experiment. Cells were then cultured at 37°C for 2 - 18 hours, depending on the experiment.

2.7.5 Image analysis

Fluorescent-Gelatin film degradation

Gelatin film degradation was quantified using Fiji. Area of degradation was calculated using the gelatin fluorescence image which was converted to greyscale and thresholded. The threshold was set the same for all the pictures analysed, to have an objective mean of analysis. Area and area fraction were measured. The DAPI-stained corresponding image was converted to a binary image to count the number of cells in the microscopic field. The degraded area per cell was calculated as follow:

$$\text{Degraded Area per cell } (\mu m^2) = \frac{\text{Total Degraded Area}}{\text{Number of Cells}}$$

Mean degraded areas were plotted using Prism and statistical significance was calculated using one-way ordinary ANOVA with Tukey's multiple comparison test.

Fluorescent-Gelatin Film degradation by GFP-tagged KIF-transfected HT-1080 cells

Gelatin film degradation was quantified using Volocity, measuring the fluorescence intensity of the gelatin area underneath each single cell. The area was defined using the cell shape obtained from the images picturing the actin staining. Average fluorescence intensity of the gelatin layer beneath GFP-tagged KIF-transfected HT-1080 cells was compared to the average fluorescence intensity beneath un-transfected HT-1080 cells within the same sample. Mean values were plotted using Prism and statistical significance was calculated using an unpaired T test.

2.8 Collagen film degradation assay

2.8.1 Reagents and materials

Reagents and materials were purchased from the following sources: bovine collagen type I PureCol from Inamed Biomaterials; Cellmatrix type I-A collagen from Nitta; 10x RPMI-1640 from Sigma Aldrich; Corning® CellBIND® 12-well plates from Corning.

2.8.2 Collagen-coating of 12-well dish

Ice-cold PureCol (3 mg/ml) and Cellmatrix type I-A (3 mg/ml) collagen were mixed on ice in the ratio 1:1. Nine portions of the mixture were supplemented with one portion of 10x RPMI-1640.1M NaOH was used to adjust the solution at neutral pH and serum-free DMEM was added to obtain a final concentration of collagen of 2 mg/ml. Wells within a CellBIND® 12-well plate were

coated with 100 µL of collagen, by adding 500 µL and removing 400 µL. Collagen-coated dishes were incubated at 37°C for 5 hours to allow the collagen to set completely.

2.8.3 Culture of cells on collagen-coated dishes and collagen staining

Cells were transfected with the specific siRNA and incubated at 37°C. After 48 hours, they were trypsinised, seeded onto the polymerized collagen and incubated for 72 hours. Then, they were removed from each well by washing three times with 1x PBS and incubating overnight with Trypsin. Remaining collagen layer was fixed using 4% formaldehyde in PBS for 30 minutes and stained with R-250 Coomassie brilliant blue. Each well was then washed with de-staining solution and with dH_2O, before it was let to dry. Digested area was visualised as white areas against the blue collagen background.

2.8.4 Image analysis

Collagen degradation was quantified using Fiji by measuring the integrated density of the collagen layer. Mean results were plotted using Prism and statistical significance was calculated using one-way ordinary ANOVA with Tukey's multiple comparison test.

2.9 Cell surface biotinylation

2.9.1 Reagents and materials

Reagents and materials were purchased from the following sources: Sulfo-NHS biotin from Thermo Scientific; magnesium chloride ($MgCl_2$) from Merck Biosciences; lysine, proteinase inhibitor cocktail and deoxycholic acid from Sigma Aldrich; MyOne StreptavidinT1 beads from Invitrogen.

2.9.2 General solutions

- Washing solution (1x PBS (+)): 100mM $MgCl_2$, 1M $CaCl_2$ in 1x PBS
- Sulfo-NHS Biotin solution: Sulfo-NHS Biotin (2mg/ml) in PBS (+)
- Lysine solution: 25mM lysine in PBS (+)
- RIPA buffer: 1% TritonX-100, 1% deoxycolic acid, 50 mM Tris-HCl (pH7.5), 150 mM NaCl, proteinase inhibitor cocktail (1:1000), 0.02% NaN_3

2.9.3 Procedure

Transfected cells were washed three times on ice with ice cold 1x PBS (+) and then, they were incubated with 1 ml of Sulfo-NHS-Biotin solution for 30 minutes at 4°C; lysine solution was used to stop the reaction. Cells were lysed with 180 µL of 1% SDS in PBS, containing proteinase inhibitor cocktail (1:1000) and 1620 µL of RIPA buffer, and the lysates were subjected to sonication. Biotinylated proteins were isolated incubating the samples with MyOne StreptavidinT1 for 1 hour at 4°C. They were then eluted from the beads applying 55 µL of 1x loading buffer. The samples were subjected to electrophoresis and analysed by WB.

2.10 Transwell collagen invasion assay

2.10.1 Reagents and materials

8 µm polyethylene terephthalate (PET) track-etched membrane culture transwells were purchased from VWR.

2.10.2 Procedure

PET transwells were inserted into wells of a 24-well plate (Figure 2.3). PET membranes were coated with 20 µL of neutralised collagen by adding 90 µL and removing 70 µL. Neutralised collagen was prepared as previously described for coating 12-well plates for collagen film degradation assay. Coated inserts were incubated at 37°C for 30 minutes to let the collagen polymerise. Inserts were transferred under a tissue culture hood and incubated overnight to dry the collagen completely. 1 x 10^4 cells suspended in 200 µL of serum-free DMEM were seeded on top of the collagen-coated insert. 700 µL of DMEM supplemented with 10% (v/v) FBS was added to the bottom well. Cells were incubated at 37°C for 18 hours in the presence or absence of GM6001. Collagen was carefully removed from the top of each insert with a cotton swab and samples were fixed with 4% formaldehyde for 30 minutes (Figure 2.3). Invasive cells were stained with DAPI and visualised with a Nikon TE2000-E microscope.

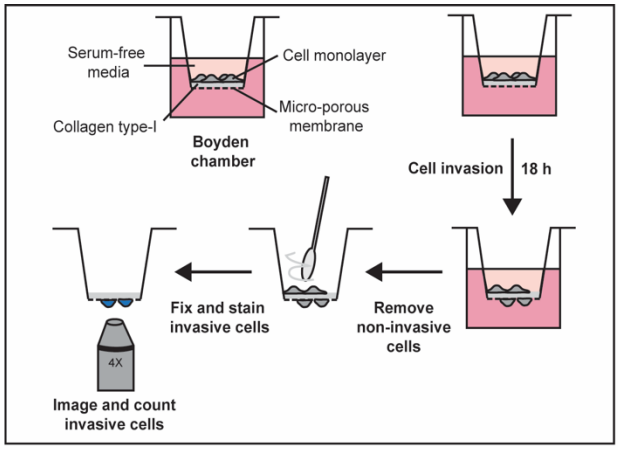


Figure 2.3: Set up of transwell invasion assay

HT-1080 cells transfected with siRNAs targeting KIFs were seeded atop of a collagen-coated insert and cultured for 18 hours. Non-invasive cells were removed with a cotton swab. Invasive cells were fixed, stained with DAPI and imaged.

2.10.3 Transwell invasion quantification

To count cells that had invaded through the PET membranes, Volocity software was employed. Average number of invaded cells was calculated considering six inserts per treatment. Averages were plotted using Prism and statistical significance was calculated using one-way ordinary ANOVA with Tukey's multiple comparison test.

2.11 Microcarrier beads invasion assay

2.11.1 Reagents and materials

Reagents and materials were purchased from the following sources: 1M HEPES buffer from Lonza Biosciences; Cytodex 3 microcarrier beads from VWR.

2.11.2 Procedure

A suspension of Cytodex 3 microcarrier beads in serum-free DMEM (8 x 10^3 beads/ml) was kindly provided by Dr. Itoh. 0.5 x 10^5 cells were incubated with 200 beads in 500 µL of DMEM supplemented with 10% (v/v) FBS, antibiotics and 10mM HEPES. The cells/beads suspension was attached horizontally to a shaking platform and incubated at 37°C 6 - 7 hours or until cells had formed a confluent monolayer on the surface of the beads. Cell-coated beads were left to settle on ice and they were washed three times with serum-free DMEM to remove un-attached cells. After the third wash, the supernatant was removed to reach a minimal volume of 50 µL and cell-coated beads were kept on ice. In the meantime, nine portions of Cellmatrix type I-A collagen were mixed with 10x RMPI-1640 in a pre-cooled 50 ml tube. The pH of the collagen solution was adjusted to 8. 250 µL of cell-coated beads were mixed with 500 µL of neutralised collagen by gently pipetting on ice. The suspension was immediately transferred to the well of a 12-well plate and incubated at 37°C for 1 hour to let the collagen polymerise. After the incubation, 1 ml of DMEM, supplemented with 10% (v/v) FBS and with or without GM6001, was added to each well. Cells were let migrate from the surface of the beads for 18 hours (Figure 2.4) and after, they were fixed with 4% formaldehyde for 30 minutes. Images were acquired using a light microscope equipped with a CCD camera.

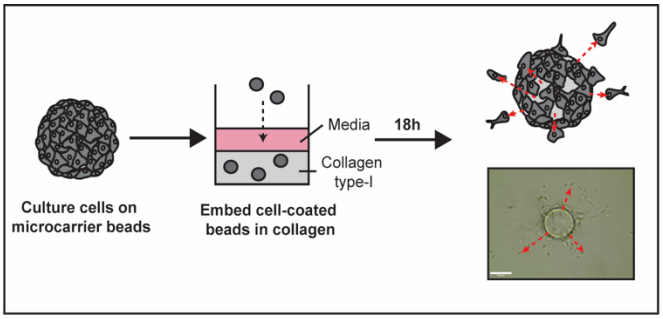


Figure 2.4: Set up of microcarrier beads invasion assay

HT-1080 cells were transfected with siRNAs targeting KIFs and cultured on gelatin-coated microcarrier beads. Cell-coated beads were embedded in collagen type I and incubated for 18 hours to let cells migrate. Images were acquired with a light microscope equipped with a CCD camera. The line tool was used to measure the distance from the surface of the bead and the nuclei of well-focused cells. Examples of migrated distances are shown as dotted red arrows. The scale bar is 130 µm.

2.11.3 Quantification of cellular invasion through the collagen matrix

To quantify collagen invasion, the distance between a cell nucleus and the surface of the bead (dashed red lines, Figure 2.4) was measured using the line tool of Fiji. Only well-focused cells were considered and migrated distances were calculated for 100 cells per treatment. Mean migrated distances were plotted using Prism and statistical significance was calculated using one-way ordinary ANOVA with Tukey's multiple comparison test.

2.12 Wound-healing assay

2.12.1 Reagents and materials

Culture inserts consisting of two reservoirs separated by a 500-µm-thick wall were purchased from Ibidi.

2.12.2 Procedure

Each reservoir of a culture insert was filled with 70 µL of cell suspension (2 x 10^5 cells/ml) and cells were incubated until becoming fully confluent. The inserts were gently removed and the gap was visualised with a light microscope equipped with a CCD camera. Cells were let migrate into the gap for 6 hours during which the process of cell migration was monitored. Cells were fixed with 4% formaldehyde for 15 minutes and images of the gap closure were captured by an Evos® XL Core Imaging System for a transmitted-light microscope equipped with 10X objective.

2.12.3 Quantification of wound closure

To measure the percentage of wound closure, Fiji was employed. For each condition, the ROI corresponding to the initial wound-gap (ROI-I) and the one, delimited by the migration front after 6 hours of incubation (ROI-F), were calculated. The percentage of wound closure was calculated as follow:

$$\text{Wound Closure}\ (\%) = \frac{(\text{ROI} - \text{I}) - (\text{ROI} - \text{F})}{\text{ROI} - \text{I}} * 100$$

Mean percentages were plotted using Prism and statistical significance was calculated using one-way ordinary ANOVA with Tukey's multiple comparison test.

2.13 Live cell imaging

2.13.1 Reagents and materials

Reagents and materials were purchased from the following sources: cell permeant Coumarin HaloTag® ligand from Promega; glass-bottomed 8-well chambers from Ibidi.

2.13.2 General Solutions

- 5x HaloTag® ligand working solution: HaloTag® ligand (1:200) in DMEM supplemented with 10% (v/v) FBS

2.13.3 Procedure

HT-1080 cells were transfected with GFP-tagged KIFs, Halo-tagged KIFs and MT1-RFP and after 36 hours they were seeded at a density of 4×10^3 cells/well on gelatin-coated glass-bottomed 8-well chambers. After 12 hours, medium was replaced with fresh DMEM supplemented with 10% (v/v) FBS and cells were subjected to live imaging. In case HT-1080 cells had been transfected with Halo-tagged KIFs, live-cell labelling was carried out before live images were acquired. Medium was replaced with fresh DMEM supplemented with 10% (v/v) FBS and with HaloTag® ligand working solution (1:5). Cells were incubated for 15 minutes at 37°C. After, 1/5 of the medium was replaced with fresh DMEM supplemented with 10% (v/v) FBS and this washing step was repeated three times. Finally, medium was completely replaced with fresh DMEM supplemented with 10% (v/v) FBS and cells were subjected to live cell imaging. Live images were acquired by either confocal laser scanning microscopy or total internal

reflection fluorescence (TIRF) microscopy (details specified below). Both microscopes were equipped with an environmental chamber to maintain temperature at 37°C and CO_2 at 5%. Time-lapse images were acquired every 3 to 30 seconds, depending on the experiment.

2.13.4 Tracking of MT1-RFP-positive vesicles trafficked by GFP-tagged KIFs

Tracking of MT1-RFP-containing vesicles trafficked by GFP-tagged KIFs was carried out using the Track Mate plugin in Fiji (236). Image time sequences of GFP-tagged KIFs and MT1-RFP were merged and calibrated. The crop settings of the plugin where used to focus on the area of interest. Vesicles were identified using the LoG detector and their diameter was estimated at 1.5 μm. HyperStack displayer was selected as view and blob quality was employed as filter to diminish background detection. Tracking was performed by Simple LAP Tracker using 2 μm as linking and gap-closing maximum distances. The gap-closing maximum frame gap was set at 2. Tracks below an average spot quality were excluded. Mean, maximum, minimum velocities and vesicle diameters were calculated automatically by the plugin. Data were plotted using Prism and statistical significance was calculated by either a parametric unpaired T test or a one-way ordinary ANOVA with Tukey's multiple comparison test.

2.14 Image acquisition

All widefield images were captured on an inverted Nikon TE2000-E widefield microscope with Volocity Acquisition software (PerkinElmer). These

objective lenses were used: 4X objective lens (Plan Fluor 4X/Numerical aperture (NA): 0.13), 10X objective lens (UPLSAPO 10X/NA 0.30 DIC), and 20X objective lens (UPLSAPO 20X/NA 0.45). Confocal laser scanning microscopy imaging was performed on a PerkinElmer Spinning Disk Confocal Microscope based on a Nikon TE 2000-U Eclipse motorized inverted microscope with DIC optics. A 60X objective lens was used: 60X (Plan Apo 60×/NA 1.40). Volocity software (PerkinElmer, Coventry, UK) was used for acquisition. Confocal laser scanning microscopy was also performed on a Nikon Ti2 Microscope in Galvano scanning mode, equipped with a Nikon A1 LFOV camera. A 60X objective lens was used (Bertrand lens 60X/ NA 1.4). Nikon Elements software was used for the acquisition and image deconvolution. For TIRF microscopy an Olympus microscope in TIRF mode (CellTIRF-4Line system; Olympus), equipped with an EMCCD camera (Evolve) was used. A 150X objective lens was used (UPLSAPO 150 X/ NA 1.45). For total internal reflection fluorescence structured illumination microscopy (TIRF-SIM) a custom-built system was employed. The system was equipped with a grating pattern, generated by a ferroelectric special modulator (SML, ForthDimention Displays, QXGA3DM), a high-NA TIRF objective (Olympus Plan-Apochromat 100X/ NA1.49) and sCMOS cameras (Hamamatsu, Orca Flash 4.0 v2 sCMOS).

2.15 Image processing and analysis

Fiji, Volocity (PerkinElmer) and Nikon elements (Nikon instruments Inc) were used for image visualisation, processing and analysis.

Quantification of MT1-MMP and β1 integrin fluorescence intensity at the substrate-attachment side

To measure the amount of either β1 integrin and MT1-MMP at the substrate-attachment side, the corresponding fluorescence intensities (FIs) were measured by Fiji. TIRF images were analysed by defining a region of interest (ROI), corresponding to the cell body (ROI-CB), and a rectangular ROI in the background (ROI-B). FIs were calculated as follow:

$$\mathrm{FI} = \mathrm{FI}(\mathrm{ROI}-\mathrm{CB}) - \mathrm{FI}(\mathrm{ROI}-\mathrm{B})$$

30 cells were analysed for each condition. ROI-B dimension and position was kept the same throughout the course of the analysis. Mean FIs were plotted using Prism and statistical significance was calculated using one-way ordinary ANOVA with Tukey's multiple comparison test.

Quantification of the overall amount of MT1-MMP on the cell surface

To measure the overall amount of MT1-MMP on the cell surface of HT-1080 cells, FIs were analysed by Volocity measurement module software. Extended focus images of HT-1080 cells stained for cell surface endogenous MT1-MMP, captured by spinning disk confocal microscope were used. 30 cells were analysed for each condition. Mean FIs were plotted using Prism and statistical significance was calculated using one-way ordinary ANOVA with Tukey's multiple comparison test.

Quantification of GFP-tagged KIFs and MT1-RFP co-localisation

Co-localisation between GFP-tagged KIFs and MT1-RFP was quantified using the Coloc 2 plugin in Fiji. This plugin automatically calculates the Pearson's correlation coefficient (PCC), that measures the correlation between two fluorophores, for a selected ROI. PCC can reach the maximum value of 1, when the intensities of two fluorophores are perfectly and linearly related, and the

minimum value of −1, when these intensities are perfectly but inversely related to one another. Before being analysed, two-colour channel images were subjected to background subtraction. The ROI was selected using the selection tool. Coloc2 plugin was run and Pearson's correlation coefficients (PCCs) were calculated. This procedure was used on two-colour channel images of cells cultured on 2D matrices and on two-colour channel stacks, picturing cells cultured in 3D collagen matrices. Mean PCCs were plotted using Prism and statistical significance was calculated using one-way ordinary ANOVA with Tukey's multiple comparison test. The Co-localisation Threshold plugin was used to generate co-localised pixel maps to compare KIF13A-GFP and MT1-RFP co-localisation with KIF3A-GFP and MT1-RFP co-localisation at the nuclear area and cell edge. For the purpose of this calculation, the nuclear area was considered comprising all the regions around the nucleus of a cell, excluding all membrane protrusions, while the cell edge area was only comprising the membrane protrusions.

2.16 Analysis of genomic alterations of *Kinesin* genes in cancer

To analyse genomic alterations of *Kif13a* and *Kif9* genes in cancer, cBioPortal (237, 238) (https://www.cbioportal.org) was employed. CBioPortal is an open-access analysis tool to explore large-scale cancer genomic datasets. The Cancer Genome Atlas (TCGA) PanCancer Atlas studies were selected to visualise and analyse *Kif13a* and *Kif9* gene alterations. The TCGA PanCancer Atlas is the most recent version of datasets that can be found on cBioPortal. It collects data, including clinical data, mutations, copy number, RNAseq,

normalised across cancer types and it is continuously updated. The analysis was carried out querying first for *Kif13a* and *kif9* mutations across the selected studies and then for *Kif13a* and *Kif9* amplifications and deletions. The onco query language was employed to write queries. Graphs showing the alterations' frequencies across the TCGA studies and onco-prints were generated through the specific tabs and survival analysis was carried out comparing the median months overall survival of patients with or without the queried gene alteration. The Human Protein Atlas (https://www.proteinatlas.org) was consulted to check whether *Kif13a* or *Kif9* genes were prognostic markers for specific cancer types.

CHAPTER 3:

CHARACTERISATION OF KIFs INVOLVED IN CELL SURFACE LOCALISATION OF MT1-MMP

3.1 Introduction

Previous studies in Dr. Itoh's group found that MT1-MMP cell-surface localisation is achieved by targeted intracellular trafficking of MT1-MMP-containing vesicles along microtubules and that KIFs play a role. There are 39 N-type KIFs in humans that transport cargoes to the cell periphery (239); among those, some are only expressed in neuronal cells or implicated in cell division. Therefore, 17 KIFs were chosen as potential candidates and they were targeted with a siRNA library to study their possible role in MT1-MMP-containing vesicle transport in HT-1080 human fibrosarcoma cells. As shown in Figure 3.1, it was found that the KD of four KIFs (KIF13A, KIF3A, KIF9 and KIF1C) notably affected MT1-MMP-mediated gelatin film degradation. The aim of this Chapter is to characterise the role of these four KIFs in MT1-MMP intracellular trafficking.

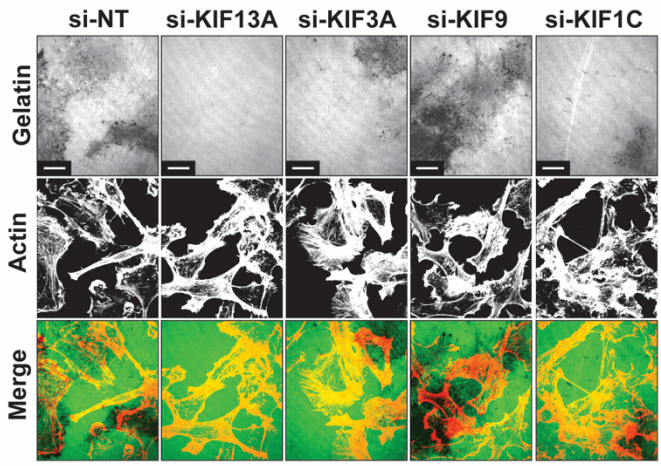


Figure 3.1: The KD of KIF13A, KIF3A, KIF9 and KIF1C alters MT1-MMP-mediated gelatin film degradation in HT-1080 cells

HT-1080 cells were transfected with siRNAs targeting the selected KIFs and subjected to gelatin film degradation assay. Cells were stained with phalloidin to visualise actin (red in the merge). Gelatin is green in the merge images. Scale bars are 22 μm.

3.2 Results

3.2.1 MT1-MMP-dependent F-gelatin film degradation by HT-1080 cells is inhibited by KD of KIF13A, KIF3A, KIF1C and enhanced by KD of KIF9

To confirm that KIF13A, KIF3A, KIF9 and KIF1C were involved in MT1-MMP intracellular trafficking, I analysed the effect of silencing these genes on MT1-MMP-dependent gelatin film degradation. In this assay, fluorescently labelled gelatin is used as a substrate and its degradation results in the detection of dark non-fluorescent areas against a fluorescent background. Average degraded area per cell (μm^2) can be measured as described in Chapter 2 (Paragraph 2.7.5). In HT-1080 cells, gelatin degradation is only attributed to the endogenous MT1-MMP. As shown in Figure 3.2, gelatin degradation was completely abolished when cells were cultured in the presence of GM6001 (10 μM), a broad-spectrum inhibitor of MMPs, or DX2400 (200 nM), a potent and specific biologic inhibitor for MT1-MMP (240). On the other hand, TIMP-1, that is unable to inhibit MT1-MMP up to the concentration of 1 μM, did not affect the degradation (Figure 3.2).

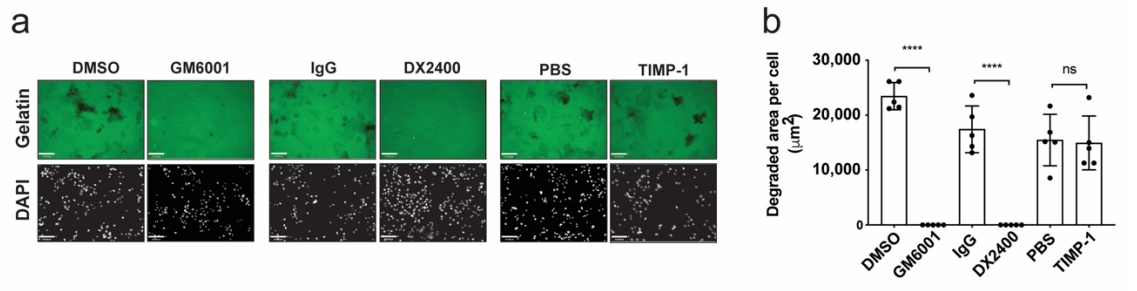


Figure 3.2: Gelatin film degradation is dependent on endogenous MT1-MMP in HT-1080 cells

a HT-1080 cells were subjected to gelatin film degradation assay in the presence of GM6001 (10 µM), DX2400 (200 nM), TIMP-1 (200 nM) and the relative controls. Scale bars are 130 µm. **b** Quantification of the degradation area (µm^2) per cell in HT-1080 cells. Data are presented as mean of five independent microscopic fields of view and are representative of three independent experiments. One-way ordinary Anova with Tukey's multiple comparisons test. Error bars are standard deviations (SDs); **** $P < 0.0001$; ns: non-significant.

HT-1080 cells were transfected with siRNAs against the above KIFs and NT siRNA (si-NT) and KD efficiency was evaluated (Figure 3.5). After 72 hours, transfected cells were re-seeded on cover slips coated with Alexa-488-labelled gelatin and cultured for 7 hours. Cells were then fixed and stained for nuclei using DAPI. As shown in Figure 3.3 a, silencing these *kinesin* genes resulted in notable changes of MT1-MMP-dependent gelatin film degradation: KIF13A, KIF3A and KIF1C KD notably decreased gelatin film degradation, while silencing *Kif9* gene increased the degradation of the underlying matrix. As shown Figure 3.3 b, the difference between the average area (µm^2) degraded by si-NT transfected cells and that degraded by cells transfected with siRNAs targeting these KIFs, was statistically significant ($P < 0.0001$). Since KIF5B had been previously reported to traffic MT1-MMP-containing vesicles (108, 211, 241), I also examined the

gelatinolytic activity of si-KIF5B-transfected cells. However, there was no effect on gelatin degradation (Figure 3.4).

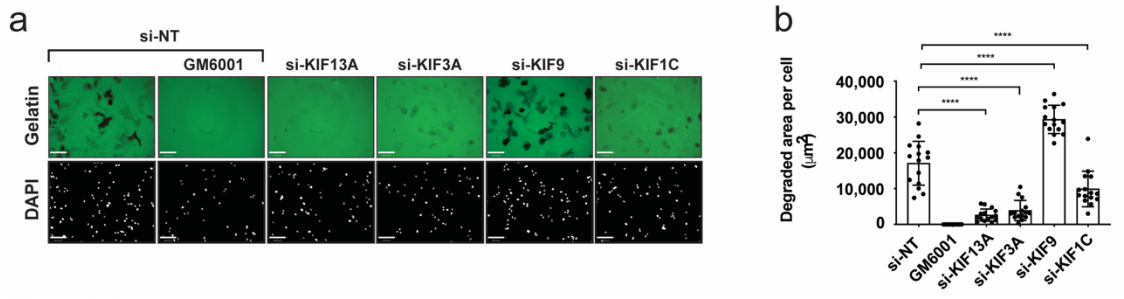


Figure 3.3: The KD of KIF13A, KIF3A, KIF9 and KIF1C alters MT1-MMP-mediated gelatin film degradation in HT-1080 cells

a HT-1080 cells were transfected with siRNAs targeting the selected KIFs and subjected to gelatin film degradation assay in the presence or absence of GM6001 (10 µM). Scale bars are 130 µm. **b** Quantification of the degradation area (µm^2) per cell in HT-1080 cells transfected with the specified siRNAs. Data are presented as the mean of 15 independent microscopic fields of view and are representative of five independent experiments. One-way ordinary Anova with Tukey's multiple comparisons test. Error bars SD, **** P < 0.0001.

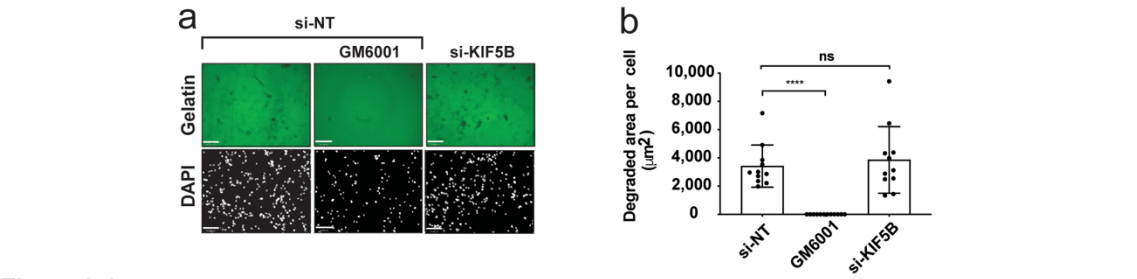


Figure 3.4: The KD of KIF5B does not alter MT1-MMP-mediated gelatin film degradation in HT-1080 cells

a HT-1080 cells were transfected with siRNAs targeting KIF5B and subjected to gelatin film degradation assay in the presence or absence of GM6001 (10 µM). Scale bars are 130 µm. **b** Quantification of the degradation area (µm^2) per cell in HT-1080 cells transfected with the specified siRNAs. Data are presented as the mean of 10 independent microscopic fields of view

and are representative of three independent experiments. One-way ordinary Anova with Tukey's multiple comparisons test. Error bars are SD; **** P < 0.0001; ns: non-significant.

The efficiency of silencing was confirmed by reverse transcription polymerase chain reaction (RT-PCR). DNA bands were quantified using Fiji as explained in Chapter 2 (Paragraph 2.2.6). KIF3A KD was almost complete, with KIF3A mRNA level down by 95% (Figure 3.5 a). On the contrary, KIF13A and KIF1C mRNA levels were only reduced by 47% and 56% respectively (Figure 3.5 a). As shown in Figure 3.5 a, among KIF9 splice variants (v1-3), only KIF9-v1 was efficiently knocked down, whereas KIF9-v2/v3 mRNA level was only down by 39%. To confirm that the decrease in mRNA levels reflected lower protein levels, cell lysates of HT-1080 cells transfected with si-NT, si-KIF13A and si-KIF1C, were subjected to WB. As shown in the Figure 3.5 b, KIF3A and KIF1C antibodies confirmed high efficiencies of KD. KIF5B antibody also showed that KIF5B protein level was down by 87% (Figure 3.5 b). Unfortunately, it was not possible to find good commercial anti-KIF9 and anti-KIF13A antibodies.

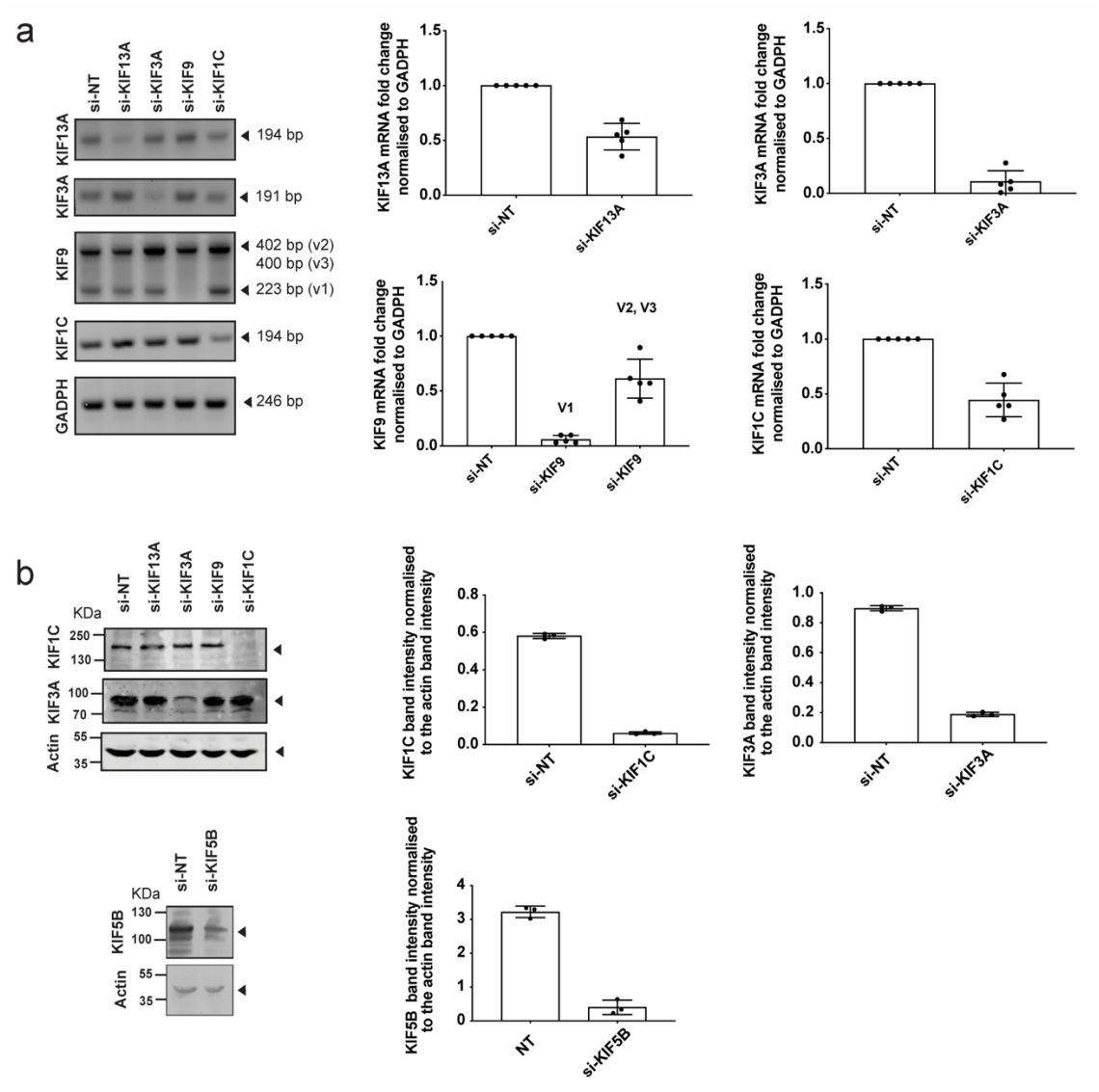


Figure 3.5: Efficiency of KIF KD in HT-1080 cells

a Efficiency of KIF KD by one-step RT-PCR. Quantification of KIF13A, KIF3A, KIF9 and KIF1C mRNAs relative to GADPH mRNA. The data are representative of three independent experiments. **b** Efficiency of KIF3A and KIF1C KD by WB. HT-1080 cells were transfected with siRNAs targeting the selected KIFs. Cell lysates were analysed by WB using the indicated antibodies. Arrow heads point bands of interest. Quantification of the intensity of KIF3A, KIF1C and KIF5B protein bands relative to actin.

To confirm that silencing KIF13A, KIF3A, KIF9 and KIF1C did not affect MT1-MMP mRNA levels, I again employed RT-PCR. As shown in Figure 3.6,

silencing of *Kif13a*, *Kif3a*, *Kif9* and *Kif1c* genes did not affect expression of MT1-MMP.

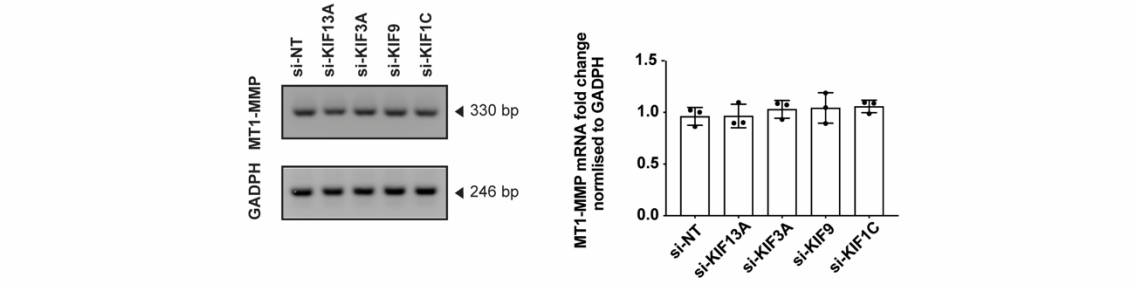


Figure 3.6: The KD of KIF13A, KIF3A, KIF9 and KIF1C does not alter MT1-MMP expression at the mRNA level

RT-PCR to quantify MT1-MMP mRNA level in HT-1080 cells transfected with siRNAs targeting the selected KIFs. Quantification of MT1-MMP mRNA relative to GADPH. Data are representative of three independent experiments.

3.2.2 MT1-MMP-dependent F-gelatin film degradation by HT-1080 cells is not affected by overexpression of GFP-tagged KIF13A, KIF3A, KIF9 and KIF1C

Given that the KD of these KIFs was affecting MT1-MMP-dependent gelatin film degradation, I tested whether their overexpression had any functional effect. HT-1080 cells were transfected with GFP-tagged KIF13A, KIF3A, KIF9 and KIF1C and overexpression was confirmed by confocal microscopy (Figure 3.7 a) and WB as previously shown in Chapter 2 (Figure 2.1 b). After 48 hours, cells were re-seeded on Alexa-568 labelled gelatin. After 4 hours, cells were fixed and stained with Alexa-488 Phalloidin, to visualise actin. As shown in Figure 3.7, MT1-MMP-dependent gelatin film degradation was not affected by the overexpression of any of these GFP-tagged KIFs. These results were confirmed

by quantifying the average fluorescence intensity of the gelatin layer beneath transfected and un-transfected cells (Figure 3.7).

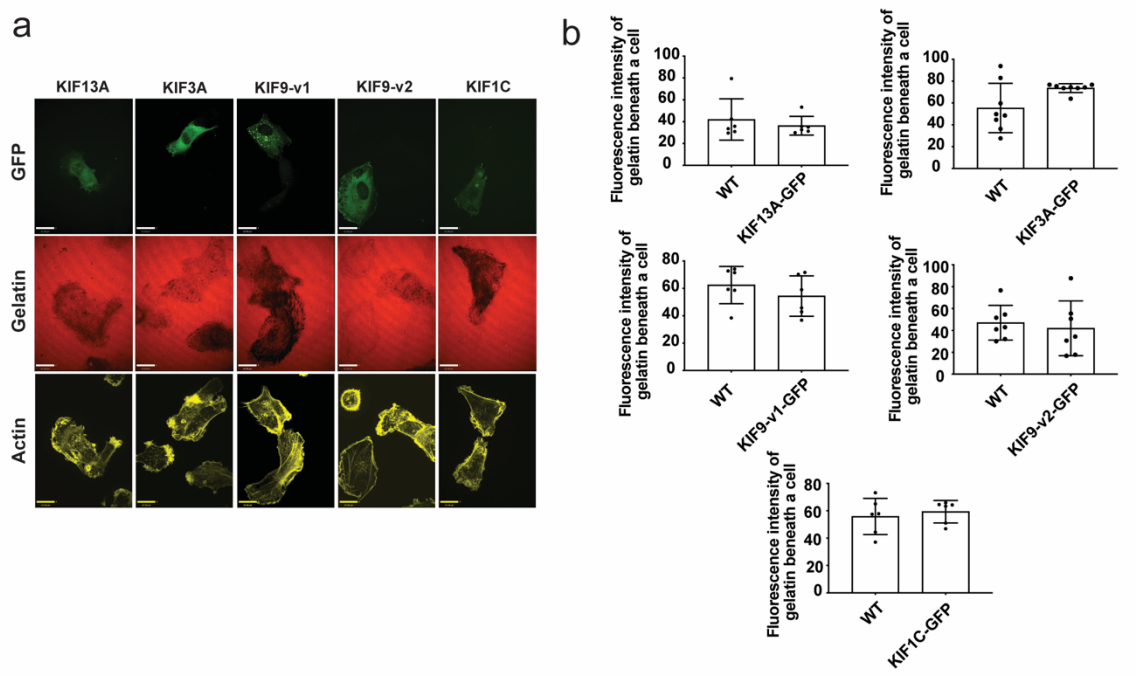


Figure 3.7: Overexpression of GFP-tagged KIFs does not influence MT1-MMP-dependent gelatin film degradation by HT-1080 cells

a HT-1080 cells were transfected with GFP-tagged KIFs (green) and subjected to gelatin film degradation assay (gelatin layer is red). Cells were stained with DyLight 650 Phalloidin to visualise actin (yellow) and they were imaged by confocal microscopy. Representative images of three independent experiments are shown. Scale bars are 22 µm. **b** Quantification of the gelatin degradation by HT-1080 cells transfected with GFP-tagged KIFs. Data are presented as the average fluorescence intensities of the gelatin layer beneath 15 cells. Data are representative of three independent experiments. Error bars are SDs.

3.2.3 MT1-MMP-dependent collagen film degradation by HT-1080 cells is inhibited by KD of KIF13A, KIF3A, KIF1C and enhanced by KD of KIF9

Next, I examined the effect of KIF13A, KIF3A, KIF9 and KIF1C KD on cellular collagenolytic activity of MT1-MMP by subjecting HT-1080 cells to collagen film degradation assay. In HT-1080 cells, collagen film degradation is entirely dependent on endogenous MT1-MMP (Figure 3.8).

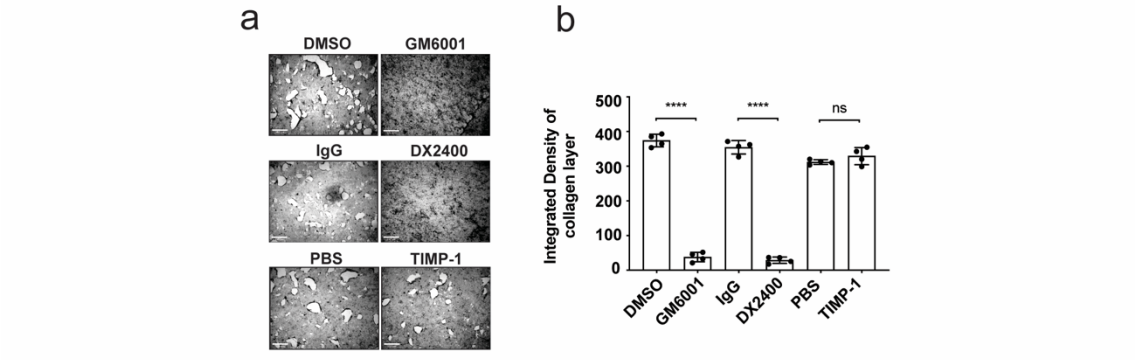


Figure 3.8: Gelatin film degradation is mediated by endogenous MT1-MMP in HT-1080 cells

a HT-1080 cells were subjected to collagen film degradation assay in the presence of GM6001 (10 μM), DX2400 (200 nM), TIMP-1 (200 nM) and the relative controls. Scale bars are 300 μm. **b** Quantification of the integrated density of the collagen layer in HT-1080 cells. Data are presented as mean of four independent microscopic fields of view and are representative of three independent experiments. One-way ordinary Anova with Tukey's multiple comparisons test. Error bards are SDs; **** $P < 0.0001$; ns: non-significant.

Cells were transfected with siRNAs targeting KIFs and after 48 hours they were re-seeded on a thin layer of fibrillar collagen type I and cultured for another 72 hours. Cells were then removed after extensive trypsinisation and remaining collagen was fixed and stained with Coomassie Blue. Collagen degradation was

quantified by Fiji as explained in Chapter 2 (Paragraph 2.8.4). As shown in Figure 3.9 a, silencing of *Kif13a*, *Kif3a* and *Kif1c* genes notably decreased collagen film degradation, compared to the control. On the contrary, KIF9 KD markedly enhanced the degradation of collagen. I plotted the average integrated densities of the collagen layer (Figure 3.9 b) and found that the differences described were all statistically significant. Thus, the effect of silencing these *kinesin* genes on the collagenolytic activity of HT-1080 cells was in line with what I observed for the gelatin film degradation assay.

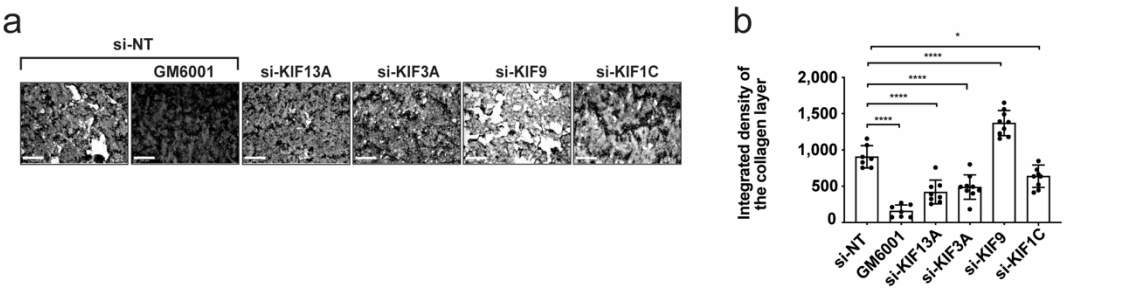


Figure 3.9: The KD of KIF13A, KIF3A, KIF9 and KIF1C alters MT1-MMP-mediated collagen film degradation in HT-1080 cells

a HT-1080 cells were transfected with siRNAs targeting the selected KIFs and subjected to collagen film degradation assay in the presence or absence of GM6001 (10 μM). Scale bars are 130 μm. **b** Quantification of the integrated density of the collagen layer in HT-1080 cells transfected with the specified siRNAs. Data are presented as the mean of eight independent microscopic fields of view and are representative of five independent experiments. One-way ordinary Anova with Tukey's multiple comparisons test. Error bars are SDs; **** $P < 0.0001$; * $P < 0.05$.

3.2.4 MT1-MMP-dependent proMMP-2 activation by HT-1080 cells is inhibited by KD of KIF13A, KIF3A, KIF1C and enhanced by KD of KIF9

Next, I tested the effect of silencing *Kif13a*, *Kif3a*, *Kif9* and *Kif1c* genes on proMMP-2 activation. ProMMP-2 activation can be induced by adding collagen type I (100 µg/ml) to the culture medium and analysed by subjecting supernatants to gelatin zymography. As shown in Figure 3.10 a, cells that were not stimulated with collagen type I failed to process proMMP-2 (P, 72 kDa) to lower-molecular-weight species, while collagen stimulation induced proMMP-2 conversion to its active form (A, 66 kDa). Gelatinolytic bands were quantified as described in Chapter 2 (Paragraph 2.5.5). Like gelatin and collagen film degradation assays, DX-2400 clearly inhibited proMMP-2 activation, suggesting that proMMP-2 activation is solely dependent on endogenous MT1-MMP in HT-1080 cells (Figure 3.10).

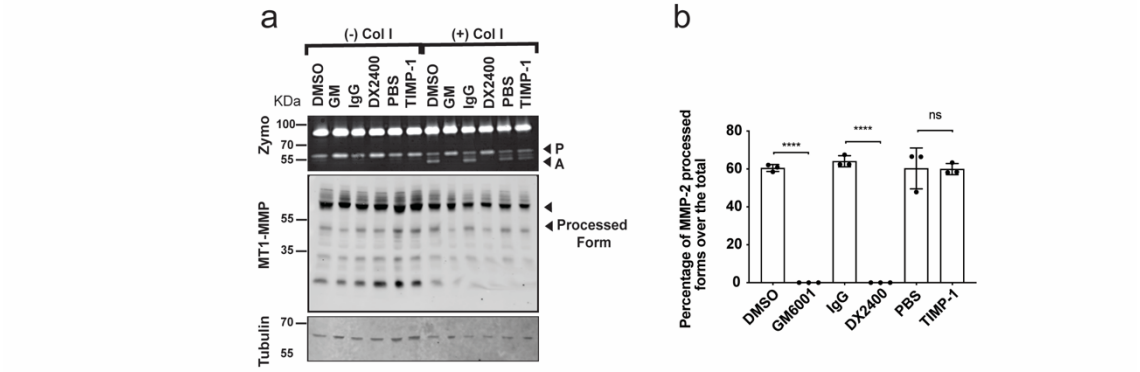


Figure 3.10: Pro-MMP-2 activation is only dependent on endogenous MT1-MMP in HT-1080 cells

a HT-1080 cells were cultivated in the presence or absence of collagen I (100 µg/ ml) and the above drugs for 24 h. Culture media from the assay were analysed by zymography (Zymo). P, pro-MMP-2; A, active MMP-2. Cell lysates were analysed by WB using the indicated antibodies. Arrow heads point bands of interest. **b** Quantification of the percentage of MMP-2 processed

forms over the total in HT-1080 cells, treated as specified above. Data are presented as mean of three blots representative of three independent experiments. One-way ordinary Anova with Tukey's multiple comparisons test. Error bars are SDs; **** P < 0.0001; ns: non-significant.

To examine the effect of knocking down these KIFs, HT-1080 cells were transfected with si-NT and siRNAs targeting these KIFs. After 48 hours, media were changed to serum-free DMEM with or without collagen type I (100 µg/ml). After 24 hours, media were recovered and subjected to gelatin zymography. As shown in Figure 3.11 a, media recovered from si-NT-transfected cells, not subjected to collagen stimulation, contained both proMMP-2 (P) and an intermediate form (68 KDa). The KD of KIF13A, KIF3A and KIF1C completely abolished the appearance of this intermediate form, while silencing *Kif9* gene enhanced processing of proMMP-2 to intermediate and active forms (Figure 3.11 a). Upon collagen stimulation, si-NT-transfected cells converted majority of the enzyme to its active form (A, 65 kDa). The KD of KIF13A and KIF3A significantly decreased this activation and KIF1C KD also seemed to moderately diminish it. On the other hand, silencing *Kif9* gene enhanced the production of MMP-2 active form in comparison to the control (Figure 3.11 a). Average percentages of proMMP-2 processed forms over the total were calculated and plotted, confirming that the differences discussed above were all statistically significant (Figure 3.11 b, c). Silencing these *kinesin* genes did not considerably alter the amount of pro or active MT1-MMP, when compared to the control (Figure 3.11 a) but it changed MT1-MMP processing to its autolytic form (45 kDa). As shown in Figure 3.11 d, the percentages of MT1-MMP autolytic form in si-KIF13A-, si-KIF3A- or si-KIF1C-transfected cells were significantly lower than the control. On the other hand, there was no statistically significant difference between si-KIF9- and si-NT-

transfected cells (Figure 3.11 d). Therefore, I concluded that the KD of KIF13A, KIF3A, KIF9 and KIF1C notably affected MT1-MMP-mediated cell functions on the cell surface.

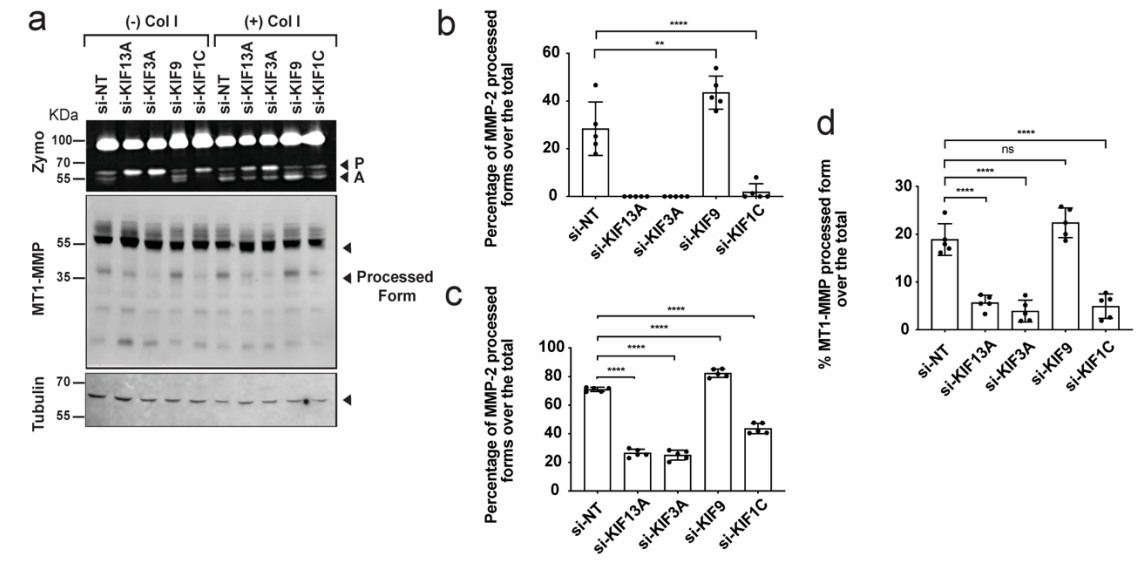


Figure 3.11: The KD of KIF13A, KIF3A, KIF9 and KIF1C alters MT1-MMP-mediated proMMP-2 activation and MT1-MMP processing

a HT-1080 cells transfected with the specified siRNAs were cultivated in the presence or absence of collagen I (100 µg/ ml) for 24 h. Culture media from the assay were analysed by zymography (Zymo). P, proMMP-2; A, active MMP-2. Cell lysates were analysed by WB using the indicated antibodies. Arrows point bands of interest. **b,c** Quantification of the percentage of MMP-2 processed forms over the total of HT-1080 cells transfected with the specified siRNAs and cultured in the presence or absence of collagen I. Data are presented as mean of five blots representative of eight independent experiments. One-way ordinary Anova with Tukey's multiple comparisons test. Error bars are SDs; **** $P < 0.0001$; ** $P < 0.01$. **d** Quantification of the percentage of MT1-MMP processed forms over the total. Data are presented as mean of five blots, representative of five independent experiments. One-way ordinary Anova with Tukey's multiple comparisons test. Error bars are SDs; **** $P < 0.0001$; ns: non-significant.

3.2.5 The KD of KIF13A, KIF3A, KIF9 and KIF1C does not affect MT1-MMP cell surface expression

To investigate whether the KD of these KIFs was altering MT1-MMP cell surface expression, I carried out cell surface biotinylation assay. HT-1080 cells were transfected with siRNAs targeting these KIFs and cell surface molecules were biotinylated with Sulfo-NHS-Biotin. Cells were lysed and lysates were incubated with streptavidin-conjugated beads to isolate biotinylated proteins that were subjected to WB using an anti-MT-Loop antibody. As shown in Figure 3.12 a, b, the KD of these four KIFs did not alter MT1-MMP cell surface expression. This result was confirmed by confocal microscopy. HT-1080 cells transfected with siRNAs targeting these four KIFs were stained for cell surface MT1-MMP and actin. As shown in Figure 3.12 c, d, the fluorescence intensity of MT1-MMP on the cell surface was not altered by silencing these *kinesin* genes. Hence, I hypothesized that the effects of the KD of these KIFs might be attributed to changes of MT1-MMP distribution to the cell-matrix interface.

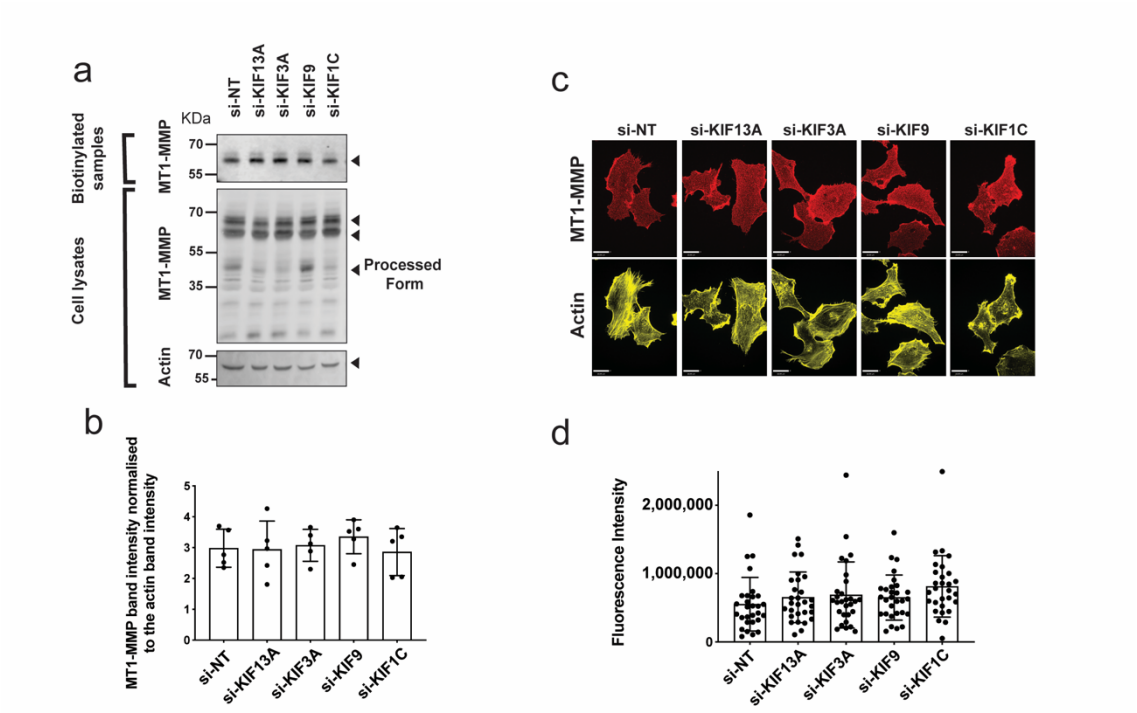


Figure 3.12: The KD of KIF13A, KIF3A, KIF9 and KIF1C does not affect the overall amount of MT1-MMP on the cell surface

a HT-1080 cells were transfected with siRNAs targeting the selected KIFs and subjected to surface biotinylation assay. Proteins eluted from the streptavidin beads were analysed by WB using anti-Loop MT1-MMP antibody. Whole cell lysates were analysed by WB using 1D8 anti MT1-MMP and anti actin antibodies. Arrows point bands of interest. **b** Quantification of the biotinylated sample blot in HT-1080 cells. Data are presented as mean of five blots, representative of five independent experiments. Error bars are SDs. **c** HT-1080 cells were transfected with siRNAs targeting the selected KIFs. After 72 hours, cells were stained with anti-MT-Loop MT1-MMP (red) antibody without permeabilisation and Alexa-568 Phalloidin to visualise actin (yellow) and they were imaged by confocal microscopy. Extended focus representative images of five independent experiments are shown. Scale bars are 22 µm. **d** Quantification of the overall cell surface MT1-MMP in HT-1080 cells. Data are presented as mean of the fluorescence intensities calculated for 30 cells. Error bars are SDs.

3.2.6 The KD of KIF13A, KIF3A and KIF9 alters MT1-MMP localisation to the cell matrix interface

To visualise MT1-MMP at the cell matrix interface, TIRF microscopy was employed. TIRF microscopy is an optical technique designed to image fluorescent molecules that are very close to a solid substance with a high refractive index like coverglass. The thickness of the excitation depth can be reduced to 100 nm (1/6 of confocal microscopy), increasing the resolution significantly and reducing the collection of out-of-focus light (242). HT-1080 cells transfected with siRNAs targeting these KIFs were fixed and stained for cell surface MT1-MMP with an anti-MT-Loop antibody and subjected to TIRF microscopy applying identical laser intensities to all samples. As shown in Figure 3.13 a, the KD of KIF13A and KIF3A noticeably reduced MT1-MMP fluorescence signal at the cell-matrix interface, while silencing *Kif9* gene increased it in comparison to the control. I confirmed that these results were statistically significant by measuring MT1-MMP fluorescence intensity in 30 cells for each treatment and calculating mean values (Figure 3.13 d). Interestingly, the KD of KIF1C did not change MT1-MMP localisation at the substrate-attachment cell side (Figure 3.13 a, b) when compared to the control. Nevertheless, MT1-MMP localisation at the cell matrix interface was significantly higher than when KIF13A was knocked down, and lower than when *Kif9* gene was silenced (Figure 3.13 a. b).

To confirm that knocking down these four KIFs was not impairing cell attachment to the gelatin-coated coverglass, HT-1080 cells transfected with siRNAs targeting these KIFs were stained for β1 integrin with an anti-β1 integrin antibody and subjected to TIRF microscopy applying identical laser intensities to

all samples. As shown in Figure 3.13 c, the fluorescence intensity of β1 integrin at the substrate-attachment side was not altered. Along with TIRF imaging of HT-1080 cells stained for β1 integrin, interference reflection microscopy (IRM) was employed to monitor overall cell adherence to the coverglass. IRM uses interference patterns generated by the thin spaces between coverglass and the apposed cell membrane. This technique was first applied to cell biology in 1964 by Curtis (243) and it is still extensively used to study processes that happen close to the cell membrane, without employing fluorescence. As shown in Figure 3.13 c, d, IRM data confirmed that silencing these four *kinesin* genes did not alter cell attachment to the substratum. Therefore, I concluded that the KD of these KIFs altered MT1-MMP localisation at the cell-matrix interface without impairing cell attachment to the substratum.

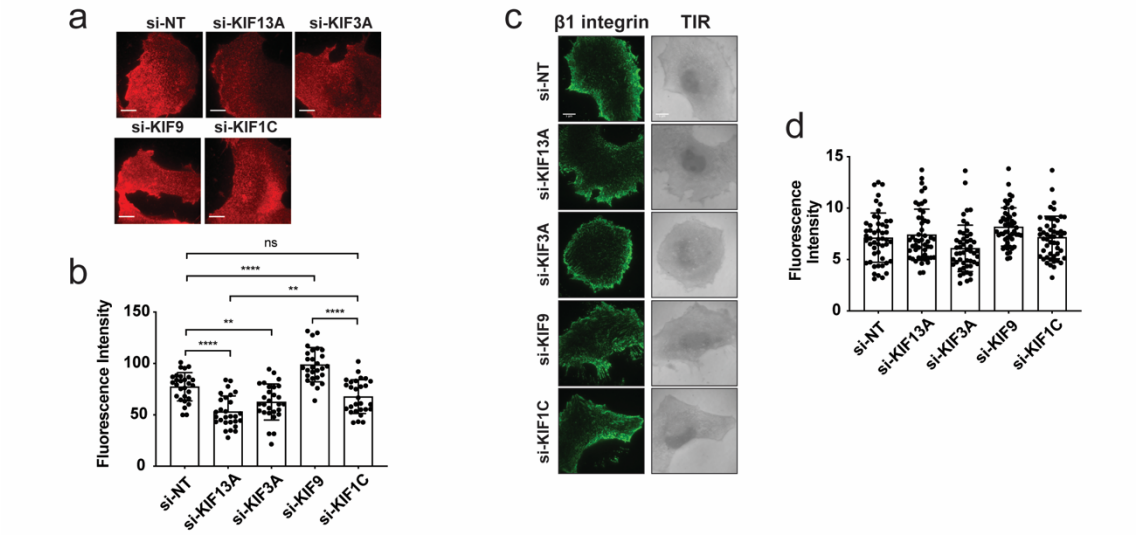


Figure 3.13: The KD of KIF13A, KIF3A, KIF9 and KIF1C modifies MT1-MMP localisation at the substrate-attachment side

a HT-1080 cells were transfected with siRNAs targeting the selected KIFs. After 72 hours, cells were stained with anti-β1 integrin (green) antibody without permeabilisation and they were imaged by TIRF microscopy. Representative images of three independent experiments are shown. Scale

bars are 10 μm. **b** Quantification of MT1-MMP expression at the substrate-attachment side in HT-1080 cells. Data are presented as mean of the fluorescence intensities calculated for 30 cells. One-way ordinary Anova with Tukey's multiple comparisons test. Error bars are SDs; **** $P < 0.0001$; ** $P < 0.01$; ns: non-significant. **c** HT-1080 cells were transfected with siRNAs targeting the selected KIFs. After 72 hours, cells were stained with anti-β1 integrin (green) antibody without permeabilisation and they were imaged by TIRF and IRM microscopies. Representative images of three independent experiments are shown. Scale bars are 10 μm. **d** Quantification of β1 integrin expression at the substrate attachment side in HT-1080 cells. Data are presented as mean of the fluorescence intensities of 30 cells. Error bars are SDs.

3.2.7 The KD of KIF13A, KIF3A and KIF9 affects MT1-MMP-mediated cell invasion through a microporous membrane

Transwell collagen invasion assay was employed to test whether the KD of these KIFs was affecting MT1-MMP-mediated cell invasion though a microporous membrane. The assay was carried out as previously described in Chapter 2 (Paragraph 2.10). The microporous membrane of transwell plastic inserts was coated with a thin layer of collagen type I and was intended to mimic the basement membrane that cancer cells encounter during the process of invasion. The collagen-coated transwells were placed into the wells of a 24-well plate, filled with DMEM supplemented with FBS, that acted as chemoattractant. HT-1080 cells transfected with siRNAs targeting these KIFs were re-suspended in serum-free DMEM and re-seeded on the upper compartment of the transwell. After 18 hours, cells remained on top of the insert were removed, while those that had migrated to the other side were fixed and stained with DAPI. Invaded cells were imaged by wide-field microscopy and counted. I confirmed that in HT-1080 cells, invasion through the thin layer of collagen was only attributed to

endogenous MT1-MMP. As shown in Figure 3.14, transwell invasion is completely abolished when cells are cultured in the presence of GM6001 or DX2400, while it is not affected by TIMP-1. As indicated in Figure 3.15, I found that the number of invaded cells was significantly diminished when cells were transfected with si-KIF13A or si-KIF3A than when they were transfected with si-NT. On the other hand, KD of KIF9 considerably augmented HT-1080 cell invasiveness in comparison to the control. Silencing KIF1C did not alter MT1-MMP-dependent invasion through the collagen.

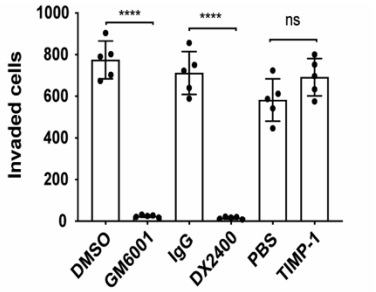


Figure 3.14: Transwell invasion is only dependent on endogenous MT1-MMP in HT-1080 cells

HT-1080 cells were subjected to transwell invasion assay in the presence of GM6001 (10 μM), DX2400 (200 nM), TIMP-1 (200 nM) and relative control solutions. MT1-MMP-dependent cell invasion was quantified. Data are presented as mean of the number of cells migrated through six transwells for each treatment and are representative of three independent experiments. Error bars are SDs; **** $P < 0.0001$; ns: non-significant.

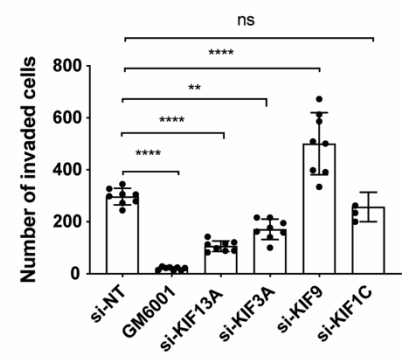


Figure 3.15: The KD of KIF13A, KIF3A, KIF9 and KIF1C alters MT1-MMP-dependent transwell invasion

HT-1080 cells were subjected to transwell invasion assay using Boyden chambers, in the presence or absence of GM6001 (10 μM) and the MT1-MMP-dependent cell invasion was quantified. Data are presented as mean of the number of cells migrated through six transwells for each treatment and are representative of three independent experiments. Error bars are SDs; **** $P < 0.0001$; ** $P < 0.01$; ns: non-significant.

3.2.8 The KD of KIF13A, KIF3A, KIF9 and KIF1C diminishes MT1-MMP-dependent cell migration in 3D collagen

Microcarrier beads invasion assay was carried out to investigate whether the KD of these KIFs had an effect on HT-1080 cells' ability to migrate through a 3D collagen gel. Cells were allowed to attach to gelatin-coated beads for 7 hours. Cell-coated beads were then suspended in collagen type I and incubated for 18 hours to let cells migrate from the surface of the beads into the collagen matrix. Migrated distances were calculated and mean values were plotted as described in Chapter 2 (Paragraph 2.11.3). Firstly, I checked if the migratory mode of HT-1080 cells through the collagen matrix was only MT1-MMP-dependent. As showed in Figure 3.16, migration of HT-1080 cells was almost completely abolished in the presence of GM6001 or DX2400, while it was not significantly

altered by TIMP-1. Hence, I concluded that HT-1080 cell migration through the collagen matrix was entirely dependent on the endogenous MT1-MMP.

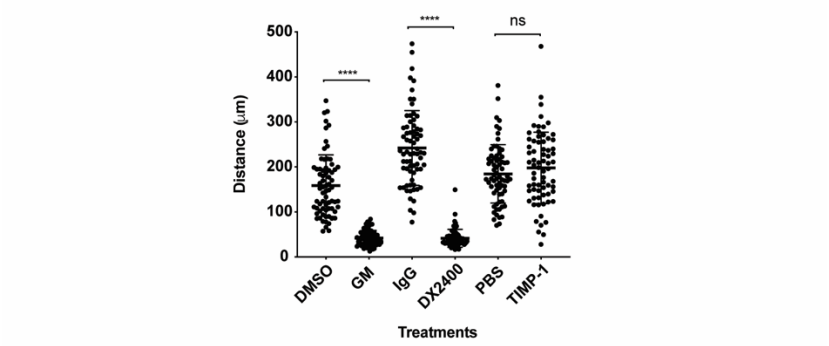


Figure 3.16: Cell migration through 3D collagen is only dependent on endogenous MT1-MMP

HT-1080 cells were subjected to beads invasion assay in the presence of GM6001 (10 μM), DX2400 (200 nM), TIMP-1 (200nM) and relative control solutions. Quantification of beads invasion assay by HT-1080 cells. Data are presented as mean of the distance migrated by 100 cells for each treatment and are representative of three independent experiments. One-way ordinary Anova with Tukey's multiple comparisons test. Error bars are SDs; **** $P < 0.0001$; ns: non-significant.

HT-1080 cells transfected with siRNAs targeting these KIFs were subjected to this assay. As illustrated in Figure 3.17, silencing *Kif13A*, *Kif3A* and *Kif1C* genes significantly decreased HT-1080 cells migration in comparison to the control. Surprisingly, even si-KIF9-transfected cells migrated considerably less than si-NT transfected ones.

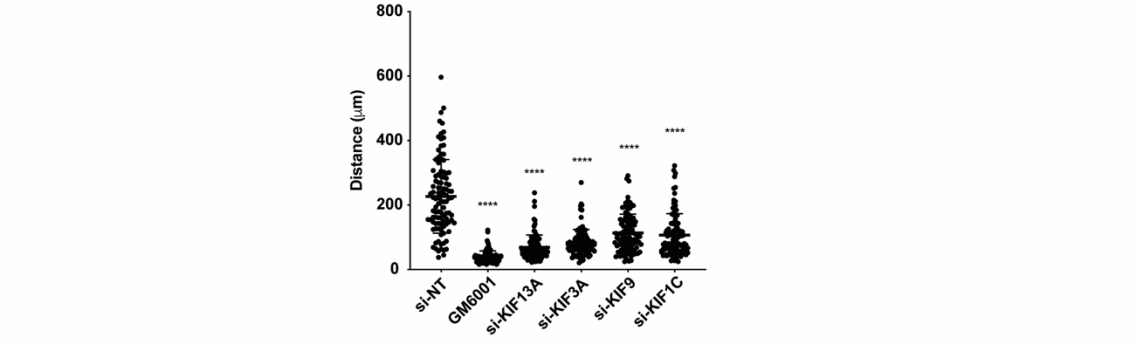


Figure 3.17: The KD of KIF13A, KIF3A, KIF9 and KIF1C diminishes MT1-MMP-dependent cell migration in 3D collagen

HT-1080 cells were transfected with siRNAs targeting the selected KIFs and subjected to beads invasion assay in the presence or absence of GM6001 (10 μM). Data are presented as mean of the distance migrated by 100 cells for each treatment and are representative of three independent experiments. One-way ordinary Anova with Tukey's multiple comparisons test. Error bars are SDs; **** $P < 0.0001$.

To assess whether silencing these *kinesin* genes was not impairing basic mechanisms of cell locomotion, a wound healing assay was performed on plastic. HT-1080 cells transfected with siRNAs targeting these four KIFs were used to fill the two reservoirs of culture inserts and incubated until confluent. Then, the culture inserts were removed and the cells were let migrate into the gap for 6 hours. As shown in Figure 3.18 a, the final wound gap observed for cells transfected with siRNAs targeting KIF13A, KIF3A and KIF9 was not notably different to that of control cells. To confirm these results, I calculated the percentage of wound closure for each condition, as previously explained in Chapter 2, and verified that there was no statistically significant difference between control and si-KIF13A-, si-KIF3A-, si-KIF9-transfected cells (Figure 3.18 b). On the other hand, the percentage of wound closure calculated for HT-1080 cells transfected with si-KIF1C was relatively lower than the control ($P = 0.019$).

Thus, these data suggest that the KD of KIF13A, KIF3A and KIF9 has no effect on the cell migration machinery, but influences MT1-MMP-dependent cell migration through a 3D collagen matrix.

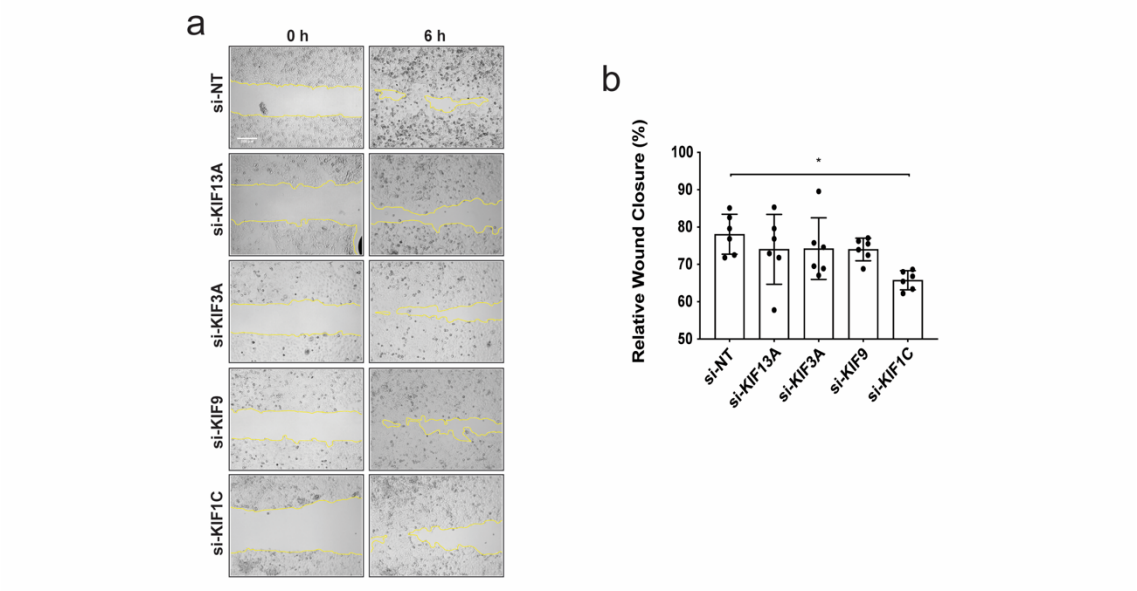


Figure 3.18: The KD of KIF13A, KIF3A, KIF9 and KIF1C does not affect wound closure

a HT-1080 cells were transfected with siRNAs targeting the selected KIFs and subjected to wound healing assay on plastic. Images of 0 h and 6 h time points are shown. Images are representative of three independent experiments. Yellow lines highlight the migration front. Scale bar is 200 μm. **b** Quantification of wound healing assay by HT-1080 cells. Data are presented as mean of the percentage of wound closure relative to the initial gap area. Error bars are SDs; * $P < 0.05$.

3.2.9 MT1-MMP-dependent collagen film degradation by RASFs is inhibited by KD of KIF13A, KIF3A, KIF1C and enhanced by KD of KIF9

Next, I investigated whether these four KIFs could have a role in MT1-MMP intracellular trafficking in human rheumatoid arthritis synovial fibroblasts (RASFs) as RASFs' invasion is MT1-MMP-dependent (24). RASFs from three

different donors were transfected with siRNAs targeting these four KIFs and subjected to collagen film degradation assay as described in Chapter 2 (Paragraph 2.8). As illustrated in Figure 3.19 a, KIF13, KIF3A and KIF1C KD notably diminished the degradation of the collagen matrix by RASFs, while silencing *Kif9* gene enhanced collagenolysis. These results were quantified measuring the integrated density of the collagen layer and mean values were plotted in Figure 3.19 b. There were statistically significant differences between the collagenolytic activity of targeting siRNA-transfected cells and the control. Therefore, these four KIFs are likely to play a role in transporting MT1-MMP-containing vesicles in RASFs as in HT-1080 cells.

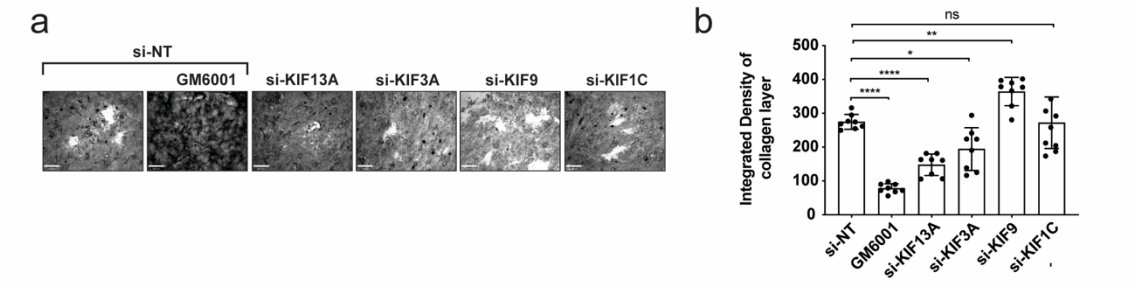


Figure 3.19: The KD of KIF13A, KIF3A, KIF9 and KIF1C alters MT1-MMP-mediated collagen film degradation by RASFs

a RASFs were transfected with siRNAs targeting the selected KIFs and subjected to collagen film degradation assay in the presence or absence of GM6001 (10 μM). Scale bars are 130 μm. **b** Quantification of the integrated density of the collagen layer in RASFs transfected with the specified siRNAs. Data are presented as mean of eight independent microscopic fields of view and are representative of five independent experiments. One-way ordinary Anova with Tukey's multiple comparisons test. Error bars are SDs; **** $P < 0.0001$; ** $P < 0.01$; * $P < 0.05$; ns: non-significant.

3.2.10 MT1-MMP-dependent gelatin film degradation by MDA-MB-231 cells is not affected by KD of KIF13A, KIF3A, KIF9 and KIF1C

Given the potential role played by these KIFs in MT1-MMP intracellular trafficking in HT-1080 fibrosarcoma cells and RASFs, I decided to investigate their function in MDA-MB-231 cells. MDA-MB-231 is a triple negative human breast cancer (TNBC) cell line that lacks expression of receptors for progesterone, oestrogen and human epidermal growth factor receptor 2 (HER2). MDA-MB-231 cells are de-differentiated epithelial cancer cells, highly aggressive and invasive. It has been extensively shown that MDA-MB-231 cells use MT1-MMP for their invasion by localising the enzyme at the invadopodia structure (88, 93, 111). MDA-MB-231 were transfected with siRNAs targeting these four KIFs and subjected to gelatin film degradation assay. The efficiency of silencing was confirmed by RT-PCR and WB (Figure 3.20 a, b). As shown in Figure 3.21 a, MDA-MB-231 cells transfected with si-NT showed typical invadopodia-dependent gelatin film degradation. Interestingly, cells transfected with siRNAs targeting KIFs showed similar gelatinolytic activity (Figure 3.21 a, b). KIF5B had been previously reported to associate with MT1-MMP-containing vesicles in MDA-MB-231 cells (210, 211), thus I investigated the effect of KIF5B KD. As illustrated in Figure 3.21 a, b, silencing *Kif5b* gene did not show any effect on the gelatinolytic capacity of MDA-MB-231 cells. In conclusion, MDA-MB-231 cells do not seem to employ KIF13A, KIF3A, KIF9, KIF1C or KIF5B to traffic MT1-MMP-containing vesicles to the cell surface.

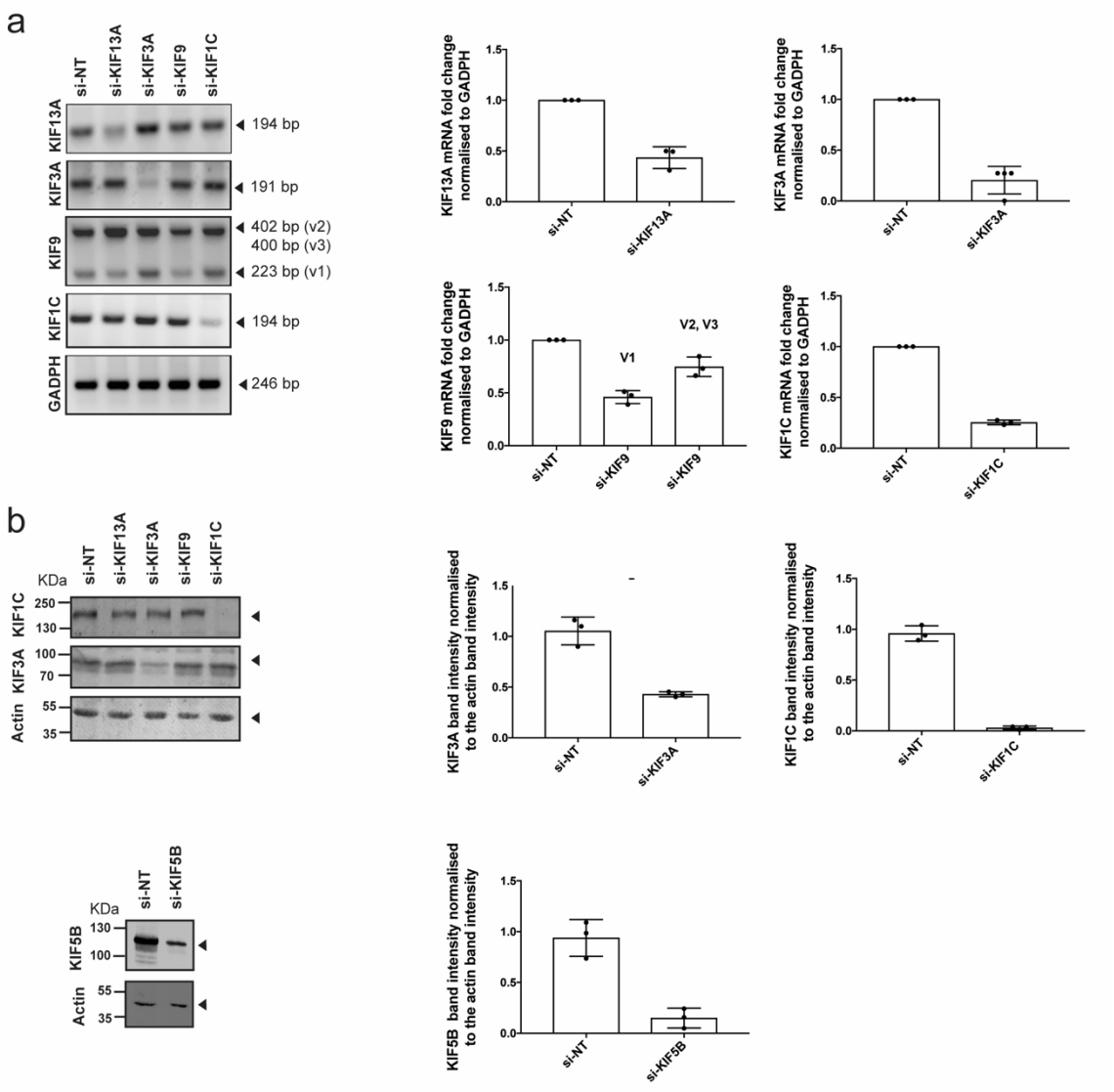


Figure 3.20: Efficiency of KIF KD in MDA-MB-231 cells

a Efficiency of KIF KD by one-step RT-PCR. Quantification of KIF13A, KIF3A, KIF9 and KIF1C mRNAs relative to GADPH mRNA. The data are representative of three independent experiments. **b** Efficiency of KIF3A and KIF1C KD by WB. MDA-MB-231 cells were transfected with siRNAs targeting the selected KIFs. Cell lysates were analysed by WB, using the indicated antibodies. Arrow heads point bands of interest. Quantification of the intensity of KIF3A, KIF1C and KIF5B protein bands relative to actin.

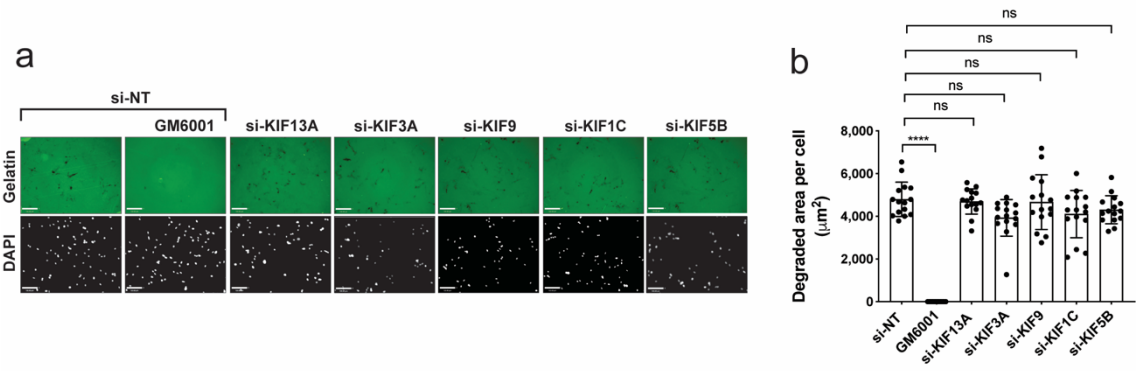


Figure 3.21: The KD of KIF13A, KIF3A, KIF9, KIF1C and KIF5B does not affect MT1-MMP-mediated gelatin film degradation by MDA-MB-231

a MDA-MB-231 cells were transfected with siRNAs targeting the selected KIFs and subjected to gelatin film degradation in the presence or absence of GM6001 (10 µM). Scale bars are 130 µm. **b** Quantification of the degradation area (μm^2) per cell in MDA-MB-231 cells transfected with the specified siRNAs. Data are presented as the mean of 15 independent microscopic fields of view and are representative of five independent experiments. One-way ordinary Anova with Tukey's multiple comparisons test. Error bars are SDs; **** $P < 0.0001$; ns: non-significant.

3.2.11 MT-Loop region is dispensable for efficient MT1-MMP-dependent gelatin film degradation by MDA-MB-231 cells

Since MDA-MB-231 cells seemed to use different KIFs to localise MT1-MMP to invadopodia, I next examined the effect of MT-Loop deletion on MT1-MMP-mediated gelatin film degradation in this cell line. MT-Loop is an eight-amino-acid loop present in the catalytic domain of MT1-MMP, that is required for the enzyme to localise to the cell adhesion complex in different cell types including HT-1080, COS-7, squamous carcinoma (A431) and HeLa cells (112). In these cells, deletion of MT-Loop region significantly reduces MT1-MMP degrading capacity against gelatin and collagen. MDA-MB-231 and COS-7 cells were transfected with FLAG-tagged MT1-MMP (MT1-F) and MT-Loop deleted

MT1-F (ΔLoop MT1-F) and after 48 hours they were re-seeded on Alexa 488-labelled gelatin film and incubated for 4 hours. Cells were fixed and stained with anti-FLAG antibody, Alexa 568 Phalloidin and DAPI to respectively visualise actin and nuclei. Samples were imaged by confocal microscopy applying identical laser intensities to all samples. As indicated in Figure 3.22, when COS-7 cells expressing similar levels of MT1-F and ΔLoop MT1-F were compared, ΔLoop MT1-F-expressing cells did not degrade gelatin in an efficient manner, as previously reported (112). On the other hand, ΔLoop MT1-F-expressing MDA-MB-231 cells degraded gelatin as efficiently as the MT1-F-expressing ones. MDA-MB-231 cells express endogenous MT1-MMP. Nevertheless, these cells were incubated on gelatin for only 4 making the degradation only dependent on the exogenously expressed proteinase. These data indicate that MT-Loop region was dispensable for MT1-MMP-dependent gelatin film degradation in MDA-MB-231 cells.

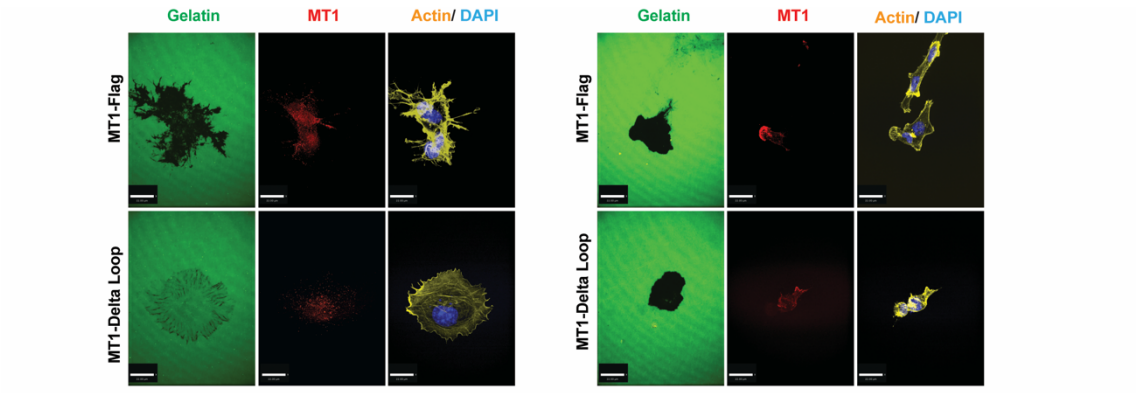


Figure 3.22: MT1-Loop region is not required for efficient MT1-MMP mediated gelatin film degradation by MDA-MB-231

MDA-MB-231 cells and COS-7 cells were transfected with MT1-F and ΔLoop MT1-F and they were subjected to gelatin film degradation. Incubation on the gelatin film lasted 4 hours. Cells

were stained with anti-FLAG antibody, phalloidin and DAPI. Gelatin is shown in green, MT1-F is red, actin is yellow and nuclei are blue. Scale bars are 22 μm.

3.3 Discussion

Localisation of MT1-MMP to the leading edge is a crucial step to promote cell migration and invasion (244). Precise mechanisms that regulate MT1-MMP cell surface exposure are still largely unknown and have been attracting growing interest from the scientific community in the last decade. Dr. Itoh's research group and others have shown a close interaction of MT1-MMP with microtubules in fixed specimens (Chapter 1, Paragraph 1.5) (209) and that MT1-MMP positive vesicles actively travel along microtubules (Chapter 1, Paragraph 1.5) (108). Studies on primary human macrophages have also shown that MT1-MMP trafficking along microtubules is powered by KIFs, in particular by KIF5B, KIF3A/3B (108). Studies in Dr. Itoh's research group analysed the possible involvement of 17 different human KIFs in MT1-MMP intracellular trafficking in HT-1080 cells. The effects of the KD of these selected KIFs in HT-1080 cells were evaluated by analysing MT1-MMP-dependent gelatin film degradation. It was found that the KD of four KIFs (KIF13A, KIF3A, KIF9 and KIF1C) noticeably affected MT1-MMP-dependent gelatin film degradation. Studies presented in this Chapter aimed to characterise the role of KIF13A, KIF3A, KIF9 and KIF1C in MT1-MMP cell surface exposure and MT1-MMP-dependent cellular invasion.

Silencing *Kif13a*, *Kif3a*, *Kif9* and *Kif1c* genes was confirmed to markedly alter MT1-MMP-mediated gelatin film degradation. The KD of KIF13A, KIF3A and KIF1C reduced MT1-MMP-mediated gelatin film degradation, while the KD of KIF9 increased the gelatinolytic activity. Unexpectedly, overexpression of these

KIFs tagged with GFP did not alter MT1-MMP-mediated gelatin film degradation. MT1-MMP intracellular trafficking most likely involves the activity of multiple KIFs, which may compete with each other or work together to deliver the proteinase to the cell surface. Consequently, increasing the amount of one motor protein does not necessarily mean that there will be more or less proteinase to be transported to the cell surface. Moreover, very little is known about how KIFs recognise MT1-MMP-containing vesicles and whether there is competition for a limited number of binding sites or adaptor molecules. The effects of the KD of these KIFs in HT-1080 cells were further evaluated by analysing other MT1-MMP-dependend proteolytic activities at the cell surface, including collagen degradation and proMMP-2 activation. Collagen film degradation was significantly altered by silencing these *kinesin* genes: the KD of KIF13A, KIF3A and KIF1C diminished degradation of the collagen film, while silencing *Kif9* gene enhanced it. Similarly, the KD of KIF13A, KIF3A and KIF1C noticeably reduced proMMP-2 activation whereas silencing *Kif9* gene increased it. TIMP-2 is necessary for MT1-MMP to carry out proMMP-2 activation on the cell surface (245). Hence, the effects of silencing these *kinesin* genes on proMMP-2 activation could be a consequence of an altered trafficking of TIMP-2 to the cell surface. The KD of these KIFs did not change the amount of pro or active MT1-MMP but it significantly modified MT1-MMP processing to 44 - 45 kDa species. MT1-MMP processing to lower-molecular-weight species is known to be attributed to MT1-MMP itself or active MMP-2 and to regulate MT1-MMP proteinase activity on the cell surface (68, 78, 79). Therefore, it was not surprising to notice that KIF13A, KIF3A and KIF1C KDs decreased the production of 44 - 45 kDa MT1-MMP, whereas silencing *Kif9* gene enhanced MT1-MMP processing. I hypothesised that the effects on MT1-MMP

processing to lower molecular mass species by either MT1-MMP itself or active MMP-2 were a response to the alterations of MT1-MMP functional activities on the cell surface.

Given that the KD of these selected KIFs noticeably and consistently affected several MT1-MMP-dependent functions on the cell surface, I postulated that cell surface expression of MT1-MMP might have been altered. Surprisingly, cell surface biotinylation and confocal imaging of HT-1080 cells stained for cell surface MT1-MMP showed that silencing these *kinesin* genes did not cause any change to the overall level of MT1-MMP on the cell surface. Interestingly, TIRF imaging of HT-1080 cells stained for cell surface MT1-MMP, revealed that KIF13A and KIF3A KDs diminished MT1-MMP localisation at the substrate-attached cell side, whereas silencing *Kif9* gene augmented it. KIF1C KD did not alter MT1-MMP localisation at the cell-matrix interface, suggesting that this motor protein might have not been directly involved in MT1-MMP intracellular trafficking. Lower MT1-MMP levels at the cell-matrix interface support the decrease in MT1-MMP-dependent gelatinolytic and collagenolytic activities; likewise, increased MT1-MMP-dependent gelatin and collagen film degradation by HT-1080 cells, upon KIF9 KD, was explicated by a higher expression of the proteinase at the substrate attachment sites.

ProMMP-2 activation on the cell surface occurs as a result of multi-molecular interactions. MT1-MMP forms a homo-dimeric complex on the cell surface and TIMP-2 binds and inhibits one of the MT1-MMP molecules by interacting through its N-terminal inhibitory domain with the catalytic domain of the proteinase (90). The C-terminal domain of TIMP-2 in the complex is exposed and has affinity to proMMP-2 hemopexin domain, thus forming a proMMP-2-

TIMP-2-$(MT1\text{-}MMP)_2$ ternary complex. Finally, the MT1-MMP within the complex, free from TIMP-2, cleaves proMMP-2 pro-peptide and triggers the activation (90, 246). ProMMP-2 activation requires MT1-MMP homo-dimerisation but it is not exactly known how the activation process is spatially regulated on the cell surface and whether it only occurs at the leading edge of migrating cells, or at the substrate attachment sites (90, 246). It has been shown that MT1-MMP dimerisation is a dynamic event that consistently occurs at the leading edge and not at the trailing edge of cells migrating in 3D collagen matrices (92). Moreover, it has been found that the expression of constitutively active Rac1 increases proMMP-2 activation at the ruffling membrane structures, without affecting MT1-MMP cell surface expression (90). Our results showed that proMMP-2 activation was affected by the KD of these KIFs, even though MT1-MMP cell surface level was not changed. I speculated that alterations to proMMP-2 activation were caused by change in MT1-MMP cell surface localisation at the substrate attachment sites and thus to MT1-MMP homo-dimeric complex formation. Therefore, I speculate that proMMP-2 activation mostly occurs at the leading edge of cells, where matrix degradation takes place.

2D cell cultures may not accurately resemble cell-cell and cell-extracellular matrix interactions in tissues, whereas 3D culture methods expose cells to an environment that better mimic conditions *in vivo*. Transwell invasion and microcarrier beads invasion assays were chosen to mimic cells breaching through a matrix barrier and migrating through collagen matrices respectively. Transwell invasion assay showed that the KD of KIF13A and KIF3A decreased MT1-MMP-dependent invasion through the collagen-coated microporous membrane, while KIF9 KD increased it. In this assay, cells form a monolayer and

they degrade collagen to breach through the porous membrane employing MT1-MMP at the cell-collagen interface. Therefore, it is not surprising that these data are consistent with what it was observed for gelatin or collagen type I degradation under 2D culture conditions. Silencing *Kif1c* gene did not affect MT1-MMP-mediated invasion, confirming that this KIF may not be directly involved in MT1-MMP intracellular trafficking. Microcarrier beads invasion assay indicated that the KD of all of these KIFs diminished MT1-MMP-mediated migration through 3D collagen. Hence, KIF13A and KIF3A were proved to have a positive role in MT1-MMP-dependent cellular functions. Unexpectedly, silencing *Kif9* gene also diminished MT1-MMP-dependent migration through collagen in a significant manner. Cells cultured in 3D collagen matrices encounter an environment totally different from what they experience on the commonly used 2D surfaces. Therefore, their morphologies range from dendritic, to stellate to bipolar depending on the matrix stiffness (247), rather than being characterised by lamellar and flattened extensions like lamellipodia. On 2D surfaces, cells have a forced asymmetry, exemplified by a top and a bottom side, through which they form integrin-dependent adhesion contacts as focal adhesions (248). In 3D matrices, there are a limited number of adhesion sites accessible to cells, that interact through integrin-mediated 3D cell matrix-interactions and are subjected to a change in mechanical stability due to matrix-entanglement (247). Consequently, it is not surprising that the KD of KIF9 enhances MT1-MMP-dependent cellular functions when HT-1080 cells are cultured atop of 2D surfaces, whereas it diminishes MT1-MMP-mediated migration through 3D collagen. KIF1C KD also decreased MT1-MMP-mediated 3D migration of HT-1080 cells. Previous studies have found that KIF1C transports α5β1-integrins to

the trailing edge of human epithelial cells, stabilising cell tails and supporting forward movement (231). I speculated that KIF1C was playing a similar role in HT-1080 cells and thus its KD caused significantly less 3D migration. This hypothesis was supported to an extent by performing a wound-healing assay on HT-1080 cells: the percentage of wound closure of si-KIF1C-transfected cells was significantly lower than the control.

As observed for HT-1080 cells, silencing *Kif13a*, *Kif3a* and *Kif1c* genes decreased collagenolytic activity of RASFs, while the KD of KIF9 enhanced the degradation of underlying collagen. I speculated that MT1-MMP trafficking machinery in RASFs might employ the same motors as HT-1080 cells. It has been previously reported that RASFs express high levels of MT1-MMP and that this proteinase has a key role in promoting synovial invasion by its collagenolytic activity (24). Therefore, MT1-MMP intracellular trafficking by KIFs has a great importance for the understanding of RA pathogenesis. Unfortunately, I did not have sufficient time to investigate the effect of silencing these *kinesin* genes on other MT1-MMP-dependent cellular functions but this analysis will be done in the future.

In contrast with RASFs, MDA-MB-231 cells seemed to utilise different motor proteins to bring MT1-MMP to the cell surface. In fact, the KD of KIF13A, KIF3A, KIF9 and KIF1C did not have any effect on MT1-MMP-dependent gelatin film degradation. KIF3A has been previously reported to associate with MT1-MMP-positive vesicles in MDA-MB-231 cells (211). Moreover, its KD has been reported to reduce MT1-MMP-dependent gelatin film degradation and invasion through collagen type I (211). Our data did not confirm that silencing *Kif3a* gene had a negative effect on MDA-MB-231 cells' gelatinolytic activity. On average, si-

KIF3A-transfected MDA-MB-231 cells had a lower gelatinolytic activity than the control but the difference was not statistically significant (P = 0.08). As previously described in Chapter 2, gelatin film degradation by MDA-MB-231 cells was run for 15 hours and gelatinolytic activity was quantified on images acquired with a wide-field microscope equipped with a 10X objective. Marchesin et al. (211) reported to run the assay for only 4 hours and quantified gelatin degradation on images captured with a confocal microscope equipped with a 63X objective. It is likely that incubating MDA-MB-231 cells on gelatin for 15 instead of 4 hours flattened the differences between the gelatinolytic capacity of si-KIF3A-transfected cells and of si-NT-transfected ones. More experiments would be needed to further assess the role of KIF3A in MT1-MMP intracellular trafficking in MDA-MB-231 cells. KIF5B was also reported to have a role in MT1-MMP cell surface exposure in MDA-MB-231 cells (211). Authors found that KIF5B KD diminished MT1-MMP-dependent gelatin film degradation and migration through 3D collagen by MDA-MB-231 cells (211). My data did not again confirm that KIF5B KD suppressed MT1-MMP-dependent gelatin film degradation. Unfortunately, I did not have sufficient time to investigate further about KIF5B involvement in MT1-MMP cell surface exposure. Anyway, it is highly likely MT1-MMP intracellular trafficking machinery in MDA-MB-231 cells is different than other cell types like HT-1080 cells. MT-Loop region has been demonstrated to be crucial for efficient MT1-MMP-dependent proteolytic activities in HT-1080, COS-7, HeLa and A431 cells (112). Nevertheless, I found that MT-Loop region was dispensable for MDA-MB-231 cells to efficiently degrade the underlying gelatin film. MT-Loop was found to be important for its association with β1 integrin-containing cell adhesion complexes in the cell lines mentioned above (112).

Since MDA-MB-231 cells degrade gelatin film exclusively at the invadopodia, I hypothesised that the mechanism of MT1-MMP localisation at these was different.

This Chapter aimed to characterise KIFs involved in MT1-MMP intracellular trafficking. My data showed that MT1-MMP cell surface exposure is regulated by multiple KIFs. I hypothesise that when HT-1080 cells are cultured atop of a substratum, like gelatin or collagen, KIF13A and KIF3A potentially transport MT1-MMP-containing vesicles to substrate attachment sites (Figure 3.23 a). On the other hand, KIF9 may carry these vesicles to areas distinct from substrate attachment sites (Figure 3.23 a). In all likelihood, the KD of KIF9 increases MT1-MMP-mediated cellular functions, simply because there are more MT1-MMP-containing vesicles free to be carried to the substrate attachment sites by KIF13A and KIF3A. Therefore, I postulate that different kinesin-mediated trafficking pathways compete with each other. When one pathway is switched off, MT1-MMP-containing vesicles may be recognised and transported by another. When HT-1080 cells are embedded in 3D collagen, KIF13A, KIF3A and KIF9 carry MT1-MMP to the leading edge, mediating MT1-MMP-dependent 3D migration (Figure 3.23 b).

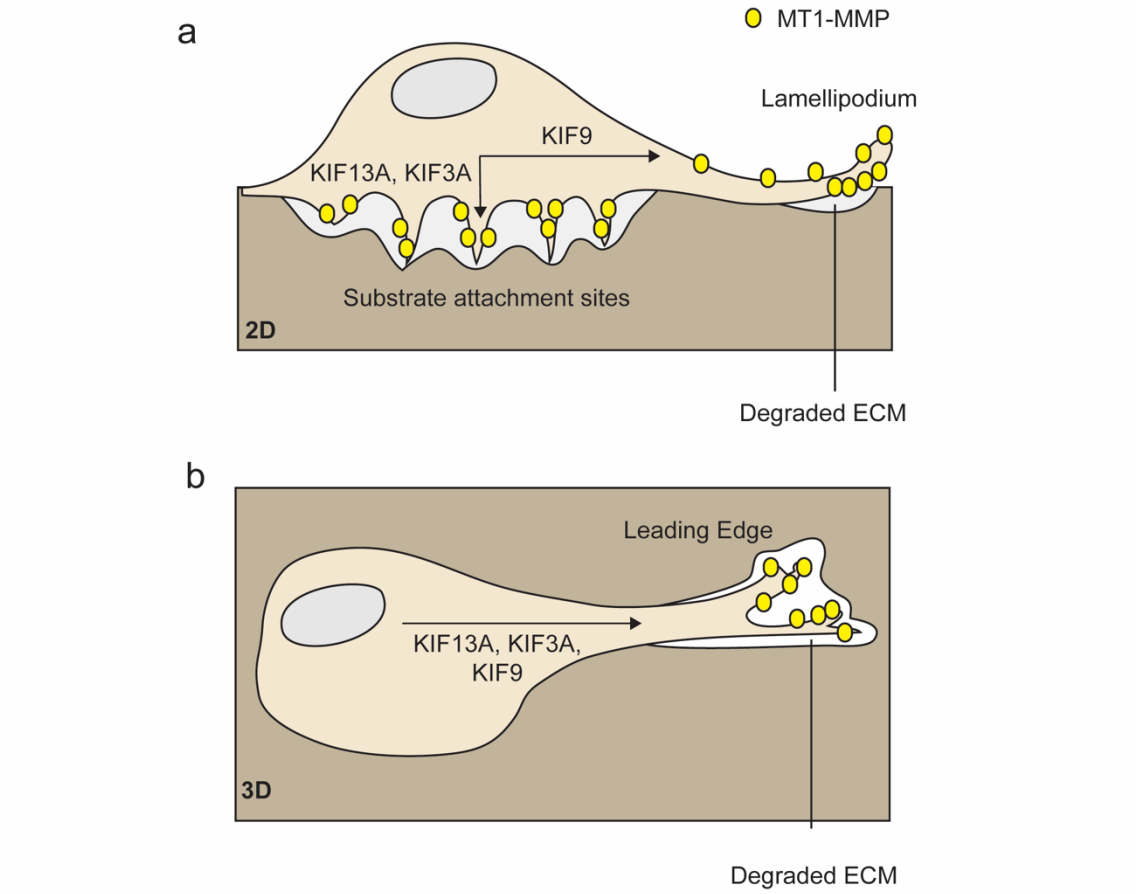


Figure 3.23: Multiple KIFs regulate MT1-MMP intracellular trafficking

a When cells are cultured atop a 2D surface KIF13A and KIF3A potentially transport MT1-MMMP to the substrate attachment sites, while KIF9 may traffic the proteinase to different areas like the lamellipodium. **b** When cells are embedded in a 3D matrix like collagen, KIF13A, KIF3A and KIF1C may all transport MT1-MMP to the leading edge.

In future experiments, it will be important to better investigate the role of KIF13A, KIF3A and KIF9 in MT1-MMP intracellular trafficking in RASFs. It would be interesting to test the effect of silencing *Kif13a*, *Kif3a* and *Kif9* genes on RASFs invasion and migration employing transwell invasion and microcarrier beads invasion assays. Very little is known about the mechanisms that MDA-MB-231 cells employ to localise MT1-MMP to the cell-matrix adhesion. Hence, it

would be crucial to perform experiments to identify and characterise KIFs involved in MT1-MMP cell surface exposure in this cell line.

CHAPTER 4:

DYNAMIC REGULATION OF MT1-MMP INTRACELLULAR TRAFFICKING BY KIF13A, KIF3A, KIF9 AND KIF1C

4.1 Introduction

MT1-MMP-containing vesicles are trafficked along microtubules bidirectionally (108) and different KIFs have been shown to mediate their anterograde movement, depending on the cell type. In primary human macrophages, KIF5B and KIF3A/3B have been reported to regulate MT1-MMP anterograde transport along microtubules (108); KIF5B has been also shown to traffic MT1-MMP to the cell surface of breast cancer cells (211); in gastric cancer cells and glioma cells, KIF1B has been identified as a mediator of MT1-MMP intracellular trafficking mechanisms (212, 249). As previously discussed in Chapter 1 (Paragraph 1.5), KIF1B did not seem to contribute to MT1-MMP transport in HT-1080 cells. In Chapter 3, I have shown that the KD of KIF13A, KIF3A and KIF9 significantly alters MT1-MMP cell surface exposure in HT-1080 cells, influencing MT1-MMP-dependent cellular functions. KIF13A, KIF3A and KIF9 are likely to play crucial roles in MT1-MMP intracellular transport. These KIFs could either work cooperatively or mediate different trafficking pathways, competing for the same MT1-MMP-containing vesicles. So far there have been no publications on the interplay between different KIFs in the context of MT1-MMP intracellular transport. Shedding light on these aspects of MT1-MMP cell surface localisation would provide significant insights in understanding underlying mechanisms of MT1-MMP-mediated cell migration. This Chapter aims to investigate the dynamic regulation of KIF13A, KIF3A, KIF9 and KIF1C in orchestrating MT1-MMP cell surface exposure.

4.2 Results

4.2.1 KIF13A, KIF3A, KIF9 and KIF1C KD influences MT1-MMP intracellular distribution in HT-1080 cells

Since the KD of KIF13A, KIF3A, KIF9 and KIF1C changed MT1-MMP distribution on the cell surface but not its overall expression, I next investigated whether the KD of these KIFs had any effect on MT1-MMP distribution within the cytoplasm. HT-1080 cells, transfected with siRNAs targeting these KIFs, were fixed, permeabilised and stained for MT1-MMP with an anti-MT-Loop MT1-MMP antibody, then imaged by confocal microscopy, applying identical laser intensities to all samples. As shown in Figure 4.1 a, silencing these *kinesin* genes, particularly *Kif13a* and *Kif3a*, seemed to notably change MT1-MMP fluorescence intensity. Nevertheless, I calculated MT1-MMP overall fluorescence intensity for each treatment and found that there was no statistically significant difference when comparing targeting siRNA-transfected cells with the control (Figure 4.1 b). Next, I categorised cells as positive, partially positive or negative for MT1-MMP localisation to actin-rich ruffling membrane structures and put together the data from 100 cells for each treatment (Figure 4.1 c). In NT-siRNA-transfected cell population, over 80% of cells were either positive or partially positive and only less then 10% were negative for MT1-MMP localisation to the ruffling membrane structures. The KD of KIF13A brought the percentage of cells that were either positive or partially positive down to 48% and increased that of negative cells to 52% (Figure 4.1 c). Similarly, when KIF3A was knocked down, positive cells were only 7%, there were no partially positive cells and negative ones were up to 93% (Figure 4.1 c). In si-KIF9-transfected cell population, all the cells were either

positive or partially positive. Silencing *Kif1c* gene did not significantly alter MT1-MMP localisation to ruffling membrane structures. Statistical significance was examined employing a Chi-square test. The test revealed that knocking down different *kinesin* genes, was producing dissimilar MT1-MMP distribution ($P < 0.0001$). Si-NT-transfected HT-1080 cells often exhibited a peri-nuclear accumulation of MT1-MMP, presumably overlapping with the endoplasmic reticulum and Golgi apparatus (Figure 4.1 a). Upon KIF13A and KIF3A KD, this accumulation was notably decreased (Figure 4.1). To evaluate MT1-MMP differential distribution within the cytoplasm, I employed a wide-field microscope equipped with a 10X lens (Figure 4.1 d) and counted the number of cells presenting a peri-nuclear accumulation of the proteinase. I found that MT1-MMP peri-nuclear accumulation within the cytoplasm significantly diminished when *Kif13a* and *Kif3a* genes were silenced (Figure 4.1 d). As illustrated in Figure 4.1 e, I confirmed that the KD of KIF13A and KIF3A resulted in a statistically significant decrease of the percentage of cells with peri-nuclear accumulation of MT1-MMP. 13 different fields of view per treatment were taken into consideration. Therefore, I concluded that the KD of these KIFs altered MT1-MMP distribution within the cytoplasm of HT-1080 cells.

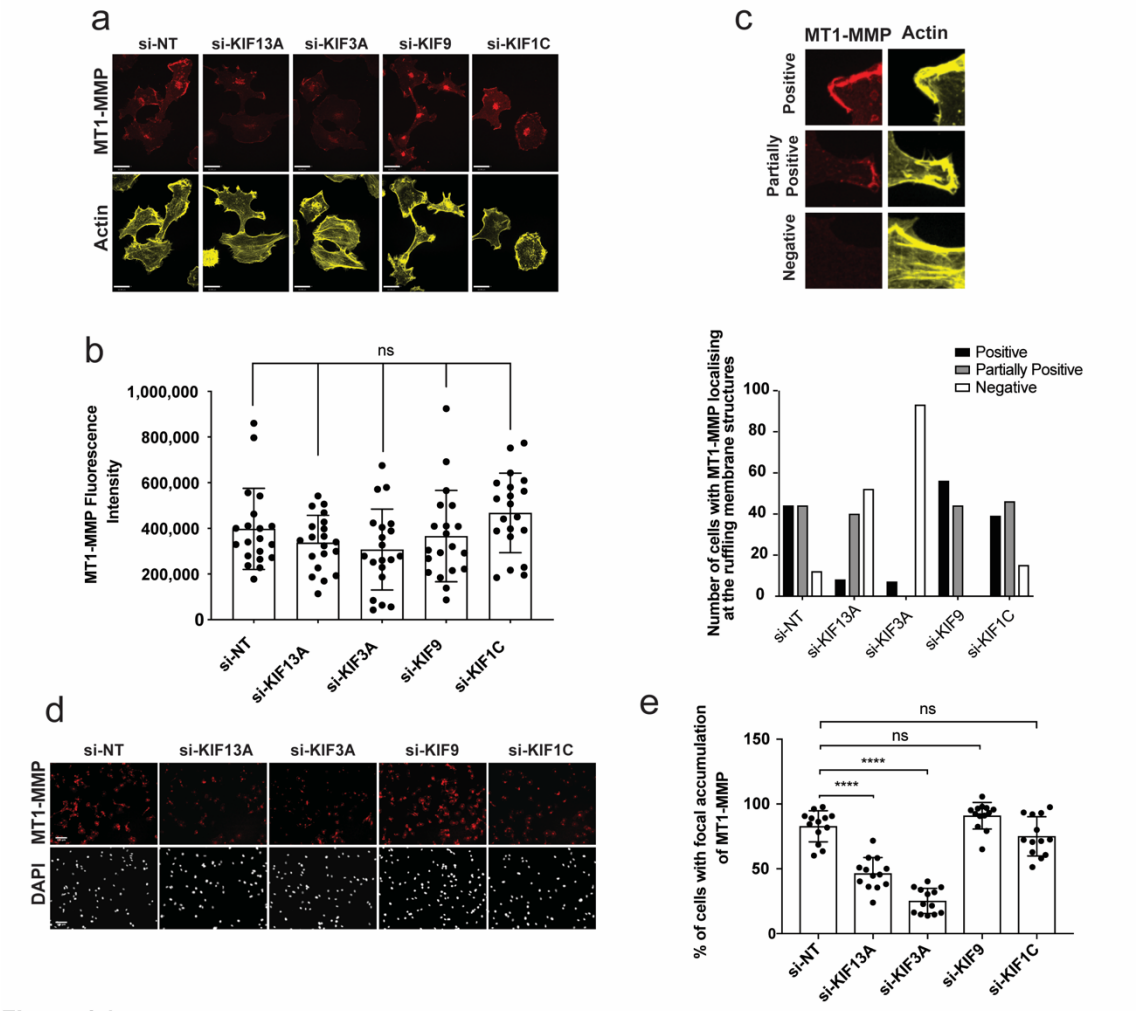


Figure 4.1: MT1-MMP distribution in the cytoplasm and its accumulation at the ruffling membrane structures and perinuclear area

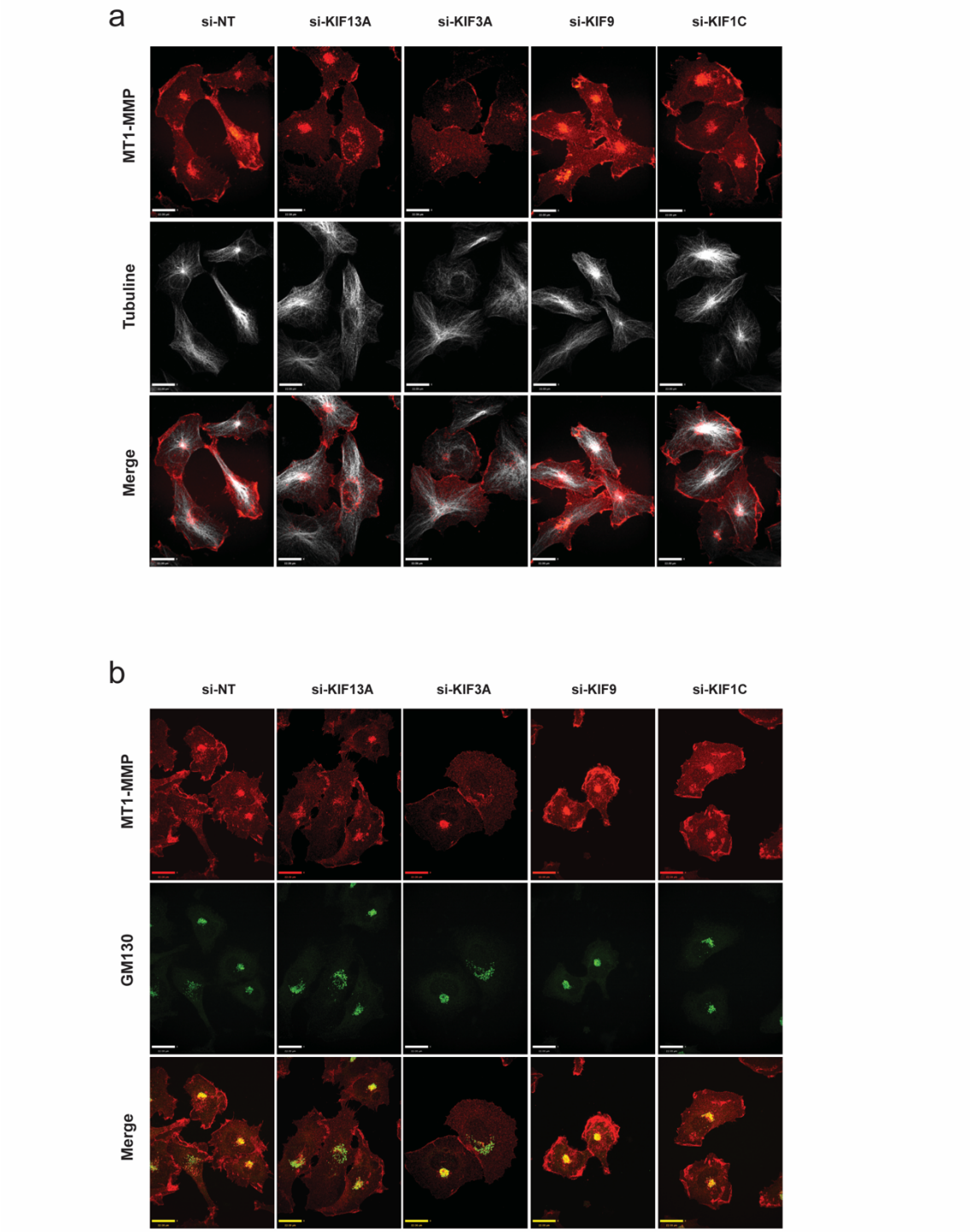
a HT-1080 cells were transfected with siRNAs targeting the selected KIFs. After 72 hours, cells were stained with anti-MT-Loop MT1-MMP (red) antibody with permeabilisation and Alexa 568 Phalloidin to visualise actin (yellow) and they were imaged by confocal microscopy. Extended focus representative images of five independent experiments are shown. Scale bars are 22 μm. **b** Quantification of the overall MT1-MMP fluorescence intensity within the cell body. 20 cells per treatment were analysed. Data are presented as mean fluorescence intensities. One-way ordinary Anova with Tukey's multiple comparisons test. Error bars are SDs; ns: non-significant**. c** Representative images of positive, partially positive and negative localisation of MT1-MMP (red) at the ruffling membrane structures. 100 cells per treatment were categorised for MT1-MMP localisation at the ruffling membrane structures. Statistical significance was tested using a Chi-

squared test (P < 0.0001). **d** HT-1080 cells were transfected with siRNAs targeting the selected KIFs. After 72 hours, cells were stained with anti-MT-Loop-MT1-MMP (red) antibody with permeabilisation and DAPI (white) and they were imaged by wide-field microscopy. Representative images of three independent experiments are shown. Scale bars are 130 µm. **e** Quantification of the percentage of cells presenting a peri-nuclear accumulation of MT1-MMP. 13 fields of view per treatment were analysed. Data are presented as mean percentages. One-way ordinary Anova with Tukey's multiple comparisons test. Error bars are SDs; **** P < 0.0001; ns: non-significant.

4.2.2 MT1-MMP localisation to the MTOC, *cis*-Golgi and *trans*-Golgi

To study MT1-MMP distribution to the different cellular compartments, HT-1080 cells, transfected with siRNAs targeting these KIFs, were fixed, permeabilised and stained for MT1-MMP with an anti-MT1-MMP antibody and for the microtubule organising centre (MTOC), *cis*- or *trans*-Golgi. In migrating fibroblasts, the MTOC or centrosome is located between the nucleus and the leading edge (250). The MTOC was stained using an anti-α-tubulin antibody. As illustrated in Figure 4.2 a, in si-NT-transfected cells, MT1-MMP was focally accumulated around the MTOC and the KD of these KIFs did not disrupt the microtubule integrity nor the distribution of MT1-MMP peri-nuclear accumulation around the MTOC (Figure 4.2 a). MT1-MMP was also found to co-localise with Golgi components such as GM130, a *cis*-Golgi marker, and TGN38, a *trans*-Golgi marker, and silencing these *kinesin* genes did not alter co-localisation of MT1-MMP peri-nuclear accumulation with these two Golgi compartments (Figure 4.2 b, c). Overall, I postulated that regardless of silencing these *kinesin* genes, MT1-

MMP peri-nuclear accumulation partially overlapped with the MTOC and with the *cis*- and *trans*-Golgi compartments.



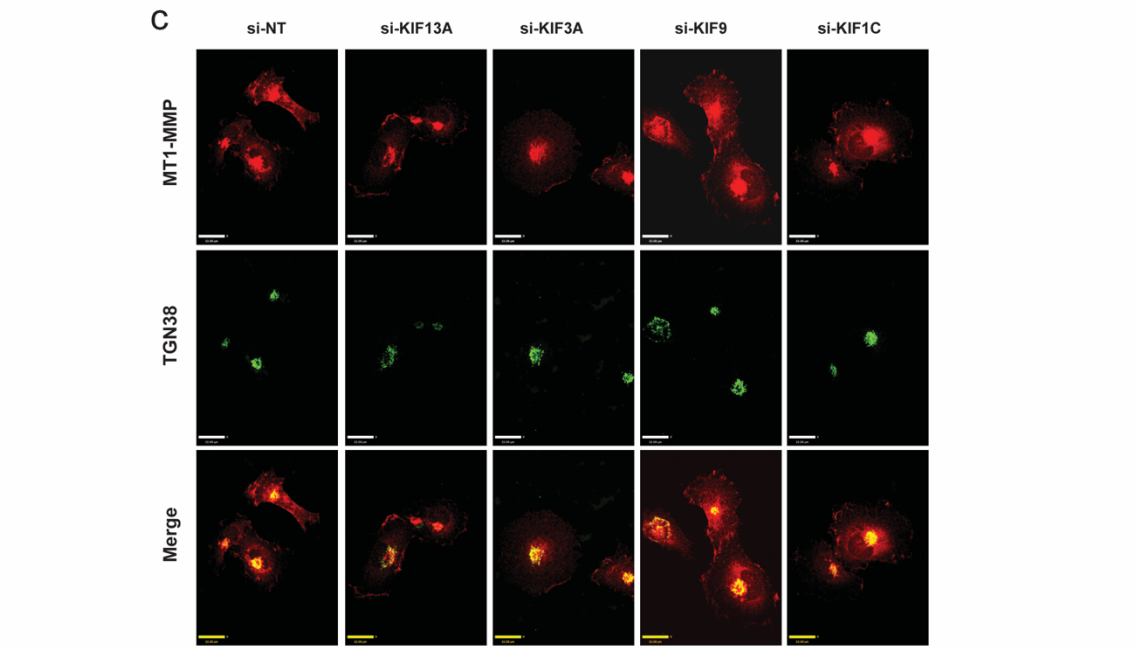


Figure 4.2: MT1-MMP localisation to the MTOC, cis- and trans-Golgi

a HT-1080 cells were transfected with siRNAs targeting the selected KIFs. After 72 hours, cells were stained with anti-MT-Loop MT1-MMP (red) antibody with permeabilisation and anti-α tubulin (grey) antibody and they were imaged by confocal microscopy. Extended focus representative images of three independent experiments are shown. Scale bars are 22 μm. **b** HT-1080 cells were transfected with siRNAs targeting the selected KIFs. After 72 hours, cells were stained with anti-MT-Loop MT1-MMP (red) antibody with permeabilisation and anti-GM130 (green) antibody and they were imaged by confocal microscopy. Extended focus representative images of three independent experiments are shown. Scale bars are 22 μm. **c** HT-1080 cells were transfected with siRNAs targeting the selected KIFs. After 72 hours, cells were stained with anti-MT-Loop MT1-MMP (red) antibody with permeabilisation and anti-TGN38 (green) antibody and they were imaged by confocal microscopy. Representative images of three independent experiments are shown. Scale bars are 22 μm.

4.2.3 MT1-MMP co-localisation with Rab5 and Rab7

To assess the effect of knocking down KIF13A, KIF3A, KIF9 and KIF1C on endo/exocytic circuities, I tested whether MT1-MMP distribution to early and late endosomes was influenced. Rab5 and Rab7 are small GTPases that have emerged been reported to be critical for MT1-MMP endo/exocytic circuities (85, 110). Rab5 has been reported to regulate vesicle trafficking from the plasma membrane to the early endosomes and to mediate homotypic fusion of these compartments (251, 252). Therefore, Rab5 is used as early endosome marker. Rab7 is critically involved in mediating vesicle trafficking from early to late endosomes and from late endosomes to lysosomes (253, 254). Hence, this Rab GTPase is used as a late endosome marker. HT-1080 cells transfected with siRNAs targeting these KIFs were co-stained with an anti-MT1-MMP antibody and an anti-Rab5 or anti-Rab7 antibody. As shown in Figure 4.3 a, Rab5 distribution was found to partially overlap with MT1-MMP peri-nuclear accumulation, regardless of the KD of these KIFs. Co-localisation of MT1-MMP with Rab7 was also found un-altered (Figure 4.3 b). As a result, I hypothesised that silencing *Kif13a*, *Kif3a*, *Kif9* and *Kif1c* genes did not significantly alter MT1-MMP distribution to early and late endosomes.

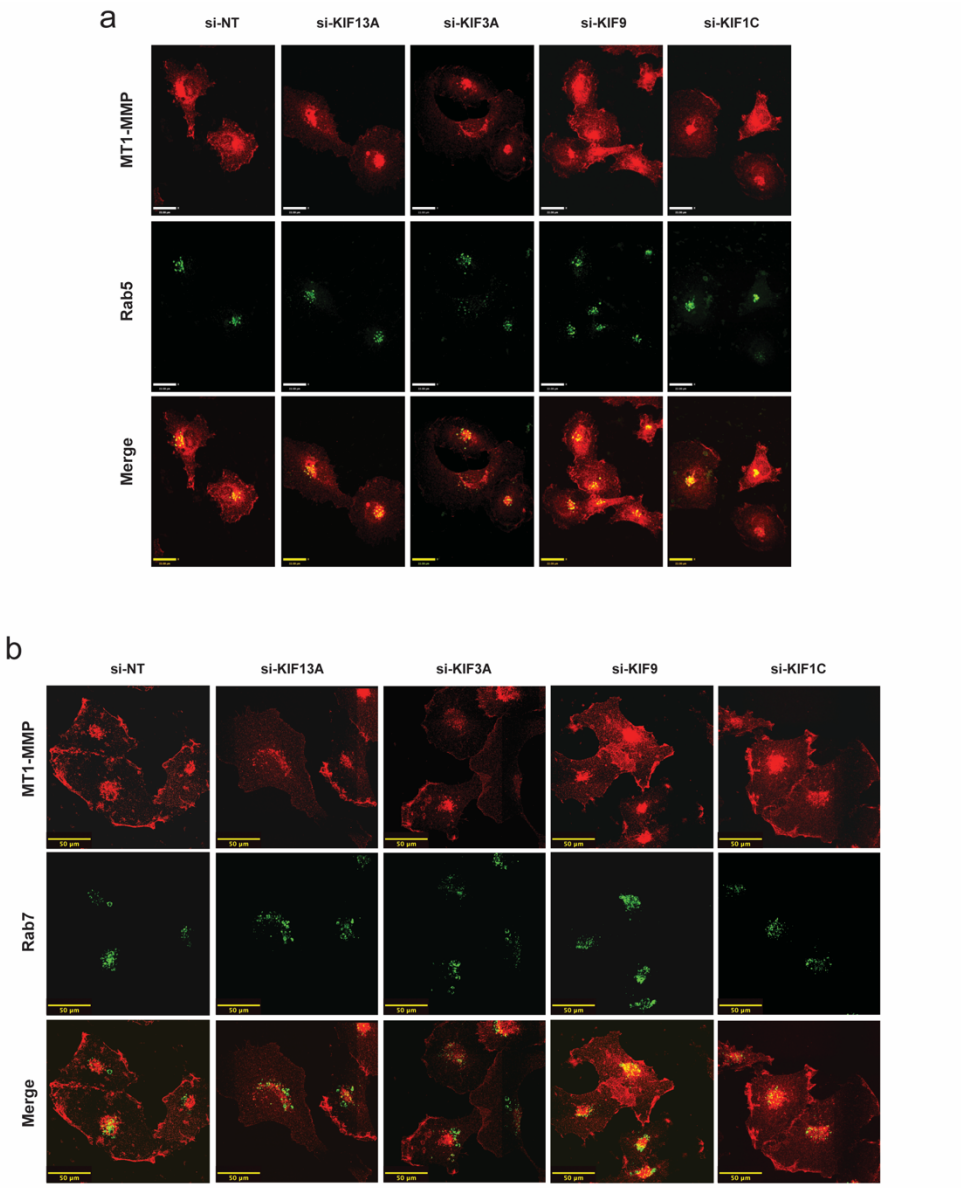


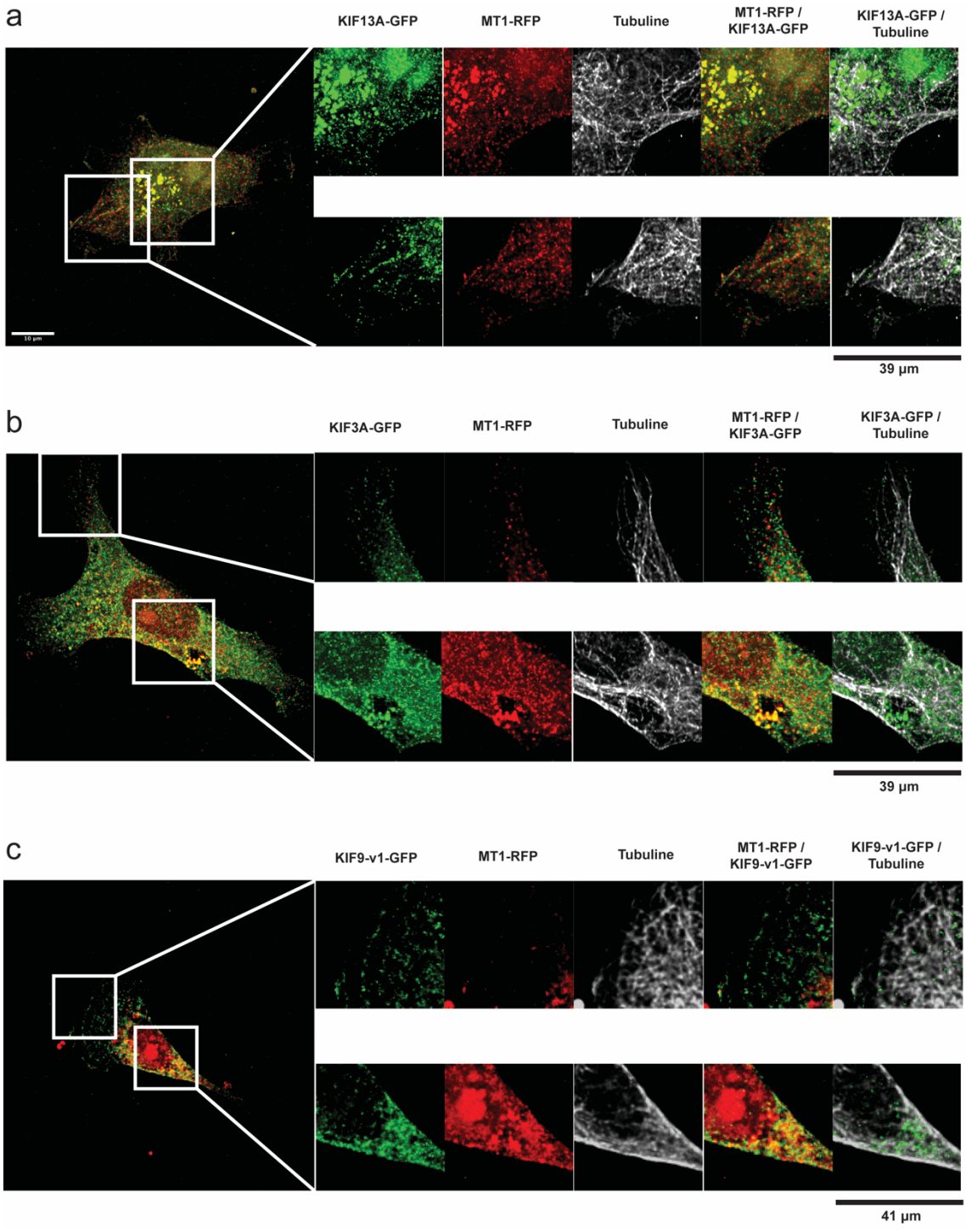
Figure 4.3: MT1-MMP co-localisation with Rab5 and Rab7

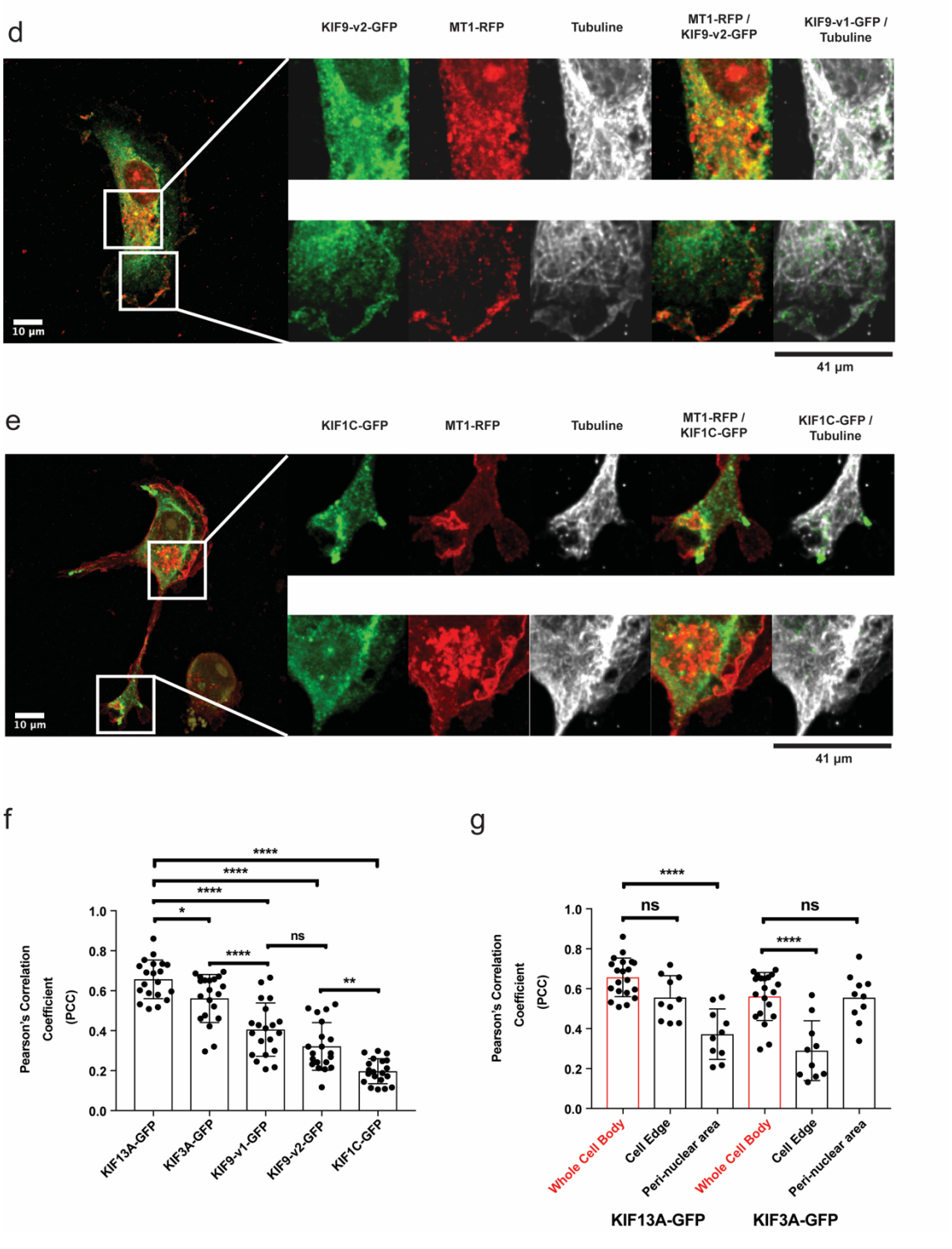
a, b HT-1080 cells were transfected with siRNAs targeting the selected KIFs. After 72 hours, cells were stained with anti-MT-Loop MT1-MMP (red) antibody with permeabilisation and with anti-Rab5 (green) or anti-Rab7 (green) antibodies. Extended focus representative images of three independent experiments are shown. Scale bars are 22 μm.

4.2.4 Co-localisation of GFP-tagged KIFs and MT1-RFP in HT-1080 cells cultured on a gelatin matrix

To study the involvement of these microtubule-associated motor proteins with MT1-MMP intracellular trafficking, GFP-tagged constructs of wild type KIF13A, KIF3A, KIF9-v1, KIF9-v2 and KIF1C were analysed for co-localisation with MT1-RFP. GFP-tagged KIFs were generated as described in Chapter 2 (Paragraph 2.2.13). HT-1080 cells were co-transfected with MT1-RFP and GFP-tagged constructs, they were cultured on gelatin-coated coverslips and imaged by confocal microscopy. KIF13A, KIF3A and KIF9-v1 but not KIF9-v2 and KIF1C clearly co-localised with MT1-RFP. As shown in Figure 4.4 a, KIF13A-GFP co-localised with MT1-RFP-positive vesicles either at the peri-nuclear area and at the cell periphery and these vesicles were associated with the microtubule filaments. Vesicles double positive for KIF3A-GFP and MT1-RFP, associating with the microtubule system, could be detected at the peri-nuclear area but not at the cell periphery (Figure 4.4 b). KIF9-v1-GFP was also found to co-localise with MT1-RFP at the peri-nuclear area but not at the cell periphery (Figure 4.4 c). Nevertheless, KIF9-v1-GFP-transfected HT-1080 cells did not have a MT1-RFP cytoplasmic signal with a clear vesicular-like distribution (Figure 4.4 c). As indicated in Figure 4.4 d, very few KIF9-v2-GFP- and MT1-RFP-positive vesicles could be identified and they were only detected at the peri-nuclear area. KIF1C-GFP did not seem to overlap with MT1-RFP and was strongly accumulated at the tips of membrane protrusions (Figure 4.4 e). To further analyse co-localisation between GFP-tagged KIFs and MT1-RFP, I quantified the Pearson's correlation coefficient (PCC) as described in Chapter 2 (Paragraph 2.15). As shown in Figure

4.4 f, KIF13A-GFP had the highest degree of co-localisation with MT1-RFP, followed by KIF3A-GFP. KIF9-v2-GFP and KIF1C-GFP exhibited the lowest co-localisation level with MT1-RFP, with mean PCC values around 0.3 and 0.2 respectively (Figure 4.4 f). Having observed that the distribution of MT1-RFP co-localised with KIF13A-GFP and KIF3A-GFP was not homogeneous within the whole cell body, I quantified PCC values for either peri-nuclear area and cell periphery. These two areas were defined as described in Chapter 2 (Paragraph 2.15). As indicated in Figure 4.4 g, KIF13A-GFP degree of co-localisation with MT1-RFP at the cell periphery was significantly higher than at the peri-nuclear area, whereas it was the opposite for KIF3A-GFP. These results were confirmed generating co-localised pixel maps as shown in Figure 4.4 h. Taken together these data suggested that, KIF13A-GFP, KIF3A-GFP and KIF9-v1-GFP co-localised with MT1-RFP-positive vesicles at the peri-nuclear area but only KIF13A-GFP- and MT1-RFP-positive vesicles could be detected at the cell periphery.


a
KIF13A-GFP
MT1-RFP
Tubuline
MT1-RFP / KIF13A-GFP
KIF13A-GFP / Tubuline
39 µm
b
KIF3A-GFP
MT1-RFP
Tubuline
MT1-RFP / KIF3A-GFP
KIF3A-GFP / Tubuline
39 µm
c
KIF9-v1-GFP
MT1-RFP
Tubuline
MT1-RFP / KIF9-v1-GFP
KIF9-v1-GFP / Tubuline
41 µm


d
KIF9-v2-GFP
MT1-RFP
Tubuline
MT1-RFP / KIF9-v2-GFP
KIF9-v1-GFP / Tubuline
10 µm
41 µm
e
KIF1C-GFP
MT1-RFP
Tubuline
MT1-RFP / KIF1C-GFP
KIF1C-GFP / Tubuline
10 µm
41 µm
f
Pearson's Correlation Coefficient (PCC)
KIF13A-GFP
KIF3A-GFP
KIF9-v1-GFP
KIF9-v2-GFP
KIF1C-GFP
g
Pearson's Correlation Coefficient (PCC)
ns
Whole Cell Body
Cell Edge
Peri-nuclear area
KIF13A-GFP
KIF3A-GFP

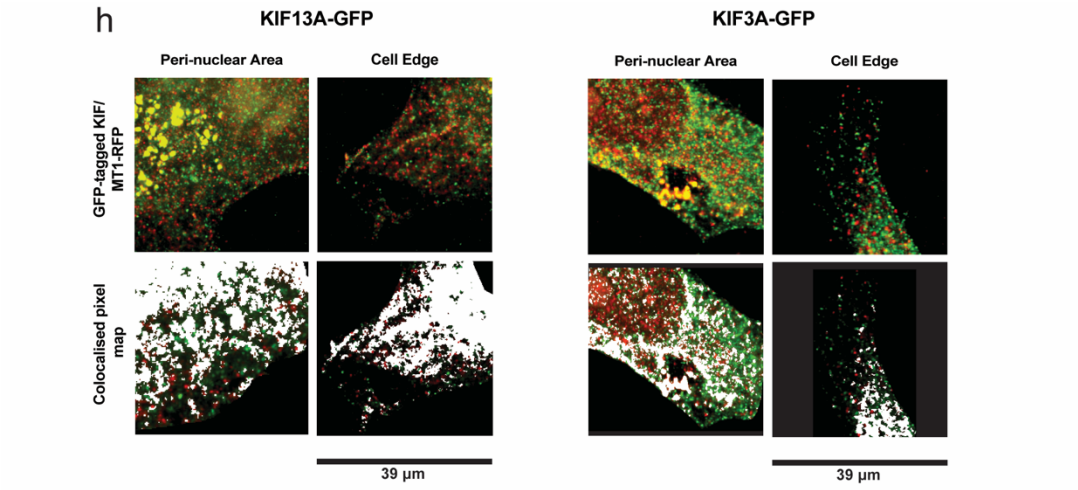


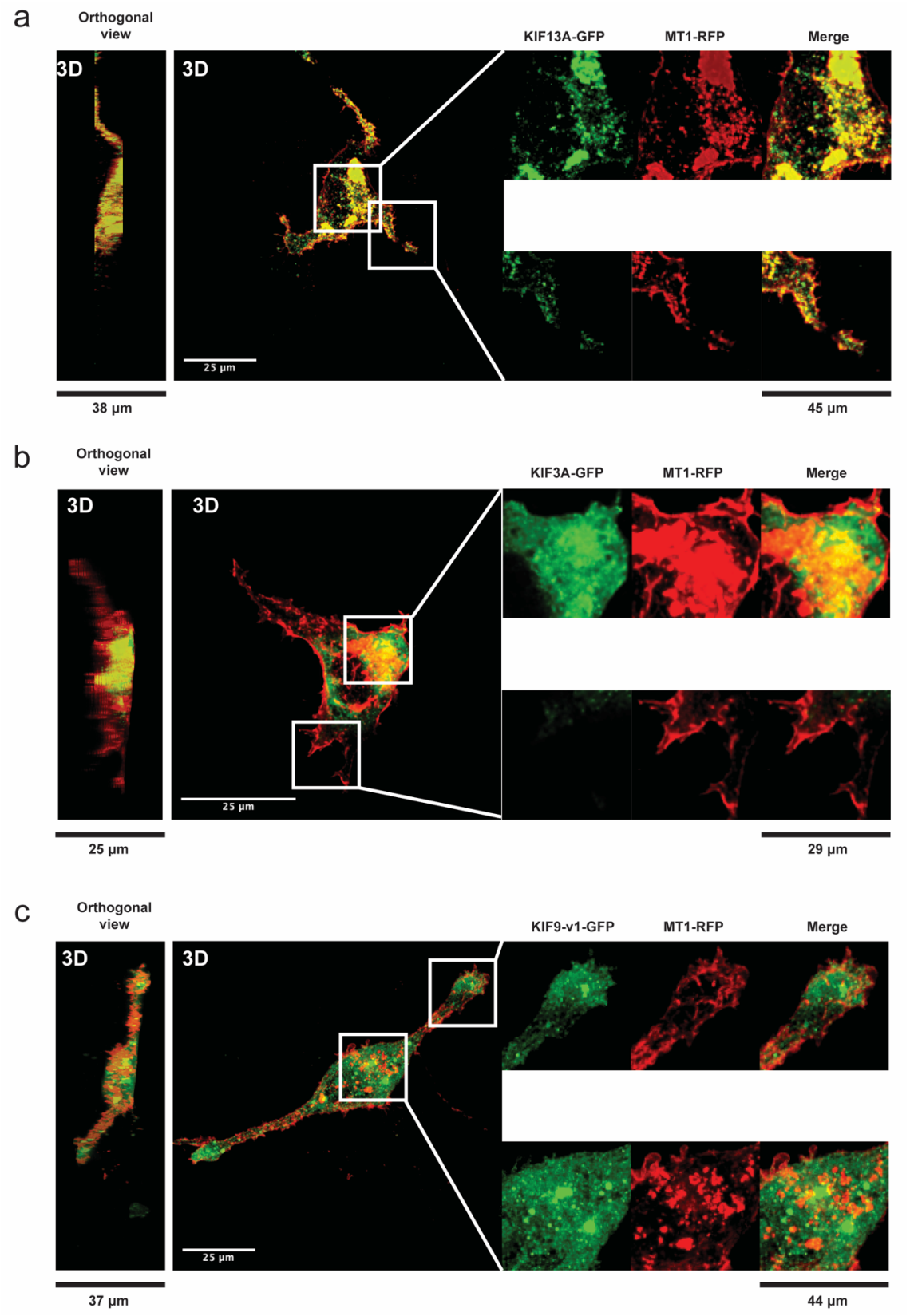
Figure 4.4: GFP-tagged KIFs and MT1-RFP co-localisation in HT-1080 cultured on gelatin-coated cover glass

a, b, c, d, e HT-1080 cells transfected with GFP-tagged KIFs (green) and MT1-RFP (red) were cultured on gelatin-coated cover glass. Cells were stained for tubulin (grey) with anti-α-tubulin antibody. Extended focus representative images are shown. White boxes enclose enlarged areas. Scale bars are 10 µm. **f** Quantification of co-localisation between GFP-tagged KIFs and MT1-RFP. Data are presented as the mean of 20 PCCs calculated for 20 different cells per treatment and are representative of three independent experiments. One-way ordinary Anova with Tukey's multiple comparisons test. Error bars are SDs; * $P < 0.05$; ** $P < 0.01$; **** $P < 0.0001$; ns: non-significant. **g** Quantification of co-localisation between KIF13A-GFP/ MT1-RFP and KIF3A-GFP/ MT1-RFP. Data are presented as the mean of PCCs calculated for the whole cell body, the cell edge and peri-nuclear area and are representative of three independent experiments. One-way ordinary Anova with Tukey's multiple comparisons test. Error bars are SDs; **** $P < 0.0001$; ns: non-significant. **h** Representative GFP-tagged-KIFs/ MT1-RFP merge images showing the peri-nuclear area and the cell edge with the relative co-localised pixel maps.

4.2.5 Co-localisation of GFP-tagged KIFs and MT1-RFP in HT-1080 cells cultured in a 3D collagen matrix

To analyse the positioning of MT1-RFP-positive vesicles under 3D culture conditions, HT-1080 cells co-transfected with MT1-RFP and GFP-tagged KIFs were embedded in a 3D collagen matrix and imaged by confocal microscopy. KIF13A-GFP and MT1-RFP co-localised at either the peri-nuclear area and membrane protrusions (Figure 4.5 a). The cytoplasmic distribution of MT1-RFP was in vesicle-like structures and there were several vesicles positive for both KIF13A-GFP and MT1-RFP (Figure 4.5 a). KIF3A-GFP only overlapped with MT1-RFP around the nucleus and not at the tips of the membrane protrusions (Figure 4.5 b). The orthogonal view also confirmed that co-localised pixels were limited to the peri-nuclear area (Figure 4.5 c). HT-1080 cells co-transfected with GFP-tagged KIF9-v1 and MT1-RFP showed a distinct vesicular distribution of the proteinase within the cell body (Figure 4.5 c). Nevertheless, very few vesicles positive for both KIF9-v1-GFP and MT1-RFP could be spotted around the nucleus and none at the tips of membrane protrusions (Figure 4.5 c). Under these culture conditions, KIF9-v2-GFP and KIF1C-GFP did not seem to overlap with MT1-RFP (Figure 4.5 d, e). As shown in Figure 4.5 e, KIF1C accumulated at the tips of membrane protrusions as observed for HT-1080 cells cultured on a gelatin matrix. PCC values confirmed that even when cells were cultured in 3D collagen, KIF13A-GFP had the highest degree of co-localisation with MT1-RFP (Figure 4.5 f). KIF9-v2-GFP and KIF1C-GFP showed again the least co-localisation level with MT1-RFP, with the latter presenting a negative average PCC value (Figure 4.5 f). PCC average values for KIF3A-GFP and KIF9-v1-GFP were respectively

around 0.4 and 0.3, both lower than those calculated when cells were cultured on a gelatin matrix (Figure 4.5 f). Overall, when cells were cultured in 3D collagen, KIF13A-GFP, KIF3A-GFP and KIF9-v1-GFP seemed to overlap with MT1-RFP-positive vesicles. KIF13A-GFP showed the highest degree of co-localisation with MT1-RFP, that had the clearest vesicle-like structure distribution within the cytoplasm.


a
Orthogonal view
KIF13A-GFP
MT1-RFP
Merge
3D
3D
25 µm
38 µm
45 µm
b
Orthogonal view
KIF3A-GFP
MT1-RFP
Merge
3D
3D
25 µm
25 µm
29 µm
c
Orthogonal view
KIF9-v1-GFP
MT1-RFP
Merge
3D
3D
25 µm
37 µm
44 µm

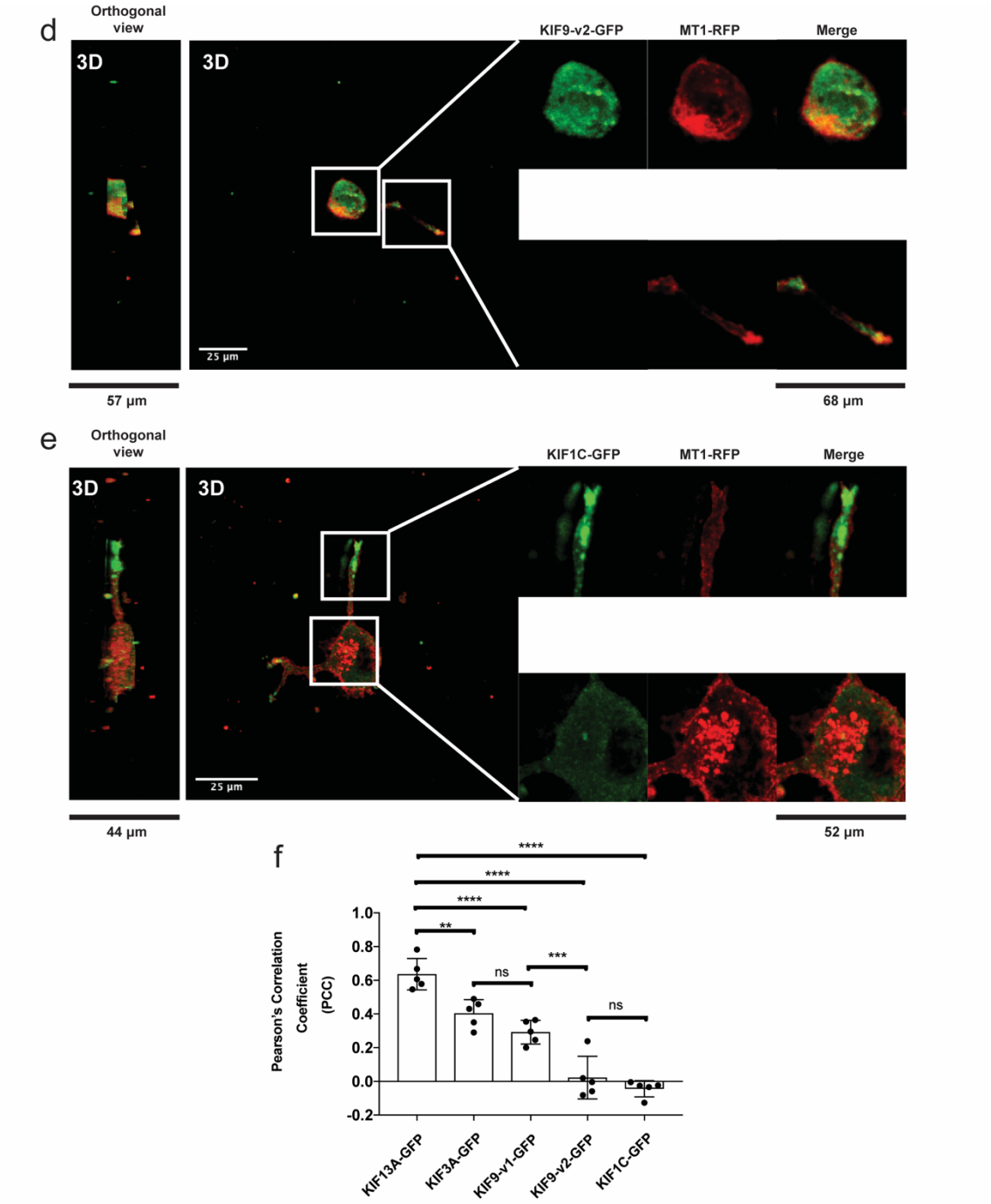


Figure 4.5: GFP-tagged KIFs and MT1-RFP co-localisation in HT-1080 cultured in a 3D collagen matrix

a, b, c, d, e HT-1080 cells transfected with GFP-tagged KIFs (green) and MT1-RFP (red) were embedded in 3D collagen and imaged by confocal microscopy. Extended focus representative images and the corresponding orthogonal views are shown. White boxes enclose enlarged areas. Scale bars are 25 µm. **f** Quantification of co-localisation between GFP-tagged KIFs and MT1-

RFP. Data are presented as the mean of five PCCs calculated for five different cells per treatment and are representative of three independent experiments. One-way ordinary Anova with Tukey's multiple comparisons test. Error bars are SDs; ** P < 0.01; *** P < 0.001; **** P < 0.0001; ns: non-significant.

4.2.6 GFP-tagged KIF13A, KIF3A and KIF9-v1 transport MT1-RFP-positive vesicles.

To get direct evidence that KIF13A, KIF3A and KIF9-v1 were mediating MT1-MMP vesicle trafficking, HT-1080 cells co-transfected with GFP-tagged KIFs and MT1-RFP were imaged by time-lapse confocal microscopy. As illustrated in Figure 4.6 a, b, numerous vesicles positive for KIF13A-GFP and MT1-RFP could be observed travelling towards the cell edge and accumulating at the tips of ruffling membrane structures. KIF13A-GFP and MT1-RFP did not only accumulate together at the peri-nuclear area but also in regions closer to the cell periphery. In Figure 4.6 b, I used a white square box to enclose the area around one of these peripheral cytosolic aggregates. In the enlarged version of this area, the white arrows point at different KIF13A and MT1-RFP double positive vesicles, that could be watched and tracked in the live videos. These vesicles were continuously moving from the aggregate towards the cell periphery (Figure 4.6 b). Overexpression of KIF13A-GFP generated a distribution of MT1-RFP-positive vesicles in tubular-like structures, extending from the peri-nuclear areas to the cell periphery (Figure 4.6 a, b). Vesicles double positive for MT1-RFP and KIF13A-GFP could also be detected around the peri-nuclear area (Figure 4.6 c). Vesicles were tracked using the Track Mate plugin in Fiji (236) as described in Chapter 2 (Paragraph 2.13.4). I analysed 47 and 44 tracks at the cell periphery

and peri-nuclear area respectively and calculated their mean, maximum and minimum velocities (Figure 4.6 d, e, f). Velocities of vesicles moving within the peri-nuclear area or at the cell periphery were not statistically different. The mean diameter of vesicles at the peri-nuclear area was significantly greater than that at the cell edge (Figure 4.6 g).

Time-lapse TIRF microscopy of HT-1080 cells co-transfected with KIF13A-GFP and MT1-RFP was employed to investigate KIF13A-GFP-dependent peripheral trafficking of MT1-RFP-positive vesicles. As previously discussed in Chapter 3 (Paragraph 3.2.6), TIRF microscopy is designed to image fluorescent molecules that are very close to the coverglass-sample interface, so it is ideal to visualise any KIF13A-GFP-mediated MT1-RFP trafficking, happening at or near the cell surface. Moreover, TIRF microscopy facilitates live cell imaging because it causes low phototoxicity (255). As shown in Figure 4.6 h, vesicles positive for both MT1-RFP and KIF13A-GFP were spotted at the substrate-attached side. Time-lapse IRM image time sequence (Figure 4.6 j) showed that HT-1080 cells, migrating on a gelatin-coated glass surface, formed highly adherent protrusions, where MT1-RFP accumulated. These highly adherent protrusions were identified as dark areas against the grey background. Dark pixels result from destructive interference between the light reflected by the cell membrane and the light reflected by the glass surface. Hence, dark pixels mean high proximity. MT1-RFP positive vesicles formed a tubule-like structure, pointing to the area where the highly adherent membrane protrusion was developing (Figure 4.6 j). KIF13A-GFP-positive vesicles appeared at the tip of this MT1-RFP tubular structure prior to the formation of the protrusion (Figure 4.6 j).

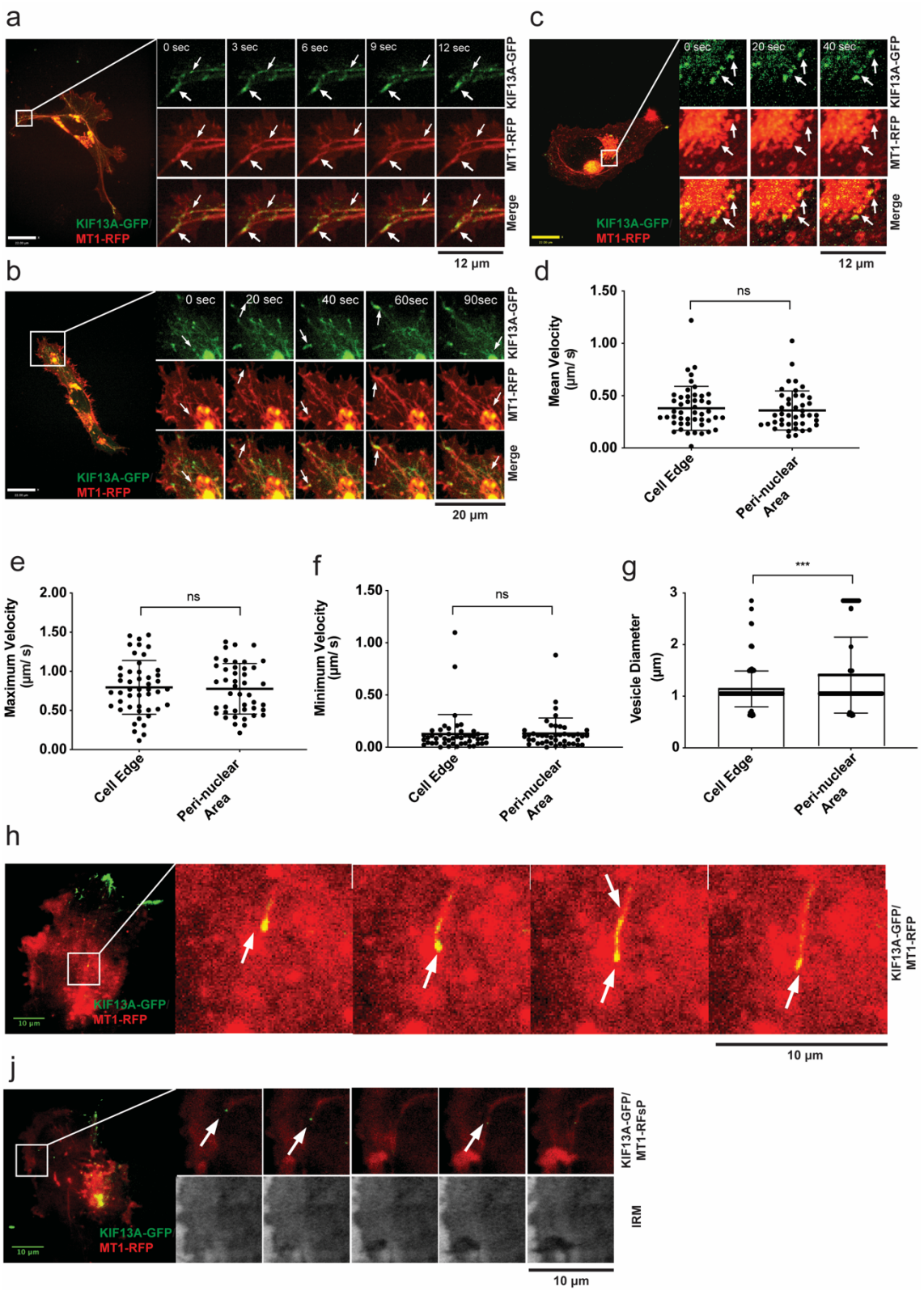


Figure 4.6: KIF13A transports MT1-MMP-containing vesicles at the ruffling membrane structures and the substrate-attachment side

a, b, c HT-1080 cells were transfected with KIF13A-GFP (green) and MT1-RFP (red) and they were subjected to live cell imaging by confocal microscopy. Representative image time sequences are shown. White arrows point vesicles of interest. Scale bars are 22 μm. **d, e, f** Quantification of mean, maximum and minimum velocities of vesicles of interest at the leading edge and nuclear area. Data are representative of five independent experiments and are calculated for 47 and 44 trajectories for the cell edge and the peri-nuclear area respectively. Unpaired T test with Welch's correction. Error bars are SDs; ns: non-significant. **g** Quantification of vesicle diameter at the cell edge and peri-nuclear area. Data are representative of five independent experiments and are calculated for 129 vesicles for the leading edge and the peri-nuclear area. Unpaired T test with Welch's correction. Error bars are SDs. *** $P < 0.001$. **h, j** HT-1080 cells transfected with KIF13A-GFP (green) and MT1-RFP (red) were subjected to live cell imaging by TIRF microscopy. Representative image time sequences are shown. White arrows point vesicles of interest. IRM, internal reflection microscopy. Scale bar is 10 μm.

Vesicles double positive for KIF3A-GFP and MT1-RFP were observed around the peri-nuclear area of HT-1080 cells. Time-lapse confocal imaging (Figure 4.7 a, b) showed that these vesicles were either moving linearly or oscillating around the same spot (Figure 4.7 a, b). I analysed 26 and 24 different linear and oscillatory trajectories respectively. By comparing the mean, maximum and minimum velocities of vesicles with linear trajectories with the respective values of those with an oscillatory movement, I could not detect any statistically significant differences (Figure 4.7 c, d, e). The average diameters of vesicles with linear or oscillatory trajectories were also not different (Figure 4.7 f).

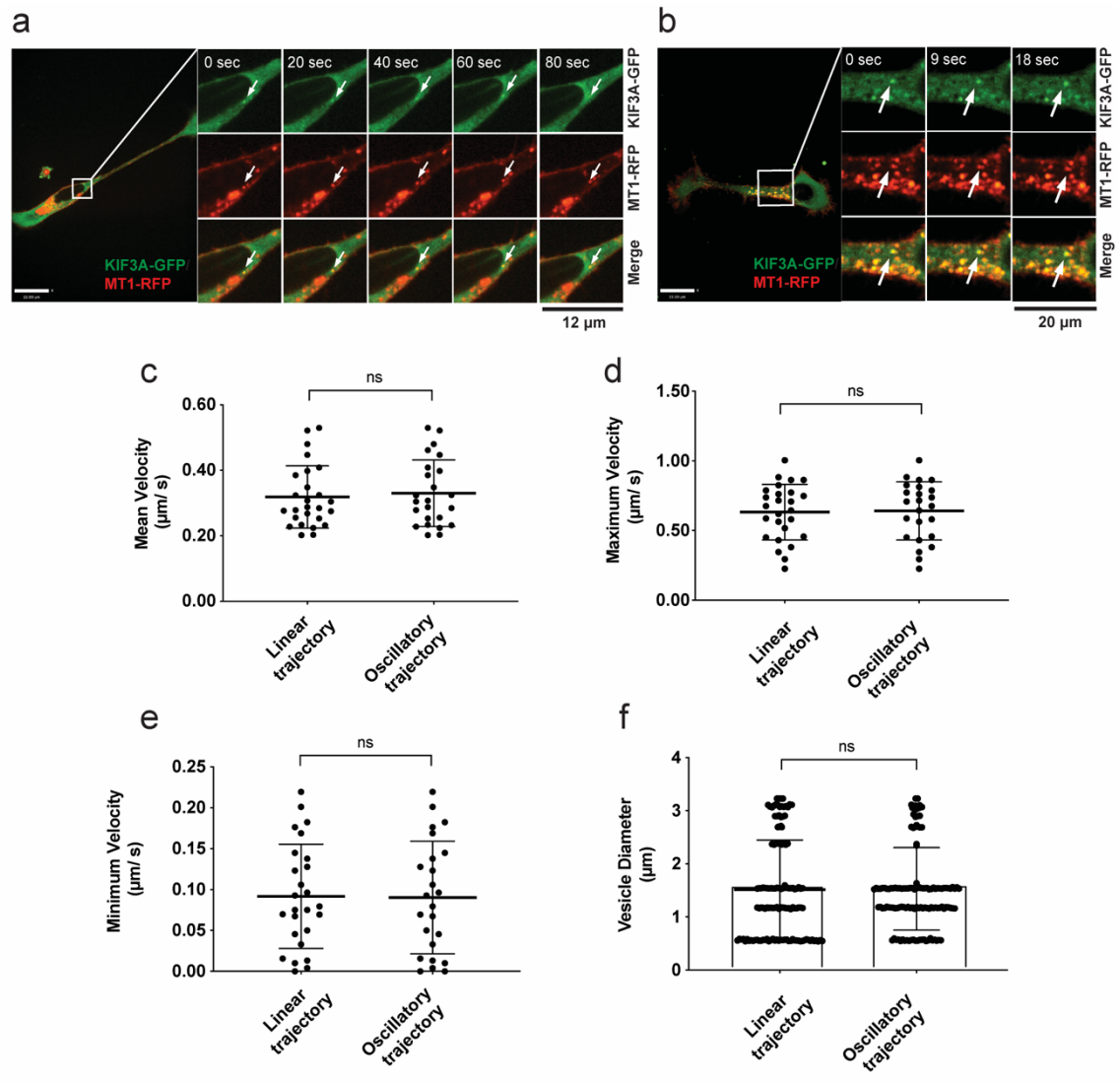


Figure 4.7: KIF3A transport MT1-MMP-containing vesicles around the perinuclear area

a, b HT-1080 cells transfected with KIF3A-GFP (green) and MT1-RFP (red) and they were subjected to live cell imaging by confocal microscopy. Representative image time sequences are shown. White arrows point vesicles of interest. Scale bars are 22 µm. **c, d, e** Quantification of mean, maximum and minimum velocities of vesicles of interest with linear or oscillatory trajectories. Data are representative of five independent experiments and are calculated for 26 and 24 linear and oscillatory trajectories respectively. Unpaired T test with Welch's correction. Error bars are SDs; ns: non-significant. **f** Quantification of vesicle diameter. Data are representative of five independent experiments and are calculated for 129 vesicles for each group. Unpaired T test with Welch's correction. Error bars are SDs; ns: non-significant.

KIF9-v1-GFP- and MT1-RFP positive vesicles could also be detected at the peri-nuclear area (Figure 4.8). Nevertheless, they were not characterised by linear or oscillatory trajectories, as for KIF13A-GFP or KIF3A-GFP, because their fluorescence intensity was fading over time (Figure 4.8). This observation led me to hypothesis that these vesicles were moving out of plane along the Z axis. I analysed 27 trajectories and calculated their average mean, maximum and minimum velocities as well as their average vesicle diameter (Table 4.1). These trajectories were generated considering only the time points when the vesicles were clearly visible. Velocities calculated for these trajectories referred to the vesicles' movement within the XY plane. As shown in Table 4.1 and Figure 4.8, MT1-RFP-positive vesicles trafficked by KIF9-v1-GFP were slower and larger than those transported by KIF13A-GFP or KIF3A-GFP.

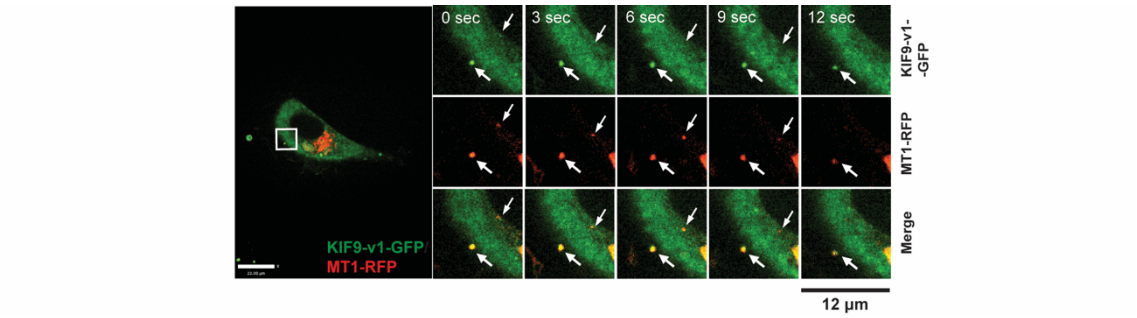


Figure 4.8: KIF9-v1-GFP and MT1-RFP positive vesicles localises at the perinuclear area

HT-1080 cells transfected with KIF9-v1-GFP (green) and MT1-RFP (red) were subjected to live cell imaging by confocal microscopy. Representative image sequence is shown. White arrows point vesicles of interest. Scale bar is 22 µm.

Table 4.1: Average velocities and diameters of MT1-RFP-positive vesicles transported by KIF13A-GFP, KIF3A-GFP and KIF9-v1-GFP

KIF	Trajectory	Cell Area	Mean Velocity (µm/s)	Maximum Velocity (µm/s)	Minimum Velocity (µm/s)	Vesicle Diameter (µm)
KIF13A	Linear	Cell Edge	0.38 ± 0.21	0.79 ± 0.34	0.13 ± 0.19	1.14 ± 0.35
	Linear	Peri-nuclear	0.36 ± 0.19	0.78 ± 0.32	0.13 ± 0.15	1.41 ± 0.73
KIF3A	Linear	Peri-nuclear	0.32 ± 0.09	0.63 ± 0.20	0.09 ± 0.06	1.51 ± 0.93
	Oscillatory	Peri-nuclear	0.33 ± 0.10	0.63 ± 0.20	0.09 ± 0.07	1.53 ± 0.77
KIF9-v1	Oscillatory	Peri-nuclear	0.16 ± 0.06	0.39 ± 0.11	0.035 ± 0.024	1.89 ± 0.74

To clarify the role of KIF9-v2 and KIF1C in MT1-MMP intracellular transport, HT-1080 cells co-transfected with MT1-RFP and one of these two GFP-tagged KIFs were subjected to time-lapse confocal imaging. As indicated in Figure 4.10 a, no vesicles positive for both MT1-RFP and KIF9-v2-GFP could be observed. It was not possible to spot MT1-RFP-containing vesicles trafficked by KIF1C-GFP but this motor protein clearly accumulated at the tip of the trailing edge (Figure 4.10 b). In summary, these live-cell imaging data strengthened the hypothesis that KIF13A, KIF3A and KIF9-v1 were directly involved in MT1-MMP intracellular trafficking. KIF13A seemed to have a prominent role for MT1-MMP transport around the cell edge, while KIF3A and KIF9-v1 within the peri-nuclear area. On the contrary, KIF9-v2 and KIF1C did not appear to be required for MT1-MMP trafficking.

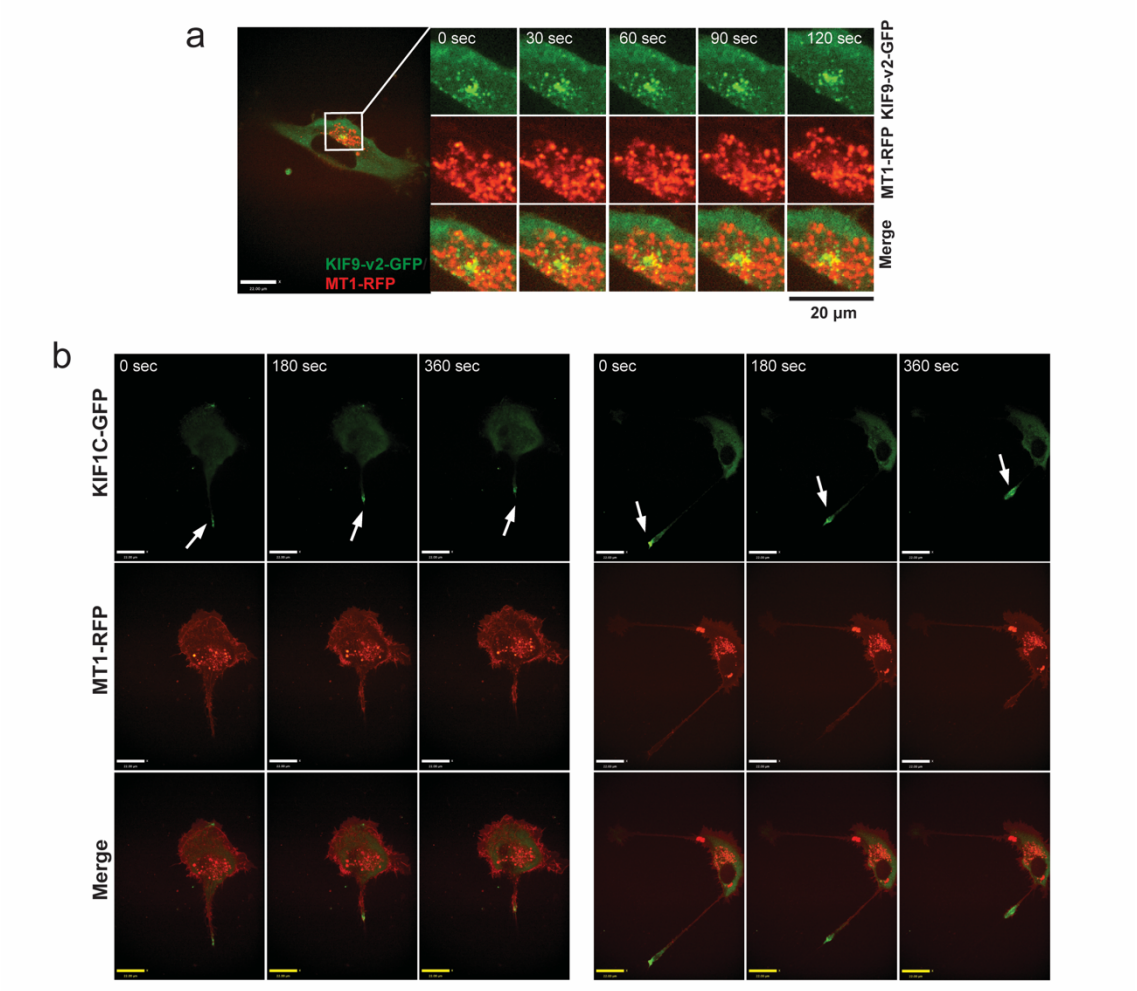


Figure 4.9: KIF9-v2-GFP and KIF1C do not directly contribute to MT1-MMP intracellular trafficking mechanisms

a HT-1080 cells were transfected with KIF9-v2-GFP (green) and MT1-RFP (red) and they were subjected to live cell imaging by confocal microscopy. Representative image time sequence is shown. Scale bars are 22 µm. **b** HT1080 cells were transfected with KIF1C-GFP (green) and MT1-RFP (red) and they were subjected to live cell imaging by confocal microscopy. Representative image time sequences are shown. White arrows point trailing edges. Scale bars are 22 µm.

4.2.7 GFP-tagged KIF13A and KIF3A collaboratively transport MT1-RFP-containing vesicles

As KIF13A, KIF3A and KIF9-v1 seemed to be directly involved in MT1-MMP intracellular trafficking, I next investigated whether they were acting independently or in collaboration with each other. HT-1080 cells were transfected with si-KIF13A, si-KIF3A and a combination of the two and they were subjected to gelatin film degradation assay. As shown in Figure 4.11 a, knocking down KIF13A, KIF3A or both, significantly decreased gelatin film degradation in comparison to the control. Co-silencing *Kif13a* and *Kif3a* genes was as efficient as silencing *Kif13a* gene alone in reducing gelatinolytic activity of HT-1080 cells but significantly more effective than knocking down KIF3A only (Figure 4.11 a, b). KIF13A and KIF3A co-KD brought KIF13A and KIF3A mRNAs down by 40% and 60% respectively. These data suggested that KIF13A and KIF3A might be functioning in the same pathway to achieve MT1-MMP cell surface exposure.

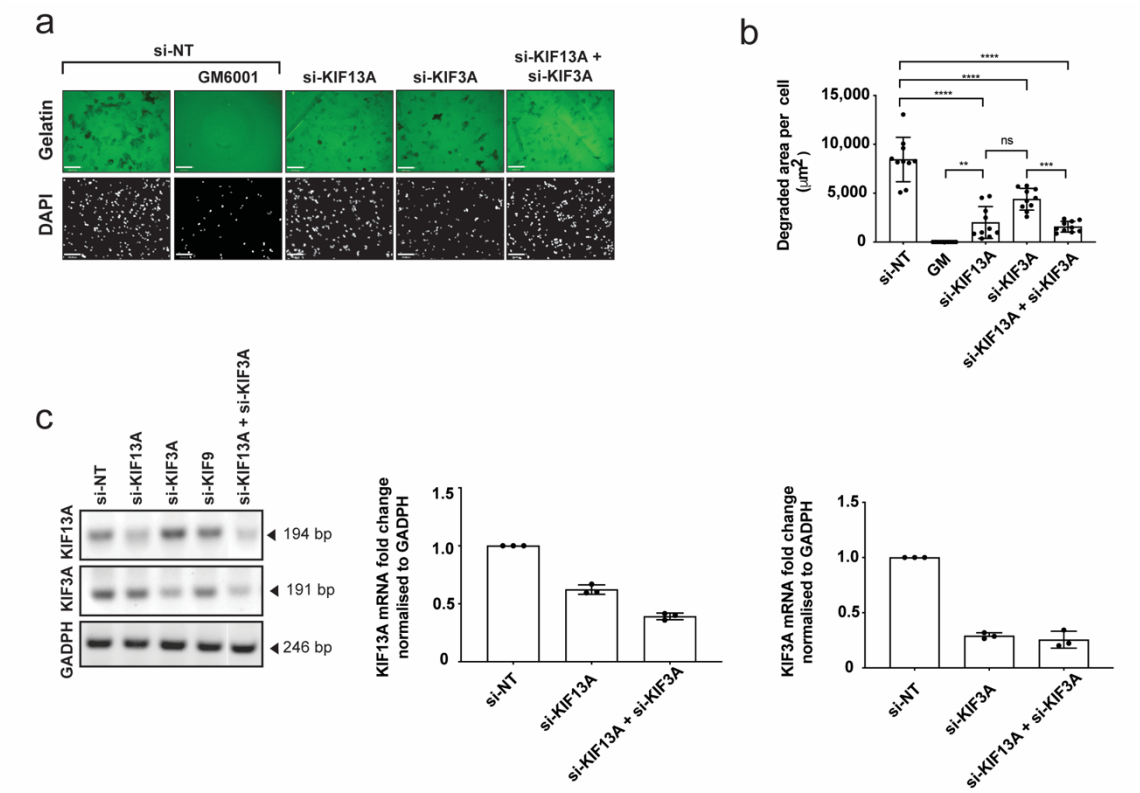


Figure 4.10: Effect of concomitant KD of KIF13A and KIF3A on MT1-MMP-mediated gelatin film degradation

a HT-1080 cells were transfected with siRNAs targeting the selected KIFs and subjected to gelatin film degradation assay in the presence or absence of GM6001 (10 µM). Scale bars are130 µm. **b** Quantification of the degradation area (µm^2) per cell in HT1080 cells transfected with the specified siRNAs. Data are presented as mean of 10 independent microscopic fields of view and are representative of three independent experiments. One-way ordinary Anova with Tukey's multiple comparisons test. Error bars are SDs; **** P < 0.0001; *** P < 0.001; ** P < 0.01; ns: non-significant. **c** Efficiency of KIF KD by one-step RT-PCR. Quantification of KIF13A and KIF3A mRNA fold changes relative to GADPH mRNA. The data are representative of three independent experiments.

To visualise KIF13A and KIF3A at the same time, HT-1080 cells were co-transfected with KIF13A-GFP, KIF3A-HaloTag and MT1-RFP and they were imaged by time-lapse confocal microscopy. KIF3A-HaloTag was visualised by

live-cell labelling with HaloTag Coumarin ligand that has a major excitation peak at 353 nm and an emission maximum at 434 nm. The level of KIF3A-HaloTag protein expression was relatively low and I had to test several laser power and exposure time conditions to find the best compromise to limit the oxidative DNA damage. This oxidative damage is evident for cells exposed to violet light [340-380 nm] that is used to excite blue fluorophores (256). As illustrated in the Panels a and b of Figure 11, KIF13A-GFP, KIF3A-HaloTag and MT1-RFP co-localised around the peri-nuclear area. As pointed by the arrows coloured as the three different channels, vesicles triple positive for these two KIFs and MT1-RFP were spotted moving around the cytoplasm. Sometimes, MT1-RFP-containing vesicles were transported towards the cell edge by both KIF13A-GFP and KIF3A-HaloTag until MT1-RFP fluorescence signal faded and the two KIFs travelled back to the centre of the cell (Panel a). More frequently, KIF13A-GFP and KIF3A-HaloTag co-localised with MT1-RFP-positive vesicles that were close to the nucleus and were not moving much within the XY plane (Panel b and peri-nuclear area of Panel c). As mentioned above, KIF3A-HaloTag signal level was quite low and resulted in grainy confocal images and limited the number of vesicles that could be tracked. I analysed five trajectories of MT1-RFP-containing vesicles trafficked by KIF13A-GFP and KIF3A-HaloTag and calculated their average mean, maximum and minimum velocities (Table 4.2). I also calculated mean velocities of KIF13A-GFP (0.77μm/s) and KIF3A-HaloTag (1.02 μm/s) after they dissociated from the MT1-MMP-containing vesicle that they were carrying (Figure 4.11a). Interestingly, KIF13A-GFP appeared to be slower than KIF3A-HaloTag.

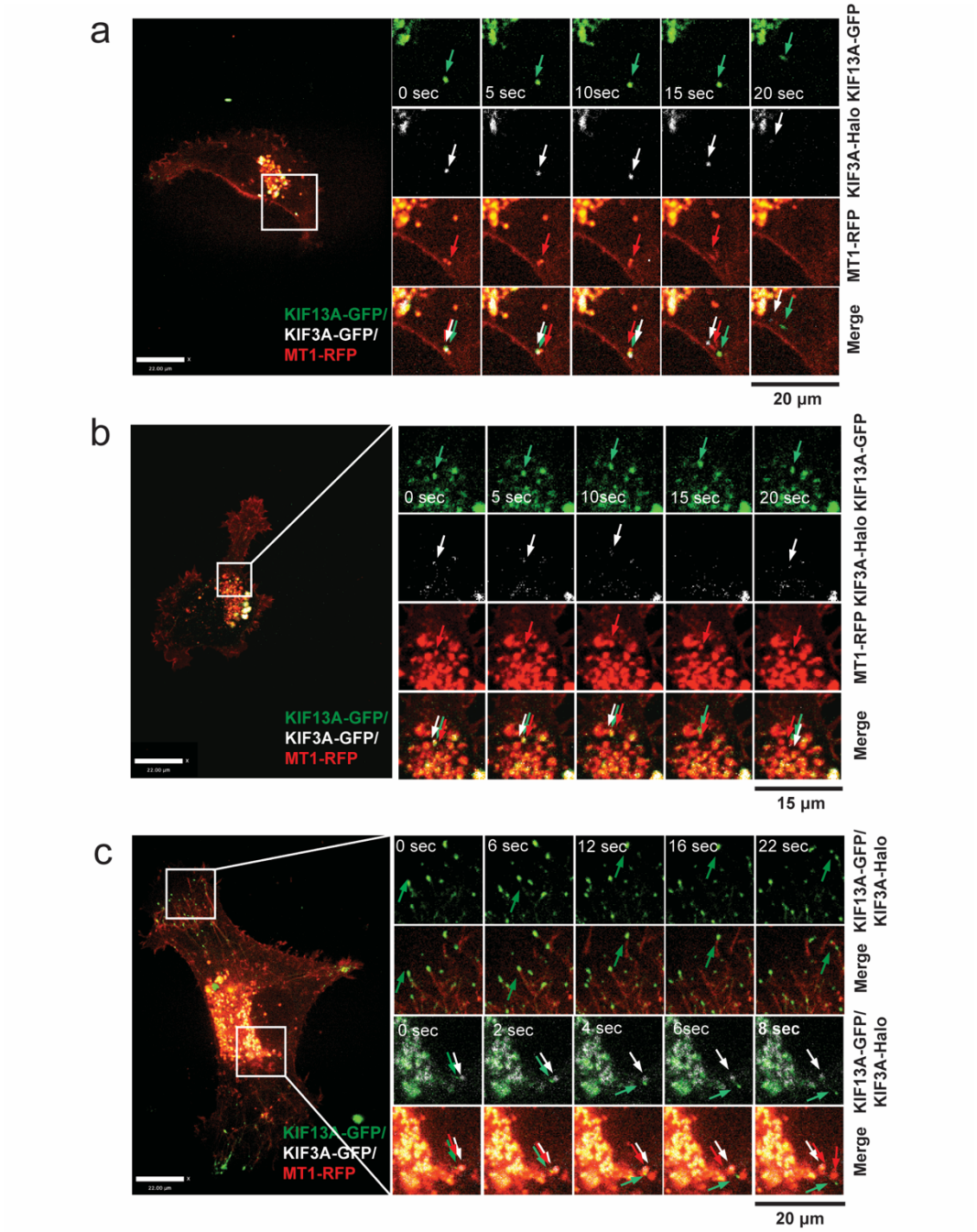
Table 4.2: Average velocities of MT1-RFP-positive vesicles transported by KIF13A-GFP and KIF3A-HaloTag

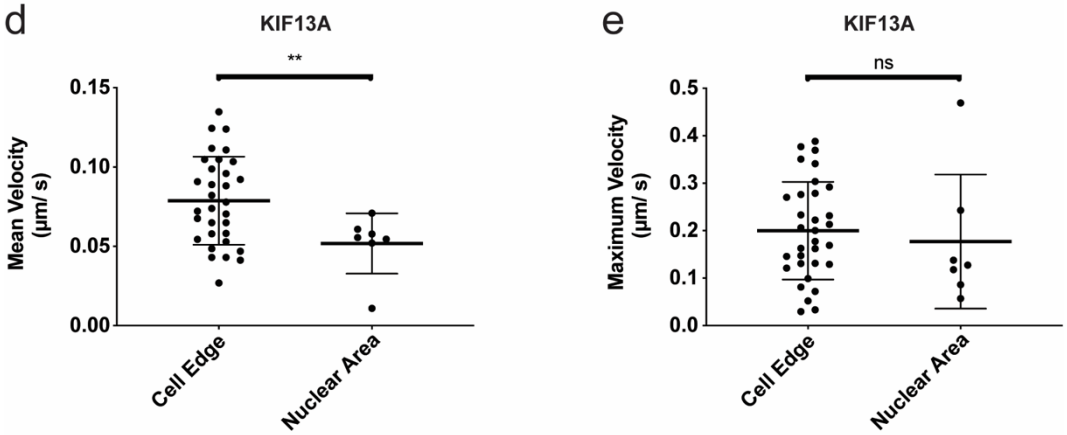
KIF	Mean Velocity (µm/s)	Maximum Velocity (µm/s)	Minimum Velocity (µm/s)
KIF13A-GFP/ KIF3A-HaloTag	0.57 ± 0.33	1.08 ± 0.65	0.06 ± 0.03

No co-localisation between KIF13A-GFP, KIF3A-Halotag and MT1-RFP was detected at the cell edge (Figure 4.11c). As previously reported, only KIF13A-GFP co-localised with MT1-RFP at the peripheral areas. I analysed seven and 32 trajectories of MT1-RFP-positive vesicles transported by KIF13A-GFP at the peri-nuclear area and cell edge respectively and calculated their average mean, maximum and minimal velocities. When KIF3A-Halotag was expressed, mean velocity of vesicles trafficked by KIF13A-GFP was significantly higher at the cell edge than the peri-nuclear areas (Figure 4.11 d), while no differences were observed comparing maximum and minimum velocities (Figure 4.11 e, f). The analysis of 11 oscillatory and 10 linear trajectories of MT1-RFP-containing vesicles, trafficked by KIF3A-HaloTag, indicated that their average maximum and minimum velocities were not statistically different (Figure 4.11 h, I). On the other hand, average mean velocity of vesicles moving linearly was higher than those oscillating when KIF13A-GFP was expressed (Figure 4.11 g).

To further investigate whether MT1-RFP peripheral trafficking was only dependent on KIF13A-GFP, HT-1080 cells co-transfected with KIF13A-GFP, KIF3A-HaloTag and MT1-RFP were subjected to time-lapse imaging by TIRF microscopy. As shown in Figure 11 j, MT1-RFP and KIF13A-GFP but not KIF3A-

HaloTag co-localised at the cell periphery of the substrate-attached side. KIF3A-HaloTag fluorescence signal was bluer and overlapping with KIF13A-GFP and MT1-RFP only around the peri-nuclear area (Figure 4.11 j). To sum up, KIF13A and KIF3A seemed to collaborate for the transport of MT1-MMP-containing vesicles around the peri-nuclear area, whereas KIF13A appeared to be the sole motor protein to traffic the proteinase towards the cell periphery.


a
0 sec
5 sec
10sec
15 sec
20 sec
KIF13A-GFP/
KIF3A-GFP/
MT1-RFP
KIF3A-Halo KIF13A-GFP
MT1-RFP
Merge
20 µm
b
0 sec
5 sec
10sec
15 sec
20 sec
KIF13A-GFP/
KIF3A-GFP/
MT1-RFP
MT1-RFP KIF3A-Halo KIF13A-GFP
Merge
15 µm
c
0 sec
6 sec
12 sec
16 seo
22 sec
KIF13A-GFP/
KIF3A-GFP/
MT1-RFP
KIF13A-GFP/
KIF3A-Halo
Merge
0 sec
2 sec
4 sec
6sec
8 sec
KIF13A-GFP/
KIF3A-Halo
Merge
20 µm


d
KIF13A
**
Mean Velocity (µm/ s)
0.15
0.10
0.05
0.00
Cell Edge
Nuclear Area
e
KIF13A
ns
Maximum Velocity (µm/ s)
0.5
0.4
0.3
0.2
0.1
0.0
Cell Edge
Nuclear Area

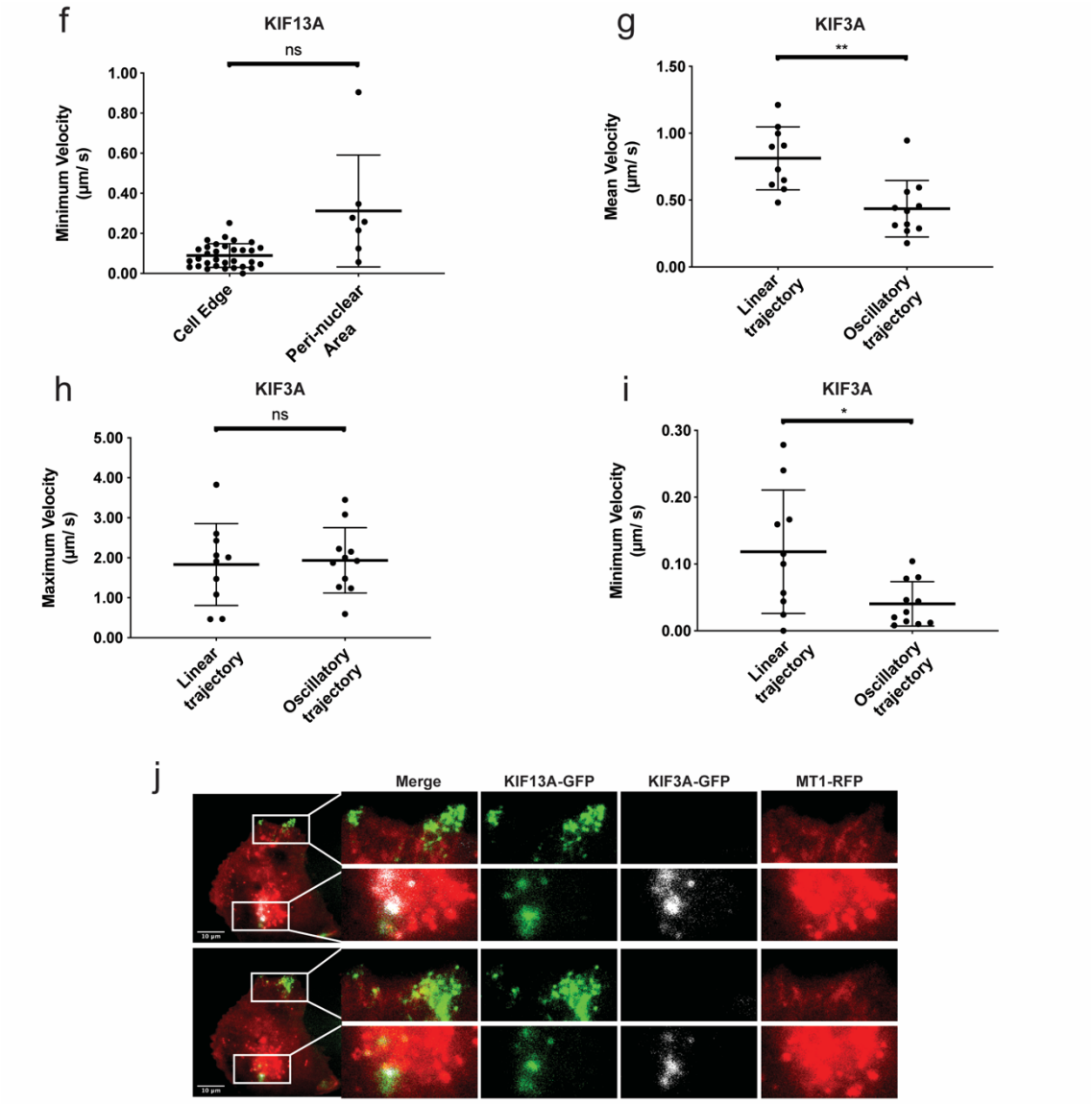


Figure 4.11: KIF13A and KIF3A collaboratively transport MT1-MMP-containing vesicle

a, b, c HT-1080 cells were transfected with KIF13A-GFP (green), KIF3A-GFP (white) and MT1-RFP (red) and they were subjected to live cell imaging by confocal microscopy. Representative image time sequences are shown. Arrows point vesicles of interest. Scale bars are 22 µm. **d, e, f** Quantification of mean, maximum and minimum velocities of MT1-RFP-containing vesicles transported by KIF13A-GFP at the cell edge and nuclear area. Data are representative of three independent experiments and are calculated for 32 and seven trajectories for the cell edge and the nuclear area respectively. Unpaired T test with Welch's correction. Error bars are SDs; ** $P < 0.01$; ns: non-significant. **g, h, i** Quantification of mean, maximum and minimum velocities of MT1-RFP-containing vesicles transported by KIF3A-GFP with linear or oscillatory trajectories. Data are

representative of three independent experiments and are calculated for 10 linear and 11 oscillatory trajectories. Unpaired T test with Welch's correction. Error bars are SDs; ** P < 0.01, ns: non-significant. **j** HT-1080 cells were transfected with KIF13A-GFP (green), KIF3A-GFP (white) and MT1-RFP (red) and they were subjected to live cell imaging by TIRF microscopy. Representative images from two different time points are shown. Scale bars are 10 μm.

4.2.8 KD of KIF3A or KIF13A diminishes KIF9-induced increase of MT1-MMP-dependent gelatinolytic activity of HT-1080 cells

To examine relationships between KIF3A and KIF9, I again employed a gelatin film degradation assay. HT-1080 cells were transfected with si-KIF3A, si-KIF9 and a combination of the two and they were cultivated on a fluorescently-labelled gelatin film. As previously reported, silencing *kif3A* gene decreased gelatinolytic activity, whereas knocking down KIF9 enhanced it (Figure 4.12 a). HT-1080 cells co-transfected with si-KIF3A and si-KIF9 degraded gelatin significantly more than those transfected with only si-KIF3A (P = 0.022) and notably less than when only *kif9* gene was silenced (P < 0.0001) (Figure 4.12 a, b). KIF3A and KIF9-v1 mRNA levels were both down by 80% when HT-1080 cells were co-transfected with both si-KIF3A and si-KIF9 (Figure 4.12 c). As reported in Chapter 3, KIF9-v2 and KIF9-v3 were not knocked down by si-KIF9 nor by the combination of si-KIF3A and si-KIF9. Interestingly, when KIF3A was knocked down, KIF9-v1 mRNA level was up by almost 15%, suggesting that the expression levels of these two motor proteins might be linked. To visualise possible interactions between KIF3A and KIF9-v1, HT-1080 cells were co-transfected with KIF9-v1-GFP, KIF3A-HaloTag and MT1-RFP. HaloTag Coumarin ligand was again employed to label KIF3A-HaloTag. As shown in

Figure 4.13, few MT1-RFP-containing vesicles, positive for both KIF3A and KIF9-v1 were located around the nucleus where MT1-RFP was accumulated. Hence, the background signal was quite high and vesicles could not be tracked. Unfortunately, I did not have sufficient time to explore the potential collaboration between KIF3A and KIF9-v1 further.

HT-1080 cells were also co-transfected with si-KIF13A, si-KIF9 and a combination of the two and they were subjected to gelatin film degradation assay (Figure 4.14 a, b). When *kif13A* and *kif9* genes were co-silenced, HT-1080 cells degraded gelatin more than when only *kif13A* gene was silenced ($P = 0.015$) and significantly less than when only KIF9 was knocked down ($P < 0.0001$). KIF13A remaining mRNA was around 30% when KIF13A and KIF9 were co-knocked down, while KIF9-v1 mRNA was down by almost 60%. Regrettably, I did not have sufficient time to study potential cooperation between KIF13A and KIF9-v1 for the trafficking of MT1-MMP. Overall, more experiments would be needed to understand whether KIF9-v1 works together with KIF13A or KIF3A to traffic MT1-MMP to the cell surface.

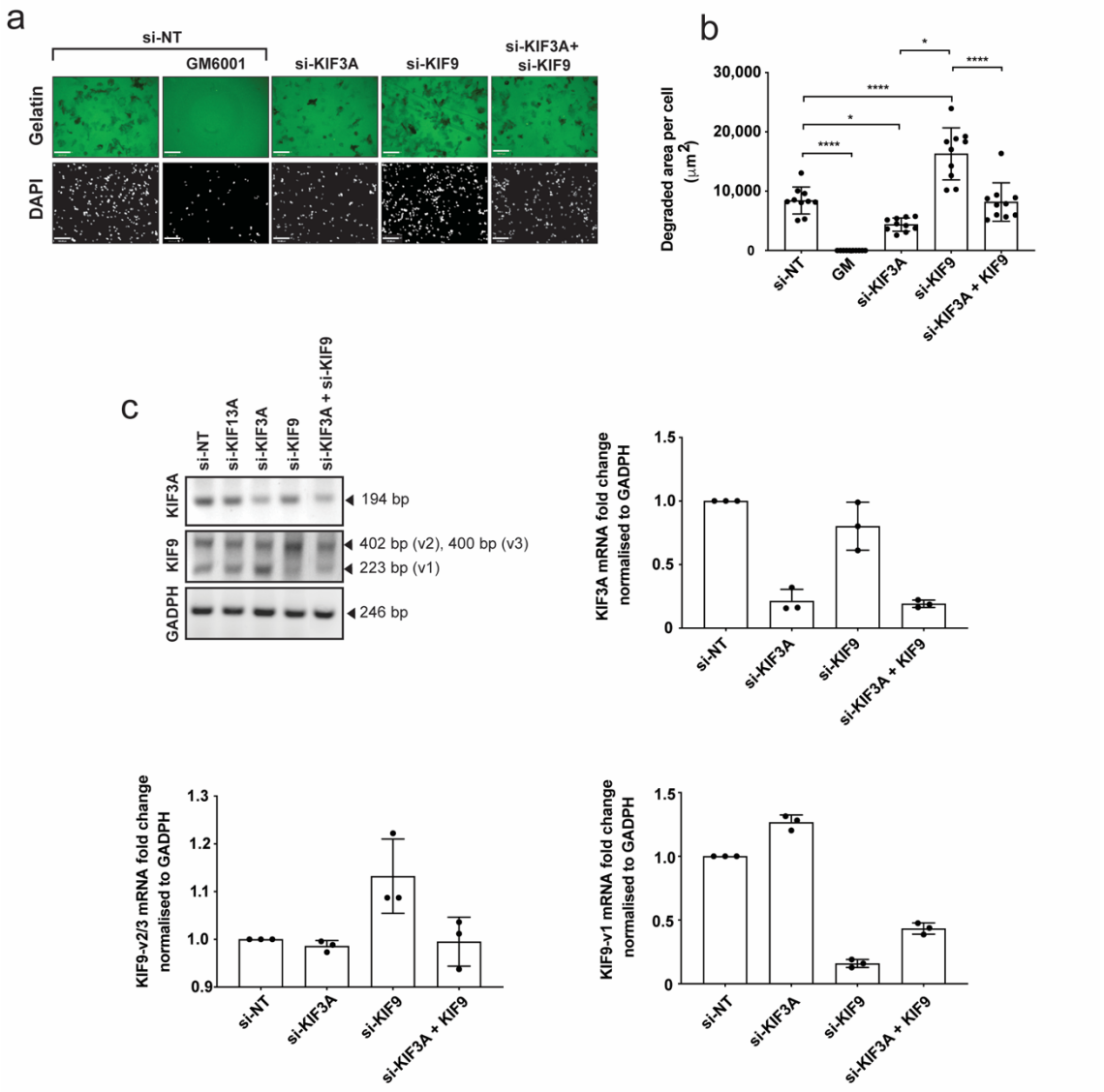


Figure 4.12: Effect of KIF3A and KIF9 co-KD on MT1-MMP-mediated gelatin film degradation

a HT-1080 cells were transfected with siRNAs targeting the selected KIFs and subjected to gelatin film degradation assay in the presence or absence of GM6001 (10 μM). Scale bars are 130 μm. **b** Quantification of the degradation area (μm^2) per cell in HT-1080 cells transfected with the specified siRNAs. Data are presented as mean of 10 independent microscopic fields of view and are representative of three independent experiments. One-way ordinary Anova with Tukey's multiple comparisons test. Error bars are SDs; **** $P < 0.0001$; ** $P < 0.01$; * $P < 0.05$. **c** Efficiency of KIF KD by one-step RT-PCR. Quantification of KIF3A, KIF9-v1and KIF9-v2/3 mRNAs relative to GADPH mRNA. The data are representative of three independent experiments.

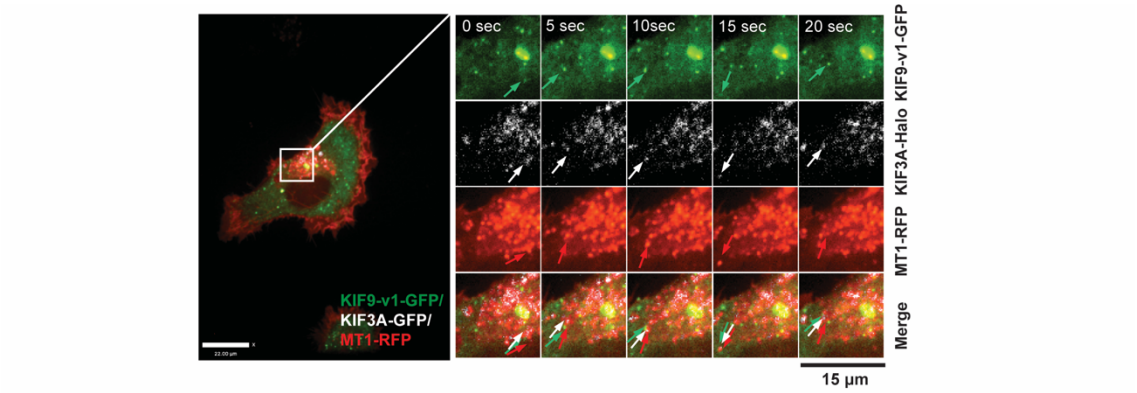


Figure 4.13: KIF3A and KIF9-v1 transport MT1-MMP-containing vesicles around the nuclear area

HT-1080 cells were transfected with KIF9-v1-GFP (green), KIF3A-GFP (white) and MT1-RFP (red) and they were subjected to live cell imaging by confocal microscopy. Representative image time sequences are shown. Arrows point vesicles of interest. Scale bar is 22 µm.

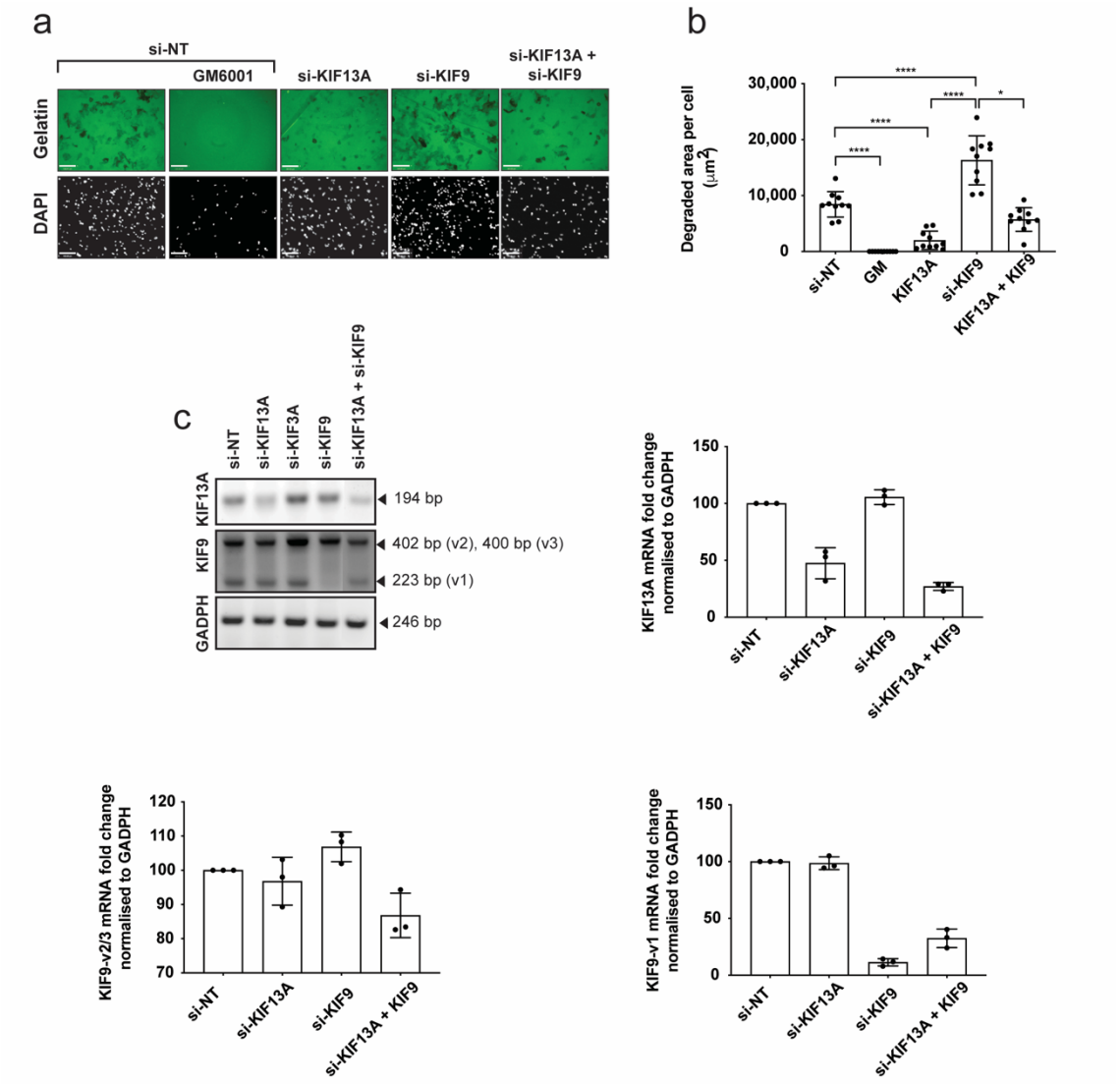


Figure 4.14: Effect of KIF13A and KIF9 co-KD on MT1-MMP-mediated gelatin film degradation

a HT-1080 cells were transfected with siRNAs targeting the selected KIFs and subjected to gelatin film degradation assay in the presence or absence of GM6001 (10 μM). Scale bars are 130 μm. **b** Quantification of the degradation area (μm^2) per cell in HT-1080 cells transfected with the specified siRNAs. Data are presented as mean of 10 independent microscopic fields of view and are representative of three independent experiments. One-way ordinary Anova with Tukey's multiple comparisons test. Error bars are SDs; **** $P < 0.0001$; * $P < 0.05$. **c** Efficiency of KIF knockdown by one-step RT-PCR. Quantification of KIF13A, KIF9-v1 and KIF9-v2/3 mRNAs relative to GADPH mRNA. The data are representative of three independent experiments.

4.3 Discussion

This Chapter focuses on the dynamic regulation of MT1-MMP vesicle trafficking by KIF13A, KIF3A and KIF9. Data presented in Chapter 3 highlighted that these motor proteins may mediate different MT1-MMP trafficking pathways, that may compete or work together, to deliver the proteinase to the cell surface. Therefore, I carried out several experiments to investigate whether knocking down any of these motor proteins had an impact on the distribution of MT1-MMP within the cytoplasm and its localisation to the cell edge. The KD of KIF13A and KIF3A significantly diminished both MT1-MMP peri-nuclear accumulation and localisation to the cell edge, while silencing *kif9* gene increased them in comparison to the control. MT1-MMP peri-nuclear accumulation partially overlapped with the MTOC and the *cis*- and *trans*-Golgi compartments, as previously reported for human melanoma cells (257), fibrosarcoma cells (209) and primary human macrophages (108). Differences in the percentages of cells characterised by this MT1-MMP peri-nuclear accumulation are likely depending on the altered trafficking of the proteinase towards the cell surface. The less MT1-MMP being transported to the substrate attachment sites by KIF13A or KIF3A the more MT1-MMP might be available for the lysosomes to be degraded. The KD of KIF3A had the greatest effect in diminishing MT1-MMP peri-nuclear accumulation. Lysosome anterograde movement has been shown to depend on several kinesins including KIF3A (258, 259) but its mechanisms of coupling are not well understood. The KD of KIF3A possibly shifts lysosome population to the central cytoplasm, reducing their transport towards the cell periphery and thus affecting MT1-MMP distribution to these cellular compartments. Peri-nuclear

MT1-MMP accumulation also partially overlapped with Rab5 and Rab7, used as markers for early and late endosomes respectively. These data are not sufficient to draw a conclusion on whether these KIFs are influencing MT1-MMP endo/exocytic circuities and more experiments would be needed to study this aspect further.

Co-expression of GFP-tagged KIFs and MT1-RFP revealed that KIF13A and KIF3A bound to MT1-RFP-positive vesicles associated to the microtubules, when cells were cultured on a gelatin film or embedded in 3D collagen. KIF13A was the sole KIF to overlap with MT1-RFP at the cell periphery. In Chapter 3, I reported that only KIF9-v1 mRNA levels were significantly decreased after transfection of HT-1080 cells with si-KIF9. As stated on the Database Resources of the National Center for Biotechnology Information (NCBI, Bethesda (MD)), KIF9 has three different splice variants: KIF9-v1, KIF9-v2 and KIF9-v3. KIF9-v2 and KIF9-v3 only differ in their non-coding regions and they both encode for a 790 amino acid-protein. KIF9-v1 has 70 amino acid less than KIF9-v2 and KIF9-v3 in its coiled-coil region, but identical motor and cargo-binding domains. Given the selectivity of si-KIF9 for KIF9-v1 (Chapter 3, Figure 3.5), I hypothesised that this was the only KIF9 variant to be involved in MT1-MMP intracellular trafficking. This assumption was strengthened by comparing KIF9-v1-GFP and KIF9-v2-GFP co-localisation with MT1-RFP. KIF9-v1-GFP was observed to co-localise with MT1-RFP-positive vesicles around the peri-nuclear area of HT-1080 cells cultured on a gelatin film or in 3D collagen. In contrast, KIF9-v2-GFP did not overlap with MT1-RFP for any of the culture conditions used. To my knowledge, this is the first time that KIF9 splice variants are shown to differently participate in the intracellular trafficking of a specific protein. It has been previously reported

that alternative splicing can influence trafficking of specific cargoes. For instance, regulation of Kinesin-1 exon 15 splicing affects GABA-B receptor transport towards dendrites and consequently neurotransmission (260). KIF1C-GFP did not co-localise with MT1-RFP but it markedly accumulated at the tips of membrane protrusions.

Time-lapse confocal imaging of HT-1080 cells transfected with GFP-tagged KIFs and MT1-RFP was employed to better define the role of these KIFs in MT1-MMP intracellular trafficking. Vesicles positive for MT1-RFP and KIF13A-GFP accumulated at the cell periphery and could also be detected in the central area of the cytoplasm. KIF13A-GFP overexpression caused the formation and localised at highly dynamic MT1-RFP tubular structures, extending from the cytosol to the cell edge. The motor activity of KIF13A was already reported to modulate vesicle tubulation *in vitro* (219). Overexpression of KIF13A-YFP was previously found to cause the development of Rab11-positive tube-like structures extending to the cell periphery (215). KIF13A-YFP extensively localised to these tubules, concentrating at the tips (215). This behaviour was explained by a model in which KIF13A mediates the generation, extension and peripheral transport of Rab11-dependent recycling endosomes from sorting endosomes (215). This model was further refined through other studies which confirmed the primary role of KIF13A for the biogenesis of recycling endosomes from sorting endosomes (216, 261, 262). Therefore, it is reasonable to hypothesise that KIF13A might be playing a role in mobilising MT1-MMP from recycling endosomes to sorting endosomes, influencing its recycling back to the cell surface. In fact, MT1-RFP-positive tubular structures were mostly originating from peripheral cytosolic aggregates that might be acting as stations to sort endocytic cargoes. Moreover,

time-lapse TIRF microscopy showed that these tubular structures pointed towards areas where highly adherent membrane protrusions were developing and were decorated with KIF13A-GFP. Hence, KIF13A-dependent mobilisation of MT1-MMP from sorting endosomes might direct the spatial localisation of new membrane protrusions, directing cell migration and invasion. MT1-RFP-positive vesicles trafficked by KIF13A-GFP around the peri-nuclear area or cell periphery proceeded with mean, maximum and minimum speeds in the range of 0.1 - 0.8 μm/s (Table 4.1). These velocities were comparable with reported measurements of anterograde movement of 5-HT_{1A} receptor by KIF13A (0.7 ± 0.3 μm/s) (219). Nevertheless, KIF13A-labelled vesicles moved significantly faster towards the tips of hippocampal neurones dendrites (1.56 ± 0.06 μm/s) (263). MT1-RFP-positive vesicles decorated with KIF13A-GFP were significantly bigger within the peri-nuclear area than at the cell periphery. It is possible than the two vesicle populations represent diverse states of maturity. The larger peri-nuclear vesicles might be acting as storage agglomerates of multiple MT1-RFP-positive vesicles from which peripheral vesicles originate. MT1-RFP-containing vesicles trafficked by KIF3A presented an oscillatory or linear trajectory and moved within the central area of the cytoplasm with mean, maximum and minimum speeds in the range of 0.09 - 0.6 μm/s (Table 4.1). These velocities were comparable with measurements of MT1-MMP mCherry vesicles trafficked by KIF3A in primary human macrophages (0.78 ± 0.20 μm/s) (108) and of other KIF3A-transported cargoes like fodrin in mouse neurons (0.5 – 0.6 μm/s) (150) and ciliary opsin in human retinal epithelial cells (0.7 μm/s) (264). As discussed above, KIF9-v1-GFP trafficked MT1-RFP vesicles that were slower but larger than those trafficked by KIF13A or KIF3A (Table 4.1). No measurements of vesicle movement driven by

KIF9 variants have been previously reported. It is noteworthy that MT1-RFP vesicles labelled with KIF9-v1 faded over time without changing their X and Y positions, thus most likely moving along the Z plane. It is reasonable to speculate that KIF9-v2 and KIF1C are not directly involved in MT1-MMP intracellular trafficking. In particular, live cell imaging data showed a consistent accumulation of KIF1C at the trailing edge of migrating cells. These results strengthened the hypothesis that this KIF might stabilise the trailing edge of migrating cells to support forward movement also in HT-1080 cells as previously reported for human epithelial cells (231).

Data presented in this Chapter demonstrate that KIF13A and KIF3A cooperate with each other to create the networks to deliver MT1-MMP to the cell surface. This result provides significant insights in understanding MT1-MMP vesicle trafficking and it also elucidates the roles of these KIFs. Many single-molecule studies on individual motors have been carried out and scientists have long analysed how the tug-of-war between kinesins and minus-end-directed dynein determines the directionality of cargo transport along microtubules (265, 266). On the other hand, very little is known about collaboration of multiple plus-end-directed kinesins for the intracellular trafficking of cargoes. Kinesin-1 and kinesin-2 have been reported to cooperate for mRNA transport in the developing *Xenopus Laevis* oocyte (267). Heterotrimeric and homodimeric Kinesin-2 motors collaborate with one another to regulate the development of *Caenorhabditis Elegans* amphid channel cilia on chemosensory neurons (268, 269). These motors work redundantly to traffic the same intraflagellar transport particles along the initial segment of the cilia, at a velocity that is intermediate between the free-sliding rate of each kinesin alone (0.7 μm/s) (269). Only homodimeric kinesin-2

transports intraflagellar particles to the ciliary distal segment (268, 269). Pan et al. (269) elaborated a mathematical model to predict the way heterotrimeric and homodimeric kinesin-2 collaborate, uncovering for the first time how different plus-end-directed kinesins can work together to traffic the same cargo. This motility model might well represent also how KIF13A and KIF3A cooperate to traffic MT1-MMP. In fact, it is reasonable to hypothesise that KIF13A and KIF3A transport MT1-MMP together within the central cytoplasmic area but only KIF13A delivers the proteinase to the cell surface. KIF13A and KIF3A might either exert an alternating action or undergo mechanical competition, dragging each other to move MT1-MMP vesicles along the microtubules (Figure 4.14). Then, KIF13A proceeds alone to deliver MT1-MMP at the substrate attachment sites and at the tips of ruffling membrane structures. KIF3A seemed also to work together with KIF9-v1 to traffic MT1-MMP within the central cytoplasmic area. Nevertheless, the accumulation of unbound KIF9-v1-GFP within the cytoplasm caused obscuration of vesicle labelling and made the tracking analysis impossible. Therefore, more experiments are needed to better understand whether KIF3A and KIF9-v1 work together to traffic MT1-MMP and also if there is any collaboration between KIF9-v1 and KIF13A.

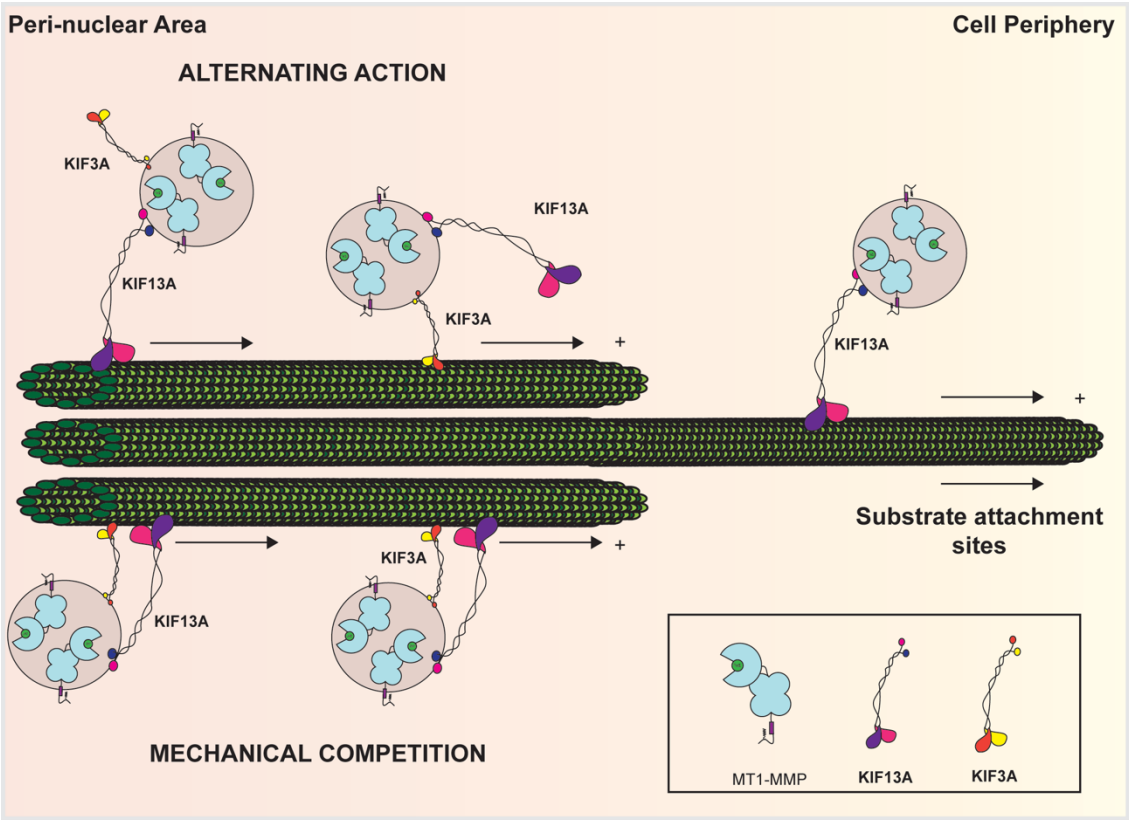


Figure 4.15: KIF13A and KIF3A collaborate to traffic MT1-MMP to the cell surface

Hypothetical model showing sequential transport of MT1-MMP vesicles from the perinuclear area to the cell periphery. KIF13A and KIF3A move MT1-MMP vesicles along the microtubule within the central cytoplasmic areas. When these vesicles are closer to the cell periphery, KIF13A alone deliver the proteinase to the substrate attachment sites or to the tips or ruffling membrane structures.

Taken together, data in this Chapter strongly suggest that KIF13A, KIF3A and KIF9-v1 are major players of MT1-MMP intracellular trafficking pathways. When HT-1080 cells are cultured atop a substratum, KIF13A and KIF3A cooperate to move MT1-MMP vesicles within the central cytoplasmic areas with average mean velocities around 0.6 μm/s (Figure 4.14). Once MT1-MMP vesicles are closer to the cell periphery, KIF3A dissociates and only KIF13A proceeds to deliver the proteinase to the substrate attachment sites and the tips of ruffling

membrane structures (Figure 4.14). KIF13A most likely also directs MT1-MMP mobilisation from sorting endosomes to recycling endosomes and its recycling back to the cell surface. KIF9-v1 might transport MT1-MMP to the top side of the cell, moving along the Z plane and possibly collaborating with KIF3A within the peri-nuclear area.

In future experiments, it would be important to further investigate the interplay between KIF13A, KIF3A and KIF9-v1 to achieve MT1-MMP delivery to the cell surface. It would be fascinating to understand how these KIFs coordinate with endo/exocytic circuities and cytoskeletal rearrangements to achieve MT1-MMP localisation to the cell surface. It might be worth trying other strategies to label kinesin constructs. Recently, Yang et al. (263) have reported the successful use of fluorescently labelled-tail domains instead of fluorescently-tagged full length kinesins to track vesicles transported by members of the Kinesin-1, -2 and -3 families in hippocampal neurons. These alternative fluorescently-labelled constructs markedly reduced the background signal (212). It could also be interesting to tag endogenous kinesins with fluorophores by genome engineering with CRISPR-Cas9. This strategy would allow to only look at the endogenous motor proteins avoiding overexpression.

CHAPTER 5:

THE ROLE OF KIF13A AND KIF9 IN THE METASTATIC POTENTIAL OF HT-1080 CELLS

5.1 Introduction

MT1-MMP promotes cell migration and invasion by degrading the ECM and it has been implicated with cancer invasion and metastasis (27). Metastasis is a complex multi-step process that involves the degradation of both the ECM and basement membranes allowing cancer cells to migrate from the primary tumor to distant tissues and organs. In Chapter 3, I showed that KIF13A, KIF3A and KIF9 mediate MT1-MMP intracellular trafficking when cells are cultured on a substratum or are embedded in a collagen gel. In Chapter 4, I confirmed that when cells are cultured atop a substratum, KIF13A and KIF3A collaborate to carry MT1-MMP-containing vesicles around the perinuclear area but only KIF13A carries the proteinase to the substrate attachment sites and the ruffling membrane structures. KIF9-v1 seems to be the only KIF9 splice variant to be directly involved in MT1-MMP intracellular trafficking, transporting the proteinase within the central cytoplasmic area. KIF3A is a relatively well-characterised kinesin and it has already been identified as major player of MT1-MMP intracellular trafficking in primary macrophages (108). On the contrary, KIF13A and KIF9 have been poorly studied and have never been associated with MT1-MMP localisation to the cell surface. Therefore, I decided to further characterise these two kinesins by examining the effect of their KD in MT1-MMP-dependent HT-1080 cell metastasis. This study would help to understand how kinesin-mediated MT1-MMP intracellular trafficking contributes to MT1-MMP-driven cell invasion and metastasis *in vivo*.

An experimental pulmonary metastatic model was chosen to evaluate the role of KIF13A and KIF9 in HT-1080 cell metastasis. This model is based on the

injection of cancer cells into the lateral tail vein of nude mice. The injection results in pulmonary metastasis that can be counted under a dissecting microscope (270) (Figure 5.1). This experimental metastasis model has been already employed to study the metastatic potential of HT-1080 cells (271-274). HT-1080 cells, stably expressing luciferase, were generated to monitor the development of metastatic lesions in the lungs by bioluminescent imaging. These cells were lentivirally transduced to express shRNAs targeting either *Kif13a* or *Kif9* genes, under the control of a tetracycline-on (Tet-on) inducible promoter. The aim of this Chapter is to describe the generation and characterisation of these cells and to discuss their employment in the pulmonary metastatic model that was selected.

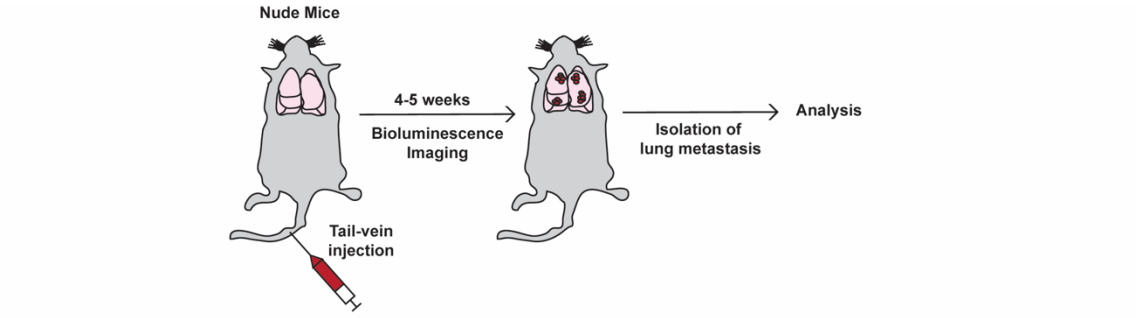


Figure 5.1: Schematic representation of an experimental pulmonary metastatic model

Luciferase-labelled cancer cells are injected in the lateral tail vein of nude mice. Mice are monitored for 4 - 5 weeks by whole-animal imaging to follow the development of lung metastasis. After, mice are sacrificed and lungs are isolated for analysing metastasis.

5.2 Results

5.2.1 MT1-MMP-dependent F-gelatin film degradation by NanoLuc® luciferase-expressing HT-1080 cells is inhibited by the KD of KIF13A, KIF3A and KIF1C and enhanced by the KD of KIF9

NanoLuc® luciferase-expressing HT-1080 cells were generated as described in Chapter 2 (Paragraph 2.1.6). To verify whether they behave similarly to wild type HT-1080 cells, cells were transfected with siRNAs targeting KIF13A and KIF9 and subjected to F-gelatin film degradation assay. As shown in Figure 5.2, the KD of KIF13A decreased the gelatinolytic activity of luciferase-expressing HT-1080 cells, whereas the KD of KIF9 enhanced it in comparison to the control. Quantification of gelatin film degradation confirmed that these differences were statistically significant (Figure 5.2). Therefore, I concluded that the insertion of luciferase gene into the genome did not alter the effect of KIF13A and KIF9 KD on vesicle transport of MT1-MMP to substrate attachment sites.

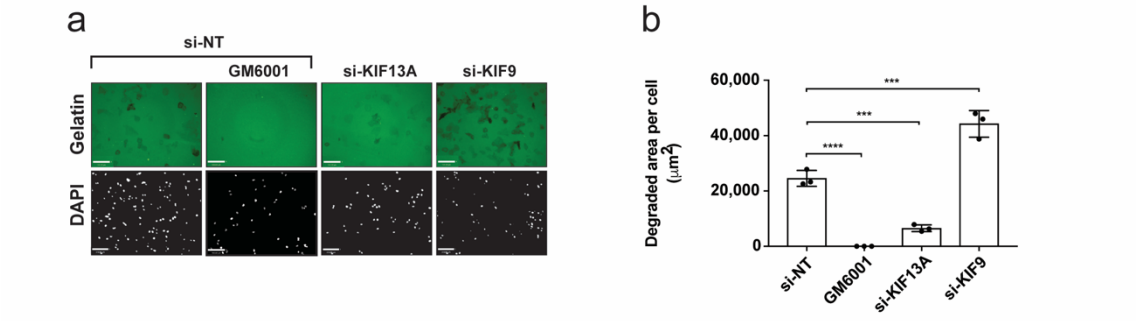


Figure 5.2: The KD of KIF13A and KIF9 alters MT1-MMP-mediated gelatin film degradation by luciferase-labelled HT1080 cells

a Luciferase-labelled HT1080 cells were transfected with siRNAs targeting KIF13A and KIF9 and subjected to gelatin film degradation in the presence or absence of GM6001 (10 μM). Scale bars

are 130 μm. **b** Quantification of the degradation area (μm^2) per cell. Data are presented as the mean of three independent microscopic fields of view and are representative of three independent experiments. One-way ordinary Anova with Tukey's multiple comparisons test. Error bars are SDs; **** P < 0.0001.

5.2.2 Characterisation of NanoLuc® luciferase-expressing HT-1080 stably expressing TRIPZ inducible lentiviral shRNAs targeting KIF13A or KIF9

Initially, I decided to target KIF13A and KIF9 employing Tet-off TRIPZ inducible lentiviral shRNA constructs, which were generated from the corresponding commercial Tet-on shRNAs, as described in Chapter 2 (Paragraph 2.2.14). The Tet-off inducible expression system does not require mice to be fed with doxycycline upon injection of cells into the tail vein, thus it is easier to handle. Doxycycline is usually administered through drinking water (275) but this antibiotic is known to adsorb UVA light and to be highly unstable in solution (276), forcing scientists to store doxycycline-containing water in tinted bottles and to replace it every few days. Therefore, it is much easier to employ Tet-off system. Unfortunately, transduction of luciferase-expressing HT-1080 cells with Tet-off TRIPZ inducible lentiviral shRNA constructs failed. Most likely, generation of Tet-off TRIPZ shRNA-expressing lentiviral particles was unsuccessful and luciferase-expressing HT-1080 cells could not be efficiently infected. Therefore, the commercially available Tet-on shRNAs, targeting KIF13A (sh-KIF13A) and KIF9 (sh-KIF9), were employed to generate lentiviral particles and used to transduce luciferase-expressing HT-1080 cells as previously explained in Chapter 2 (Paragraph 2.1.7). Transduction efficiency was monitored

by checking the expression of the TurboRFP reporter gene by wide-field fluorescent microscopy. As shown in Figure 5.3 a, TurboRFP fluorescence signal was barely detectable, suggesting that constructs were not efficiently delivered into the cells. Therefore, I transduced two more times and found that TurboRFP fluorescence signal notably increased (Figure 5.3 a). RT-PCR was employed to evaluate the KD efficiency of KIF13A and KIF9. As shown in Figure 5.3 b, KIF13A mRNA level was down by 50%, whereas sh-KIF9 construct failed to efficiently decrease KIF9-v1 mRNA level, that was diminished by more than 95% when the corresponding siRNA was used for transfection (Chapter 3, Figure 3.5 a). These cells were further characterised by F-gelatin film degradation (Figure 5.3 c). Luciferase-expressing HT-1080 cells, expressing Tet-on TRIPZ inducible NT shRNA (sh-NT) degraded gelatin similarly to those expressing sh-KIF13A or sh-KIF9 (Figure 5.3 d). Hence, I concluded that these cells were not suitable for the experimental pulmonary metastatic model.

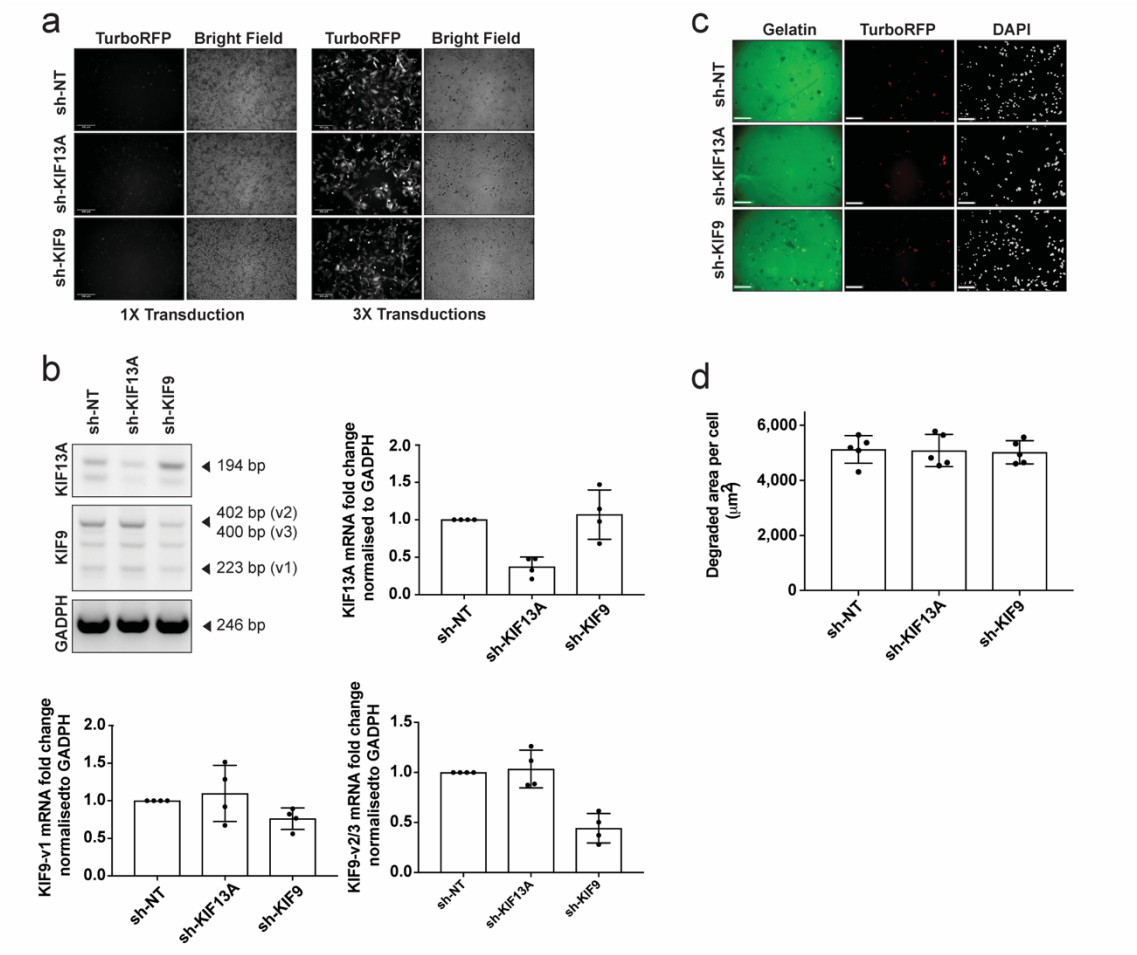


Figure 5.3: Characterisation of NanoLuc® luciferase-labelled HT1080 stably expressing Tet-on TRIPZ inducible lentiviral shRNAs targeting KIF13A or KIF9

a Luciferase-labelled HT1080 cells were transduced one or three times with Tet-on TRIPZ inducible lentiviral shRNAs targeting KIF13A and KIF9 and they were subjected to wide-field microscopy to check the expression of the TurboRFP reporter gene. Scale bars are 130 µm. **b** Efficiency of KIF KD by one-step RT-PCR. Quantification of KIF13A and KIF9 mRNA fold change relative to GADPH. The data are representative of three independent experiments. **c** Luciferase-labelled HT1080 cells expressing Tet-on TRIPZ inducible lentiviral shRNAs targeting KIF13A and KIF9 were subjected to gelatin film degradation. Scale bars are 130 µm. **d** Quantification of the degradation area (μm^2) per cell. Data are presented as the mean of five independent microscopic fields of view and are representative of three independent experiments.

5.2.3 Genomic alterations of Kif13a and Kif9 genes across The Cancer Genome Atlas (TCGA) studies

Since I could not evaluate the effects of knocking down KIF13A and KIF9 on MT1-MMP-dependent HT-1080 cells' metastatic potential through the experimental pulmonary metastatic model, I decided to take a broader approach. As previously mentioned, KIF13A and KIF9 have been poorly characterised and little is known about their potential role in cancer. Therefore, cBioPortal (http://cbioportal.org) (237, 238) was employed to search for mutations, amplifications and deep deletions of *Kif13a* and *Kif9* genes in The Cancer Genome Atlas (TCGA) database. The term amplification indicates a high copy-number level per gene, whereas deep deletion implies a deep loss in the copy-number level per gene and often refers to a homozygous deletion.

Somatic mutations of *Kif13a* and *Kif9* genes could be detected in 2.3% and 1.2% of samples respectively and they were found across several types of cancer (Figure 5.4). Fisher's exact test revealed that *Kif13a* and *Kif9* somatic mutations were not mutually exclusive but there was statistically significant co-occurrence ($P < 0.001$). Interestingly, both *Kif13a* and *Kif9* mutations were mostly detected in melanoma and uterine carcinoma (Figure 5.4). The biological significance of these mutations could not be determined because of their consistent distribution through the protein sequence and their uniqueness to each sample.

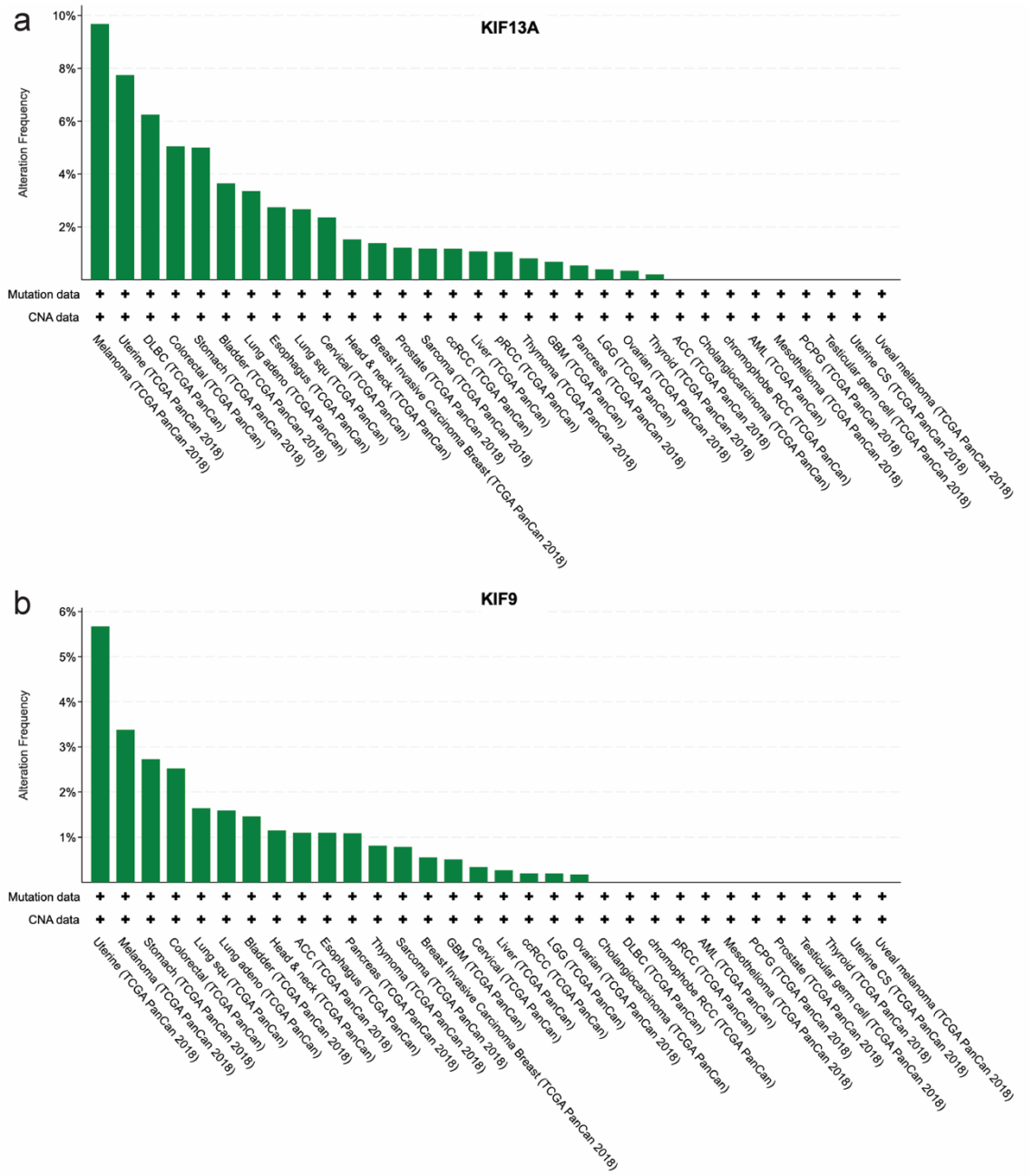


Figure 5.4: Analysis of *Kif13a* and *Kif9* gene mutations in TCGA PanCancer Atlas studies

a, b *Kif13a* and *Kif9* gene mutations across TCGA PanCancer Atlas studies. In order of appearance DLBC: diffuse large B-cell lymphoma; ccRCC: kidney renal clear cell carcinoma; GBM: glioblastoma multiforme; LGG: brain lower grade glioma; ACC: adrenocortical carcinoma.

Oncoprints are compact representations made to visualise genomic alterations across a set of cases. The oncoprint of *Kif13a* and *Kif9* amplifications and deep

deletions showed that *Kif13a* was amplified in 1.3% of samples and deleted in 0.2% of them, while *Kif9* was amplified in only 0.1% of samples and deleted in 0.5% of them (Figure 5.5 a). These gene alterations were distributed across several cancer types from TCGA (Figure b c). As shown in Figure 5.5 b, almost eight in 100 patients, diagnosed with ovarian serous cystadenocarcinoma, presented a *Kif13a* gene amplification. Unfortunately, I could not correlate the overall patients' survival status with this amplification because this information was not available for all the profiled patients. *Kif13a* gene was also amplified for more than 6% of bladder urothelial cancer patients (Figure 5.5 c) but correlation with their overall survival status could again not be assessed. This type of analysis could be run for other cancer studies like cholangiocarcinoma, breast invasive and lung squamous carcinomas but P values, calculated using a Logrank test, were not statistically significant. *Kif9* gene was deleted in more than 6% of patients diagnosed with diffuse large B-cell lymphoma (DLBC) and about 3% of those affected by kidney renal clear carcinoma (ccRCC). For these two studies, it was again not possible to correlate the gene alteration with the patients' overall survival status. Taken together these data suggest that the biological significance of *Kif13a* and *Kif9* gene mutations cannot be assessed. Interestingly, this analysis highlights that *Kif13a* and *Kif9* have altered expression profiles in several cancer types and that *Kif13a* gene is mostly amplified, while *Kif9* gene is mainly deleted.

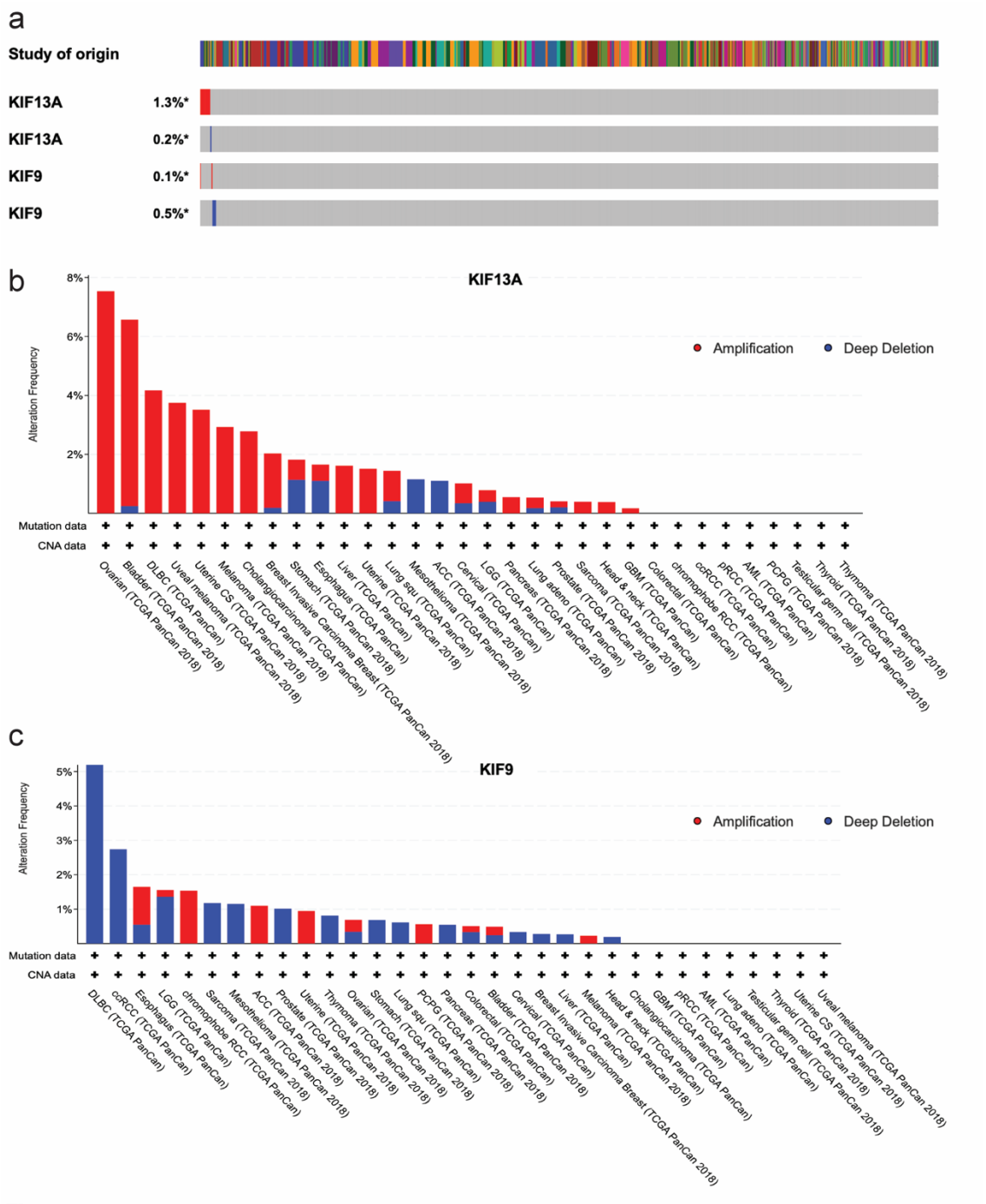


Figure 5.5: Analysis of *Kif13a* and *Kif9* gene amplifications and deep deletions in TCGA PanCancer Atlas studies

a Oncoprint of *Kif13a* and *Kif9* gene amplifications and deep deletions across the TCGA PanCancer Atlas studies. Each colour in the study of origin bar represents a distinct cancer study. **b** *Kif13a* gene amplifications and deep deletions across TCGA PanCancer Atlas studies. **c** *Kif9*

gene amplifications and deep deletions across TCGA PanCancer Atlas studies. In order of appearance: DLBC: diffuse large B-cell lymphoma; ACC: adrenocortical carcinoma; LGG: brain lower grade glioma; GBM: glioblastoma multiforme; ccRCC: kidney renal clear cell carcinoma; PCPG: pheochromocytoma and paraganglioma.

5.3 Discussion

To date, KIF13A and KIF9 have never been described to mediate MT1-MMP-containing vesicle transport to the cell surface. These two motor proteins, particularly KIF9, are not very well studied and my findings represent an important contribution for their characterisation. In Chapter 3, I showed that when cells are cultured atop a substratum, the KD of KIF13A decreases MT1-MMP-mediated cellular functions on the cell surface, whereas the KD of KIF9 enhances them. Interestingly, silencing of both *Kif13a* and *Kif9* genes notably diminishes MT1-MMP-dependent invasion through a 3D collagen gel. It is reasonable to speculate that KIF13A may support MT1-MMP-dependent cancer cell invasion and metastasis by trafficking the proteinase to the leading edge. On the other hand, it is less obvious to speculate how KIF9 may influence MT1-MMP-mediated invasion and metastasis. It is possible to hypothesise that its function may sustain cell migration through the ECM, but may contrast MT1-MMP-dependent transmigration through the basement membrane, a process that is well-mimicked by the transwell invasion assay that I performed. To better investigate how KIF13A and KIF9 contribute to MT1-MMP-mediated cancer cell invasion and metastasis, I attempted to employ an experimental pulmonary metastatic model *in vivo* by generating Tet-on luciferase-expressing HT-1080 cells expressing sh-

KIF13A or sh-KIF9. In this Chapter, I described the method used to generate this stable cell line. Luciferase-expressing HT-1080 cells were successfully generated and insertion of the luciferase gene into the genome did not seem to change the effect of silencing *Kif13a* and *Kif9* genes on their gelatinolytic activity. These cells were also effectively transduced with lentiviral particles expressing Tet-on TRIPZ inducible sh-KIF13A or sh-KIF9. Nevertheless, after three lentiviral transductions of the cells, the efficiency of KIF13A and KIF9 KD was still low and there was no difference between the gelatinolytic activity of cells expressing sh-KIF13A, sh-KIF9 and sh-NT. Therefore, I decided to stop this experiment. As previously mentioned, this model is based on the injection of cancer cells directly into the systemic circulation through the lateral tail vein (270), which results in the development of lung metastasis because the pulmonary capillary bed is the first encountered by cancer cells (270). This experiment was planned to be carried out by the research group of one of our collaborators, Professor Masaki Inada, who is based at the department of Technology and Agriculture at the University of Tokyo. Considering the experimental conditions already described by other authors (271-274), nude mice of 4 - 8-week-old would be injected with 5 x 10^4 - 1 x 10^6 luciferase-expressing HT-1080 cells, expressing Tet-on inducible sh-NT, sh-KIF13A and sh-KIF9 and sacrificed 20 - 28 days after injection. Lung colonisation would be examined during the course of the experiment by performing whole-mouse in vivo bioluminescence imaging. Mice would need to be fed Tet-containing water throughout the experiment. After the sacrifice, lungs would be fixed and metastasis would be counted under a dissecting microscope. To make sure that only MT1-MMP-dependent lung colonisation is considered, mice injected with sh-NT would also be administered DX2400 or the

corresponding IgG isotype control. As mentioned in Chapter 3, DX2400 is a potent and specific biologic inhibitor of MT1-MMP (240) and has previously been employed to achieve MT1-MMP inhibition in mice at a concentration of 20 mg/kg and injected intraperitoneally every other day (277). Therefore, this experimental setup (Figure 5.6) is a valuable tool to evaluate how suppression of KIF13A and KIF9 affects MT1-MMP-dependent invasion and metastasis of HT-1080 cells and alternative means to achieve a better KD of these kinesin genes should be considered.

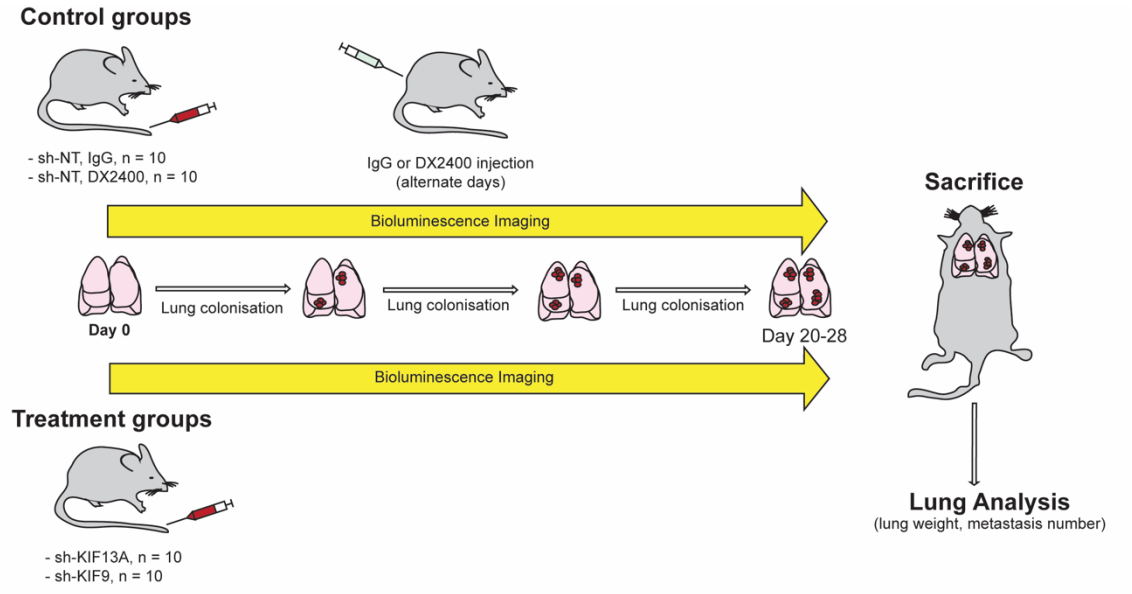


Figure 5.6: Schematic representation of a possible experimental setup

Control nude mice are injected with luciferase-labelled HT-1080 cells expressing sh-NT and administered DX2400 or IgG control every other day. Nude mice in the treatment groups are injected with luciferase-labelled HT-1080 cells expressing sh-KIF13A or sh-KIF9. All mice are fed Tet-containing water during the course of the experiment. Lung colonisation is monitored with whole-animal bioluminescence imaging. Mice are sacrificed 20 - 28 days post injection and lungs are fixed and analysed under a dissecting microscope.

Kif13A and *Kif9* genes could be silenced by genome editing techniques based on clustered regularly interspaced palindromic repeat (CRISPR)-associated (Cas) 9 system. Zheng et al. (278) showed that Cas9 coupled with two guide RNAs (gRNAs) could precisely and effectively generate DNA deletions of up to 10 kb. This approach was successfully employed to generate KIF5B knockout cells to study the role of this motor protein in the transport of keratin and vimentin intermediate filaments (279). Wei et al. (280) generated KIFC1 knockout cell lines targeting different *Kifc*1 loci to investigate the functions of this protein during the cell cycle. CRISPR/Cas9 genome editing was also employed to generate KIF3A/KIF3B double knockout cells to examine their role in intraflagellar transport in mammalian cilia (281). Therefore, CRISPR/Cas9 could also be used to generate KIF13A and KIF9 knockout luciferase-expressing HT-1080 cells. Unfortunately, I did not have sufficient time to explore this alternative strategy.

The analysis of the TCGA database revealed that the expression profile of KIF13A and KIF9 is altered in several cancer types. Amplification is the most common Kif13a gene alteration detected across the TCGA database. Remarkably, KIF13A is reported by the Pathology Atlas (https://www.proteinatlas.org/humanproteome/pathology) (282) as an unfavourable prognostic marker for liver cancer patients. The Pathology Atlas is a database within the Human Protein Atlas and collects mRNA and protein expression data from 17 different human cancers, correlating them with the patients' clinical outcome. As shown in Figure 5.7, liver cancer patients with a high expression of KIF13A had a significantly minor survival probability than those with a low expression. These results indicate that KIF13A may have a specific role in liver cancer and more generally a pro-tumorigenic potential. My

data suggest that KIF13A is a major player of MT1-MMP intracellular trafficking pathways and may mediate MT1-MMP-dependent invasion and metastasis of cancer cells. Therefore, it is reasonable to hypothesise that one of the reasons why KIF13A may have a pro-tumorigenic role is its involvement in MT1-MMP trafficking to the cell surface. KIF9 is mainly deleted rather than amplified across the TCGA database. Moreover, according to the Pathology Atlas, it is a favourable prognostic marker in renal and colorectal cancers (Figure 5.8). These results suggest that KIF9 may have an anti-tumorigenic potential for these two cancer types. According to my data, KIF9 is involved in MT1-MMP intracellular trafficking pathways and it may sustain MT1-MMP-dependent invasion through the stroma and prevent transmigration of cancer cells through the basement membrane. Overall, these data highlight that KIF13A and KIF9 may have cancer-specific roles, in part related to their involvement in MT1-MMP intracellular trafficking. As discussed above, these motor proteins are poorly studied and there are only few publications discussing their altered expression profiles in cancer. Chandrasekaran et al. (283) used cBioPortal to search for kinesin gene alterations in TCGA and reported that Kif13a gene was amplified in more than 10% of patients diagnosed with serous ovarian adenocarcinoma or bladder urothelial carcinoma. They also reported that 12% of patients with clear renal carcinoma had a homozygous deletion of kif9 gene. These percentages were slightly different than what I found though my analysis. These discrepancies are likely due to the higher number of data that have been included in the TCGA database since the authors published their review. Cho et al. (284) performed an integrate analysis of the clinical significance of specific kinesin motors, including KIF9, in low-grade glioma and glioblastoma. They showed that KIF9 expression

is linked to cancer progression and significantly lower survival probability, especially for patients diagnosed with glioblastoma (284). This is the only study to date that analyses the relationship between KIF9 and cancer progression.

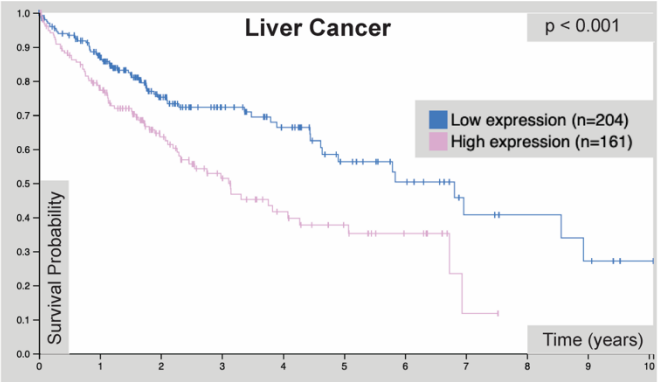


Figure 5.7: KIF13A is an unfavourable prognostic marker for liver cancer

Survival analysis of liver cancer patients characterised by a low (below cut off) or high level (above cut off) of expression of KIF13A generated through the Human Pathology Atlas. Cut off was determined automatically. X-axis shows time for survival and Y-axis the probability of survival. 1 corresponds to 100% survival. Statistical significance was calculated by Log-rank T test analysing the correlation between mRNA expression and patient survival.

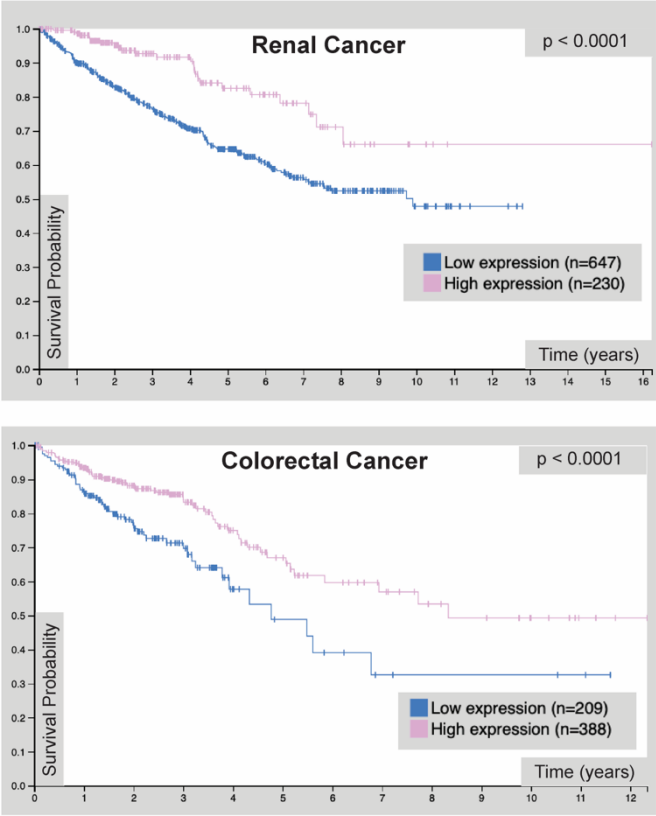


Figure 5.8: KIF9 is a favourable prognostic marker for renal and colorectal cancers

a, b Survival analysis of renal and colorectal cancer patients characterised by a low (below cut off) or high level (above cut off) of expression of KIF9 generated through the Human Pathology Atlas. Cut off was determined automatically. X-axis shows time for survival and Y-axis the probability of survival. 1 corresponds to 100% survival. Statistical significance was calculated by Log-rank T test analysing the correlation between mRNA expression and patient survival.

In future experiments, it would be crucial to investigate the correlation between KIF13A, KIF9 and cancer. Given the primary role of MT1-MMP in cancer progression (27) and the potential involvement of these kinesin motors in its intracellular trafficking, it would be essential to analyse the effect of their suppression on MT1-MMP-dependent invasion of cancer cells. Hence, the employment of alternative routes like CRISPR/Cas9, to generate KIF13A and KIF9 knockout luciferase-expressing HT-1080 cells, would be critical to widen our

knowledge about the involvement of these KIFs in cancer progression. Moreover, more bioinformatic analysis should be carried out to correlate *Kif13a* and *Kif9* gene alterations with *Mt1-mmp* gene alterations across the cancer studies of TCGA.

CHAPTER 6:

GENERAL DISCUSSION AND FUTURE PROSPECTS

6.1 General discussion

Cell migration is a key process for multicellular organisms and when it is mis-regulated it can support the development of pathological conditions such as cancer invasion and metastasis (2, 285, 286). MT1-MMP promotes cell migration and invasion by degrading pericellular ECM (14, 287). The proteinase has been shown to be overexpressed in different types of tumor cells, supporting tumor growth, invasion and metastasis (287-289). Therefore, its expression has been associated with poor overall survival in multiple cancer types (290). Cell surface exposure of MT1-MMP to the leading edge of migrating cells is an important step for the proteinase to support cellular invasion (72). Mechanisms that govern MT1-MMP polarised localisation to the plasma membrane are still unclear. Dr. Itoh's research group and others have shown that MT1-MMP cell surface exposure is achieved by targeted intracellular transport of MT1-MMP-containing vesicles along microtubule filaments and that this process is powered by KIFs. Employing a gene KD approach, Dr. Itoh's research group have also identified four KIFs (KIF13A, KIF3A, KIF9 and KIF1C) that may regulate MT1-MMP intracellular trafficking in HT-1080 cells. In this thesis, I have investigated the role of these KIFs in MT1-MMP cell surface exposure and MT1-MMP-dependent cell migration and invasion.

Multiple KIFs have been reported to mediate MT1-MMP intracellular trafficking in various cell types: KIF5B, KIF3A/3B have been shown to transport MT1-MMP-containing vesicles in primary human macrophages (108); KIF1B has been found to regulate MT1-MMP cell surface exposure in gastric cancer cells and glioma cells (212, 249); KIF3A and KIF5B have been associated with MT1-MMP vesicle transport in MDA-MB-231 cells (211). In contrast with these reports, I found that KIF5B, KIF3B and KIF1B were all dispensable for MT1-MMP localisation to the cell surface of HT-1080

cells. However, my data confirmed that KIF13A, KIF3A, KIF9 and KIF1C were all potentially involved in MT1-MMP intracellular transport in HT-1080 cells. Therefore, it is reasonable to speculate that mechanisms, which govern MT1-MMP polarised localisation, are controlled by multiple motor proteins and are potentially cell-type specific.

My data showed that when HT-1080 cells are cultured atop a substratum, the KD of KIF13A and KIF3A decreases MT1-MMP-dependent proteinase activity on the cell surface, whereas silencing *Kif9* gene enhanced it. Interestingly, silencing none of these *kinesin* genes altered overall cell surface expression of MT1-MMP, but it influenced its polarised localisation. In particular, the KD of KIF13A and KIF3A significantly diminished MT1-MMP cell surface exposure at the substrate attachment sites, while silencing *Kif9* gene increased it. These results led me to hypothesise that when HT-1080 cells are seeded on 2D matrices, KIF13A and KIF3A traffic MT1-MMP-containing vesicles to substrate attachment sites, whereas KIF9 transport the proteinase to other areas, like the dorsal cell side. My data demonstrate that kinesins can highly influence cells' ability to modify the pericellular microenvironment, by regulating MT1-MMP polarised cell surface exposure. This assumption is strikingly exemplified by the altered cells' capability to breach through a collagen-coated microporous membrane upon kinesin KD. Cell invasion through a microporous membrane mimics cell breaching through the basement membrane. Therefore, it is reasonable to speculate that kinesins may play a prominent role in basement membrane transmigration *in vivo*, influencing the progression of pathological processes like cancer cell invasion and metastasis. In future, it will be interesting to find a suitable way to assess these aspects *in vivo*, employing animal models like the pulmonary metastatic model described in Chapter 5.

Since 2D cell cultures do not accurately mimic conditions *in vivo*, I also studied the effects of silencing these *kinesin* genes on MT1-MMP-dependent migration of HT-1080 cells within a 3D collagen matrix. The KD of KIF13A, KIF3A and KIF9 significantly diminished MT1-MMP-mediated 3D migration of HT-1080 cells. Although these results are in good agreement with the observations made employing 2D culture conditions for KIF13A and KIF3A, they are opposite for KIF9. As extensively discussed in Chapter 3, this discrepancy is likely due to the different environment that cells face when they are either cultured on the commonly used 2D surfaces or completely embedded in 3D matrices. Anyway, my data suggest that KIF13A, KIF3A and KIF9 transport MT1-MMP towards the leading edge, influencing MT1-MMP-dependent 3D migration. These findings confirm that these KIFs do not only potentially control basement membrane transmigration *in vivo* but also cell migration and invasion through the stromal matrices. Considering these results, it will be even more interesting to find a suitable model to test this hypothesis *in vivo*. Above all, it would be really fascinating to better understand how the pericellular microenviroment could influence KIF9-dependent MT1-MMP intracellular trafficking pathways. To my knowledge, it has never been reported that a kinesin can differently regulate the polarised cell surface exposure of one of its cargoes, depending on whether the cell needs to transmigrate through the basement membrane or to migrate through the stroma.

MT1-MMP-dependent cell migration relies on the polarised localisation of the proteinase on the cell surface and this process needs to coordinate with the dynamics of motility-associated structures. KIF1C is likely to play a role in at least some of the mechanisms that drive the generation of membrane protrusions. This hypothesis is supported by the fact that silencing *Kif1c* gene significantly decreased some of the MT1-MMP-dependent proteolytic activities but did not alter the proteinase localisation

to substrate attachment sites. Similarly, Wiesner and co-workers (179) have shown that KIF1C influences MT1-MMP-dependent matrix degradation at podosomes without altering the proteinase localisation at these membrane protrusions. KIF1C has been reported to regulate podosome dynamics and is transported to the cell periphery upon activation of protein kinesin C (PKC) before podosome formation is initiated (234). It has also been reported that KIF1C stabilises the trailing edge of epithelial cells during migration by trafficking α5β1 integrins (231). It is still unknown whether KIF1C contributes to the dynamics of other motility associated structures like lamellipodia or invadopodia, but it is likely that it may play a role.

KIF13A, KIF3A and KIF9 seem to also regulate MT1-MMP intracellular trafficking mechanisms also in RASFs. These cells have been found to contribute to the growing pannus in the inflammatory milieu of joints and to also invade into healthy cartilage (291, 292). MT1-MMP is highly expressed in RASFs and contributes to their invasiveness (24). Hence, understanding how this proteinase is trafficked to the cell surface would help researchers to find new targets to treat RA. Different subsets of RASFs have been identified and described recently (293). Sub-lining fibroblasts are thymus cell antigen 1 positive ($THY1^+$) and express genes encoding chemokines and cytokines, mediating inflammation (293). Lining fibroblasts are $THY1^-$ and responsible for bone and cartilage degradation (293). It would be interesting to investigate whether MT1-MMP intracellular trafficking pathways are different in these subsets and whether they contribute to the phenotype of these cells. These findings would likely help setting up more effective treatments for RA, directly targeting specific subsets of RASFs.

Unlike RASFs, MDA-MB-231 cells do not seem to employ KIF13A, KIF3A and KIF9 to achieve MT1-MMP cell surface exposure. KIF5B has been reported to mediate MT1-MMP intracellular trafficking in this cell type (211) but my data did not confirm

that KIF5B is involved in MT1-MMP localisation to the cell surface of MDA-MB-231 cells. As previously discussed in Chapter 3, this discrepancy may depend on the different experimental conditions used to run the gelatin film degradation assay and to quantify MT1-MMP gelatinolytic activity. Wang and co-workers (210) found that KIF5B localises to MT1-MMP-containing vesicles in MDA-MB-231 cells and that this process depends on phospholipase D2 (PLD2). In future, it would be important to better investigate the role of KIF5B for the trafficking of MT1-MMP in MDA-MB-231 cells. Since KIF5B co-localisation with MT1-MMP-positive vesicles was analysed for MDA-MB-231 cells stably expressing MT1-GFP, it would be important to check whether this result is reproducible when endogenous MT1-MMP is stained. It would also be crucial to screen for potential KIFs involved in MT1-MMP intracellular trafficking mechanisms, employing the same gene KD approach that was used by Dr Itoh's research group in HT-1080 cells.

Dynamics of MT1-MMP intracellular trafficking by KIF13A, KIF3A and KIF9 were investigated by employing time-lapse confocal imaging of HT-1080 cells expressing fluorescently-tagged KIFs and MT1-RFP. I showed that KIF13A traffics MT1-MMP-positive vesicles around the peri-nuclear area as well as at the cell periphery. In particular, this KIFs seemed to mediate MT1-MMP delivery to the substrate attachment sites and the tips of ruffling membrane structures, when HT-1080 cells are cultured on a 2D matrix. Vesicles positive for MT1-MMP and KIF3A moved within the peri-nuclear area with an oscillatory or linear trajectory. These imaging experiments also revealed that KIF9-v1 and not KIF9-v2 carries MT1-MMP-containing vesicles in HT-1080 cells. Vesicles positive for KIF9-v1 and MT1-MMP exhibited a very limited XY movement and rather travelled out of plane over time. MT1-MMP-positive vesicles trafficked by KIF13A moved with velocities in the range of 0.1

- 0.7 μm/s and this result was in good keeping with previously reported measurements of vesicles transported by the same KIF (219). MT1-MMP was trafficked by KIF3A with velocities in the range of 0.09 – 0.6 μm/s. These measurements were also in good agreement with velocities calculated for MT1-MMP-containing vesicles in primary human macrophages (108).

KIF13A and KIF3A cooperate to achieve MT1-MMP cell surface exposure in HT-1080 cells. This collaboration takes place within the peri-nuclear area until KIF13A takes over and delivers the proteinase to the cell periphery. This result represents one of the most novel findings of my work. As extensively described in Chapter 4, cooperation between different plus-end directed KIFs for the intracellular trafficking of cargoes has not been very well described so far. Pan and co-workers (269) were the first to elaborate a mathematical model to explain how plus-end directed motors cooperate to traffic the same cargo. According to this model, KIFs could either have an alternating action or undergo mechanical competition. Considering the velocity measurements and the observations I made through time-lapse confocal imaging experiments, it is currently not possible to rule out one of the two hypotheses. However, collaboration between multiple plus-end directed motors to traffic the same cargo might be used as an additional way to fine tune networks of intracellular transport. Moreover, it might also be employed to prevent cargoes from falling off the microtubule filaments. It has been shown that post-translational modifications of tubulin and microtubule-binding proteins can act as guidance cues for polarised kinesin transport (199). These cues control kinesin loading and navigation on microtubule tracks as well as cargo delivery. Since KIF13A and KIF3A belong to different families and are regulated by distinct guidance cues, it is likely that when

one's affinity for the microtubule tracks is diminished, the other can prevent the cargo from falling off, holding to the microtubule filaments.

It is still largely unknown whether KIF-driven intracellular trafficking of MT1-MMP plays a role in the invasion and metastatic potential of cancer cells *in vivo*. Wang and co-workers (210) are the only to have studied this aspect so far. They employed the mice mammary tumor virus (MMTV)-Neu transgenic mouse breast cancer model and found that PLD2-phosphatidic acid (PA)-KIF5B signalling mediates MT1-MMP cell surface exposure in breast cancer cells and influences their metastatic potential to the lungs (210). PLD2-generated PA couples MT1-MMP-containing vesicles with KIF5B, which carries the proteinase to the plasma membrane of breast cancer cells (210). The authors claim that targeting this exocytic pathway could be a successful therapeutic strategy for metastatic breast cancer patients. Although I was unable to test the role of KIF13A and KIF9 in the invasion and metastatic potential of HT-1080 cells *in vivo*, I could show that the expression profile of KIF13A and KIF9 is altered in several cancer types by employing a bioinformatic approach. According to this analysis, KIF13A has a pro-tumorigenic potential and its high expression is correlated with poor survival in liver cancer patients (282). These results are at least in part explained by the fact that this KIF mediates MT1-MMP intracellular trafficking mechanisms and its KD reduces MT1-MMP-dependent transwell invasion and migration through 3D collagen. My analysis also showed that KIF9 is deleted in several cancer types and it is a favourable prognostic marker in renal and colorectal cancers. These results could also be partially explained by the fact that this KIF is involved in MT1-MMP cell surface exposure. However, since its KD promotes MT1-MMP-dependent transwell invasion, but reduces MT1-MMP-driven migration through 3D collagen, experiments *in vivo* would better explain its anti-tumorigenic potential.

6.2 Future prospects

I have shown that KIF13A, KIF3A and KIF9-v1 play a role in MT1-MMP intracellular trafficking and influence MT1-MMP-dependent cellular functions on the cell surface in HT-1080 cells and potentially in RASFs. Although, I have elucidated how these three KIFs differentially contribute to transport of MT1-MMP-containing vesicles, further research is required to fully understand the detailed mechanism. For instance, it is unknown which adaptor molecules mediate the interaction between MT1-MMP-positive vesicles and these KIFs. Dr. Itoh's research group have previously found that the eight amino acid insertion within the catalytic domain of MT1-MMP, named MT-Loop, is required for the enzyme to localise at the cell adhesion complex of the cells (112). Recently, they have also identified several candidates that associate with MT-Loop by employing a proteomic approach. These molecules could potentially mediate the interaction between MT1-MMP-containg vesicles and KIFs, playing a key role in the regulation of KIF-driven MT1-MMP localisation to the leading edge of migrating cells. PA is the only molecule that has been reported to mediate the interaction between a kinesin motor and MT1-MMP-containing vesicles (210). Since most KIFs play indispensable roles during development and homeostasis of adult organisms, it would not be possible to target them to control the MT1-MMP-dependent unwanted cell invasion that drives pathological conditions like RA or cancer (126, 294). Therefore, the identification of adaptor molecules would potentially provide alternative ways to specifically target KIF-driven MT1-MMP intracellular trafficking. For instance, PLD2 and not KIF5B has been proposed as a potential target to treat metastatic breast cancer patients (210).

Overexpression of fluorescently-labelled KIFs was employed to investigate the interplay between KIF13A, KIF3A and KIF9-v1 to achieve MT1-MMP cell surface

exposure. Although this experimental approach has been an invaluable resource to study the dynamics of KIF-mediated MT1-MMP intracellular trafficking, there are some pitfalls. For instance, overexpression of fluorescently-labelled KIFs can lead to altered protein localisation within the cytoplasm as well as to altered protein functions. These pitfalls were well exemplified when HT-1080 cells were transfected with KIF3A-GFP. The overexpression of this motor protein caused its accumulation in the cytoplasm, which generated a high background signal, that greatly limited the tracking analysis. In future, CRISPR-Cas9 genome editing could be used to tag the KIFs of our interest with fluorescent proteins. This experimental approach would overcome the pitfalls I have experienced so far and would enable a better understanding of the interplay between KIF13A, KIF3A and KIF9-v1.

CRISPR-Cas9 genome editing could also be useful to generate KIF13A and KIF9 knockout HT-1080 cells that could then be used for the experimental pulmonary metastatic model I have extensively described in Chapter 5. Finding ways to test the role of KIF13A and KIF9 in the MT1-MMP-dependent invasion and metastatic potential of cancer cells *in vivo* is of great importance.

6.3 Conclusions

In this work, I have confirmed that MT1-MMP intracellular trafficking mechanisms are driven by KIFs. Anterograde movement of MT1-MMP is powered by KIF13A, KIF9 and KIF9-v1 in HT-1080 cells. These three KIFs can highly influence cell surface exposure of the enzyme and consequently MT1-MMP-dependent cellular functions on the cell surface. These findings bring a great contribution to the understanding of MT1-MMP intracellular trafficking and considerably expand the knowledge about KIF13A and KIF9, which have been poorly described so far. Overall,

my work sheds light on some of the mechanisms that regulate MT1-MMP cell surface localisation and suggests KIF-driven MT1-MMP intracellular transport as a potential target to prevent un-wanted cellular invasion.

CHAPTER 7:

BIBLIOGRAPHY

1. Vicente-Manzanares M, Webb DJ, & Horwitz AR (2005) Cell migration at a glance. *J Cell Sci* 118(Pt 21):4917-4919.
2. Franz CM, Jones GE, & Ridley AJ (2002) Cell migration in development and disease. *Dev Cell* 2(2):153-158.
3. Abercrombie M, Heaysman JE, & Pegrum SM (1970) Locomotion of Fibroblasts in Culture .1. Movements of Leading Edge. *Experimental Cell Research* 59(3):393-+.
4. Abercrombie M, Heaysman JE, & Pegrum SM (1970) Locomotion of Fibroblasts in Culture .3. Movements of Particles on Dorsal Surface of Leading Lamella. *Experimental Cell Research* 62(2-3):389-+.
5. Abercrombie M, Heaysman JE, & Pegrum SM (1970) Locomotion of Fibroblasts in Culture .2. Ruffling. *Experimental Cell Research* 60(3):437-+.
6. Friedl P & Wolf K (2009) Proteolytic interstitial cell migration: a five-step process. *Cancer Metastasis Rev* 28(1-2):129-135.
7. Liotta LA (1986) Tumor invasion and metastases--role of the extracellular matrix: Rhoads Memorial Award lecture. *Cancer Res* 46(1):1-7.
8. Wolf K*, et al.* (2003) Compensation mechanism in tumor cell migration: mesenchymal-amoeboid transition after blocking of pericellular proteolysis. *Journal of Cell Biology* 160(2):267-277.
9. Wolf K*, et al.* (2013) Physical limits of cell migration: Control by ECM space and nuclear deformation and tuning by proteolysis and traction force. *Journal of Cell Biology* 201(7):1069-1084.

10. Sato H, Takino T, & Miyamori H (2007) Roles of membrane-type matrix metalloproteinase-1 in tumor invasion and metastasis. *Clin Exp Metastas* 24(4):242-242.
11. Page-McCaw A, Ewald AJ, & Werb Z (2007) Matrix metalloproteinases and the regulation of tissue remodelling. *Nat Rev Mol Cell Bio* 8(3):221-233.
12. Nagase H, Visse R, & Murphy G (2006) Structure and function of matrix metalloproteinases and TIMPs. *Cardiovasc Res* 69(3):562-573.
13. Loffek S, Schilling O, & Franzke CW (2011) Series "matrix metalloproteinases in lung health and disease": Biological role of matrix metalloproteinases: a critical balance. *Eur Respir J* 38(1):191-208.
14. Gifford V & Itoh Y (2019) MT1-MMP-dependent cell migration: proteolytic and non-proteolytic mechanisms. *Biochem Soc Trans* 47(3):811-826.
15. Blobel G*, et al.* (1979) Translocation of proteins across membranes: the signal hypothesis and beyond. *Symp Soc Exp Biol* 33:9-36.
16. Gomis-Ruth FX (2003) Structural aspects of the metzincin clan of metalloendopeptidases. *Mol Biotechnol* 24(2):157-202.
17. Coleman JE (1998) Zinc enzymes. *Curr Opin Chem Biol* 2(2):222-234.
18. Gupta SP & Patil VM (2012) Specificity of binding with matrix metalloproteinases. *Exp Suppl* 103:35-56.
19. Rosenblum G*, et al.* (2007) Insights into the structure and domain flexibility of full-length pro-matrix metalloproteinase-9/gelatinase B. *Structure* 15(10):1227-1236.
20. Murphy G*, et al.* (1992) The C-terminal domain of 72 kDa gelatinase A is not required for catalysis, but is essential for membrane activation and

modulates interactions with tissue inhibitors of metalloproteinases. *Biochem J* 283 (Pt 3):637-641.

21. Arnold LH*, et al.* (2011) The interface between catalytic and hemopexin domains in matrix metalloproteinase-1 conceals a collagen binding exosite. *J Biol Chem* 286(52):45073-45082.
22. Itoh Y (2015) Membrane-type matrix metalloproteinases: Their functions and regulations. *Matrix Biol* 44-46:207-223.
23. Hotary K, Allen E, Punturieri A, Yana I, & Weiss SJ (2000) Regulation of cell invasion and morphogenesis in a three-dimensional type I collagen matrix by membrane-type matrix metalloproteinases 1, 2, and 3. *J Cell Biol* 149(6):1309-1323.
24. Miller MC*, et al.* (2009) Membrane type 1 matrix metalloproteinase is a crucial promoter of synovial invasion in human rheumatoid arthritis. *Arthritis Rheum* 60(3):686-697.
25. Ohkawara H, Ikeda K, Ogawa K, & Takeishi Y (2015) Membrane Type 1-Matrix Metalloproteinase (Mt1-Mmp) Identified as a Multifunctional Regulator of Vascular Responses. *Fukushima J Med Sci* 61(2):91-100.
26. Pap T*, et al.* (2000) Differential expression pattern of membrane-type matrix metalloproteinases in rheumatoid arthritis. *Arthritis and Rheumatism* 43(6):1226-1232.
27. Seiki M (2003) Membrane-type 1 matrix metalloproteinase: a key enzyme for tumor invasion. *Cancer Lett* 194(1):1-11.
28. Sato H*, et al.* (1994) A matrix metalloproteinase expressed on the surface of invasive tumour cells. *Nature* 370(6484):61-65.

29. Rozario T & DeSimone DW (2010) The extracellular matrix in development and morphogenesis: a dynamic view. *Dev Biol* 341(1):126-140.

30. Shoulders MD & Raines RT (2009) Collagen structure and stability. *Annu Rev Biochem* 78:929-958.

31. Ricard-Blum S (2011) The collagen family. *Cold Spring Harb Perspect Biol* 3(1):a004978.

32. Amar S, Smith L, & Fields GB (2017) Matrix metalloproteinase collagenolysis in health and disease. *Biochim Biophys Acta Mol Cell Res* 1864(11 Pt A):1940-1951.

33. Holmbeck K*, et al.* (1999) MT1-MMP-deficient mice develop dwarfism, osteopenia, arthritis, and connective tissue disease due to inadequate collagen turnover. *Cell* 99(1):81-92.

34. Zhou ZJ*, et al.* (2000) Impaired endochondral ossification and angiogenesis in mice deficient in membrane-type matrix metalloproteinase I. *P Natl Acad Sci USA* 97(8):4052-4057.

35. Taylor SH*, et al.* (2015) Matrix metalloproteinase 14 is required for fibrous tissue expansion. *Elife* 4:e09345.

36. Tanjore H & Kalluri R (2006) The role of type IV collagen and basement membranes in cancer progression and metastasis. *Am J Pathol* 168(3):715-717.

37. Taniwaki K*, et al.* (2007) Stroma-derived matrix metalloproteinase (MMP)-2 promotes membrane type 1-MMP-dependent tumor growth in mice. *Cancer Research* 67(9):4311-4319.

38. Knauper V*, et al.* (1996) Cellular mechanisms for human procollagenase-3 (MMP-13) activation. Evidence that MT1-MMP (MMP-14) and gelatinase

a (MMP-2) are able to generate active enzyme. *J Biol Chem* 271(29):17124-17131.

39. Knäuper V*, et al.* (2002) Cellular activation of proMMP-13 by MT1-MMP depends on the C-terminal domain of MMP-13. *FEBS Lett* 532(1-2):127-130.
40. Kajita M*, et al.* (2001) Membrane-type 1 matrix metalloproteinase cleaves CD44 and promotes cell migration. *J Cell Biol* 153(5):893-904.
41. Endo K*, et al.* (2003) Cleavage of syndecan-1 by membrane type matrix metalloproteinase-1 stimulates cell migration. *J Biol Chem* 278(42):40764-40770.
42. Deryugina EI*, et al.* (2001) MT1-MMP initiates activation of pro-MMP-2 and integrin alphavbeta3 promotes maturation of MMP-2 in breast carcinoma cells. *Exp Cell Res* 263(2):209-223.
43. Adams RR, Tavares AA, Salzberg A, Bellen HJ, & Glover DM (1998) pavarotti encodes a kinesin-like protein required to organize the central spindle and contractile ring for cytokinesis. *Genes Dev* 12(10):1483-1494.
44. Sithu SD*, et al.* (2007) Membrane-type 1-matrix metalloproteinase regulates intracellular adhesion molecule-1 (ICAM-1)-mediated monocyte transmigration. *Journal of Biological Chemistry* 282(34):25010-25019.
45. Mori H*, et al.* (2002) CD44 directs membrane-type 1 matrix metalloproteinase (MT1-MMP) to lamellipodia by associating with its hemopexin-like domain (PEX). *Molecular Biology of the Cell* 13:208a-208a.
46. Deryugina EI, Ratnikov BI, Postnova TI, Rozanov DV, & Strongin AY (2002) Processing of integrin alpha(v) subunit by membrane type 1 matrix

metalloproteinase stimulates migration of breast carcinoma cells on vitronectin and enhances tyrosine phosphorylation of focal adhesion kinase. *Journal of Biological Chemistry* 277(12):9749-9756.

47. Rozanov DV, Hahn-Dantona E, Strickland DK, & Strongin AY (2004) The low density lipoprotein receptor-related protein LRP is regulated by membrane type-1 matrix metalloproteinase (MT1-MMP) proteolysis in malignant cells. *Journal of Biological Chemistry* 279(6):4260-4268.
48. Chan KM*, et al.* (2012) MT1-MMP Inactivates ADAM9 to Regulate FGFR2 Signaling and Calvarial Osteogenesis. *Developmental Cell* 22(6):1176-1190.
49. Yamamoto K*, et al.* (2017) Inhibition of Shedding of Low-Density Lipoprotein Receptor-Related Protein 1 Reverses Cartilage Matrix Degradation in Osteoarthritis. *Arthritis Rheumatol* 69(6):1246-1256.
50. Lehti K, Rose NF, Valavaara S, Weiss SJ, & Keski-Oja J (2009) MT1-MMP promotes vascular smooth muscle dedifferentiation through LRP1 processing. *Journal of Cell Science* 122(1):126-135.
51. Itoh Y & Seiki M (2004) MT1-MMP: an enzyme with multidimensional regulation. *Trends Biochem Sci* 29(6):285-289.
52. Lohi J, Lehti K, Valtanen H, Parks WC, & Keski-Oja J (2000) Structural analysis and promoter characterization of the human membrane-type matrix metalloproteinase-1 (MT1-MMP) gene. *Gene* 242(1-2):75-86.
53. Haas TL, Stitelman D, Davis SJ, Apte SS, & Madri JA (1999) Egr-1 mediates extracellular matrix-driven transcription of membrane type 1 matrix metalloproteinase in endothelium. *J Biol Chem* 274(32):22679-22685.

54. Takino T*, et al.* (2016) Tip60 regulates MT1-MMP transcription and invasion of glioblastoma cells through NF-kappaB pathway. *Clin Exp Metastasis* 33(1):45-52.

55. Sroka IC, Nagle RB, & Bowden GT (2007) Membrane-type 1 matrix metalloproteinase is regulated by Sp1 through the differential activation of AKT, JNK, and ERK pathways in human prostate tumor cells. *Neoplasia* 9(5):406-417.

56. Hong IK*, et al.* (2014) The tetraspanin CD81 protein increases melanoma cell motility by up-regulating metalloproteinase MT1-MMP expression through the pro-oncogenic Akt-dependent Sp1 activation signaling pathways. *J Biol Chem* 289(22):15691-15704.

57. Petrella BL, Lohi J, & Brinckerhoff CE (2005) Identification of membrane type-1 matrix metalloproteinase as a target of hypoxia-inducible factor-2 alpha in von Hippel-Lindau renal cell carcinoma. *Oncogene* 24(6):1043-1052.

58. Petrella BL & Brinckerhoff CE (2006) Tumor cell invasion of von Hippel Lindau renal cell carcinoma cells is mediated by membrane type-1 matrix metalloproteinase. *Mol Cancer* 5:66.

59. Rowe RG*, et al.* (2009) Mesenchymal cells reactivate Snail1 expression to drive three-dimensional invasion programs. *J Cell Biol* 184(3):399-408.

60. Qin Z, Feng J, Liu Y, Deng LL, & Lu C (2016) PDGF-D promotes dermal fibroblast invasion in 3-dimensional extracellular matrix via Snail-mediated MT1-MMP upregulation. *Tumour Biol* 37(1):591-599.

61. Tomasek JJ*, et al.* (1997) Gelatinase A activation is regulated by the organization of the polymerized actin cytoskeleton. *Journal of Biological Chemistry* 272(11):7482-7487.

62. Ruangpanit N*, et al.* (2001) Gelatinase A (MMP-2) activation by skin fibroblasts: dependence on MT1-MMP expression and fibrillar collagen form. *Matrix Biol* 20(3):193-203.

63. Majkowska I, Shitomi Y, Ito N, Gray NS, & Itoh Y (2017) Discoidin domain receptor 2 mediates collagen-induced activation of membrane-type 1 matrix metalloproteinase in human fibroblasts. *J Biol Chem* 292(16):6633-6643.

64. Zhang D & Brodt P (2003) Type 1 insulin-like growth factor regulates MT1-MMP synthesis and tumor invasion via PI 3-kinase/Akt signaling. *Oncogene* 22(7):974-982.

65. Udayakumar TS, Nagle RB, & Bowden GT (2004) Fibroblast growth factor-1 transcriptionally induces membrane type-1 matrix metalloproteinase expression in prostate carcinoma cell line. *Prostate* 58(1):66-75.

66. Jiang L*, et al.* (2010) Overexpression of proto-oncogene FBI-1 activates membrane type 1-matrix metalloproteinase in association with adverse outcome in ovarian cancers. *Mol Cancer* 9:318.

67. Kaewprag J, Umnajvijit W, Ngamkham J, & Ponglikitmongkol M (2013) HPV16 oncoproteins promote cervical cancer invasiveness by upregulating specific matrix metalloproteinases. *PLoS One* 8(8):e71611.

68. d'Ortho MP*, et al.* (1998) MT1-MMP on the cell surface causes focal degradation of gelatin films. *FEBS Lett* 421(2):159-164.

69. Yu M, Sato H, Seiki M, & Thompson EW (1995) Complex Regulation of Membrane-Type Matrix Metalloproteinase Expression and Matrix Metalloproteinase-2 Activation by Concanavalin a in Mda-Mb-231 Human Breast-Cancer Cells. *Cancer Research* 55(15):3272-3277.

70. Gervasi DC*, et al.* (1996) Carbohydrate-mediated regulation of matrix metalloproteinase-2 activation in normal human fibroblasts and fibrosarcoma cells. *Biochem Biophys Res Commun* 228(2):530-538.

71. Yana I & Weiss SJ (2000) Regulation of membrane type-1 matrix metalloproteinase activation by proprotein convertases. *Mol Biol Cell* 11(7):2387-2401.

72. Itoh Y (2006) MT1-MMP: a key regulator of cell migration in tissue. *IUBMB Life* 58(10):589-596.

73. Caterina JJ*, et al.* (2000) Inactivating mutation of the mouse tissue inhibitor of metalloproteinases-2(Timp-2) gene alters proMMP-2 activation. *J Biol Chem* 275(34):26416-26422.

74. Leco KJ*, et al.* (2001) Spontaneous air space enlargement in the lungs of mice lacking tissue inhibitor of metalloproteinases-3 (TIMP-3). *J Clin Invest* 108(6):817-829.

75. English JL*, et al.* (2006) Individual Timp deficiencies differentially impact pro-MMP-2 activation. *J Biol Chem* 281(15):10337-10346.

76. Oh J*, et al.* (2001) The membrane-anchored MMP inhibitor RECK is a key regulator of extracellular matrix integrity and angiogenesis. *Cell* 107(6):789-800.

77. Nakada M*, et al.* (2001) Suppression of membrane-type 1 matrix metalloproteinase (MMP)-mediated MMP-2 activation and tumor invasion

by testican 3 and its splicing variant gene product, N-Tes. *Cancer Research* 61(24):8896-8902.

78. Lehti K, Lohi J, Valtanen H, & Keski-Oja J (1998) Proteolytic processing of membrane-type-1 matrix metalloproteinase is associated with gelatinase A activation at the cell surface. *Biochemical Journal* 334:345-353.

79. Stanton H*, et al.* (1998) The activation of ProMMP-2 (gelatinase A) by HT1080 fibrosarcoma cells is promoted by culture on a fibronectin substrate and is concomitant with an increase in processing of MT1-MMP (MMP-14) to a 45 kDa form. *J Cell Sci* 111 (Pt 18):2789-2798.

80. Osenkowski P, Toth M, & Fridman R (2004) Processing, shedding, and endocytosis of membrane type 1-matrix metalloproteinase (MT1-MMP). *J Cell Physiol* 200(1):2-10.

81. Remacle A, Murphy G, & Roghi C (2003) Membrane type I-matrix metalloproteinase (MT1-MMP) is internalised by two different pathways and is recycled to the cell surface. *J Cell Sci* 116(Pt 19):3905-3916.

82. Uekita T, Itoh Y, Yana I, Ohno H, & Seiki M (2001) Cytoplasmic tail-dependent internalization of membrane-type 1 matrix metalloproteinase is important for its invasion-promoting activity. *Journal of Cell Biology* 155(7):1345-1356.

83. Anilkumar N*, et al.* (2005) Palmitoylation at Cys574 is essential for MT1-MMP to promote cell migration. *FASEB J* 19(10):1326-1328.

84. Baker TM, Waheed S, & Syed V (2018) RNA interference screening identifies clathrin-B and cofilin-1 as mediators of MT1-MMP in endometrial cancer. *Exp Cell Res* 370(2):663-670.

85. Williams KC & Coppolino MG (2011) Phosphorylation of membrane type 1-matrix metalloproteinase (MT1-MMP) and its vesicle-associated membrane protein 7 (VAMP7)-dependent trafficking facilitate cell invasion and migration. *J Biol Chem* 286(50):43405-43416.

86. Suarez H*, et al.* (2020) Regulation of MT1-MMP Activity through Its Association with ERMs. *Cells* 9(2).

87. Baldassarre T*, et al.* (2015) Endophilin A2 Promotes TNBC Cell Invasion and Tumor Metastasis. *Mol Cancer Res* 13(6):1044-1055.

88. Castro-Castro A*, et al.* (2016) Cellular and Molecular Mechanisms of MT1-MMP-Dependent Cancer Cell Invasion. *Annu Rev Cell Dev Bi* 32:555-576.

89. Wolf K & Friedl P (2011) Extracellular matrix determinants of proteolytic and non-proteolytic cell migration. *Trends Cell Biol* 21(12):736-744.

90. Itoh Y*, et al.* (2001) Homophilic complex formation of MT1-MMP facilitates proMMP-2 activation on the cell surface and promotes tumor cell invasion. *EMBO J* 20(17):4782-4793.

91. El Azzouzi K, Wiesner C, & Linder S (2016) Metalloproteinase MT1-MMP islets act as memory devices for podosome reemergence. *J Cell Biol* 213(1):109-125.

92. Itoh Y*, et al.* (2011) Dimerization of MT1-MMP during cellular invasion detected by fluorescence resonance energy transfer. *Biochem J* 440(3):319-326.

93. Poincloux R, Lizarraga F, & Chavrier P (2009) Matrix invasion by tumour cells: a focus on MT1-MMP trafficking to invadopodia. *J Cell Sci* 122(Pt 17):3015-3024.

94. Mattila PK & Lappalainen P (2008) Filopodia: molecular architecture and cellular functions. *Nat Rev Mol Cell Biol* 9(6):446-454.

95. Fisher KE*, et al.* (2009) MT1-MMP- and Cdc42-dependent signaling co-regulate cell invasion and tunnel formation in 3D collagen matrices. *J Cell Sci* 122(Pt 24):4558-4569.

96. Li YY, Zhou CX, & Gao Y (2015) Podoplanin promotes the invasion of oral squamous cell carcinoma in coordination with MT1-MMP and Rho GTPases. *Am J Cancer Res* 5(2):514-529.

97. Krause M & Gautreau A (2014) Steering cell migration: lamellipodium dynamics and the regulation of directional persistence. *Nat Rev Mol Cell Biol* 15(9):577-590.

98. Takenawa T & Miki H (2001) WASP and WAVE family proteins: key molecules for rapid rearrangement of cortical actin filaments and cell movement. *J Cell Sci* 114(Pt 10):1801-1809.

99. Yamazaki D*, et al.* (2003) WAVE2 is required for directed cell migration and cardiovascular development. *Nature* 424(6947):452-456.

100. Yan C*, et al.* (2003) WAVE2 deficiency reveals distinct roles in embryogenesis and Rac-mediated actin-based motility. *EMBO J* 22(14):3602-3612.

101. Suetsugu S, Yamazaki D, Kurisu S, & Takenawa T (2003) Differential roles of WAVE1 and WAVE2 in dorsal and peripheral ruffle formation for fibroblast cell migration. *Dev Cell* 5(4):595-609.

102. Yonemura S*, et al.* (1998) Ezrin/radixin/moesin (ERM) proteins bind to a positively charged amino acid cluster in the juxta-membrane cytoplasmic domain of CD44, CD43, and ICAM-2. *J Cell Biol* 140(4):885-895.

103. Tarone G, Cirillo D, Giancotti FG, Comoglio PM, & Marchisio PC (1985) Rous-Sarcoma Virus-Transformed Fibroblasts Adhere Primarily at Discrete Protrusions of the Ventral Membrane Called Podosomes. *Experimental Cell Research* 159(1):141-157.

104. Chen WT (1989) Proteolytic Activity of Specialized Surface Protrusions Formed at Rosette Contact Sites of Transformed-Cells. *J Exp Zool* 251(2):167-185.

105. Linder S (2007) The matrix corroded: podosomes and invadopodia in extracellular matrix degradation. *Trends in Cell Biology* 17(3):107-117.

106. Murphy DA & Courtneidge SA (2011) The 'ins' and 'outs' of podosomes and invadopodia: characteristics, formation and function. *Nat Rev Mol Cell Bio* 12(7):413-426.

107. Linder S (2009) Invadosomes at a glance. *J Cell Sci* 122(Pt 17):3009-3013.

108. Wiesner C, Faix J, Himmel M, Bentzien F, & Linder S (2010) KIF5B and KIF3A/KIF3B kinesins drive MT1-MMP surface exposure, CD44 shedding, and extracellular matrix degradation in primary macrophages. *Blood* 116(9):1559-1569.

109. Wiesner C, El Azzouzi K, & Linder S (2013) A specific subset of RabGTPases controls cell surface exposure of MT1-MMP, extracellular matrix degradation and three-dimensional invasion of macrophages. *J Cell Sci* 126(Pt 13):2820-2833.

110. Linder S & Scita G (2015) RABGTPases in MT1-MMP trafficking and cell invasion: Physiology versus pathology. *Small GTPases* 6(3):145-152.

111. Frittoli E, Palamidessi A, Disanza A, & Scita G (2011) Secretory and endo/exocytic trafficking in invadopodia formation: the MT1-MMP paradigm. *Eur J Cell Biol* 90(2-3):108-114.

112. Woskowicz AM, Weaver SA, Shitomi Y, Ito N, & Itoh Y (2013) MT-LOOP-dependent localization of membrane type I matrix metalloproteinase (MT1-MMP) to the cell adhesion complexes promotes cancer cell invasion. *J Biol Chem* 288(49):35126-35137.

113. Wang Y & McNiven MA (2012) Invasive matrix degradation at focal adhesions occurs via protease recruitment by a FAK-p130Cas complex. *J Cell Biol* 196(3):375-385.

114. Stenmark H (2009) Rab GTPases as coordinators of vesicle traffic. *Nat Rev Mol Cell Biol* 10(8):513-525.

115. Frittoli E*, et al.* (2014) A RAB5/RAB4 recycling circuitry induces a proteolytic invasive program and promotes tumor dissemination. *J Cell Biol* 206(2):307-328.

116. Kajiho H*, et al.* (2016) RAB2A controls MT1-MMP endocytic and E-cadherin polarized Golgi trafficking to promote invasive breast cancer programs. *EMBO Rep* 17(7):1061-1080.

117. Steffen A*, et al.* (2008) MT1-MMP-dependent invasion is regulated by TI-VAMP/VAMP7. *Curr Biol* 18(12):926-931.

118. Planchon D*, et al.* (2018) MT1-MMP targeting to endolysosomes is mediated by flotillin upregulation. *J Cell Sci*.

119. Macpherson IR*, et al.* (2014) CLIC3 controls recycling of late endosomal MT1-MMP and dictates invasion and metastasis in breast cancer. *J Cell Sci* 127(Pt 18):3893-3901.

120. Monteiro P*, et al.* (2013) Endosomal WASH and exocyst complexes control exocytosis of MT1-MMP at invadopodia. *J Cell Biol* 203(6):1063-1079.

121. Castagnino A*, et al.* (2018) Coronin 1C promotes triple-negative breast cancer invasiveness through regulation of MT1-MMP traffic and invadopodia function. *Oncogene*.

122. Loskutov YV*, et al.* (2015) NEDD9/Arf6-dependent endocytic trafficking of matrix metalloproteinase 14: a novel mechanism for blocking mesenchymal cell invasion and metastasis of breast cancer. *Oncogene* 34(28):3662-3675.

123. Bravo-Cordero JJ*, et al.* (2007) MT1-MMP proinvasive activity is regulated by a novel Rab8-dependent exocytic pathway. *EMBO J* 26(6):1499-1510.

124. Schliwa M & Woehlke G (2003) Molecular motors. *Nature* 422(6933):759-765.

125. Cuffaro D*, et al.* (2019) Design, synthesis and biological evaluation of bifunctional inhibitors of membrane type 1 matrix metalloproteinase (MT1-MMP). *Bioorgan Med Chem* 27(1):196-207.

126. Hirokawa N, Noda Y, Tanaka Y, & Niwa S (2009) Kinesin superfamily motor proteins and intracellular transport. *Nat Rev Mol Cell Biol* 10(10):682-696.

127. Vale RD, Reese TS, & Sheetz MP (1985) Identification of a novel force-generating protein, kinesin, involved in microtubule-based motility. *Cell* 42(1):39-50.

128. Vale RD, Schnapp BJ, Reese TS, & Sheetz MP (1985) Movement of organelles along filaments dissociated from the axoplasm of the squid giant axon. *Cell* 40(2):449-454.

129. Allen RD, Allen NS, & Travis JL (1981) Video-enhanced contrast, differential interference contrast (AVEC-DIC) microscopy: a new method capable of analyzing microtubule-related motility in the reticulopodial network of Allogromia laticollaris. *Cell Motil* 1(3):291-302.

130. Brady ST (1985) A novel brain ATPase with properties expected for the fast axonal transport motor. *Nature* 317(6032):73-75.

131. Miki H, Setou M, Kaneshiro K, & Hirokawa N (2001) All kinesin superfamily protein, KIF, genes in mouse and human. *Proc Natl Acad Sci U S A* 98(13):7004-7011.

132. Endow SA, Kull FJ, & Liu H (2010) Kinesins at a glance. *J Cell Sci* 123(Pt 20):3420-3424.

133. Kull FJ, Sablin EP, Lau R, Fletterick RJ, & Vale RD (1996) Crystal structure of the kinesin motor domain reveals a structural similarity to myosin. *Nature* 380(6574):550-555.

134. Sablin EP, Kull FJ, Cooke R, Vale RD, & Fletterick RJ (1996) Crystal structure of the motor domain of the kinesin-related motor ncd. *Nature* 380(6574):555-559.

135. Marx A, Hoenger A, & Mandelkow E (2009) Structures of kinesin motor proteins. *Cell Motil Cytoskeleton* 66(11):958-966.

136. Rath O & Kozielski F (2012) Kinesins and cancer. *Nat Rev Cancer* 12(8):527-539.

137. Rice S*, et al.* (1999) A structural change in the kinesin motor protein that drives motility. *Nature* 402(6763):778-784.

138. Shang Z*, et al.* (2014) High-resolution structures of kinesin on microtubules provide a basis for nucleotide-gated force-generation. *Elife* 3:e04686.

139. Liu D, Liu X, Shang Z, & Sindelar CV (2017) Structural basis of cooperativity in kinesin revealed by 3D reconstruction of a two-head-bound state on microtubules. *Elife* 6.

140. Ren J*, et al.* (2018) Structural Delineation of the Neck Linker of Kinesin-3 for Processive Movement. *J Mol Biol* 430(14):2030-2041.

141. Budaitis BG*, et al.* (2019) Neck linker docking is critical for Kinesin-1 force generation in cells but at a cost to motor speed and processivity. *Elife* 8.

142. Khalil AS*, et al.* (2008) Kinesin's cover-neck bundle folds forward to generate force. *Proc Natl Acad Sci U S A* 105(49):19247-19252.

143. Hackney DD & Stock MF (2000) Kinesin's IAK tail domain inhibits initial microtubule-stimulated ADP release. *Nat Cell Biol* 2(5):257-260.

144. Seeberger C, Mandelkow E, & Meyer B (2000) Conformational preferences of a synthetic 30mer peptide from the interface between the neck and stalk regions of kinesin. *Biochemistry-Us* 39(41):12558-12567.

145. Karcher RL, Deacon SW, & Gelfand VI (2002) Motor-cargo interactions: the key to transport specificity. *Trends Cell Biol* 12(1):21-27.

146. Hirokawa N*, et al.* (1989) Submolecular domains of bovine brain kinesin identified by electron microscopy and monoclonal antibody decoration. *Cell* 56(5):867-878.

147. Stenoien DL & Brady ST (1997) Immunochemical analysis of kinesin light chain function. *Mol Biol Cell* 8(4):675-689.

148. Kamal A, Stokin GB, Yang Z, Xia CH, & Goldstein LS (2000) Axonal transport of amyloid precursor protein is mediated by direct binding to the kinesin light chain subunit of kinesin-I. *Neuron* 28(2):449-459.

149. Nakagawa T*, et al.* (2000) A novel motor, KIF13A, transports mannose-6-phosphate receptor to plasma membrane through direct interaction with AP-1 complex. *Cell* 103(4):569-581.

150. Takeda S*, et al.* (2000) Kinesin superfamily protein 3 (KIF3) motor transports fodrin-associating vesicles important for neurite building. *J Cell Biol* 148(6):1255-1265.

151. Echard A*, et al.* (1998) Interaction of a Golgi-associated kinesin-like protein with Rab6. *Science* 279(5350):580-585.

152. Seog DH, Lee DH, & Lee SK (2004) Molecular motor proteins of the kinesin superfamily proteins (KIFs): structure, cargo and disease. *J Korean Med Sci* 19(1):1-7.

153. Bartolini F & Gundersen GG (2010) Formins and microtubules. *Biochim Biophys Acta* 1803(2):164-173.

154. Meiring JCM, Shneyer BI, & Akhmanova A (2020) Generation and regulation of microtubule network asymmetry to drive cell polarity. *Curr Opin Cell Biol* 62:86-95.

155. Lawrence CJ*, et al.* (2004) A standardized kinesin nomenclature. *J Cell Biol* 167(1):19-22.

156. Hirokawa N (1998) Kinesin and dynein superfamily proteins and the mechanism of organelle transport. *Science* 279(5350):519-526.

157. Pfister KK, Wagner MC, Stenoien DL, Brady ST, & Bloom GS (1989) Monoclonal antibodies to kinesin heavy and light chains stain vesicle-like structures, but not microtubules, in cultured cells. *J Cell Biol* 108(4):1453-1463.

158. Hirokawa N & Noda Y (2008) Intracellular transport and kinesin superfamily proteins, KIFs: structure, function, and dynamics. *Physiol Rev* 88(3):1089-1118.

159. Miki H, Okada Y, & Hirokawa N (2005) Analysis of the kinesin superfamily: insights into structure and function. *Trends Cell Biol* 15(9):467-476.

160. Henson JH*, et al.* (1997) The heterotrimeric motor protein kinesin-II localizes to the midpiece and flagellum of sea urchin and sand dollar sperm. *Cell Motil Cytoskeleton* 38(1):29-37.

161. Setou M, Nakagawa T, Seog DH, & Hirokawa N (2000) Kinesin superfamily motor protein KIF17 and mLin-10 in NMDA receptor-containing vesicle transport. *Science* 288(5472):1796-1802.

162. Yamazaki H, Nakata T, Okada Y, & Hirokawa N (1995) KIF3A/B: a heterodimeric kinesin superfamily protein that works as a microtubule plus end-directed motor for membrane organelle transport. *J Cell Biol* 130(6):1387-1399.

163. Gilbert SP, Guzik-Lendrum S, & Rayment I (2018) Kinesin-2 motors: Kinetics and biophysics. *J Biol Chem* 293(12):4510-4518.

164. Drummond IA (2012) Cilia functions in development. *Curr Opin Cell Biol* 24(1):24-30.

165. Huangfu D*, et al.* (2003) Hedgehog signalling in the mouse requires intraflagellar transport proteins. *Nature* 426(6962):83-87.

166. Siddiqui N & Straube A (2017) Intracellular Cargo Transport by Kinesin-3 Motors. *Biochemistry (Mosc)* 82(7):803-815.

167. Sekine Y*, et al.* (1994) A novel microtubule-based motor protein (KIF4) for organelle transports, whose expression is regulated developmentally. *J Cell Biol* 127(1):187-201.

168. Tokai N*, et al.* (1996) Kid, a novel kinesin-like DNA binding protein, is localized to chromosomes and the mitotic spindle. *EMBO J* 15(3):457-467.

169. Zhou J*, et al.* (2019) KIF11 Functions as an Oncogene and Is Associated with Poor Outcomes from Breast Cancer. *Cancer Res Treat* 51(3):1207-1221.

170. Hizlan D*, et al.* (2006) Structural analysis of the ZEN-4/CeMKLP1 motor domain and its interaction with microtubules. *J Struct Biol* 153(1):73-84.

171. Hill E, Clarke M, & Barr FA (2000) The Rab6-binding kinesin, Rab6-KIFL, is required for cytokinesis. *EMBO J* 19(21):5711-5719.

172. Nislow C, Lombillo VA, Kuriyama R, & McIntosh JR (1992) A plus-end-directed motor enzyme that moves antiparallel microtubules in vitro localizes to the interzone of mitotic spindles. *Nature* 359(6395):543-547.

173. Yen TJ*, et al.* (1991) CENP-E, a novel human centromere-associated protein required for progression from metaphase to anaphase. *EMBO J* 10(5):1245-1254.

174. Bancroft J, Auckland P, Samora CP, & McAinsh AD (2015) Chromosome congression is promoted by CENP-Q- and CENP-E-dependent pathways. *Journal of Cell Science* 128(1):171-184.

175. Craske B & Welburn JPI (2020) Leaving no-one behind: how CENP-E facilitates chromosome alignment. *Essays Biochem*.

176. Messin LJ & Millar JB (2014) Role and regulation of kinesin-8 motors through the cell cycle. *Syst Synth Biol* 8(3):205-213.

177. Shrestha S, Hazelbaker M, Yount AL, & Walczak CE (2019) Emerging Insights into the Function of Kinesin-8 Proteins in Microtubule Length Regulation. *Biomolecules* 9(1).

178. Li YH*, et al.* (2010) KIF6 Polymorphism as a Predictor of Risk of Coronary Events and of Clinical Event Reduction by Statin Therapy. *Am J Cardiol* 106(7):994-998.

179. Cornfine S*, et al.* (2011) The kinesin KIF9 and reggie/flotillin proteins regulate matrix degradation by macrophage podosomes. *Mol Biol Cell* 22(2):202-215.

180. Gache V, Gomes ER, & Cadot B (2017) Microtubule motors involved in nuclear movement during skeletal muscle differentiation. *Molecular Biology of the Cell* 28(7):865-874.

181. Camlin NJ, McLaughlin EA, & Holt JE (2017) Motoring through: the role of kinesin superfamily proteins in female meiosis. *Hum Reprod Update* 23(4):409-420.

182. Maddika S, Sy SMH, & Chen JJ (2009) Functional Interaction between Chfr and Kif22 Controls Genomic Stability. *Journal of Biological Chemistry* 284(19):12998-13003.

183. Zhou RY, Niwa S, Homma N, Takei Y, & Hirokawa N (2009) KIF26A Is an Unconventional Kinesin and Regulates GDNF-Ret Signaling in Enteric Neuronal Development. *Cell* 139(4):802-813.

184. Terabayashi T*, et al.* (2012) Phosphorylation of Kif26b promotes its polyubiquitination and subsequent proteasomal degradation during kidney development. *PLoS One* 7(6):e39714.

185. Wang L*, et al.* (2018) The Atypical Kinesin KIF26A Facilitates Termination of Nociceptive Responses by Sequestering Focal Adhesion Kinase. *Cell Rep* 24(11):2894-2907.

186. Hunter AW*, et al.* (2003) The kinesin-related protein MCAK is a microtubule depolymerase that forms an ATP-hydrolyzing complex at microtubule ends. *Mol Cell* 11(2):445-457.

187. Ems-McClung SC & Walczak CE (2010) Kinesin-13s in mitosis: Key players in the spatial and temporal organization of spindle microtubules. *Semin Cell Dev Biol* 21(3):276-282.

188. She ZY & Yang WX (2017) Molecular mechanisms of kinesin-14 motors in spindle assembly and chromosome segregation. *J Cell Sci* 130(13):2097-2110.

189. Verhey KJ & Hammond JW (2009) Traffic control: regulation of kinesin motors. *Nat Rev Mol Cell Biol* 10(11):765-777.

190. Stock MF*, et al.* (1999) Formation of the compact confomer of kinesin requires a COOH-terminal heavy chain domain and inhibits microtubule-stimulated ATPase activity. *J Biol Chem* 274(21):14617-14623.

191. Coy DL, Hancock WO, Wagenbach M, & Howard J (1999) Kinesin's tail domain is an inhibitory regulator of the motor domain. *Nat Cell Biol* 1(5):288-292.

192. Hackney DD & Stock MF (2008) Kinesin tail domains and Mg2+ directly inhibit release of ADP from head domains in the absence of microtubules. *Biochemistry-Us* 47(29):7770-7778.

193. Dietrich KA*, et al.* (2008) The kinesin-1 motor protein is regulated by a direct interaction of its head and tail. *Proc Natl Acad Sci U S A* 105(26):8938-8943.

194. Espeut J*, et al.* (2008) Phosphorylation relieves autoinhibition of the kinetochore motor Cenp-E. *Mol Cell* 29(5):637-643.

195. Lee JR*, et al.* (2004) An intramolecular interaction between the FHA domain and a coiled coil negatively regulates the kinesin motor KIF1A. *EMBO J* 23(7):1506-1515.

196. Cai D, Hoppe AD, Swanson JA, & Verhey KJ (2007) Kinesin-1 structural organization and conformational changes revealed by FRET stoichiometry in live cells. *J Cell Biol* 176(1):51-63.

197. Horgan CP & McCaffrey MW (2011) Rab GTPases and microtubule motors. *Biochem Soc Trans* 39(5):1202-1206.

198. Delevoye C & Goud B (2015) Rab GTPases and kinesin motors in endosomal trafficking. *Methods Cell Biol* 130:235-246.

199. Atherton J, Houdusse A, & Moores C (2013) MAPping out distribution routes for kinesin couriers. *Biol Cell* 105(10):465-487.

200. Farrell CM, Mackey AT, Klumpp LM, & Gilbert SP (2002) The role of ATP hydrolysis for kinesin processivity. *J Biol Chem* 277(19):17079-17087.

201. Svoboda K, Schmidt CF, Schnapp BJ, & Block SM (1993) Direct observation of kinesin stepping by optical trapping interferometry. *Nature* 365(6448):721-727.

202. Kaseda K, Higuchi H, & Hirose K (2003) Alternate fast and slow stepping of a heterodimeric kinesin molecule. *Nat Cell Biol* 5(12):1079-1082.

203. Yildiz A, Tomishige M, Vale RD, & Selvin PR (2004) Kinesin walks hand-over-hand. *Science* 303(5658):676-678.

204. Wang W, Cao L, Wang C, Gigant B, & Knossow M (2015) Kinesin, 30 years later: Recent insights from structural studies. *Protein Sci* 24(7):1047-1056.

205. Howard J, Hudspeth AJ, & Vale RD (1989) Movement of microtubules by single kinesin molecules. *Nature* 342(6246):154-158.

206. Asbury CL, Fehr AN, & Block SM (2003) Kinesin moves by an asymmetric hand-over-hand mechanism. *Science* 302(5653):2130-2134.

207. Wade RH & Kozielski F (2000) Structural links to kinesin directionality and movement. *Nat Struct Biol* 7(6):456-460.

208. Hoeprich GJ, Thompson AR, McVicker DP, Hancock WO, & Berger CL (2014) Kinesin's neck-linker determines its ability to navigate obstacles on the microtubule surface. *Biophys J* 106(8):1691-1700.

209. Remacle AG*, et al.* (2005) The transmembrane domain is essential for the microtubular trafficking of membrane type-1 matrix metalloproteinase (MT1-MMP). *J Cell Sci* 118(Pt 21):4975-4984.

210. Wang Z*, et al.* (2017) Binding of PLD2-Generated Phosphatidic Acid to KIF5B Promotes MT1-MMP Surface Trafficking and Lung Metastasis of Mouse Breast Cancer Cells. *Dev Cell* 43(2):186-197 e187.

211. Marchesin V*, et al.* (2015) ARF6-JIP3/4 regulate endosomal tubules for MT1-MMP exocytosis in cancer invasion. *J Cell Biol* 211(2):339-358.

212. Dong Z*, et al.* (2013) Leptin-mediated regulation of MT1-MMP localization is KIF1B dependent and enhances gastric cancer cell invasion. *Carcinogenesis* 34(5):974-983.

213. Soppina V*, et al.* (2014) Dimerization of mammalian kinesin-3 motors results in superprocessive motion. *Proc Natl Acad Sci U S A* 111(15):5562-5567.

214. Delevoye C*, et al.* (2009) AP-1 and KIF13A coordinate endosomal sorting and positioning during melanosome biogenesis. *J Cell Biol* 187(2):247-264.

215. Delevoye C*, et al.* (2014) Recycling Endosome Tubule Morphogenesis from Sorting Endosomes Requires the Kinesin Motor KIF13A. *Cell Reports* 6(3):445-454.

216. Etoh K & Fukuda M (2019) Rab10 regulates tubular endosome formation through KIF13A and KIF13B motors. *J Cell Sci* 132(5).

217. Fehling SK*, et al.* (2013) The microtubule motor protein KIF13A is involved in intracellular trafficking of the Lassa virus matrix protein Z. *Cell Microbiol* 15(2):315-334.

218. Ramos-Nascimento A*, et al.* (2017) KIF13A mediates trafficking of influenza A virus ribonucleoproteins. *J Cell Sci* 130(23):4038-4050.

219. Zhou R, Niwa S, Guillaud L, Tong Y, & Hirokawa N (2013) A molecular motor, KIF13A, controls anxiety by transporting the serotonin type 1A receptor. *Cell Rep* 3(2):509-519.

220. Miyagishi H*, et al.* (2020) Characterization of 5-HT1A receptor and transport protein KIF13A expression in the hippocampus of stress-adaptive and -maladaptive mice. *Neurosci Lett* 733:135082.

221. Gong X, Didan Y, Lock JG, & Stromblad S (2018) KIF13A-regulated RhoB plasma membrane localization governs membrane blebbing and blebby amoeboid cell migration. *EMBO J* 37(17).

222. Kondo S*, et al.* (1994) KIF3A is a new microtubule-based anterograde motor in the nerve axon. *J Cell Biol* 125(5):1095-1107.

223. Muresan V*, et al.* (1998) KIF3C and KIF3A form a novel neuronal heteromeric kinesin that associates with membrane vesicles. *Mol Biol Cell* 9(3):637-652.

224. Hirokawa N (2000) Stirring up development with the heterotrimeric kinesin KIF3. *Traffic* 1(1):29-34.

225. Lehti MS, Kotaja N, & Sironen A (2013) KIF3A is essential for sperm tail formation and manchette function. *Mol Cell Endocrinol* 377(1-2):44-55.

226. Gaudin R*, et al.* (2012) Critical role for the kinesin KIF3A in the HIV life cycle in primary human macrophages. *J Cell Biol* 199(3):467-479.

227. Geng G*, et al.* (2018) KIF3A knockdown sensitizes bronchial epithelia to apoptosis and aggravates airway inflammation in asthma. *Biomed Pharmacother* 97:1349-1355.

228. Piddini E, Schmid JA, de Martin R, & Dotti CG (2001) The Ras-like GTPase Gem is involved in cell shape remodelling and interacts with the novel kinesin-like protein KIF9. *Embo Journal* 20(15):4076-4087.

229. Miyata H*, et al.* (2020) Testis-enriched kinesin KIF9 is important for progressive motility in mouse spermatozoa. *Faseb Journal*.

230. Dorner C*, et al.* (1998) Characterization of KIF1C, a new kinesin-like protein involved in vesicle transport from the Golgi apparatus to the endoplasmic reticulum. *J Biol Chem* 273(32):20267-20275.

231. Theisen U, Straube E, & Straube A (2012) Directional persistence of migrating cells requires Kif1C-mediated stabilization of trailing adhesions. *Dev Cell* 23(6):1153-1166.

232. Gabrych DR, Lau VZ, Niwa S, & Silverman MA (2019) Going Too Far Is the Same as Falling Short(dagger): Kinesin-3 Family Members in Hereditary Spastic Paraplegia. *Front Cell Neurosci* 13:419.

233. Kopp P*, et al.* (2006) The kinesin KIF1C and microtubule plus ends regulate podosome dynamics in macrophages. *Mol Biol Cell* 17(6):2811-2823.

234. Efimova N*, et al.* (2014) Podosome-regulating kinesin KIF1C translocates to the cell periphery in a CLASP-dependent manner. *J Cell Sci* 127(Pt 24):5179-5188.

235. Lee PL, Ohlson MB, & Pfeffer SR (2015) Rab6 regulation of the kinesin family KIF1C motor domain contributes to Golgi tethering. *Elife* 4.

236. Tinevez JY*, et al.* (2017) TrackMate: An open and extensible platform for single-particle tracking. *Methods* 115:80-90.

237. Cerami E*, et al.* (2012) The cBio cancer genomics portal: an open platform for exploring multidimensional cancer genomics data. *Cancer Discov* 2(5):401-404.

238. Gao J*, et al.* (2013) Integrative analysis of complex cancer genomics and clinical profiles using the cBioPortal. *Sci Signal* 6(269):pl1.

239. Hirokawa N & Tanaka Y (2015) Kinesin superfamily proteins (KIFs): Various functions and their relevance for important phenomena in life and diseases. *Exp Cell Res* 334(1):16-25.

240. Devy L*, et al.* (2009) Selective inhibition of matrix metalloproteinase-14 blocks tumor growth, invasion, and angiogenesis. *Cancer Res* 69(4):1517-1526.

241. Thapa N & Anderson RA (2017) PLD and PA Take MT1-MMP for a Metastatic Ride. *Dev Cell* 43(2):117-119.

242. Fish KN (2009) Total internal reflection fluorescence (TIRF) microscopy. *Curr Protoc Cytom* Chapter 12:Unit12 18.

243. Curtis AS (1964) The Mechanism of Adhesion of Cells to Glass. A Study by Interference Reflection Microscopy. *J Cell Biol* 20:199-215.

244. Linder S (2015) MT1-MMP: Endosomal delivery drives breast cancer metastasis. *J Cell Biol* 211(2):215-217.

245. Strongin AY*, et al.* (1995) Mechanism of cell surface activation of 72-kDa type IV collagenase. Isolation of the activated form of the membrane metalloprotease. *J Biol Chem* 270(10):5331-5338.

246. Itoh Y, Ito N, Nagase H, & Seiki M (2008) The second dimer interface of MT1-MMP, the transmembrane domain, is essential for ProMMP-2 activation on the cell surface. *J Biol Chem* 283(19):13053-13062.

247. Grinnell F (2003) Fibroblast biology in three-dimensional collagen matrices. *Trends Cell Biol* 13(5):264-269.

248. Rhee S (2009) Fibroblasts in three dimensional matrices: cell migration and matrix remodeling. *Exp Mol Med* 41(12):858-865.

249. Chen S*, et al.* (2016) KIF1B promotes glioma migration and invasion via cell surface localization of MT1-MMP. *Oncol Rep* 35(2):971-977.

250. Kupfer A, Louvard D, & Singer SJ (1982) Polarization of the Golgi-Apparatus and the Microtubule-Organizing Center in Cultured Fibroblasts

at the Edge of an Experimental Wound. *P Natl Acad Sci-Biol* 79(8):2603-2607.

251. Bucci C*, et al.* (1992) The Small Gtpase Rab5 Functions as a Regulatory Factor in the Early Endocytic Pathway. *Cell* 70(5):715-728.
252. Gorvel JP, Chavrier P, Zerial M, & Gruenberg J (1991) rab5 controls early endosome fusion in vitro. *Cell* 64(5):915-925.
253. Feng Y, Press B, & Wandingerness A (1995) Rab-7 - an Important Regulator of Late Endocytic Membrane Traffic. *Journal of Cell Biology* 131(6):1435-1452.
254. Bucci C, Thomsen P, Nicoziani P, McCarthy J, & van Deurs B (2000) Rab7: a key to lysosome biogenesis. *Mol Biol Cell* 11(2):467-480.
255. Mattheyses AL, Simon SM, & Rappoport JZ (2010) Imaging with total internal reflection fluorescence microscopy for the cell biologist. *J Cell Sci* 123(Pt 21):3621-3628.
256. Ge J*, et al.* (2013) Standard fluorescent imaging of live cells is highly genotoxic. *Cytometry A* 83(6):552-560.
257. Mazzone M*, et al.* (2004) Intracellular processing and activation of membrane type 1 matrix metalloprotease depends on its partitioning into lipid domains. *J Cell Sci* 117(Pt 26):6275-6287.
258. Brown CL*, et al.* (2005) Kinesin-2 is a motor for late endosomes and lysosomes. *Traffic* 6(12):1114-1124.
259. Loubery S*, et al.* (2008) Different microtubule motors move early and late endocytic compartments. *Traffic* 9(4):492-509.

260. Vidal RL*, et al.* (2007) Marlin-1 and conventional kinesin link GABAB receptors to the cytoskeleton and regulate receptor transport. *Mol Cell Neurosci* 35(3):501-512.

261. Delevoye C*, et al.* (2016) BLOC-1 Brings Together the Actin and Microtubule Cytoskeletons to Generate Recycling Endosomes. *Curr Biol* 26(1):1-13.

262. Shakya S*, et al.* (2018) Rab22A recruits BLOC-1 and BLOC-2 to promote the biogenesis of recycling endosomes. *EMBO Rep* 19(12).

263. Yang R*, et al.* (2019) A novel strategy to visualize vesicle-bound kinesins reveals the diversity of kinesin-mediated transport. *Traffic* 20(11):851-866.

264. Trivedi D, Colin E, Louie CM, & Williams DS (2012) Live-cell imaging evidence for the ciliary transport of rod photoreceptor opsin by heterotrimeric kinesin-2. *J Neurosci* 32(31):10587-10593.

265. Hendricks AG*, et al.* (2010) Motor coordination via a tug-of-war mechanism drives bidirectional vesicle transport. *Curr Biol* 20(8):697-702.

266. Rezaul K*, et al.* (2016) Engineered Tug-of-War Between Kinesin and Dynein Controls Direction of Microtubule Based Transport In Vivo. *Traffic* 17(5):475-486.

267. Messitt TJ*, et al.* (2008) Multiple kinesin motors coordinate cytoplasmic RNA transport on a subpopulation of microtubules in Xenopus oocytes. *Dev Cell* 15(3):426-436.

268. Snow JJ*, et al.* (2004) Two anterograde intraflagellar transport motors cooperate to build sensory cilia on C. elegans neurons. *Nat Cell Biol* 6(11):1109-1113.

269. Pan X*, et al.* (2006) Mechanism of transport of IFT particles in C. elegans cilia by the concerted action of kinesin-II and OSM-3 motors. *J Cell Biol* 174(7):1035-1045.

270. Khanna C & Hunter K (2005) Modeling metastasis in vivo. *Carcinogenesis* 26(3):513-523.

271. Tsai YC*, et al.* (2007) The ubiquitin ligase gp78 promotes sarcoma metastasis by targeting KAI1 for degradation. *Nat Med* 13(12):1504-1509.

272. Fuse C, Ishida Y, Hikita T, Asai T, & Oku N (2007) Junctional adhesion molecule-C promotes metastatic potential of HT1080 human fibrosarcoma. *J Biol Chem* 282(11):8276-8283.

273. Zhang L & Hill RP (2007) Hypoxia enhances metastatic efficiency in HT1080 fibrosarcoma cells by increasing cell survival in lungs, not cell adhesion and invasion. *Cancer Res* 67(16):7789-7797.

274. Hanyu A*, et al.* (2009) Functional in vivo optical imaging of tumor angiogenesis, growth, and metastasis prevented by administration of anti-human VEGF antibody in xenograft model of human fibrosarcoma HT1080 cells. *Cancer Sci* 100(11):2085-2092.

275. Saunders TL (2011) Inducible transgenic mouse models. *Methods Mol Biol* 693:103-115.

276. Zakeri B & Wright GD (2008) Chemical biology of tetracycline antibiotics. *Biochem Cell Biol* 86(2):124-136.

277. Kaneko K*, et al.* (2016) Selective Inhibition of Membrane Type 1 Matrix Metalloproteinase Abrogates Progression of Experimental Inflammatory Arthritis: Synergy With Tumor Necrosis Factor Blockade. *Arthritis Rheumatol* 68(2):521-531.

278. Zheng Q*, et al.* (2014) Precise gene deletion and replacement using the CRISPR/Cas9 system in human cells. *Biotechniques* 57(3):115-124.

279. Robert A*, et al*. (2019) Kinesin-dependent transport of keratin filaments: a unified mechanism for intermediate filament transport. *FASEB J* 33(1):388-399.

280. Wei YL & Yang WX (2019) Kinesin-14 motor protein KIFC1 participates in DNA synthesis and chromatin maintenance. *Cell Death Dis* 10(6):402.

281. Engelke MF*, et al.* (2019) Acute Inhibition of Heterotrimeric Kinesin-2 Function Reveals Mechanisms of Intraflagellar Transport in Mammalian Cilia. *Curr Biol* 29(7):1137-1148 e1134.

282. Uhlen M*, et al.* (2017) A pathology atlas of the human cancer transcriptome. *Science* 357(6352).

283. Chandrasekaran G, Tatrai P, & Gergely F (2015) Hitting the brakes: targeting microtubule motors in cancer. *Br J Cancer* 113(5):693-698.

284. Cho S & Kim D (2019) Integrative analysis of KIF4A, 9, 18A, and 23 and their clinical significance in low-grade glioma and glioblastoma multiforme. *Cancer Research* 79(13).

285. Clark AG & Vignjevic DM (2015) Modes of cancer cell invasion and the role of the microenvironment. *Curr Opin Cell Biol* 36:13-22.

286. Friedl P & Alexander S (2011) Cancer invasion and the microenvironment: plasticity and reciprocity. *Cell* 147(5):992-1009.

287. Lafleur MA, Xu D, & Hemler ME (2009) Tetraspanin proteins regulate membrane type-1 matrix metalloproteinase-dependent pericellular proteolysis. *Mol Biol Cell* 20(7):2030-2040.

288. Strongin AY (2010) Proteolytic and non-proteolytic roles of membrane type-1 matrix metalloproteinase in malignancy. *Biochim Biophys Acta* 1803(1):133-141.

289. Tomari T*, et al.* (2009) High throughput analysis of proteins associating with a proinvasive MT1-MMP in human malignant melanoma A375 cells. *Cancer Sci* 100(7):1284-1290.

290. Wu KP*, et al.* (2014) MT1-MMP is not a good prognosticator of cancer survival: evidence from 11 studies. *Tumor Biol* 35(12):12489-12495.

291. Lefevre S*, et al.* (2009) Synovial fibroblasts spread rheumatoid arthritis to unaffected joints. *Nat Med* 15(12):1414-1420.

292. Korb-Pap A, Bertrand J, Sherwood J, & Pap T (2016) Stable activation of fibroblasts in rheumatic arthritis-causes and consequences. *Rheumatology (Oxford)* 55(suppl 2):ii64-ii67.

293. Croft AP*, et al.* (2019) Distinct fibroblast subsets drive inflammation and damage in arthritis. *Nature* 570(7760):246-251.

294. Chen WT & Wang JY (1999) Specialized surface protrusions of invasive cells, invadopodia and lamellipodia, have differential MT1-MMP, MMP-2, and TIMP-2 localization. *Ann N Y Acad Sci* 878:361-371.